6th Hull Performance & Insight Conference

HullPIC'21

Edited by Volker Bertram

Sponsored by
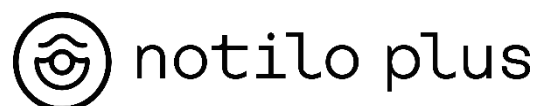
1

Index

Feature Engineering-Enhanced Vessel Performance Prediction and Modeling

Yuhuai Seah, AkzoNobel, Singapore, yuhuai.seah@akzonobel.com
Haoliang Chen, AkzoNobel, Singapore, haoliang.chen@akzonobel.com
Barry Kidd, AkzoNobel, Gateshead/UK, barry.kidd@akzonobel.com

Abstract

Over the years, the shipping industry is advancing fast as more shipping companies are relying on data to make informed decision in their vessel operations and business. At the same time, the need to better understand the data and to be able to extract meaningful accurate insights about the ships' performance presents a challenge to ship owners. Fouling control coating manufacturers face a similar issue as well. To better understand ship's hull and propeller condition and thus coatings' performance, and more importantly to support better decision-making regarding hull and propeller management and coating selection, it's important to be able to increase the performance modelling and prediction accuracy through adopting the latest performance analysis techniques. In AkzoNobel, we are continuously exploring different methodologies of analysing data provided by ship owners. One of our latest advances is to use machine learning techniques to improve performance analysis and facilitate a holistic data review. Feature engineering as one of the key steps in machine learning is investigated regarding whether it can improve the prediction accuracy. Preliminary results reveal that these techniques show promising results in extracting insights from data to understand about a vessel's performance. Here, we share preliminary work and thoughts on how some machine learning techniques could be used to assist in hull and propeller performance review and performance prediction.

1. Introduction

The exponential advancement in data analytics techniques and machine learning algorithms over the last few years have enabled shipping companies to widen their analytical toolbox and perform different types of analysis. To understand about their fleet performance, shipping companies perform various types of analysis, ranging from basic descriptive analysis of the vessel data with data visualisation tools, to making inference of performance from vessel data using statistical techniques. With an expanded capability in data analytics techniques, shipping companies are now able to explore previously undiscovered information from their data and make informed decision about their business operations.

One area of analytics widely discussed within the shipping industry is predictive analytics. Predictive analytics is the process of extracting information from data to predict future trends. In the shipping industry, companies are constantly experimenting with machine learning techniques to forecast future fuel consumption. The ability to reliably and accurately forecast fuel consumption or power requirements could significantly help shipping companies plan its ships' operation, such as the arrangement of ship maintenance and hull cleaning.

To perform predictive analysis, a machine learning framework is usually adopted and followed. A simple machine learning modelling framework is shown in Fig.1. It contains the essential steps required to perform predictive analytics. The framework can be divided into several parts: data collection and preparation, feature engineering, model selection, evaluation of model and making prediction using the trained model.

Previous studies have demonstrated the use of a machine learning modelling framework to perform predictive analytics. *Jeon et al. (2018)* adopted a big data analysis framework of predicting ship's fuel consumption. *Gundermann and McLaughlin (2018)* utilised a basic machine learning framework to perform predictive analysis. Though these papers explore the use of a machine learning modelling framework in big data vessel analysis, the particular significance and importance of the feature engineering step is seldom explored and discussed.

Feature engineering is the process of using existing information within data to identify new features by using some data mining technique. It involves the creation of new features by transforming existing features in the dataset. Feature engineering, when done right, can result in improved performance accuracy of a model. An existing non feature engineered dataset can be used to train the model to perform prediction, but it may not contain the ideal information for the model to learn from. Feature engineering modifies the dataset such that the information assists the model to learn better and thus being able to apply what it has learnt on a new set of data with high predictive accuracy. More details regarding the concept and implementation of the feature engineering concept is explained and illustrated by *Khurana et al. (2018)*.

In this preliminary study, the applicability and impacts of feature engineering on ship performance modelling will be explored and discussed by applying the technique to a group of vessel datasets

2. Methodology

Six datasets collected from different vessel types were selected were used in the machine learning modelling framework. Some of these datasets record vessels' operating information once per day (noon data), while others record once every 15 minutes. The different types of vessel data used enable us to observe how the model performs when trained with different information. Each dataset contains valuable operating information enabling ship owners to monitor the performance of their fleet. From the operating information, the operating speed, draft on sailing, wind weather condition and power consumption are extracted in this study.

After extracting relevant data for the study, the data is processed before being used to train and test the model. The processing step is important to separate unwanted noise from the valuable information which is useful for the model to learn and hopefully provide a reliable prediction performance.

A commonly used framework of machine learning modelling is shown in Fig.1. In the data collection and preparation process, data is selected based on the availability of information. Then, data is cleaned so that the quality of the data is improved. During data processing, various methods and guidelines can be applied to data filtration, treatment of missing values and identification and removal of outliers step by step. One example to follow is the data preparation and processing procedures in ISO19030. When the data are ready, feature engineering is performed on the wind Beaufort scale by grouping data of similar wind characteristic together.
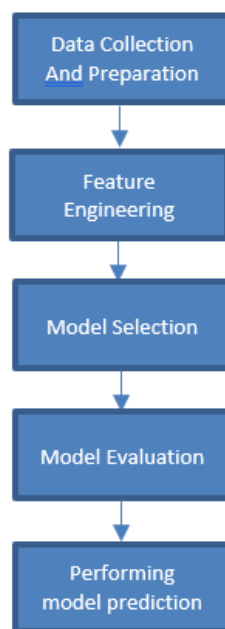
Fig.1: Modelling Framework for Machine Learning

3. Feature engineering

A new feature called wind intensity is created by grouping Beaufort scale of similar characteristic together. This is done by performing a feature engineering technique called categorical binning. Categorical binning is the assignment of a general category to combine groups in which have low frequency and similar characteristics. Combining these groups into a general category can have a positive impact on the robustness of the statistical model, since the general category provides more information to the model so it can be predicted better than when low frequency groups are provided.

The assignment of general category can vary among the different test cases, depending on the frequency distribution of the wind Beaufort scale data. For example, in one of test cases (as shown in figure 2), data belonging to Beaufort scale "0" and "1" groups can be combined to form a new category since the frequency distribution graphs show that both groups have low frequency relative to the rest of the groups, while the remaining Beaufort scale groups are not recategorized. Beaufort scale groups with low frequency count will be combined and assigned a new category.
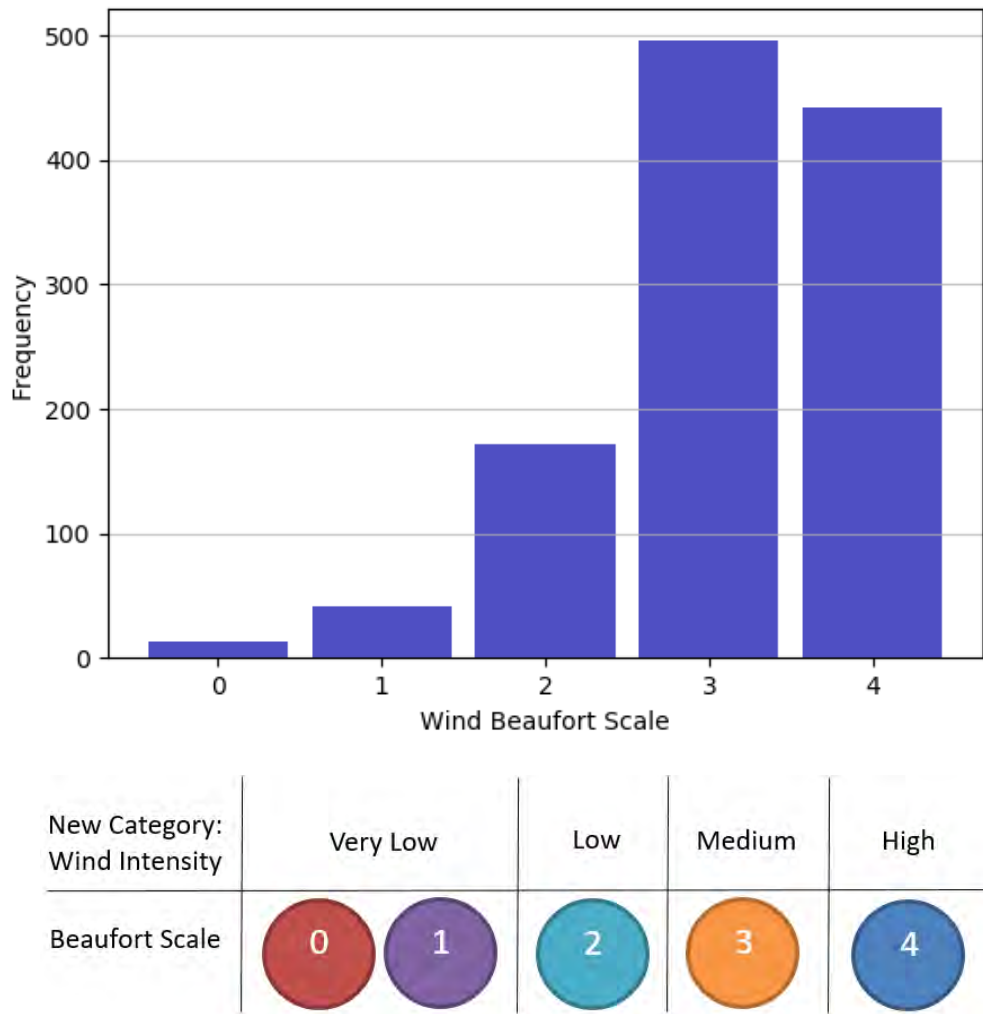
Fig.2: Frequency distribution of wind Beaufort scale of one test case and its corresponding categorization of the Beaufort scale

After performing feature engineering on wind Beaufort scale, the newly created feature comprising of the generalized category will be used to train the model in replace of the wind Beaufort scale.

6

Once feature engineering is completed, the selection of type of models follows. For simplicity sake, we choose a linear regression model for the case study. This model will then be trained using the feature engineered dataset and evaluated using performance metrics which indicate how accurate the model can predict the performance.

4. Results

To measure the predictive performance of the model, the dataset is split into training and testing datasets using the holdout method. The holdout method is a simple form of cross validation, *Sammut and Webb (2011)*, and its advantage is that it is less computationally intensive and takes lesser time in computing the predictive error of the model. In this study, two-thirds of each dataset will be allotted to the training set, while the remaining one-third will be allotted to the testing set.

The performance accuracy of the regression model is measured by using common machine learning performance metrics. The performance metrics used in this case study are the relative root mean square error (RRMSE), mean absolute error (MAE) and R-square (R^2).

RRMSE is computed by taking the root mean square error over the average value of the observed information. This performance metric considers the performance accuracy of the model to be excellent if the RRMSE is less than 0.1, *Despotovic et al. (2016)*. MAE is an average measure of sum of absolute differences between the observed and predicted values. A low MAE value implies low model prediction error. R^2 is known as the coefficient of determination and is a descriptive measure used to determine the linear association between the inputs and the response variable. A high R^2 value implies that majority of the data variability can be explained by the regression model.

Table I shows the performance metrics of the regression model across different feature engineered datasets. For each dataset, both the performance accuracy of model when trained with featured engineered dataset and raw data are measured. Datasets 1-4 are low frequency data, while datasets 5-6 are high frequency data. The first four datasets are selected from various vessel types (LNG, Container, Tanker and Bulker) and the last two datasets are selected from a cruise and tanker.

Table I: Performance metrics of model when trained with featured engineered dataset (yes column) in comparison to when raw dataset is used (no column)

Dataset No.	Frequency	Vessel Types	RRMSE		MAPE		R^2	
			No	Yes	No	Yes	No	Yes
1	Low	LNG	0.1002	0.0991	0.1267	0.1259	0.6461	0.6472
2	Low	Container	0.1797	0.1748	0.2863	0.281	0.5892	0.5930
3	Low	Tanker	0.1416	0.1415	0.1697	0.1695	0.3148	0.3156
4	Low	Bulker	0.0585	0.0581	0.0594	0.059	0.5991	0.6021
5	High	Cruise	0.0648	0.0648	0.0695	0.0695	0.9158	0.9158
6	High	Tanker	0.0762	0.0762	0.0961	0.0961	0.8994	0.8994

The table results show that there is an improvement in the performance accuracy of model using feature engineered for low-frequency datasets. The RRMSE and MAPE values decrease and the R^2 value increase. For dataset number 1, the RRMSE values of the model improved to below 0.1 when featured engineered dataset is used. On the other hand, performing categorical binning on high-frequency datasets does not have positive impact on model performance. The RRMSE, MAPE and R^2 value remain the same despite a difference in the nature of datasets used. More studies are needed to investigate which features are more significant in improving prediction accuracy for high frequency data, which is beyond the scope of this paper.
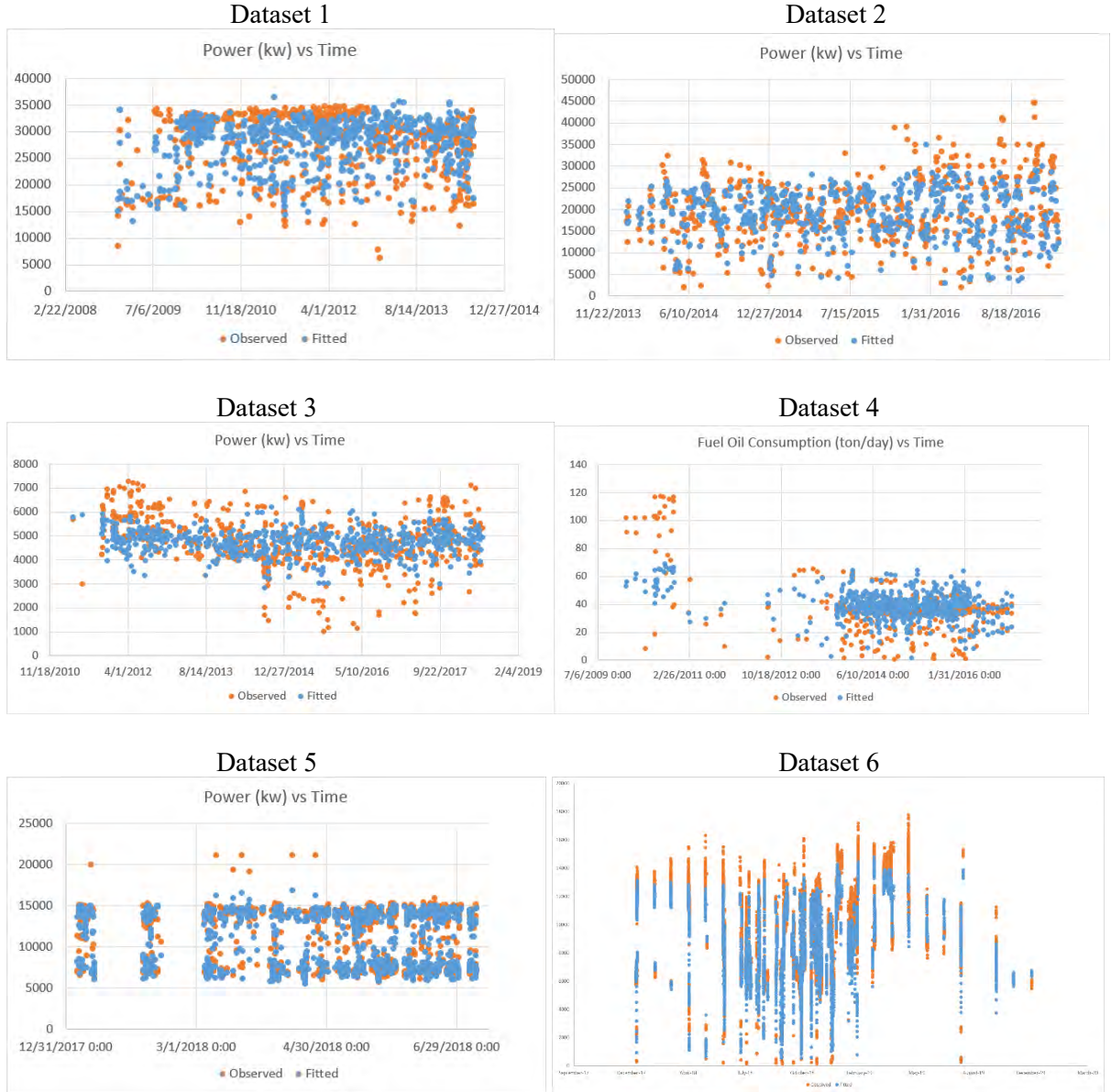
Fig.3: Time series plots of power or fuel consumption for different datasets. Predicted values are in blue and observed values are in orange.

Fig.3 shows the time series plots of the observed and predicted power across time for each dataset. Models trained with feature engineered high frequency datasets (dataset 5 & 6) tend to predict the power consumption with high accuracy, as a good proportion of predicted power overlays with the observed power. On the other hand, a lower proportion of overlay is seen for the models trained with feature engineered low frequency datasets, implying a lower prediction accuracy in the power consumption.

5. Summary and Conclusion

This paper introduces the concept of feature engineering and one of its techniques, categorical binning is applied on vessel data to explore the impact of feature engineering on model performance. When performing categorical binning, a new feature called wind intensity is created by combining Beaufort wind scale groups in which have low frequency and similar characteristics. This newly created feature replaces the Beaufort scale feature to form the feature engineered dataset. The model trained using feature engineered dataset is then compared to the model trained using non-feature engineered dataset using the regression performance metrics.

The results show that there is an improvement in model performance when feature engineered low frequency dataset are used to train the model. However, this is not the case when feature engineered high frequency dataset is used instead. It should be noted that for reporting simplicity, only the wind parameter was selected as an example in this study to explore the potential application and effects on feature engineering on vessel performance prediction. Feature selection essentially is an art of science and for high frequency data, other parameters could be more important and significant on improving the accuracy of the modeling. More studies are needed as next steps.

References

DESPOTOVIC, M.; NEDIC, V.; DESPOTOVIC, D.; CVETANOVIC, S. (2016), *Evaluation of empirical models for predicting monthly mean horizontal diffuse solar radiation,* Renewable and Sustainable Energy Reviews 56, pp.246-260

GUNDERMANN, D.; McLAUGHLIN, D. (2019), *When ISO19030 Fails: Utilizing Basic Machine Learning/Data Fitting Methods for Performance Analysis without Reference Data*, 4th HullPIC Conference, Gubbio, pp.220-228

JEON, M.; NOH, Y.; SHIN, Y.; LIM, O. K.; LEE, I.; CHO, D. (2019), *Real Ship Maritime Big Data Analysis for Prediction for Fuel Consumption*, 4th HullPIC Conference, Gubbio, pp.86-96

KHURANA, U.; SAMULOWITZ, H.; TURAGA, D. (2018), *Feature engineering for predictive modelling using reinforcement learning*, 32nd AAAI Conf. on Artificial Intelligence (AAAI-18), pp.3407-3414

SAMMUT, C.; WEBB, G.I. (2011), *Holdout Evaluation.* Encyclopedia of Machine Learning, Springer

A Step beyond the ISO 19030.2 Annex C – Evaluation of Alternative Methods for Approximating Shaft Power through Data Collection Systems

Nikolaos Bekiaris, Prisma Electronics, Greece, nikos.bekiaris@prismael.com
Lazaros Chatziagapoglou, Prisma Electronics, Greece, lazaros.chatziagapoglou@prismael.com
Christos Giordamlis, Prisma Electronics, Greece, christos@prismael.com
Fotis Dalmyras, Andriaki Shipping, Greece, fnd@andriaki.gr

Abstract

As per ISO 19030-2 Annex C, if a torque meter is not available for direct measurement of the Shaft Power, or not working, a method for estimating the engine's brake power through the use of the engine-specific SFOC reference curve is examined and analyzed. Among the challenges of any such method are the data reliability and accuracy, the great number of conditions to be applied and the factor that many of the required collected data have their own uncertainties and inconsistencies relative to sensors when measured. We will explore through the use of big data analytics, alternative ways for estimating M/E's brake power, by using specific engine's operating parameters that are collected through a LAROS data collection system. The output of this study will also define the best estimator which could be further used though Machine Learning for even more accurate estimations. More specific, through the use of up to eighteen months of operational data from 11 vessels, alternative ways of estimating engine's power are compared and analyzed. For the calculation of the reference values, filtering techniques and regression modeling are also employed. Finally, a comparative study and conclusions between the alternatives and the actual shaft power measurements are critically presented, as well as, best practices and models about the applicability and the usability of the alternatives.

1. Introduction and aim of the study

According to ISO 19030 and from general working experience, ship's speed through water and delivered power are the two primary parameters for measuring changes in hull and propeller performance. For measuring the delivered power, two are mainly the methods that ISO 19030 is suggesting:

a. One Suggested method is based on calculations of Shaft Power (Ps) from measurements of shaft torque and shaft revolutions through a proper installed & calibrated torque meter (shaft power meter), as described in details in Annex B of the specific ISO.

b. An alternative suggested method is to approximate the delivered power based on calculation of brake power from an engine-specific SFOC reference curve, as described in details in Annex C of the specific ISO.

If on a vessel a relevant shaft power meter is installed, then a high frequency automatic data collection system can collect / calculate the shaft power, either directly (as a direct output from the torque meter / shaft power meter), or through calculations from the measured shaft torque and shaft rpm.

On the other hand, the measurement of the shaft power by a high frequency automatic data collection system with the alternatively suggested by ISO 19030 method – from the engine-specific SFOC reference curve, it requires the collection of data from a larger number of parameters, where some of them are not usually available automatically, resulting on much higher uncertainty, errors and approximations, since every parameter has its own characteristics and inconsistencies when measured.

In this paper, we explore through the use of big data analytics, alternative ways for estimating M/E's brake power, by using specific engine's operating parameters that are collected through LAROS data collection system, with the final goal to define the best estimator for further use in Machine Learning.

10

2. Analysis of alternative ways for calculating shaft power

The direct method of measuring propeller shaft power is by an installed shaft power meter / torque meter connected to a high frequency automatic data collection system. Apart from that, the collection of additional measurements in a well time synchronized procedure is required in order to apply ISO 19030 criteria and filters. In the absent of such a system, below alternative ways have been considered, analyzed and compared for a universal method to be finally suggested.

Below is the theoretical presentation of each one of the explored methods, with the relevant uncertainties that each method might present.

2.1. Calculations of brake power from an engine-specific SFOC reference curve

In this method the brake horse power of the engine was estimated through the use of the engine's SFOC reference curve, which is based on the actual shop tests of the specific engine,

$$P_B = f \, (ME_{FOC\ corrected}) \qquad \text{where:}$$
$$f = SFOC\ reference\ curve$$

The $ME_{FOCcorrected}$ is the corrected ME_{FOC} according below ambient conditions:

Table I: ISO ambient conditions for F.O. consumption correction

Condition	ISO	
Cooling water inlet temp at scavenge air inlet (ºC)	25	W
Air suction ambient temp at blower (T/C) inlet (ºC)	25	A
Barometric ambient pressure at blower inlet (mbar)	1000	P
Fuel Lower Calorific Value (kJ/kg)	42700	LCV

And the typical general approach with proper corrections is:

$$ME_{FOC\ corrected} = ME_{FOC} \times \frac{LCV \times \left[1 + \dfrac{0.002 \times (P - 1000) + 0.02 \times (25 - A) + 0.06 \times (25 - W)}{100} \right]}{42700}$$

For the accurate calculations of the corrected F.O. consumption, all four above mentioned parameters are needed to be measured. As Table II shows, though, for a 10% change of any of these four parameters, while the rest of the parameters remain the same, the fuel's lower calorific value has the greatest impact.

Table II: $ME_{FOCcorrected}$ per centage change for 10% change of ambient conditions

Condition	10% increase	% change
Cooling water inlet temp at scavenge air inlet (ºC)	27.5	0.15%
Air suction ambient temp at blower (T/C) inlet (ºC)	27.5	0.05%
Barometric ambient pressure at blower inlet (mbar)	900	0.20%
Fuel Lower Calorific Value (kJ/kg)	38430	11.11%

So, for any approximation of engine's brake horse power through the use of the engine-specific SFOC curve, it is required to know the actual lower calorific value of the fuel in use. This value should either be entered manually directly into the system for the greatest accuracy – taken from the bunkered fuel oil analysis report, or through an approximating equation from fuel's density:

$$LCV = (-18837 \times \rho_{15oC}{}^2) + 15141 \times \rho_{15oC} + 43379 \qquad \text{Where:}$$

ρ_{15oC}: The density of the consumed fuel oil at 15 ºC in vacuum

Finally, the mass of consumed fuel can be obtain directly from a mass flow meter. In the event now, that the mass of consumed fuel is obtained from a volume flow meter, then the mass of fuel oil shall be calculated from the volume of the consumed fuel and the density at the actual temperature of the consumed fuel.

$$ME_{FOC} = V_{FOC} \times (\rho_{15oC} - 0.0011) \times VCF \qquad \text{Where:}$$

V_{FOC}: The volume of the consumed fuel oil

ρ_{15oC}: The density of the consumed fuel oil at 15 ^{o}C in vacuum

VCF: The Volume Correction Factor. For the VCF calculation, the actual temperature of the consumed fuel needs to be also measured. $VCF = f(Fuel\ Temp)$

The use of this method from a high frequency automatic data collection system for estimating vessel's shaft power includes below inaccuracies that should be taken in consideration during calculations:

a. The uncertainties of not measuring the other factors needed for the ISO correction of the consumed fuel oil, due to the additional equipment that are required to be installed for their proper measurement.

b. The accuracy of the installed flow meter(s). In case that the fuel oil service system is common for the M/E and the A/Es, then the final measured fuel oil consumption is also affected from the accuracy of all flow meters used for measuring the M/E's fuel oil consumption.

c. When the fuel oil consumption is measured from the flow meters, any leaks or drains (eg back wash drain from the fuel oil filter) are not possible to be measured and be excluded from the measured fuel oil consumption.

d. In case of volumetric flow meters, the accuracy is also affected with the density conversion, especially, when more than one flow meters need to be measured.

e. The condition of the Main Engine, which is perhaps the most important parameter for inaccuracies, especially for older vessels.

f. Other uncertainties including sensors reliability, piping, distortion, noise, vibrations just to mention few.

2.2. Calculations of brake power from an engine-specific Power vs Turbo Charger rpm curve

In this method the brake horse power of the engine was estimated through the use of the engine's Power vs Turbo Charger rpm curve, which is based on the actual shop tests of the specific engines.

$$P_B = f\ (T/C_{rpm})$$

The engine's turbo charger rpm (T/C_{rpm}) can easily be measured from a high frequency automatic data collection system, either directly from a local indicator, or through vessel's Alarm & Monitoring System (AMS). In case vessel's engine is equipped with two turbo chargers, then on the function the average measured rpm from the two turbo chargers was used.

In the specific method, a correction of the measured T/C_{rpm} is not required (eg ISO correction) and any inaccuracies can be found either in the accuracy of the indicator, or in the condition of the engine's turbo charger. In this method, it is very important that the cleaning intervals of the turbocharger and inter-cooler are strictly kept.

2.3. Calculations of brake power from an engine-specific Power vs scavenge air pressure curve

In this method the brake horse power of the engine was estimated through the use of the engine's Power vs Scavenge Air pressure curve, which is based on the actual shop tests of the specific engine.

$$P_B = f\ (Scav_{press})$$

The engine's scavenge air pressure ($Scav_{press}$) can be measured from a high frequency automatic data collection system, either directly from a local indicator, or through vessel's Alarm & Monitoring System (AMS).

The $Scav_{press}$ should also be corrected according to the ambient conditions in Table III.

Table III: ISO ambient conditions for $SCAV_{press}$ correction

Condition	ISO
Cooling water inlet temp at scavenge air inlet (ºC)	25
Air suction ambient temp at blower (T/C) inlet (ºC)	25

Below table shows, for a 10% change of any of these two parameters while the other parameter remains the same, the impact on the measured $Scav_{press}$.

Table IV: $SCAV_{press}$ percentage change for 10% change of ambient conditions

Condition	10% increase	% change
Cooling water inlet temp at scavenge air inlet (ºC)	27.5	-0.925%
Air suction ambient temp at blower (T/C) inlet (ºC)	27.5	1.19%

The effect of the ambient conditions in the measured $Scav_{press}$ is in general significant. An increase though in the cooling water inlet temp results to a negative change to the corrected $Scav_{press}$, while an increase in air suction ambient temp to a positive change. Usually, both temperatures rise or fall simultaneously, diminishing the effect of the ambient conditions.

2.4. Calculations of brake power from an engine-specific Power vs before & after T/C exhaust gas temperatures

In this method the brake horse power of the engine was estimated through the use of the engine's Power vs the difference of the exhaust gas temperatures before & after turbo charger curve, which is based on the actual shop tests of the specific engine.

$$P_B = f\left(T_{exh\,bef\,TC} - T_{exh\,aft\,TC}\right)$$

The exhaust gas temperatures before and after engine's turbo charger can be measured by a high frequency automatic data collection system, usually through vessel's Alarm & Monitoring System (AMS).

The $T_{exh\,bef\,TC}$ and $T_{exh\,aft\,TC}$ should also be corrected according the ambient conditions in Table V.

Table 1: ISO ambient conditions for $T_{exh\,bef\,TC}$ and $T_{exh\,aft\,TC}$ correction

Condition	ISO
Cooling water inlet temp at scavenge air inlet (ºC)	25
Air suction ambient temp at blower (T/C) inlet (ºC)	25

Table VI shows, for a 10% change of any of these two parameters while the other parameter remains the same, the impact on the measured DT_{exh} ($T_{exh\,bef\,TC} - T_{exh\,aft\,TC}$).

Table VI: DT_{exh} percentage change for 10% change of ambient conditions

Condition	10% increase	% change
Cooling water inlet temp at scavenge air inlet (ºC)	27.5	-1.067%
Air suction ambient temp at blower (T/C) inlet (ºC)	27.5	0.991%

Similarly, as $Scav_{press}$, the effect of the ambient conditions in the measured DT_{exh} is in general high. An increase though in the cooling water inlet temp results to a negative change to the corrected DT_{exh}, while

an increase in air suction ambient temp to a positive change. Usually, both temperatures rise or fall simultaneously, diminishing the effect of the ambient conditions.

2.5. Calculations of brake power from an engine-specific Power vs Fuel Rack / Index position

In this method the brake horse power of the engine was estimated through the use of the engine's Power vs Fuel Rack / Index position curve, which is based on the actual shop tests of the specific engine.

$$P_B = f\ (F.I._{pos})$$

The engine's fuel rack position (for older engines) or fuel index position (for electronic engines) ($F.I._{pos}$) can be measured from a high frequency automatic data collection system, either directly from a local indicator, or through vessel's Alarm & Monitoring System (AMS).

For the specific method, a correction of the measured $F.I._{pos}$ is not required (eg ISO correction), but the type of fuel oil, as well as the condition of the fuel pump, may have a great effect on the index, resulting in wrong estimation of the engine's power. In particular, worn fuel pumps or suction valves tend to increase the index and will thus result in a too high power estimation.

2.6. Calculations of brake power from an engine-specific Power vs M/E's Shaft RPM

In this method the brake horse power of the engine was estimated through the use of the engine's Power vs rpm curve, which is based on the actual shop tests of the specific engine.

$$P_B = f\ (SHAFT_{rpm})$$

The engine's shaft revolutions ($SHAFT_{rpm}$) can be measured from a high frequency automatic data collection system, either directly from a local indicator, or through vessel's Alarm & Monitoring System (AMS).

For the specific method, a correction of the measured $SHAFT_{rpm}$ is not required (eg ISO correction). On the other hand, vessel's loading condition and prevailing weather conditions or extreme manoeuvering can greatly affect the power output of the engine, without affecting similarly the measured shaft revolutions.

3. Vessels Selection

For this statistical analysis and comparison, data from 11 different vessels have been used, both bulker and tanker vessels of several sizes and ages. Below table presents a summary of these vessels. All above mentioned vessels of the same size, are at the same time sister vessels, Table VII.

Table VII: Selected vessels summary data

A/A	Type	Size	Built (mm/yyyy)	Latest DD
1	Tanker	VLCC #1	2009	2019
2	Tanker	VLCC #2	2009	2019
3	Tanker	Suezmax #1	2009	2019
4	Tanker	Suezmax #2	2009	2019
5	Tanker	Aframax	2010	2020
6	Bulker	Capesize	2010	2018
7	Bulker	Handymax #1	2011	2016
8	Bulker	Handymax #2	2011	2016
9	Bulker	Kamsarmax #1	2018	N/A
10	Bulker	Kamsarmax #2	2018	N/A
11	Bulker	Kamsarmax #3	2019	N/A

For the analysis, all collected data for the last 1.5 years (were available) have been used. Due to the availability of specific data, not all the above mentioned alternative ways have been used for estimating the engine's brake power. The methods implemented for each vessel are shown in Table VIII.

Table VIII: Implemented methods for each vessel for estimating engine's brake power

A/A	Vessel	$ME_{FOCcorrected}$	T/C_{rpm}	$Scav_{press}$
1	VLCC #1	Calc.	Calc.	Calc.
2	VLCC #2	Calc.	Calc.	Calc.
3	Suezmax #1	Calc.	Calc.	Calc.
4	Suezmax #2	Calc.	Calc.	Calc.
5	Aframax	Calc.	Calc.	Calc.
6	Capesize	Calc.	Calc.	Calc.
7	Handymax #1	Calc.	Calc.	Calc.
8	Handymax #2	Calc.	Calc.	Calc.
9	Kamsarmax #1	Calc.	Calc.	Calc.
10	Kamsarmax #2	Calc.	Calc.	Calc.
11	Kamsarmax #3	Calc.	Calc.	Calc.

A/A	Vessel	DT_{exh}	$F.I._{pos}$	$SHAFT_{rpm}$
1	VLCC #1	Calc.	N/A	Calc.
2	VLCC #2	Calc.	N/A	Calc.
3	Suezmax #1	Calc.	N/A	Calc.
4	Suezmax #2	Calc.	N/A	Calc.
5	Aframax	N/A	Calc.	Calc.
6	Capesize	N/A	N/A	Calc.
7	Handymax #1	Calc.	Calc.	Calc.
8	Handymax #2	Calc.	Calc.	Calc.
9	Kamsarmax #1	N/A	Calc.	Calc.
10	Kamsarmax #2	N/A	Calc.	Calc.
11	Kamsarmax #3	N/A	Calc.	Calc.

4. Data Sources

All required data – for conducting the statistical analysis and comparison between the different methods of estimating the main engine's power – have been collected through LAROS$^{TM©}$, which is a Hollistic Data Acquisition System, independent from main vendors. LAROS$^{TM©}$ is a system where wireless/ wired smart collectors are connected on any existing vessel's sensors, SCADA or equipment for collecting the agreed datasets in a single and integrated approach and transmitting them to a centrally installed server. Then the collected data are analyzed and presented on vessel's crew – if required, and transmitted – even in real time – to vessel's headquarters for further and more detailed analyses and storing. Fig.1 shows a graphical representation of LAROS$^{TM©}$ system.
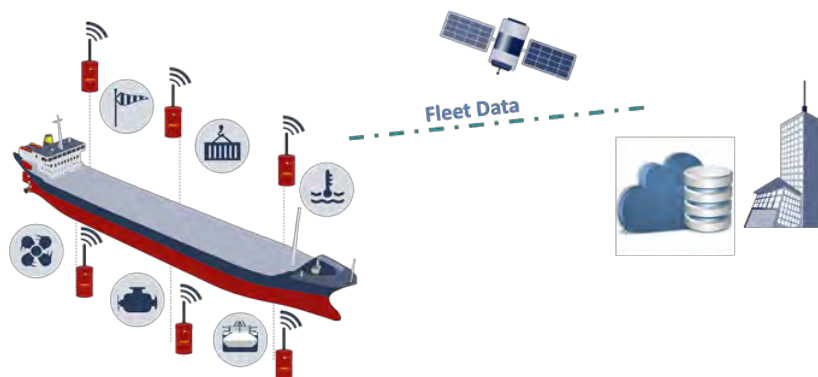

Fig.1: Graphical representation of LAROS$^{TM©}$ system

The collected data from LAROS[TM©] system may have typical three or fifteen seconds time resolution stored in the database, but for this specific analysis, a time resolution of one minute has been used. The accuracy of all collected data from LAROS[TM©] system is relative to the accuracy of each sensor / equipment providing the specific measurement. Machine Learning (ML) and Artificial Intelligence (AI) through the high frequency data collections decreased significantly the uncertainty of the collected measurements. For this reason the vessels that were used in this analysis were also selected for the reliability of the manufacturer's and the types of sensors and equipment installed.

Several times, the required data have been collected from LAROS[TM©] system through two different sources (e.g. the T/C_{rpm} have been collected both from the AMS's output, but also independently from a local installed sensor / indicator). This factor increase significantly the accuracy of the calculations and allows better monitoring and sensors' reliability of critical systems on the vessel. In this case for the estimation of the main engine's power, the average value of both measurements was finally used, with the condition of course, that the difference between the two measurements does not exceed the 0.3%. In Fig.2 such a case is visible through a high resolution time graph.
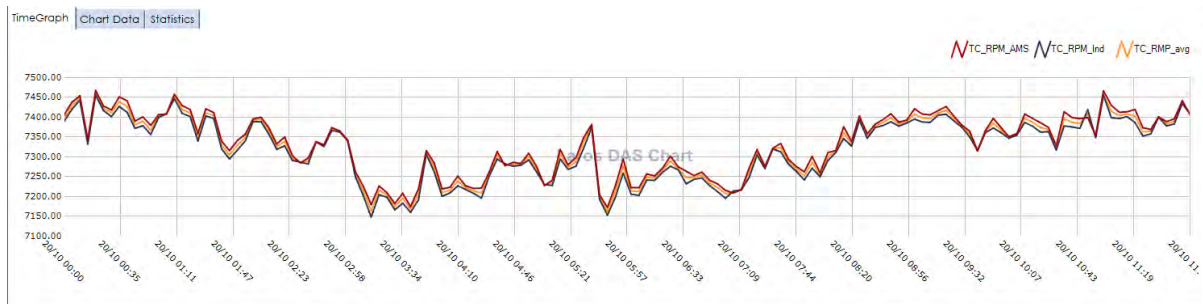
Fig.2: Averaging parameter measuring from two different sensors

5. Data Analyses

For the analyses of the data – verification of the received data, analyses, estimation of power, comparisons – as well as for the graphical representations, LAROS[TM©] Digital Analysis Software was used. Below steps were followed:

5.1. Collection of Data – Filtering of Data

All required data for the estimation of engine's power were collected as described in chapter 4, and used for the calculation of below basic parameters as analytically described in chapter 3:

$ME_{FOCcorrected}$: Main Engine's corrected fuel oil consumption (kg/min)
T/C_{rpm}: Turbo Charger rpm (rpm)
$Scav_{press}$: Scavenge Air Pressure (bar or MPa or kg/cm^2)
DT_{exh}: Difference of exhaust gas temperature before and after turbo charger (ºC)
$F.I._{pos}$: Fuel Index / Fuel Rack position (% or value)
$SHAFT_{rpm}$: Propeller Shaft rpm (rpm)

All above measurements are dynamically being cross checked for values between 25% and 100% of the relevant maximum, as in the provided engine's specific shop test. Any values lower than the 25% of the possible maximum according the engine's shop tests have been removed from calculations. For the filtering and cross checks, LAROS[TM©] Digital Analysis Software was used. Fig.3 shows such a case for the disregarded values, where the 25% of the max TC_{rpm} for the specific vessel corresponds to 4210 *rpm*.

Fig.3: Example of data filtering through LAROS$^{TM©}$ Digital Analysis Software

5.2. Estimation of Engine's Power

For the estimation of engine's power, the engines' specific shop test have been used. The tabular values from each engine's shop test and for each relevant parameter have been entered in LAROS$^{TM©}$ Digital Analysis Software. An example – for the Aframax vessel – of these data is presented in Table IX.

Table IX: Tabular format of Main Engine's Shop Tests for Aframax vessel.

Main Engine's Shop Tests										
Load (%)	Power (kW)	SFOC$_{ISO}$ (g/kWh)	ME FOC (kg/min)	TC RPM (rpm)	Pscav (kg/cm2)	T$_{EXH\_}$ BEF T/C	T$_{EXH\_}$ AFT T/C	ΔT$_{EXH\_TC}$ (°C)	Fuel Index (%)	Eng. RPM (rpm)
25%	4665.0	180.45	20.20	4210	0.360	323.3	247.2	76.0	46.8	57.3
50%	9330.0	174.96	39.18	7075	1.110	379.1	266.0	113.1	66.0	72.2
75%	13995.0	170.37	57.22	8837	2.020	386.5	239.5	147.0	84.8	82.7
90%	16794.0	171.93	69.30	9519	2.520	413.5	238.2	175.3	94.2	87.9
100%	18660.0	175.01	78.38	9925	2.82	430.4	244.8	185.6	99.2	91.0

From the above values and for each vessel and parameter, through LAROS$^{TM©}$ Digital Analysis Software third degree polynomials trendlines have been created through given conditions, criteria and filters, from which the engine's power could be estimated.

$$P_B = f(x) = A_3 \times x^3 + A_2 \times x^2 + A_1 \times x + A_0$$

where x is the parameter used for estimating the engine's power.

Through these polynomials, LAROS$^{TM©}$ Digital Analysis Software could estimate for each vessel, each parameter and each measured value the corresponding engine power.

5.3. Estimation of Power Coefficients

The estimated engine power from each parameter and measurement was compared with the actual value measured from each vessel's installed shaft power meter and the relevant coefficients in percentage were created for calculating the deviation between these two values – the estimated and the actual.

$$Coeff = \frac{(Value_{est} - Value_{actual})}{Value_{actual}} \times 100$$

Six different coefficients were created, one for each parameter:

ME_FOCcorr_Coeff: Estimated power from Main Engine's corrected fuel oil consumption
T/C_rpm_Coeff: Estimated power from engine's turbo Charger rpm
Scav_Press_Coeff: Estimated power from egnine's scavenge Air Pressure
DT_exh_Coeff: Estimated power from the difference of the exhaust gas temperature before and after turbo charger (^{o}C)
F.I._poss_Coeff: Estimated power from Fuel Index / Fuel Rack position
SHAFT_rpm_Coeff: Estimated power from Propeller Shaft rpm

These calculated dynamically coefficients, through LAROS$^{TM©}$ Digital Analysis Software were further cross checked compared and analyzed as described below, for suggesting the best practices and models about the applicability and the usability of the alternatives methods for estimating the engine's power through a high frequency automatic data collection system, without the use of a shaft power meter (torque meter).

6. Results Analysis

For the analysis of the results below procedure was followed:

1. For each vessel the average absolute value from each coefficient was calculated, as well as its standard deviation for time periods of one month and one minute time resolution, in order to verify the continuity of the results.

2. For each vessel all coefficients were plotted relative to the actual measured shaft power, in order to check if there are any patterns that could be distinguished, if any of the results should be disregarded or finally, if any ship specific general observation could be derived.

3. For each vessel the average value from each coefficient was calculated, as well as its standard deviation for the total examined period with one-minute time resolution. Then for each vessel the best coefficient and the coefficient with the smaller standard deviation were specified and finally the best one was selected.

Table X: Example of continuity check of the results

Panamax 1	January		February		March		April		May			Total	
Coefficients	Value	Stnd Dev.	Value	Stnd Dev.	Value	Stnd Dev.	Value	Stnd Dev.	Value	Stnd Dev.		Value	Stnd Dev.
Fuel rack	6.87	9.70	5.61	6.37	4.11	5.99	4.16	5.80	4.60	6.30		7.17	8.10
ME FO Cons	3.47	6.03	4.72	3.84	5.01	3.80	2.14	4.05	2.95	3.47		3.07	4.42
P scav	7.28	5.12	6.46	3.75	8.96	3.30	14.83	5.55	16.82	3.40		12.52	5.89
Shaft rpm	17.66	8.36	14.21	4.51	14.66	6.74	16.04	6.10	16.86	5.02		14.99	6.69
T/C rpm	3.95	4.41	2.28	3.10	0.82	3.23	4.51	4.16	5.23	2.69		3.93	4.44
Panamax 2	January		February		March		April		May			Total	
Coefficients	Value	Stnd Dev.	Value	Stnd Dev.	Value	Stnd Dev.	Value	Stnd Dev.	Value	Stnd Dev.		Value	Stnd Dev.
Fuel rack	12.41	6.04	9.94	10.44	5.40	9.16	9.97	9.41	9.93	6.64		8.43	9.92
ME FO Cons	8.87	2.89	9.75	3.66	10.59	3.67	11.42	3.22	10.20	6.64		9.30	4.36
P scav	15.73	4.64	15.80	3.52	----	----	16.86	3.13	17.91	4.11		14.49	5.03
Shaft rpm	16.67	5.29	14.25	5.48	16.48	5.68	11.67	5.03	16.91	5.25		14.20	6.61
T/C rpm	3.10	2.70	3.94	3.02	4.02	3.81	5.22	1.33	6.02	2.99		5.03	3.28
Panamax 3	January		February		March		April		May			Total	
Coefficients	Value	Stnd Dev.	Value	Stnd Dev.	Value	Stnd Dev.	Value	Stnd Dev.	Value	Stnd Dev.		Value	Stnd Dev.
Fuel rack	9.43	6.31	9.42	6.61	5.74	5.00	3.10	4.11	7.39	4.84		6.37	6.58
ME FO Cons	6.63	5.00	6.79	5.62	10.43	8.25	8.10	5.02	8.82	6.34		7.26	6.04
P scav	6.44	5.99	6.26	6.30	8.33	6.17	14.02	3.75	14.96	4.37		10.69	6.11
Shaft rpm	13.44	8.47	12.07	13.18	24.88	3.49	15.59	4.98	20.40	10.61		17.59	9.62
T/C rpm	4.39	4.08	4.43	3.91	5.10	3.36	2.16	2.86	3.06	3.80		3.21	4.25

6.1. Continuity of the Results

In the first step of the analysis, the continuity of the results was verified. For each vessel the average value of each coefficient, together with the relative standard deviation, was calculated for time periods of one month and compared with the total examined period for each vessel. From every month's results, the coefficient with the lower value was highlighted and compared with the coefficient with the lower average value from the total examined period. In most cases, the results were the same, or sometimes, an alteration was noticed between the first and the second-best coefficient. But in this case, also the final results for the total examined period were pretty close. Part of this table is shown in Table X.

6.2. Patterns / Observations / Disregarded Results

In the next step of the analysis, for each vessel the value of each coefficient relative to the engine load for the total examined period was plotted. The time resolution of the graphs was 1 hour, while for the averaged hourly value at least 40 measurements should have been collected.
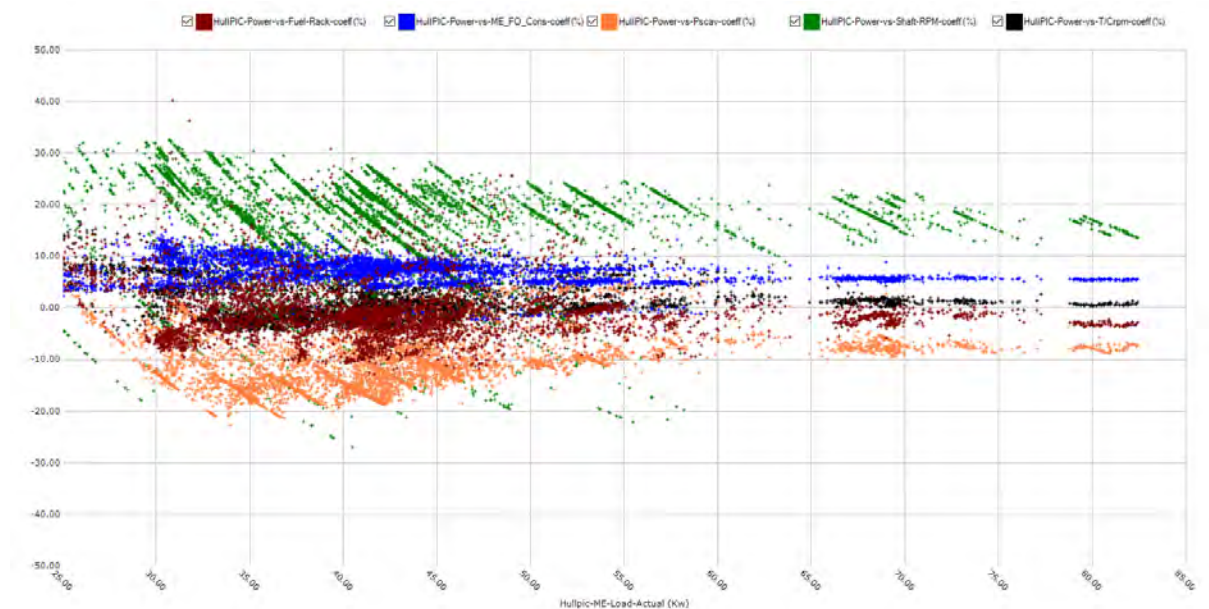
Fig.4: Example graph of actual M/E load (%) vs examined coefficients

After plotting all graphs, below items were observed:

1. In the Capesize vessel, all coefficients had much higher values than the other vessels approximately by 20%, except for the coefficient for the shaft rpm, where though the calculated values presented very high variations, as can be noticed in Fig.5 and Table XI.

Table XI: Average values of the calculated coefficients for Capesize vessel comparing all vessels

Coefficients	All Other Vessels	Capesize vessel
ME-FO-Cons (%)	9.4	29.3
Pscav (%)	-9.2	11.7
RPM (%)	7.7	10.0
T/C-rpm (%)	-3.4	25.8
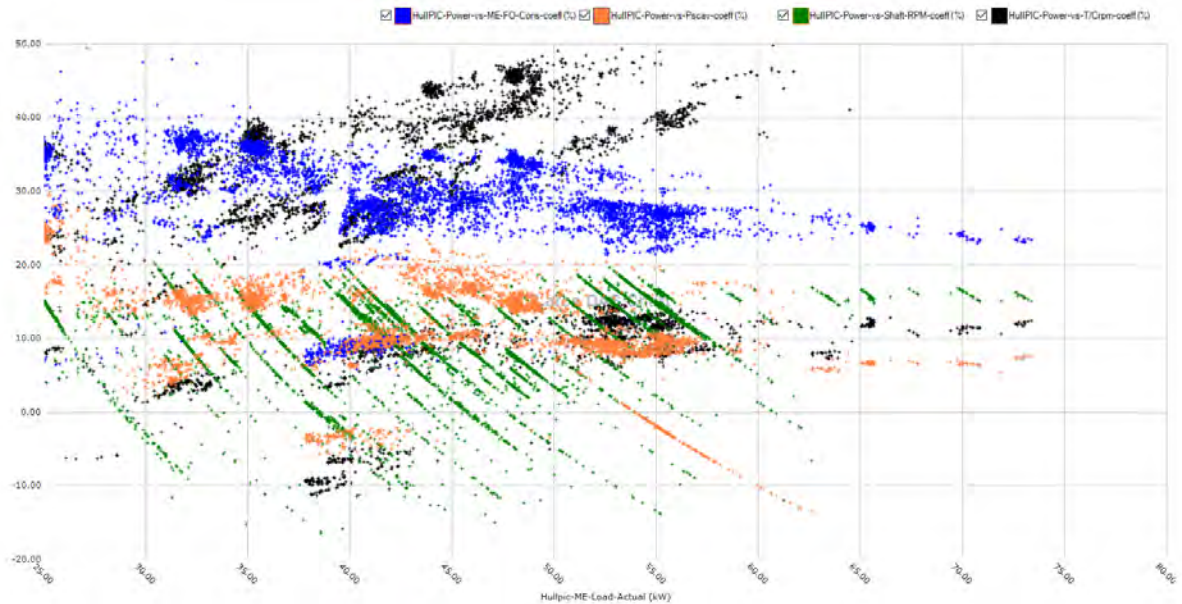
Fig.5: Graph of actual M/E load (%) vs examined coefficients for Capesize vessel
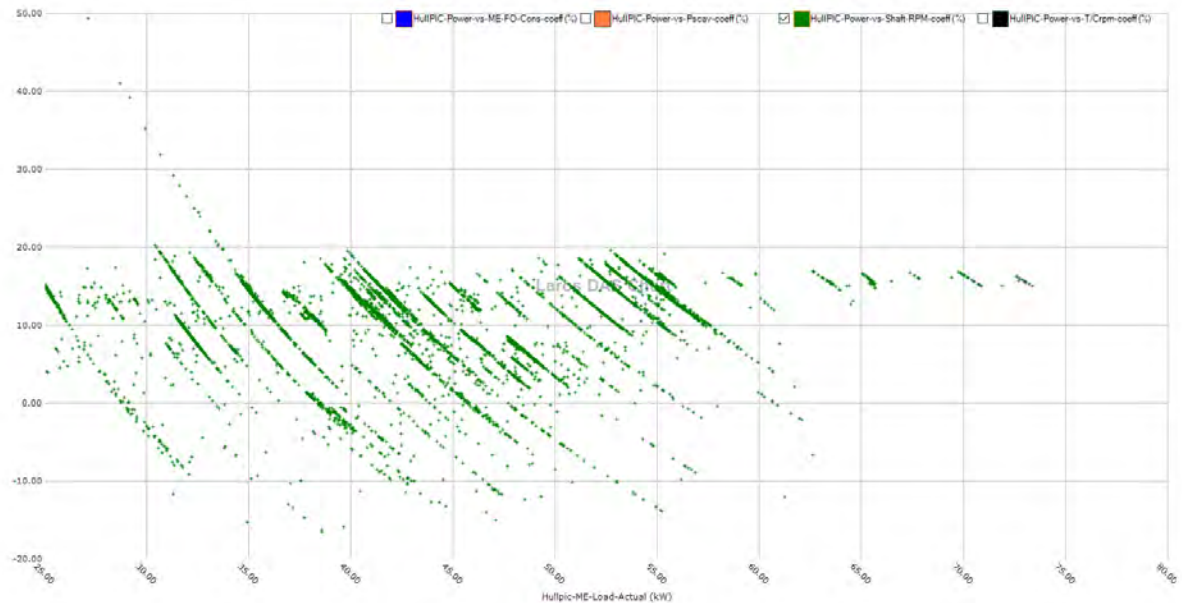
<u>Fig.6</u>: Graph of actual M/E load (%) vs SHAFT_rpm_Coeff for Capesize vessel

After noticing these high deviations, the managing company of the specific vessel was contacted and was requested to conduct a test and check the calibration of the installed shaft power meter. The test showed that the installed shaft power meter was underestimating the measured shaft power by approximate 15% and a new calibration was required. After the re-calibration of the installed shaft power meter, the calculated values of the coefficients were much closer to the similar values from the other vessels. This is visible also in below time graph. Since the available data after shaft power meter's recalibration were limited, all calculated values were disregarded for the specific vessel. This presents also a typical reason why sensor instruments and systems should be monitored by independent systems that can provide sufficient information about the actual behaviour of the sensors in daily operation.

2. The Fuel rack/index position, can be considered relative accurate, only for new electronic engines. For the electronic engines the deviation of the actual measured values was acceptable (average

20

absolute coefficient 7.3%), while the deviation for the older engines was extremely high (average absolute coefficient 60%).
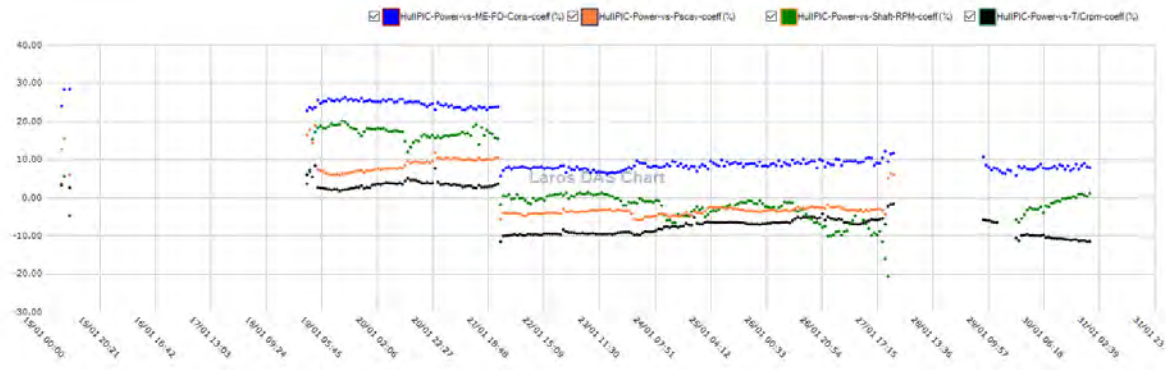
Fig.7: Graph showing the shaft power meter's point of re-calibration
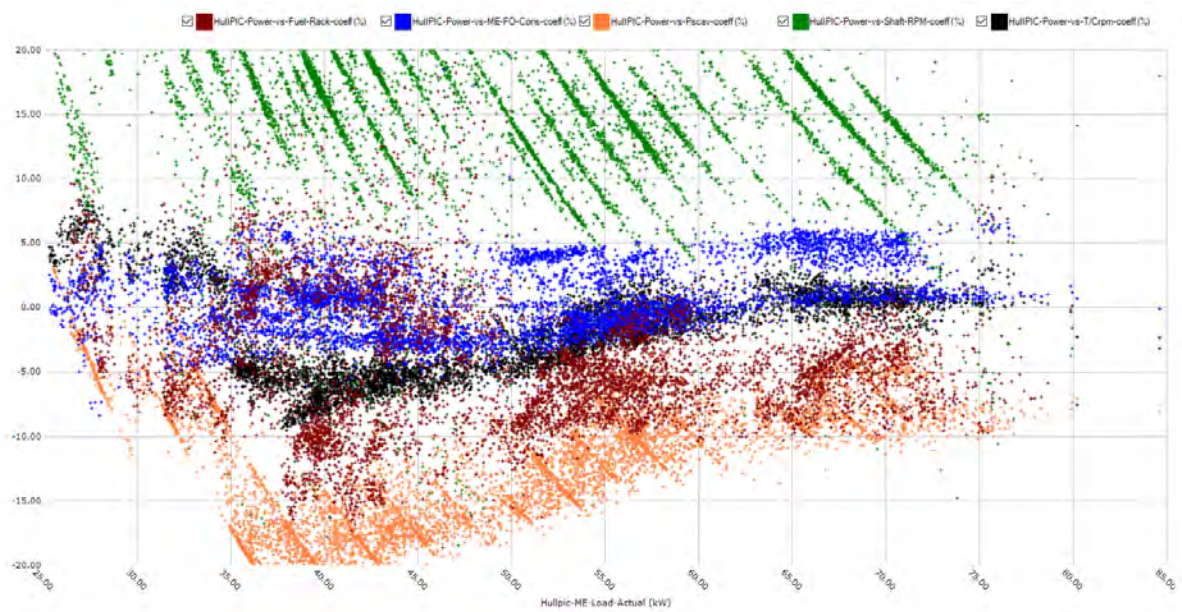
Fig.8: Graph of actual M/E load (%) vs examined coefficients for Panamax 1 vessel
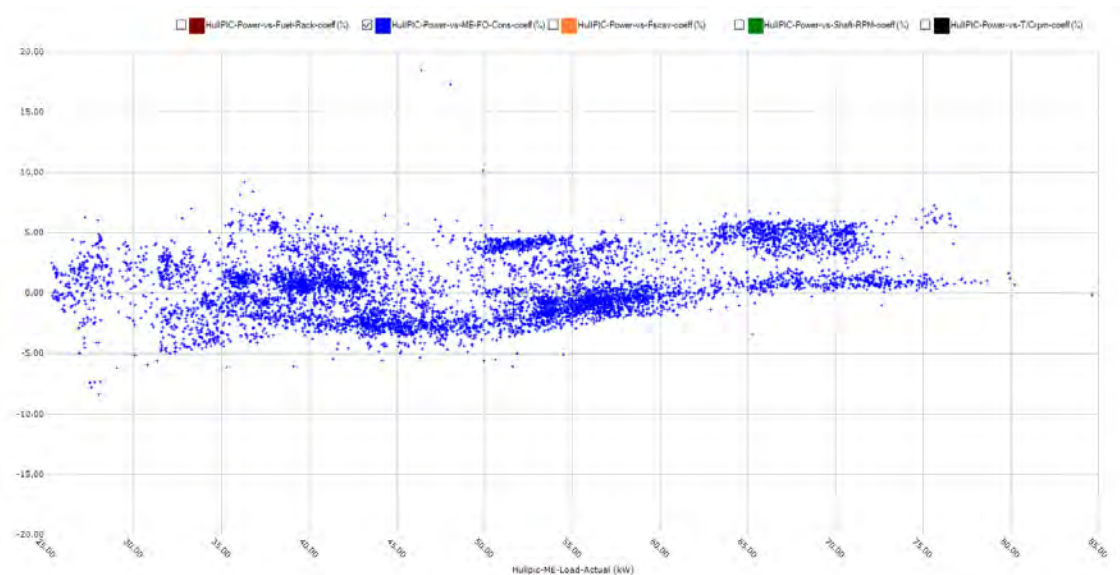
Fig.9: Graph of actual M/E load (%) vs examined ME_FOCcorr_Coeff for Panamax 1 vessel

3. The suggested method from ISO for estimating the engine's power through the M/E's F.O. consumption proved that is pretty accurate for new vessels and especially where the actual fuel's lower calorific value was used. Indeed, in all Panamax vessels, this method proved to be more accurate comparing the $Scav_{press}$ or the $Shaft_{rpm}$. This can be noticed in Fig.9.
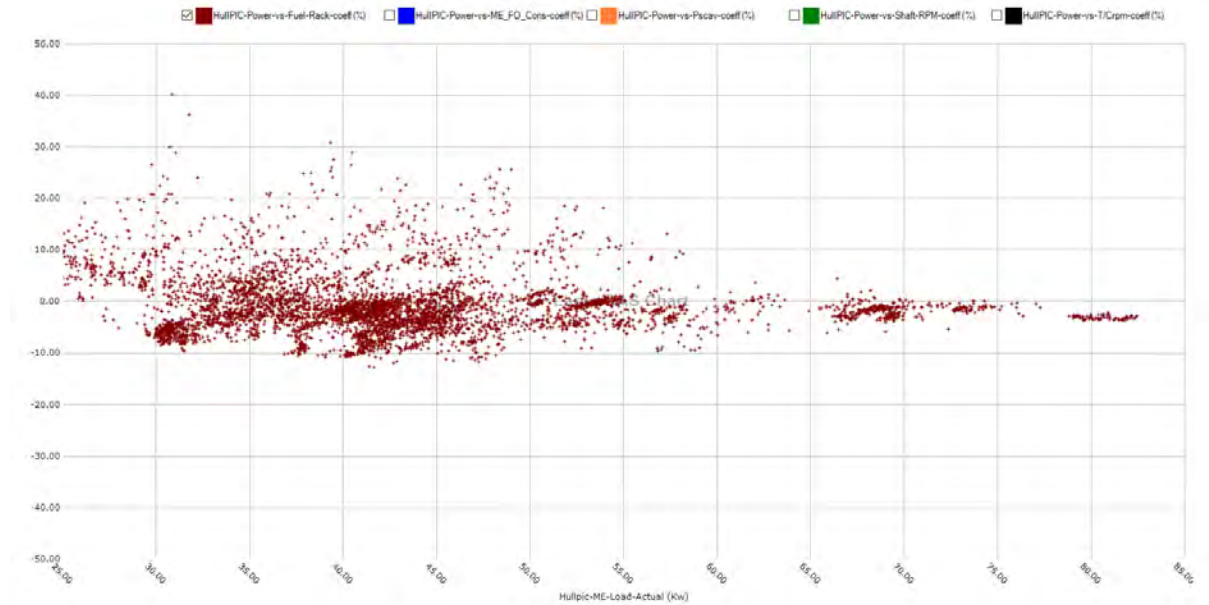
Fig.10: Graph of actual M/E load (%) vs examined F.I._poss_Coeff for new vessel (electronic engine)
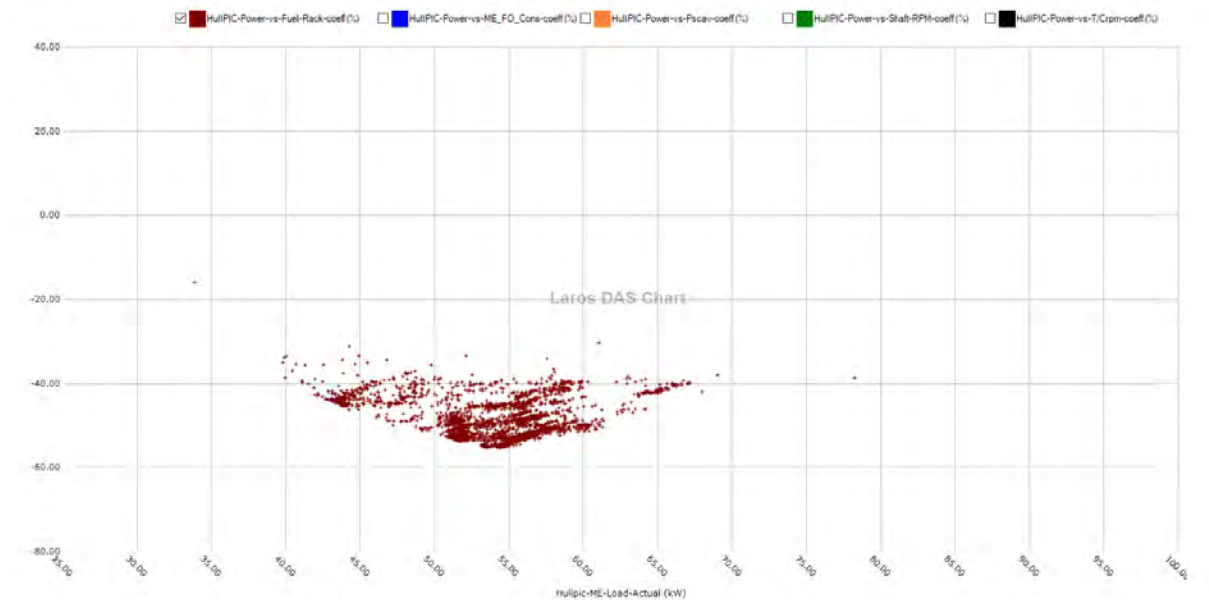
Fig.111: Graph of actual M/E load (%) vs examined F.I._poss_Coeff for old vessel (common engine)

6.3. Final parameter Selection

For the final selection, for each vessel the average value from each coefficient was calculated by LAROS$^{TM©}$ Digital Analysis Software, as well as its standard deviation, for the total examined period and with one-minute time resolution. Then, for each vessel the coefficient with the lower average absolute value and the relative smaller standard deviation was specified. The parameters with the most accurate estimations of the main engine's power for each vessel are presenting in Table XII.

Table XII: Best and 2nd best coefficients for each vessel

	Best	2nd Best
Aframax	$ME\_FOCcorr_{\_Coeff}$	$SHAFT\_rpm_{\_Coeff}$
Handymax 1	$T/C\_rpm_{\_Coeff}$	$Scav\_Press_{\_Coeff}$
Handymax 2	$T/C\_rpm_{\_Coeff}$	$Scav\_Press_{\_Coeff}$
Panamax 1	$ME\_FOCcorr_{\_Coeff}$	$T/C\_rpm_{\_Coeff}$
Panamax 2	$T/C\_rpm_{\_Coeff}$	$ME\_FOCcorr_{\_Coeff}$
Panamax 3	$T/C\_rpm_{\_Coeff}$	$F.I.\_poss_{\_Coeff}$
Suezmax 1	$T/C\_rpm_{\_Coeff}$	$Scav\_Press_{\_Coeff}$
Suezmax 2	$DT\_exh_{\_Coeff}$	$T/C\_rpm_{\_Coeff}$
VLCC 1	$T/C\_rpm_{\_Coeff}$	$Scav\_Press_{\_Coeff}$
VLCC 2	$T/C\_rpm_{\_Coeff}$	$SHAFT\_rpm_{\_Coeff}$

In seven out of ten vessels, the use of the T/C_{rpm} was the most appropriate method to be used for estimating the main engine's power when a shaft power meter is not installed. Moreover, in the two of the other three vessels, presented again the second-best selection, while only in one vessel was the third best selection.

The selection of the $ME_{FOCcorrected}$ for estimating the engine's power as ISO 19030 is suggesting is not very accurate for being used by a high frequency automatic data collection system. Of course, if the engine is new or has undertaken all proper maintenance and the measured consumption is through mass flow meters, the accuracy is increasing significantly, especially, if the exact fuel's lower calorific value is being used. The accuracy of this method could be further increased if sensors are installed, for measuring also the additional required parameters for a complete ISO correction of the consumption. Nevertheless, the above statistical analysis shows that the use of the T/C_{rpm} presents the most accurate estimator for calculating the engine's power through the use of a data collection system, in the absence of a shaft power meter.

This estimator, through the use of Machine Learning, can be further corrected based on other general vessels' parameters (e-g. weather conditions, drafts etc.)

References

ISO 19030-1 (2016), *Ships and marine technology – Measurement of changes in hull and propeller performance,* ISO, Geneva

Hull and Propeller Performance Measurement
for Offshore Support Vessels

Serena Lim, Ascenz Solutions, Singapore, serena.lim@ascenz.com
Mincui Liang, Newcastle University, United Kingdom, m.liang3@hotmail.com
Xin Wang, Newcastle University, Singapore, xin.wang@ncl.ac.uk

Abstract

ISO 19030, developed for the measurement of changes in hull and propeller performance has been applied to several types of vessels especially ocean-going vessels, such as tankers, liners, cruise ships as well as ferries and Ro-Ros. This standard however, has not been tested on Offshore Support Vessels (OSVs), which include Anchor Handling Tug Supply vessels (AHTS) and Offshore Supply Vessels. The operational conditions of such vessels are more complicated as these include up to 20 different types of operation, where vessel transit condition accounts for approximately 35% of time spent at sea. A systematic methodology is proposed to understand the vessel operational data and apply a careful filter of relevant data that can be practically applied for the use of ISO 19030 with these vessels. The outcome of hull and propeller assessment on OSVs using the proposed method complementing ISO 19030 is presented.

1. Introduction

Continuous improvement of vessel efficiency is important, besides the environmental impact contributed by the shipping industry due to burning of fuel that contributes to emissions, notably the greenhouse gases including nitrous oxide and other pollutants such as sulphur oxides, the economic impact indicates an annual saving of about US $ 3,000 million for the world fleet, *Milne (1989), Townsin (2003)*. ISO 19030:2016 part 1, 2, and 3 provides standardised methods for the measurement of hull and propeller changes and outlines the four Key Performance Indicators (KPIs) for decision making in operation strategies to enhance energy efficiency. Almost all research conducted on implementing ISO 19030, is on Ocean Going Vessels (OGVs) such as oil and LNG tankers, ferries and cruise ships, cargo and container ships and Ro-Ro vessels. The number of operating OGVs was about 53,000 in 2019, *Marinekommando (2019)*. The successful application of ISO 19030 to different types of OGV has shown that it is possible to measure hull and propeller condition and the impact of improved vessel efficiency, *Adland et al. (2018)*, reduction of fuel cost, *Nelson et al. (2013),* and lowering the greenhouse gas (GHG) emissions, *Molland et al. (2014)*.

The standard however does not address the hull and propeller changes in other vessel types such as Offshore Support Vessels (OSVs). There are about 5301 OSVs in service as of 2020, and 602 OSV in order, with an increasing number of around 7% each year (Clarkson, 2020). This amount is close to the number of container vessels in the world, a total of 5269 vessels in 2019, *BRS (2019)*. Up to 2017, the ratio of OSV to rigs is about 6.8 vessels (> 3000 dwt) vs floaters; and about 3.6 vessels (<3000 dwt) vs jack-ups. With about 457 working rigs, down from 736 rigs, at its peak in 2014. Offshore vessels are designed to assist oil exploration and construction operations. There are a variety of offshore vessels, which not only help in exploration and drilling of oil but also to provide necessary supplies to the excavation and construction units located in the high seas. There are three main types of OSV, namely the Platform Supply Vessels (PSV), Anchor Handling Tugs and Supply Vessels (AHTS) and Offshore Construction Vessels (OSCVs). Other types of OSVs also include Seismic Survey ships, Inspection, Maintenance and Repair vessels (IMR), Dive support vessels, Stand-by / Guard vessels, Remotely Operated underwater Vehicle (ROV) support vessels and various combinations of these for the various tasks of various offshore platforms and subsea installations.

As the OSVs increase in size, power, and capacity, they become multi-functional vessels, often functioning beyond their original design purpose. Since 2005, the demands of Bollard Pull have increased from around 150 to 200 tonnes, *Ahmad et al. (2005)*. The propulsion system of an OSV

differs greatly from a typical OGV. There are three main propulsion systems using on OSVs. Diesel-electric with advanced DP system becomes most popular in the OSVs market according to *Herdzik (2013)*. Diesel-electric propulsion systems are usually equipped with a Power Management System (PMS) which automatically controlling start/stop which reduces fuel consumption, a key reason for their growing popularity.

Moreover, the activities performed by OSVs are more complex, up to 22 types of operational activities of the OSV compared to OGV 7 main types of activities. In this paper, it is aimed at analyzing AHTS. AHTS is a multiutility vessel with the main function of towing and tugging, anchor handling, and emergency rescue, so it is installed with heavy equipment such as crane, anchor and winches and smart systems such as dynamic positioning systems to use the data of wind and the wave fluctuation and control the propellers automatically to maintain the ship's course and keep it steady. The operational activities are different from long voyage vessels such as navigation without load, loading and unloading supplies, buoy and anchor handling as well as towing and lifting. These flexible operations and unpredictable operation routine features determined that standard hull and propeller performance monitoring regime of OGVs cannot directly be applied to OSVs.

One of the main challenges when referencing the ISO 19030 is that OGVs are fitted with mostly fixed pitch propellers (FPP) and controllable pitch propellers (CPP). FPP which fits the propulsion system type described in the standard. However, OSVs may use Azimuth Thrusters, Z-drive, and Voith-Schneider propellers, with the purpose to carry out Dynamic Positioning (DP) because of the higher accuracy for towing and anchor handling. The thrusters are also used for manoeuvring to control the direction of the OSVs as a rudder, *Sørensen (2011)*, hence the OSVs are usually without a rudder when compared to OGVs.

Most of the energy efficiency research related to OSVs focuses on fleet size optimisation and speed optimisation. There is no solid research and literature available on their hull and propeller performance. Marine fouling is a well-known problem for OSVs. However, there is a lack of research regarding measuring the changes in the hull and propeller performance of OSVs to maximise fuel efficiency.

The ISO 19030 also advises that the delivered power is seen as the primary parameter to be considered when assessing the hull and propeller condition. However, in a fleet of OSVs, it is unlikely, or industrially challenging, to convince ship owners to install a shaft meter, from the point of view of cost and propulsion type. Moreover, the alternative quantification from ISO 19030:3 states that this method is applicable, assuming that the engine is a two-stroke main engine directly driving the propeller with no gearbox and no shaft generator (used for power take-off). OSVs are usually fitted with medium speed engines with a gearbox and shaft generator. In such a case, there are no standards available to quantify or suggest the best practice to quantify the hull and propeller condition for the OSV fleet. This paper focusses on this gap by investigating the possibility of referencing ISO 19030 to address the hull and propeller performance of these vessels.

One main advantage of exploring the hull and propeller performance monitoring for OSV is the ready availability of data. A large proportion of OSVs are fitted with Electronics Fuel Monitoring Systems (EFMS) as part of the charterer's requirement to oversee and better manage vessel activity from shore. The oil company usually charters the supply vessel instead of owning it, which is one of the highest cost elements of the operation cost for the company, which amounts to about 50% to 80% of the total operation costs.

The aim of this work was to use the readily available operational data for OSVs to test the potential and to address the lack of research regarding careful measurement of changes in hull and propeller performance of OSVs. The work will not only maximise the fuel efficiency of the vessel but will contribute to lowering the impact of offshore operations on climate change. We have begun this process by selecting an AHTS as a case study and to demonstrate proof of concept.

2. Case study preparation

The first part of the investigation is to compare the similarity of OGVs and OSVs in order to evaluate if any elements from the ISO 19030 can be adopted when addressing the hull and propeller performance monitoring regime. The operations of an OSV involves many complex operations compared to a sea going vessel. As it is designed for operations in much harsher conditions, it generally experiences tougher sea conditions. One of our goals is to look at the operational data of an OSV and evaluate if the existing data can provide useful estimates of the hull and propeller conditions.

2.1 Properties of OGVs and OSVs

Properties of OSVs are compared to OGVs to rationalise the hull and propeller performance monitoring. Table I shows the similarities and differences of these two categories of vessels.

Table I: Similarities and differences of OGVs and OSVs

Similarities	Differences
• Typical drydocking or hauled out inspection twice every 5 years • Similar options of coating used	• Number of operational profiles • Types of operational profiles • Operations in harsher conditions • Propulsion system type • Availability of delivered power data

From the aspect of hull and propeller performance evaluation, both OGVs and OSVs typically dry dock or hauled out for inspection at intervals of twice every 5 years to clean and re-paint the hull as well and cleaning the propellers where needed. The available options of coatings in the maritime industry provided for these two categories of vessels are the similar. Hence, it is worth exploring a data driven hull and propeller performance evaluation. However, due to the differences in operations and propulsion type and configuration, the application of purpose of the hull and propeller performance evaluation differs.

2.2 Vessel operations

For long voyage vessels, there are mainly four activities: anchoring at port, sea passenger, pilot on and off and manoeuvre. For OSV, the activities depend on the type of the vessel. This paper aims at analysing AHTS. AHTS is the multiutility vessel including towing and tugging oil rigs or ships to the specific oceanic areas, anchor handling and emergency rescue, so it is installed with heavy equipment such as crane, anchor and winches and smart system such as dynamic positioning system to use the data of wind and the wave fluctuation and control the propellers automatically to maintain the ship's course and keep it steady. The OSVs' operation activities are different from long voyage vessels such as navigation without load, loading and unloading supplies, buoy and anchor handling and towing, lifting etc. These flexible operation and unpredictable operation routine features determined that monitor systems of long-distance sailing cannot directly be applied to OSVs. Hence, in order to evaluate hull and propeller performances using data, the operation where an OSV is moving at near steady long distances will be used for evaluation. Using the entire year (2019) of EFMS data for an ATHS, downloaded from the Ascenz Shipulse portal, the activities that are logged is plotted in Fig.1.

The activity of interest is when the vessel is 'sailing enroute', typically when the vessel is moving from anchorage position to rigs, between rigs and vice versa. During this operation, both main engines are used for the purpose of propulsion. Fig.1 (top) shows that the vessel spends 31.0% of the time carrying out this activity, the percentage of fuel consumed during this activity is 50.5% of the year's total fuel consumption, seen in Fig.1 (bottom). These pie charts were plotted using 'Activity Manager' on the EFMS, providing a clear distinction of the fuel consumption by activity. For the purpose of this study, fuel consumption by the auxiliary engines is not considered as only fuel used for propulsion is of interest when processing the hull and propeller performance analysis.
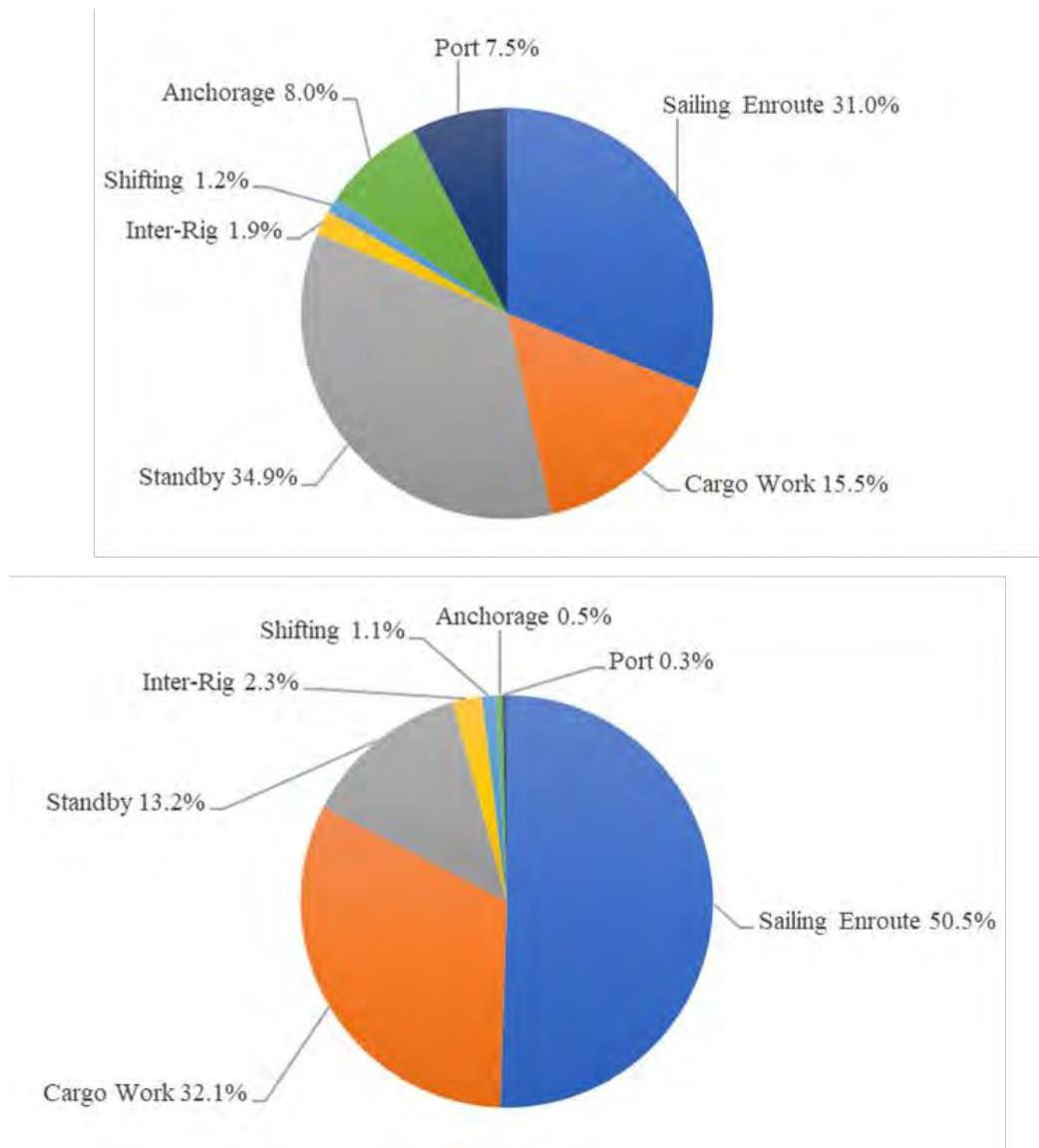
Fig.1: Time share on each main activity (top) and fuel share consumed during each activity (bottom)

3. Data gathering

ISO 19030:2 recommends automatic logging (auto-logger) of data to evaluate the hull and propeller performance. An increasing number of OSVs are equipped with EFMS, similar to auto-loggers for the purposes of transparency of fuel consumption during operations by charterer and operator. An attempt to understand the nature of the hull and propeller surface and the overall impact on the OSV performance including the complicated calculations that numerically quantifies fluid frictional drag and power needed to propel the vessel, the data is obtained by taking advantage of the well-equipped auto-logger onboard an AHTS.

The details of the dataset used are found in Table II.

Table II: Details of dataset used

Data period	1 January 2019 – 31 December 2019
Data logging interval	1 data point for each parameter every 1 minutes
Number of tags used for data validation	112
Number of tags used for data processing	12

27

Table III shows the propulsion system properties of the AHTS to put the data and analysis in context.

Table III : Candidate vessel propulsion system information

Main engine power (@100% MCR)	3678kW
Quantity of main engine	2
Auxiliary engine power (@100% MCR)	307
Quantity of auxiliary engines	2
Auxiliary generators	Main engine driven
Quantity of auxiliary generator	2
Propulsion type	Engines with reduction gear to screw shafts driving 2 controllable pitch propellers

Prior to analysis data collected from the AHTS, the gathered data are processed to check for quality. This is done using a careful step by step data validation process that uses a statistical approach to identify faults followed by a check with a covariance value among respective parameters and systems, *Lim et al. (2019)*. Since there are usually no delivered power parameters for OSVs, the fuel consumed for operational purposes is used to plot against vessel speed, Fig.2. Note that there are two engines for this vessel and the fuel consumption shown is calculated from the summation of fuel differences of inlet and outlet of both main engines in operation for the propulsion purposes. Vessel speed over ground is used for this analysis due to the limitation of the available data, it is recommended that vessel speed through water is used, where available when duplicating this methodology.

The vessel has a total of five settings of speed and the three main ones (low setting indicated by dark blue, medium setting indicated by green, and high setting indicated by yellow) that are used for analytics, omitting the slowing down and manoeuvring. Twelve months of data was used from January 2019 to December 2019. During the 'sailing enroute' condition, the vessel uses three general engine speed settings, only data with these setting have been considered for analysis to avoid vessel manoeuvring profiles, and emergencies situations when vessel has to travel at adverse speed. The data shown in Fig.2 also considers the vessel operational breakdown, where only the vessel 'sailing enroute' operation is used to evaluate the hull and propeller efficiency properties. The coefficient (indicated as 'coeff') of each best fit cubic curve is shown for each month's worth of data. However, a rough fit for January, August and December should be considered carefully since less data was available at lower speeds for a best fit curve.
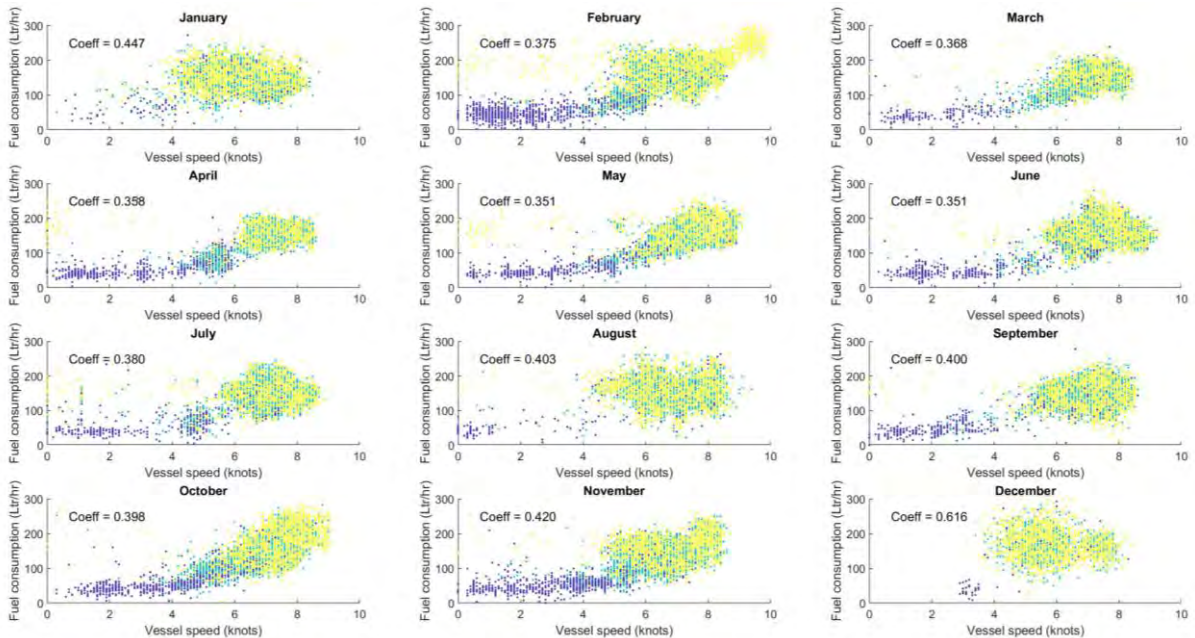

Fig.2: Fuel consumption vs vessel operational speed

4. Data analysis and discussion

The concept of data analysis presented in ISO 19030:2 has to be modified to suit the application to OSVs. For example, 1 minute interval of logging is used compared to the 15 s intervals recommended, the filtering of data when vessel is moving at straight path in sailing enroute condition to overcome the non existence of rudder. The contrast where the standard applies on mechanically directly propelled vessel whilst in comparison to the OSVs that are usually fitted with thrusters, and the ability to recognise when the operating engines are utilising the gearbox and shaft generator.

Considering the data when the vessel is in 'sailing enroute' operation, only 31.0% of the overall OSV operation in the year 2019 is used. The filter of data by speed is avoided due to the operation where the OSV is required to carry out long operations for manoeuvring and standby operations by the rig which is serviced. The other reason to use only when the vessel is in 'sailing enroute' operation is that the fuel consumed to generate power is not used to further run the shaft generator. Hence, it can be assumed that the fuel energy is transferred to the thrusters for propulsion purposes.

Following the rationale of data filtered presented in section 4, Fig.3 shows data when the vessel is moving at speed of 6 kn ± 0.1 kn. The two reference curves of six months intervals were plotted. The reference curves shift by 9.65 Ltr/hr for the vessel to move at the same speed, which is assumed that the vessel consumes additional fuel to sail at the same speed.
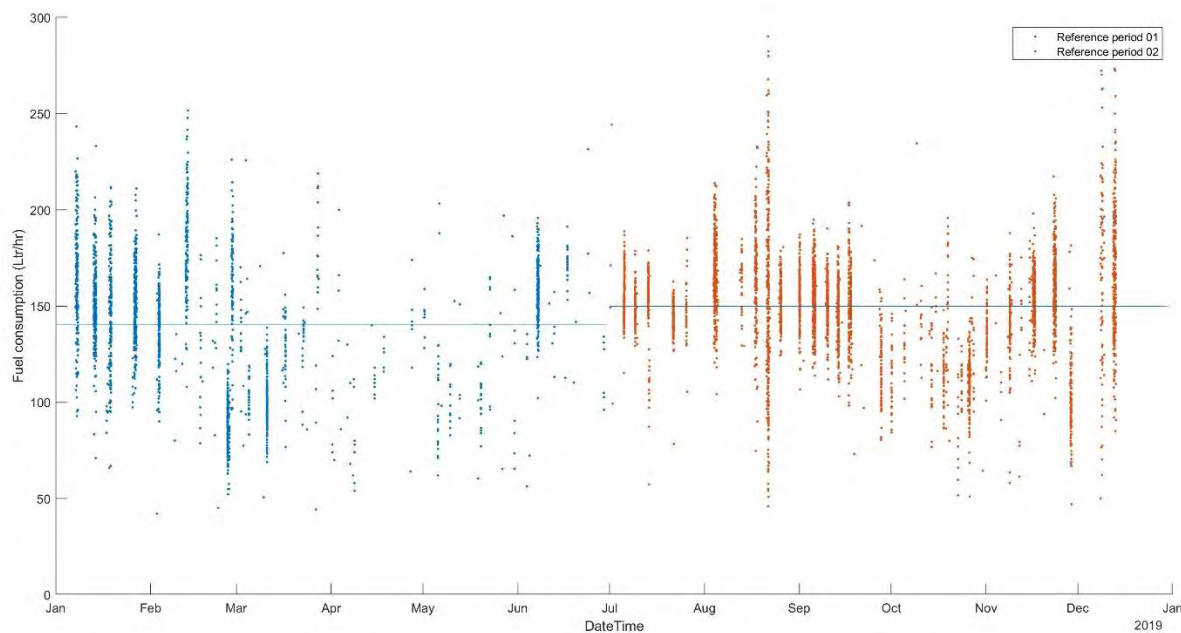
Fig.3: Fuel consumption difference at two reference periods for vessel at 6 kn ± 0.1 kn

There are no standards available to quantify or suggest the best practice to quantify the hull and propeller performance that suits an OSV fleet. In this case, the hull and propeller condition of an AHTS were evaluated by attempting to plot the changes in fuel consumption between two reference periods for the vessel moving at the same speed.

This methodology adopts the same approach as ISO 19030 by comparing changes to hull and propeller performance using the reference period. Acknowledging that the use of proxy data is tied to considerable increases in the uncertainty inherent in any sensors, where SOG is used instead of STW and that the power delivered as calculated from fuel consumption is used instead of the delivered power measured from sensor on the shaft, derived from shaft torque and shaft speed. Such analysis can be further improved by minimising the uncertainty by evaluating the performance where similar draught used or kept approximately constant over the reference period of the analysis. It is also noted that the analysis does not consider that changes in fuel quality, the global environmental effects

(though OSVs usually operate at the same location to service the particular rig), and the changes of specific fuel oil consumption (SFOC) over time due to engine degradation. Setting the limitations aside, this work explores and describes the value added to the maritime industry, which is to create valuable insights by utilising commonly available data.

5. Conclusions and future work

Hull and propeller conditions were monitored closely for long voyage vessels. This work exhibits a first data exploration to investigate the hull and propeller performance on an OSV (particularly an AHTS) using readily available data. The methodological approach developed here requires additional refinement to be carried out as well as additional validation. Further work to be carried out is to map similar methodology for:

- Longer duration OSV data sets
- Larger numbers of similar types of OSVs
- Other types of OSV and vessels that are fitted with DAS

The next phase of the research is to look at the economic sensitivity of monitoring task specific ships This will also involve moving a long distance at small fraction of the operational profile. Once it can be demonstrated that the data gathered from the vessel can be used for the hull and propeller fouling measurement, a data driven decision making tool can be developed.

Acknowledgement

References

ADLAND, R.; CARIOU, P.; JIA, H.; WOLFF, F. C. (2018), *The energy efficiency effects of periodic ship hull cleaning*, J. Cleaner Production 178, pp.1-13

AHMAD, S. (2005), *Modern Offshore Support Vessels Class and Statutory Perspectives*, Int. Conf. Technology & Operation of Offshore Support Vessels, Singapore

BRS (2019), *BRS shipping building report*, BRS Brokers, https://www.brsbrokers.com/assets/review_splits/BRS-Review2019-01-Shipbuilding.pdf

CLARKSON (2020*), Offshore support vessel,* https://www.clarksons.com/services/broking/offshore-support-vessels/

HERDZIK, J. (2013), *Problems of propulsion systems and main engines choice for offshore support vessels*, Zeszyty Naukowe/Akademia Morska W Szczecinie

ISO 19030 (2016), *Ships and marine technology – Measurement of changes in hull and propeller performance*, ISO, Geneva

LIM, S; TEO, R; SIA, T.C. (2019). *A Digital Business Model for Vessel Performance Monitoring*. In 4th Hull Performance & Insight Conference (HullPIC'19), Gubbio, Italy

MARINEKOMMANDO (2019), *Jahresbericht,* https://deutscher-marinebund.de/berichtedmb/marine kommando-jahresbericht-2019/

MOLLAND, A.F.; TURNOCK, S.R.; HUDSON, D.A.; UTAMA, I.K.A.P. (2014), *Reducing ship emissions: a review of potential practical improvements in the propulsive efficiency of future ships*, Trans. RINA Part A: Int. J. Maritime Engineering 156, pp.175-188

NELSON, M.; TEMPLE, D.W.; HWANG, J.T.; YOUNG, Y.L.; MARTINS, J.R.R.A.; COLLETTE, M. (2013), *Simultaneous optimization of propeller–hull systems to minimize lifetime fuel consumption,* Applied Ocean Research 43, pp.46-52

SØRENSEN A.J. (2011), *A survey of dynamic positioning control systems*, Annual Reviews in Control 35, pp.123-136

TOWNSIN, R.L. (2003), *The Ship Hull Fouling Penalty*, Biofouling 19:S1, pp.9-15

Vessel's Hull Cleaning: New Approach for Evaluation

Nicolas Bialystocki, StratumFive, Shoreham by Sea/UK, Nicolas.bialystocki@stratumfive.com

Abstract

This paper proposes an advantageous concept in evaluation and display of hull cleaning effectiveness. An evaluation is needed in order to give insight of the decision to carry out hull cleaning of a vessel. Whilst the popular way is long-time analysis using data from numerous voyages, a case study is described herein with only needing the correct representative voyage pre and post the event.

1. Introduction to fouling and hull cleaning

Fouling of ship's hull has been known to Naval Architects for more than 2,000 years, as it was found written in an Aramaic papyrus that a mixture of Arsenic, Sulfur and Chian Oil was applied on the hull to speed through the water, *ABS (2011)*. Along the history many other anti-fouling coating ingredients were used e.g. waxes, poisonous oils, tar, plants resins, turpentine, naphtha and the list goes further.

The aim in the search for the "perfect" coating was always to discourage attachments to the hull surface, including avoiding shipworms that could penetrate the ship's wooden hull. However, in as much as humans fight with the nature of the fouling, the phenomenon keeps rolling. More so, when a more effective solution was found, including biocides, it had negative effect on the marine life and ecosystems, thus such coatings were abolished.

As a consequence, and throughout the history, hull cleaning has been a common practice in order to reduce drag and improve ship's hydrodynamic performance. GloMEEP (Global maritime energy efficiency partnerships), https://glomeep.imo.org/technology/hull-cleaning/, defines the purpose of hull cleaning as removing biological roughness or fouling without damaging the coating.

Fouling growth on ship's hulls affect the performance of the vessel as it forms a part of the apparent slip. When a vessel is propelled, the theoretical speed (in an unyielding fluid) would be:

$$V_T = \frac{P \times N}{1852/60} \ [kts]$$

Where P and N are the propeller's pitch and revolutions, respectively.

It is noted that the speed of the vessel rarely equals to the Speed Over Ground (SOG), and that part of the difference can be attributed to weather (wind and waves) which the vessel encounters as well as to hull fouling. The apparent slip would be:

$$Apparent\_Slip = V_T - SOG \ [kts]$$

The apparent slip can be positive or negative, and in most cases it is in the range of 10-30%. This is because while the weather effect can be positive or negative, the fouling would be negative. Even in the cases of brand-new vessel, after dry-docking or after hull cleaning, it can be assumed that fouling to certain extant will be found and therefore will diminish the performance of the vessel.

Another type speed that is normally used for vessels is the Speed Through Water (STW) which is the speed of advance of the vessel relative to the water, and includes the effect of the current and wake. Real slip of a vessel would be:

$$Real\_Slip = V_T - STW \ [kts]$$

An illustration of the various speeds used for vessels is shown in Fig.1.
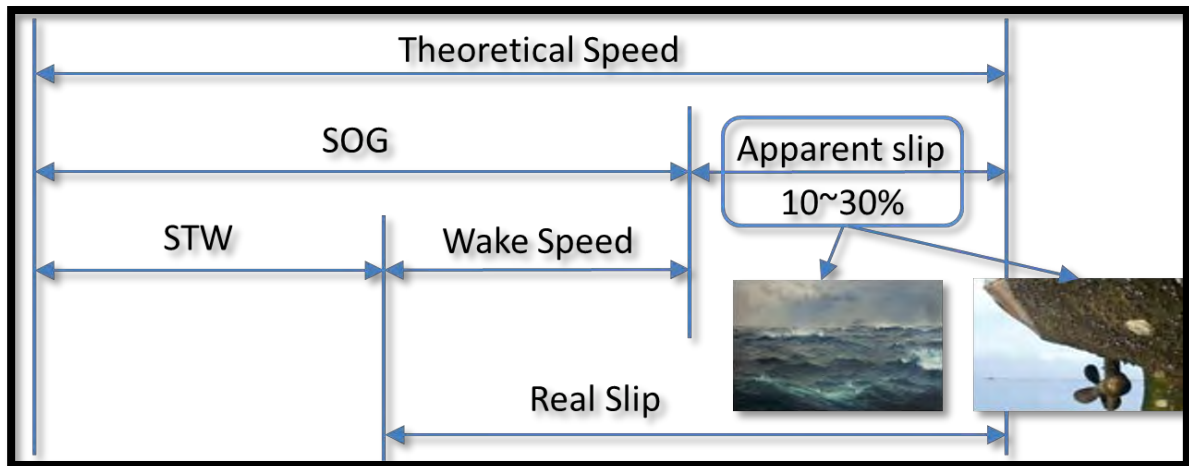
Fig.1: Speeds of vessels extracted from *Barrass (2012)*

Improving the performance of a vessel is possible by reducing her real and apparent slip, and hull cleaning is one of the answers to that. Hull cleaning by commercial diving is claimed to save 10% of the fuel bill, and by cleaning by robots between 5-15%, *Fathom (2012)*. IMO projected 320 million tons bunker demand in 2020, *Halff et al. (2019)*, which puts the hull cleaning in a favorable place market wise.

2. Factors affecting decision to carry out hull cleaning

The decision to carry out hull cleaning is affected by various considerations, some of the mains are described hereunder.

2.1 Bunker Price

Hull cleaning has its costs of the service from one side, and the time from the other. It was shown that the potential in fuel savings are in the range of 10%. Thus, higher bunker prices will thrust the decision to carry out hull cleaning forward.

2.2 Environmental Rules

IMO in way of EEOI (Energy Efficiency Operational Indicator), SEEMP (Ship Energy Efficiency Management Plan), as well as EU in way MRV (Monitoring, Reporting and Verification of CO_2 emissions) set measures are to reduce GHG (Green House Gases) emitted from shipping. All of these are strongly related to fuel consumption of world fleet. Thus, by carrying out hull cleaning, owners improve their position (and image) in meeting environmental regulations.

2.3 The Market

In a depressed market, an owner would seek to cut expenses. Ship's bunkers being a major expenditure in the transportation of goods at sea can be the way to do so, and hull cleaning can be therefore prioritized to achieve the goal and keep the business running.

2.4 Local Regulations

Ministries have the right and some have already established rules concerning hull cleaning of vessels. Example is New Zealand MPI (Ministry of Primary Industries) that demand every vessel calling NZ ports to prove that her hull was cleaned within 30 days prior to arrival to NZ.

3. Popular evaluation of hull cleaning

Hull cleaning can be done either in a drydock or afloat. Whilst the vessel is in a drydock the standard procedure would account washing, blasting, washing again and then coating the hull in typically 4-5 layers, also known as "hands", with sufficient drying time between each coat. In service hull cleaning from fouling can be done by either human diver or by a robot, and this typically lasts several hours, depending of the size of the vessel.

During hull cleaning when the vessel is afloat, evaluation of the work can be done wither in live camera broadcasting to shore, and/or by taking photos/videos and post work analysis. Example of such "on spot" evaluation is shown in Fig.2 where the hull underwater parts can be compared between before and after the cleaning.
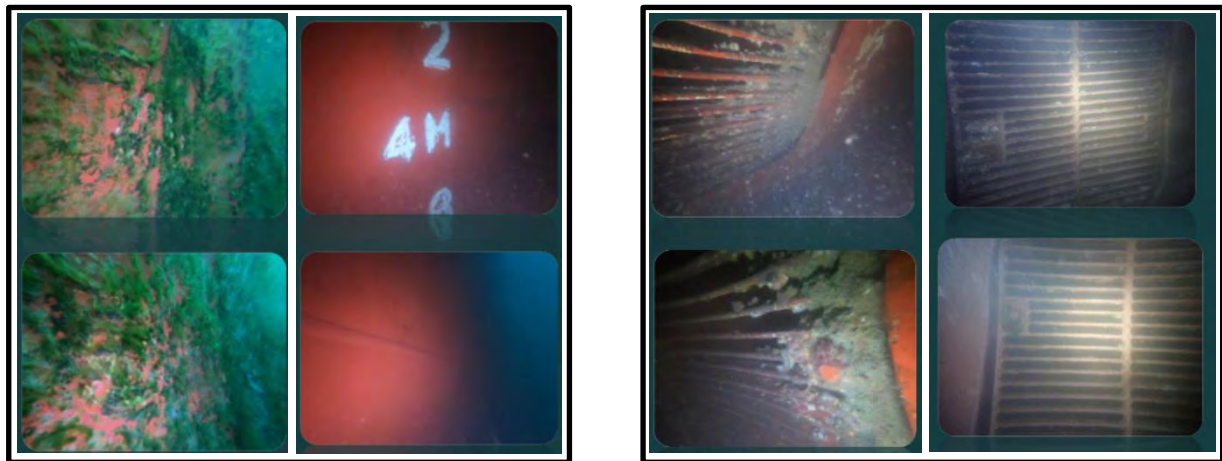
Fig.2: Pictures of hull before (left hand side) and after (right hand side) being cleaned

Common practice in evaluation of drydock and hull cleaning effectiveness on the reduction of hull resistance is by means of speed loss calculation along time prior and after cleaning of the hull. *ISO 19030 (2016)* describes the maintenance effect on the performance of a vessel over time, leaving the y-axis (hull and propeller performance) to be decided by the used of the standard.

As a consequence of common practice and the Standard, a vast variety of charts were developed from case studies and can be found in papers presented at HullPIC'18 and HullPIC'19. The performance indicators used are among other Fuel oil consumption, Power loss, Speed deviation, Hydrodynamic efficiency, Hull performance index and more.

There might be however cases, where stakeholders will find interest in the evaluation and representation of the vessel's performance in terms of speed-consumption curves, which might be more intuitively related to the fuel cost, hence voyage cost.

4. A case study of an alternative representation

An investigation with case study of a PCTC (Pure Car and Truck Carrier) vessel was carried out, to find the feasibility of an alternative representation of a dry-docking / hull cleaning effectiveness. An algorithm was developed as described herewith.

Relevant voyages that were assessed in terms of the performance of the vessel had been selected. One voyage before and after the hull cleaning operation, for laden and for ballast condition, under several restriction such as similarity of environmental condition, length of voyages and proximity to the date of hull cleaning from either side of the timeline.

NDRs (Noon Daily Reports) were used for the purpose of analysis and calculation. Speed was corrected to current, data was filtered due to weather and in view of inconsistencies, *Bialystocki and Konovessis (2016)*. On the other hand, FOC (Fuel Oil Consumption) was normalized to 24 hours. Finally, curves were plotted and the results are shown in Figs.3 and 4.

The analysis reflects daily fuel oil consumption reduction of between 14 ~ 20% in laden condition, and between -2 ~ 23% in ballast condition, dependent on the speed of the vessel.
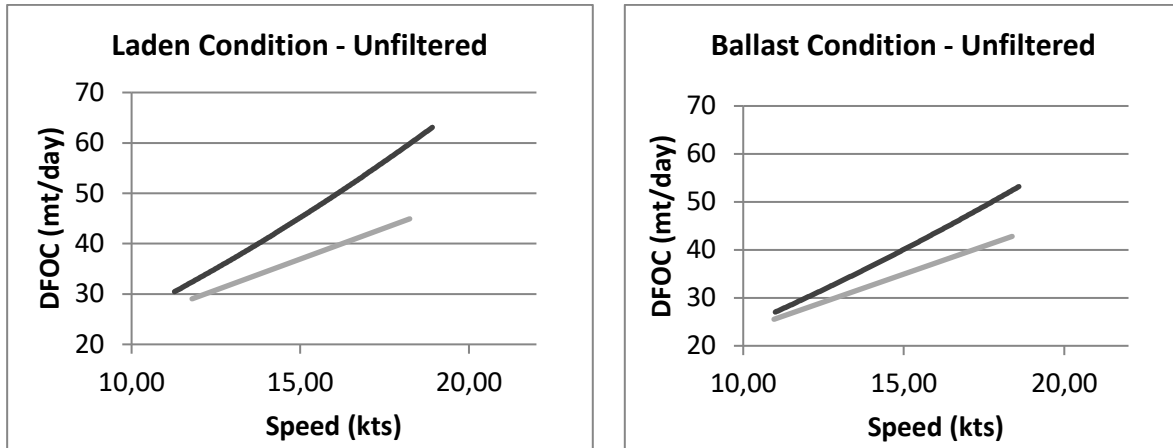
Fig.3: Performance before (upper line) and after (lower lines) drydock in each laden and ballast condition, <u>unfiltered</u>
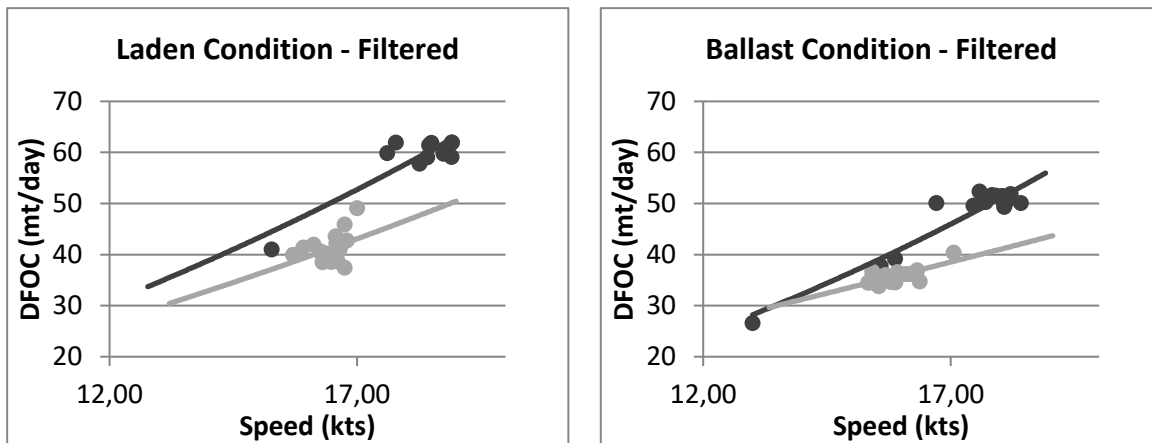
Fig.4: Performance before (upper line) and after (lower lines) drydock in each laden and ballast condition, <u>filtered</u>

5. The benefits from using the new method

The new approach for representation of ship performance by comparison and analyze voyage pre and post hull cleaning operation, clearly demonstrates and quantifies the reduction in fuel oil consumption on a specified speed. It is feasible in either laden or ballast condition. This evaluation has the following benefits in relation to the timeline performance indicator:

- **Less data** - There is no need for large datasets. In fact, to get the most accurate results, the best would be analyzing the last and first voyage, before and after the hull cleaning, respectively. In most cases these voyages would be in ballast condition, thus a further search for laden conditions would also be needed. More data sets do not necessarily mean better results, as presented by *Bertram (2019)*.

- **Faster** - Hull cleaning is a maintenance operation, which should reflect immediate improvement in performance. As such, data collection for long period is not needed and the proposed analysis can show results in very few voyages. The minimal number of required voyages for the analysis is four, namely two laden + two ballast.

- **Fuel oil consumption is IN** - While most existing analyses use speed loss as performance indicator over time, the proposed method incorporate both speed and fuel oil consumption built in the final output. This gives the user of a better picture of the performance of a vessel.

- **Large speed range** - While speed loss is in the best case normalized to a designated speed, and in the worst case, variation of speed is ignored, the proposed algorithm takes and reflects the entire peed range, even speeds less used are shown in the final plot.

- **Quicker economic check** - Fuel oil savings can be easily translated to cost savings. On the contrary, other performance indicators would need some additional calculations and assumptions in order to obtain the economic advantage.

6. Conclusions

Hull cleaning is a well-known driver to improve ship's performance. While the normal practice for evaluation of the effectiveness of this measure is long time analysis, there is a need to provide estimation at early stage after the cleaning was carried out. Within this paper it was shown that evaluation can be done by relatively small number of voyage analysis, and the outcome of speed-consumption curve is more intuitive to display results for the end user, in way of providing more workable information.

7. Further work

Further incremental improvement can be done to the process by fine tuning the draft/displacement correction to FOC, and speed correction due to wind and waves. Moreover, adaptation of the proposed method to a wired vessel is an additional challenge.

References

ABS (2011), *Surveyor – Fall 2011*, A Quarterly Magazine from ABS, Houston

BARRASS, C. B. (2012), *Ship Design and Performance for Masters and Mates,* Elsevier, Oxford

BERTRAM, V. (2019*), Some Fairy Tales in Performance Monitoring Revisited*, HullPIC'19, Gubbio

BIALYSTOCKI, N.; KONOVESSIS, D. (2016), *On the Estimation of Ship's Fuel Consumption and Speed Curve: A Statistical approach,* JOES 1, pp.157–166

FATHOM (2012), *Ship Efficiency: The Guide,* Butterworth & Heinemann, Oxford

HALFF, A.; YOUNES, L.; BOERSMA, T. (2019), *The Likely Implications of the new IMO Standards on the Shipping Industry*, Energy Policy 126, pp.277-286

ISO 19030 (2016), *Ships and marine technology – Measurement of changes in hull and propeller performance*, ISO, London

Taking In-Water Cleaning to the Next Level

Aron Frank Sørensen, BIMCO, Bagsvaerd/Denmark, afs@bimco.org

Abstract

In January 2021, a working group consisting of shipowners, cleaning companies, ports, paint manufacturers and international organisations has finalised the development of an industry standard for in-water cleaning with capture. The aim is to benefit all stakeholders involved in in-water cleaning and to ensure that: (1) the planned cleaning process is safe and effective; (2) the environmental impact is controlled whilst preserving the properties of the anti-fouling systems; (3) approval of in-water cleaners is based on testing and quality management. The paper will give a brief overview of the industry standard and share information about a newly initiated small-scale implementation project.

1. Introduction

During 2018, several shipowner members informed BIMCO of incidents involving in-water cleaners falsifying documentation. At the same time, the number of ports allowing cleaning operations were decreasing and new local and regional regulations were becoming increasingly stringent with regard to the permissible level of biofouling on ships calling at ports or waters of a coastal state.

So BIMCO took the initiative to form a working group representing the different stakeholders to develop a standard to improve the quality and safety of in-water cleaning with capture. In January 2021, the work was finalised and the following two documents that outline the performance-based requirements for the in-water cleaning with capture of a ship's hull, propeller and niche areas were published:

- Approval procedure for in-water cleaning companies
- Industry standard on in-water cleaning with capture.

The stakeholders are ships, cleaning companies, anti-fouling system (AFS) manufacturers, ports and other local authorities. The set-up ensures:

1. that the cleaning system and process are tested, audited and approved in accordance with the Approval procedure for in-water cleaning companies by an Approval Body and an independent Testing Organisation.
2. that after approval, the quality management systems of the cleaning companies are subject to periodic internal audits, whilst external audits are to be carried out by the Approval Body on an annual basis.
3. that ships, AFS manufacturers and cleaning companies will use the requirements in the Industry standard on in-water cleaning with capture for planning, conducting, and reporting on the cleaning itself.
4. that testing results can be utilised by cleaning companies to apply for local permissions from port and other relevant authorities to operate within their jurisdictions.

The Industry standard is based on responsive cleaning in other words a cleaning initiated by a marked reduction in the ship's performance. The ship will therefore need to implement procedures to monitor hull performance and biofouling growth thus avoiding that the biofouling becomes severe. Inspections of the submerged areas to show that a cleaning is needed constitutes an important part of responsive cleaning.

When planning in-water cleaning, the ship will use a cleaning company that has been approved in accordance with the Approval procedure for in-water cleaning companies.

The Industry standard does not give a detailed description of the methods and/or techniques required for carrying out the cleaning. The AFS manufacturer also has a role to play in advising the shipowner and the cleaning company on the anti-fouling coating system and the recommended cleaning methods including brush type and water pressure.

2. Inspections and planning of in-water cleaning

The *IMO (2011)* guidelines recommend the use of a biofouling management plan and biofouling record book (Resolution MEPC.207(62), 2011 Guidelines for the Control and management of Ships' Biofouling to Minimize the Transfer of Invasive Aquatic Species). The information in the IMO guidelines has formed the basis of the practical part of the Industry standard.

The biofouling management plan must specify under which conditions in-water inspections should be conducted. Some inspections are prescheduled in accordance with the ship's planned maintenance system (PMS) while others are planned in accordance with the operational profile of the ship, including after extended idle periods.

The decision to conduct an in-water inspection should be based on, but not limited to the following:

1. risk assessment of biofouling growth
2. assessment of the propulsion power and fuel consumption over a specified period (hull performance monitoring)
3. statutory and class IWS (in-water survey) between dry docks
4. availability of services provided by divers eg regular propeller polishing or cleaning or underwater repair
5. idle periods or specific lay ups for example as stipulated in a charter party or in a contract with the AFS manufacturer
6. mandatory inspection requirements according to relevant regulatory regimes before proceeding to an arrival port or waters of a coastal state
7. requested by the charterer eg due to failure of the AFS
8. inspections carried out at planned intervals in accordance with the PMS
9. inspections requested by the AFS manufacturer.

This Industry standard introduces reference areas to serve as datum areas to be used during inspections and to measure the efficacy of the cleaning.

During every inspection, attention should be paid to the reference areas and the information has to be recorded accurately. The condition of reference areas will give an indication of biofouling growth, therefore, an accurate inspection and recording of details will be of upmost importance.

The Industry standard includes detailed procedures for the planning and execution of in-water cleaning. The cleaning should be seen as an integral part of the whole biofouling management process. The top priority of the standard is to ensure that the cleaning process is carried out safely.

The figure in Annex 1 provides an overview of the communication flow between the various parties using this Industry standard when conducting hull inspection and/or cleaning.

3. Approval of In-water cleaning companies

It has been necessary to divide niche areas into different categories because the same piece of equipment cannot be used to clean all of them. Depending on the intended use of the system, the approval process may include:

a. areas on the flat sides of the hull
b. curved areas used for testing, eg the turn of bilge, and angles where the orientation of the surface changes abruptly, such as the chine, keel and skegs
c. niche areas, eg, propeller shafts, rudders, anodes and gratings
d. propellers.

A cleaning company can be approved for one or more of the above categories.

The Approval procedure for in-water cleaning companies contains the minimum requirements and test protocols for demonstrating compliance with the Industry standard and describes the approval process.

4. Testing

In-water cleaning companies will be tested for three or four different performance criteria based on their individual performance/manufacturers claims. The verification testing will take place on actual ship surfaces (submerged hull and/or niche areas) and anti-fouling coating system (AFC) (non-biocidal and/or biocidal) depending on cleaning company's claims.

The capability of the cleaning system shall be tested by an independent Testing Organisation. While being tested, the system shall be operated in the way, it is intended to be used during normal operations.

In-water cleaning companies will be tested for different performance criteria relevant to their declaration of the cleaning system's operational capabilities and performance ie (A) the capability of the system to remove macrofouling; (B) the effectiveness of the separation and/or treatment unit system at removing material, and (C and D) control of the emission to the local environment from the cleaning unit and from the separation and/or treatment unit.

The performance criteria include:

1. Limits to the type and extent of biofouling that the system is able to clean from ship surfaces (eg a height of hard calcareous fouling, fouling ratings, percentage of surface area covered with soft macro fouling and hard fouling, total amount of material that can be handled, etc.),
2. Capture and removal of material produced collected during in-water cleaning (eg largest size and percentage reduction of particulate matter in effluent water)
3. Impact to local water quality (eg levels of total suspended solids and/or AFC associate biocides) as a result of in-water cleaning.

The testing will be carried out on three different ships using a number of test samples and images. Approval will be given subject to the results of all three tests passing the performance criteria.

5. Companies and organisations behind the standard

The Industry standard has been written by an industry working group consisting of paint manufacturers, in-water cleaners, shipowners, ports, international organisations and authorities. The following were represented in the work:

Akzo Nobel, BIMCO, C-Leanship, CMA Ships, DG Diving Group, Dutch Ministry of Infrastructure and Water Management Fleet Cleaner, Hapag-Lloyd, Hempel, HullWiper, International Association of Classification Societies, International Chamber of Shipping, Minerva Shipping, Portland Port (UK), Port of Rotterdam and PPG Coatings

A reference group was asked twice to comment on the Industry standard and several parts of the standard have been updated by correspondence. Members of the reference group represented the following

AFS manufacturers, authorities, cleaning companies, international organisations representing ship owners, laboratories, research institutes, and shipowners: Bernhard Schulte Shipmanagement, Chevron Shipping CO – Houston, ECOsubsea AS, International Association of Independent Tanker Owners (INTERTANKO), Kristian Gerhard Jebsen Skipsrederi AS, Laboratory for Aquatic Research and Comparative Pathology, NACE International, SeaTec, SRN Group, TecHullClean Pte. Ltd.

Project leader, BIMCO is the world's largest international shipping association, with around 1,900 members in more than 120 countries, representing 59% of the world's tonnage. The global membership includes shipowners, operators, managers, brokers and agents. BIMCO is a not-for-profit organisation.

References

TAMBURRI, M.N.; DAVIDSON, I.C.; FIRST, M.R.; SCIANNI, C.; NEWCOMER, K.; INGLIS, G.J.; GEORGIADES, E.T.; BARNES, J.M.; RUIZ, G.M. (2020), *In-Water Cleaning and Capture to Remove Ship Biofouling: An Initial Evaluation of Efficacy and Environmental Safety*, Front. Mar. Sci. 7:437

IMO (2011), *Guidelines for the Control and Management of Ships' Biofouling to Minimize the Transfer of Invasive Aquatic Species*, International Maritime Organization, London

Annex 1 - Communication flow chart
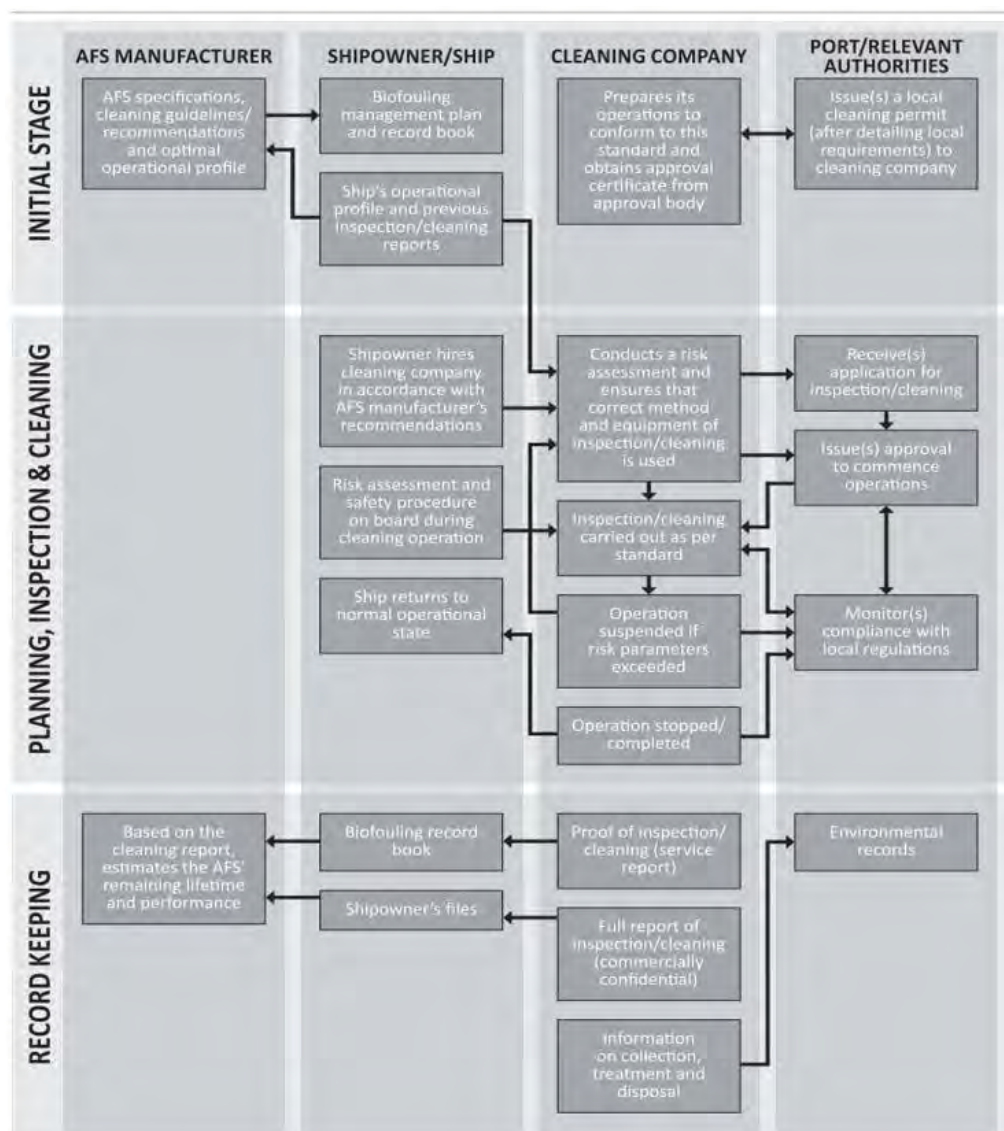
Modelling and Simulation of the Effect of Antifouling Coating on Ship Resistance

Yuanwei Zhang, Jotun A/S, Sandefjord/Norway, yuanwei.zhang@jotun.no
Irma Yeginbayeva, Jotun A/S, Sandefjord/Norway, irma.yeginbayeva@jotun.no
Angelika Brink, Jotun A/S, Sandefjord/Norway, angelika.brink@jotun.no

Abstract

Viscous flow simulations based on the equations of Reynolds-Averaged Navier-Stokes (RANS) have become an engineering tool used on a daily basis. For the hull performance, one of the main goals of such calculations is to determine frictional resistance, which is of paramount importance for ships since it directly affects their speed, fuel consumption and emissions. This paper describes a CFD method to predict the frictional performance for different antifouling coating in different roughness conditions using a ship model case. Roughness models representing different antifouling coatings were developed by using roughness functions determined in flow cell experiment. The developed roughness model was then incorporated with RANS model by means of wall function in the commercial CFD software, NUMECA. A Full-scale 3D container ship KVLCC2 model was used with different coating conditions. The results were then compared with each other to analysis the frictional resistance of different antifouling coating products.

1. Introduction

The use of antifouling coatings is an effective way to prevent the increase of frictional resistance of ships by inhibiting organism growth and settling on the hull. Such coatings play a huge role in decreasing not only the commercial costs of vessels, but also the greenhouse gas emissions of maritime industries and others. Giving that shipping has been, and still is, one of the most important and energy-efficient ways of cargo transport, there is a continually growing commercial and environmental interest and hence supporting R&D activities for the antifouling coating development and evaluations around the world.

From a hydrodynamic point of view, an antifouling coating has an initial surface roughness which affects a ship's frictional resistance already at the first place. An ideal coating should be smooth enough to improve the surface properties of a hull in the as applied condition and should be effective against marine biofouling which occurs over time. Both aspects markedly affect the frictional resistance and hence fuel consumption of a ship. Nowadays, the hotspot of antifouling paint research lies in the antifouling properties and environmental impact of the coating, e.g., the development of tin-free technologies, silylated acrylate technologies, reduction of biocides, metallic acrylate technologies, acrylic nano-capsule technology, and non-stick/fouling release silicone elastomers, *Hellio and Yebra (2009)*. However, the frictional impact of these coatings moves more and more into focus.

The International Maritime Organization has decided in its initial strategy, *IMO (2018)*, that the global emissions are to be reduced by 50 percent by 2050, compared with 2008. This started a large research activity in the field of possible technologies and the antifouling coating responsible for up to 70% of the total drag of the vessel moved into the focus. Some attempts have been made in describing the impact of different antifouling technologies on the total drag of a ship. In the studies of *Candries et al. (2003,2005)* the effect of antifouling on flat plate and cylinder was examined. Efforts were made to link the roughness of the paint to drag and hence resistance. Two of the popular types of antifouling coatings, i.e. tin-free self-polishing copolymer (SPC) and fouling-release (FRC) were applied on flat plates and cylinders respectively, and their corresponding roughness profiles were recorded. Results showed that SPC exhibits more drag as compared to foul-release. This was attributed to the higher level of roughness. *Schultz et al. (2004)* studied experimentally the relation of surface roughness and frictional resistance for a range of modern antifouling paint systems. The results indicated little differ-

ence in frictional resistance coefficient (CF) among the paint systems in the unfouled condition. Significant differences were observed in CF among the paint systems in the fouled condition for the silicone surfaces showing the largest drag penalties. *Holm et al. (2004)* presented similar results studying biocidal polishing antifouling and fouling-release coating in a rotating disk apparatus. The results showed that the antifouling control coating showed a smaller drag penalty than the fouling-release coatings. They reported a 9%-29% increase in drag for the FRC with accumulated biofilms compared to the SPC. The study reported no surface roughness evaluations for the different experimental stages and fouling conditions. Therefore, no information could be obtained on the correlation of roughness and drag characteristics for fouled coating types.

In the papers above, all the testing and measurements were conducted in small-scale panels or disks, while the comparison between different types of antifouling coatings is not yet available in a full-ship scale situation.

As discussed by *ITTC (2017)*, advances in numerical modelling methods and increases in computational power have made it possible to carry out fully non-linear simulations of ship motions, taking into account viscous effects, using Computational Fluid Dynamics (CFD).

CFD is the art of replacing the integrals or the partial derivatives of fundamental physical principles in mathematical equations with discretized algebraic forms. The governing equations are basic physical principles of mass and momentum conservation. Its use in marine research has been gaining strength in recent years. Up to date, most CFD studies on large scale scenario were focused on the effect of biofouling on ship resistance, *Khor and Xiao (2011), Demirel et al. (2017), Atencio et al. (2019)*, except a study conducted by *Demirel et al. (2014),* in which the effect of antifouling coatings on frictional resistance was predicted on a large-scale flat plate with the same wetted area of a large-scale ship.

The aim of the present study is to analysis the hydrodynamic performance of existing antifouling coatings available from Jotun AS, and fill the gap between experimental scale drag testing and full-scale ship resistance prediction by utilizing Computational Fluid Dynamics (CFD) method.

2. Roughness function

In order to understand the effect of hull-roughness on a ship's penalty drag, some background of the wall-bounded turbulent boundary layer will be explained here. The mean velocity profile in the inner portion of a turbulent boundary layer, outside of the viscous sublayer, can be expressed as a classical and universal log law (Eq.1) and is independent of the flow conditions further away.

$$U^+ = \frac{1}{k}\ln(y^+) + B \qquad \text{Eq.}(1)$$

where U^+ is the non-dimensional mean velocity in the boundary layer and y^+ is the non-dimensional normal distance from the boundary.

From numerical modeling point of view, the universalizability of the log law velocity profile is of great benefit since the velocity near the surface can be easily modelled based on Eq.(1) at any scale. This only applies when the solid surface is smooth and has no other dimensions or features that should be included in the dimensional analysis.

Characterizing the drag of a rough surface implies finding the velocity decrement caused by the frictional drag of the surface as a function of the roughness Reynolds number. This relationship is commonly known as a roughness function, $\Delta U+ = f (k+)$, *Clauser (1956)*, and is unique for a particular surface roughness geometry. Once the roughness function for a given rough surface is known, it can be used in a numerical analysis to predict the drag of any body with that particular roughness.

The most common numerical approach to model flow over rough surfaces is to modify the wall function formulation used for flow over smooth solid walls (Eq.1), by introducing the roughness function mentioned above, as Eq.(2).

$$U^+ = \frac{1}{\kappa}\ln(y^+) + B - \Delta U^+ \qquad \text{Eq. (2)}$$

In the present study, 4 types of antifouling coating from Jotun, two different biocidal self-polishing coatings (SPC-1 and SPC-2), FRC, and a type hard coating (HC), were applied on the surface of lab-scale panels (600×200 mm) first. The application was done after specification and the surface was as to be expected. To obtain the ΔU+, the full turbulent flow channel from the University of Strathclyde was utilized to measure the drag performance of the plates. Table I lists the roughness parameters of the tested coatings. In addition, 3D topographical views of the surfaces are shown in Fig.1 with an area of 40×40 mm.
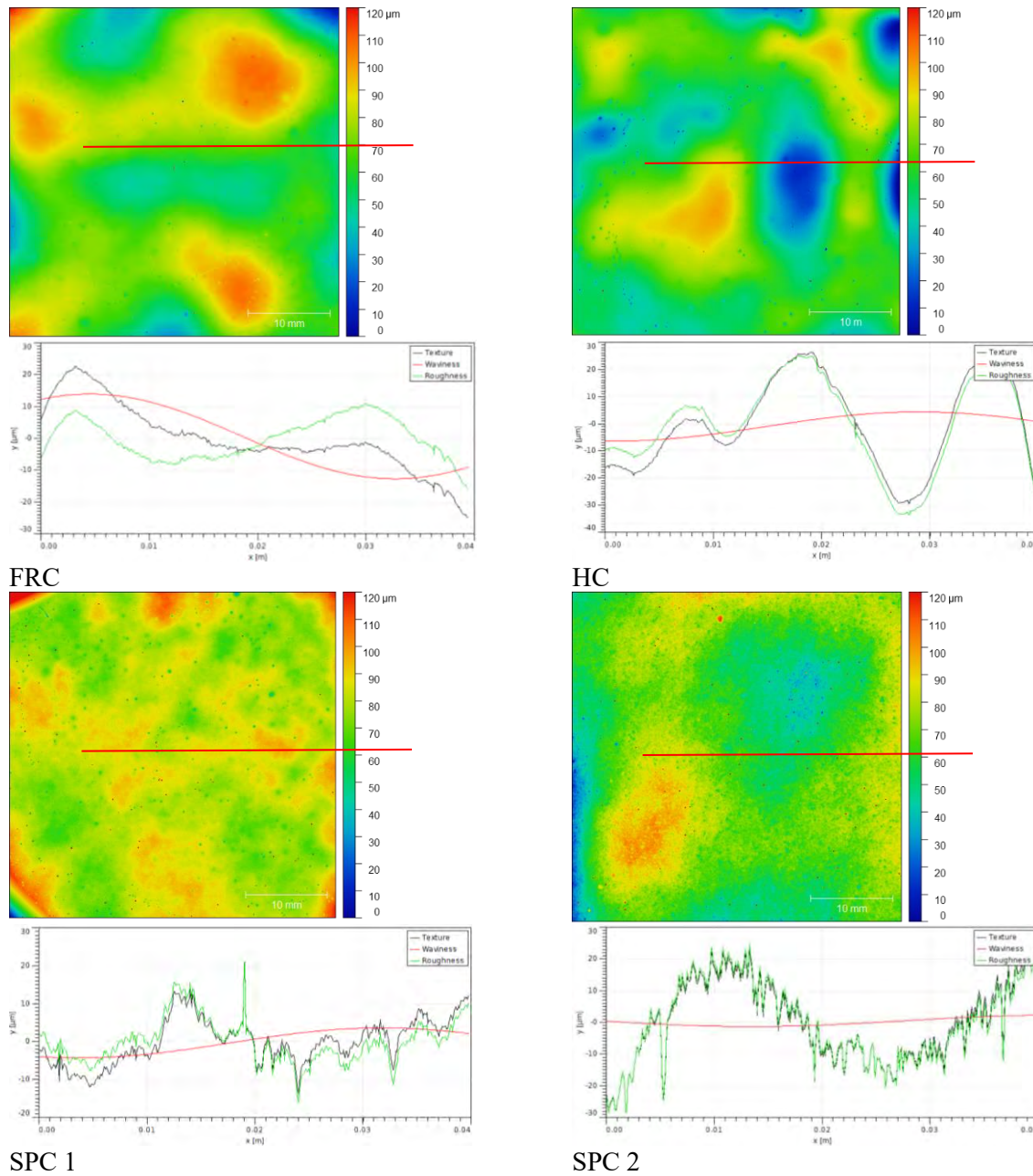

FRC

HC

SPC 1

SPC 2

Fig.1: Topographical 3D color maps and roughness/ waviness profile views of coated panels. Cut-off for 2D profiles 50 mm. The red line indicates the place of the taken 2D profile.

Table I: Roughness parameters R_q, R_{t50} and Surface Skewness S_k of the different coated panels in μm

Antifouling coating	Rq [μm]	R$_t$ (μm, cut off 50 mm)
FRC	2.54 ± 0.01	23.18 ± 8.83
HC	2.53 ± 0.22	20.34 ± 27.73
SPC-1	3.14 ± 0.03	24.31 ± 6.03
SPC-2	4.19 ± 0.02	37.05 ± 1.66

The roughness function (ΔU^+) in Eq.(2) can be obtained directly based on experimental results of the velocity shift by model fitting, as suggested by *Anders et al. (2017)*. An expression of roughness Reynolds number k^+ and ΔU^+ can be formulated as:

$$\Delta U^+ = a\ln(k^+) + b \quad \text{Eq. (3)}$$

$$k^+ = \frac{kU_\tau}{\nu} \quad \text{Eq. (4)}$$

k^+ is called roughness Reynolds number and represents the ratio of a physical roughness height to its viscous length scale. The root mean square of the absolute height (Rq) is used as k in Eq.(4). a and b are fitted parameters of the model fitting. The curve fitting plots and the fitted coefficients for different panels are shown in Fig.2.

(a) FRC   (b) HC

(c) SPC1   (d) SPC2
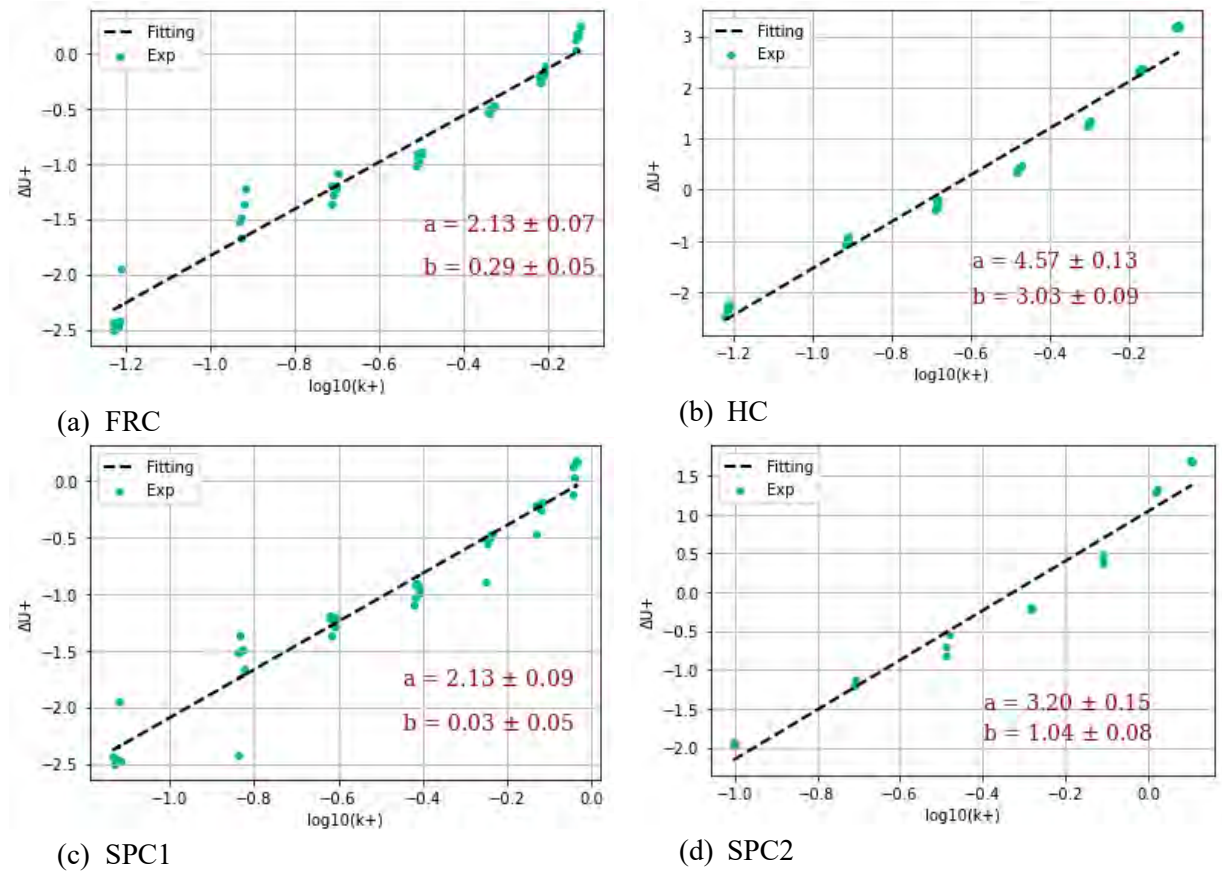
Fig.2: Roughness function model fitting based on experimental data

3. CFD model and validation

The model ship KVLCC2 (Korean Very Large Crude Carrier), 326 m long was used for simulations, as presented in Figure 3. Data for validation are available for the KVLCC2 and was therefore used as test hull. The simulations were performed with NUMECA Fine™/Marine, using a steady-state, multi-fluid model. The free surface is obtained by using the volume of fluid (VOF) method. The k-ω shear

stress transport (SST) turbulence model is used to model turbulence in the flow field. The flow over the ship surfaces is modeled by means of modifying the smooth wall function as described in the previous section.

Fig.3: Side-view of the hull geometry. Waterline is located at z = 0 m

A grid sensitivity study was carried in an earlier work using 4 domain resolutions containing 3 million, 5 million, 8 million, and 11 million cells, revealing a sufficient converging for 8 million cells, so the used cell number was 8 million. The model was validation in advance using the experimental towing tank data by MOERI and is shown in Fig.4 for the KVLCC2 in full-scale. It shows the total drag over the Froude number, which is dependent on speed. The CFD results overpredict the resistance (6% maximum) compared to the scaled towing test but show similar trends as the experimental towing tank results by MOERI. This test was scaled in accordance with the *ITTC (2017)* procedure, which demonstrated the reliability of the CFD model.
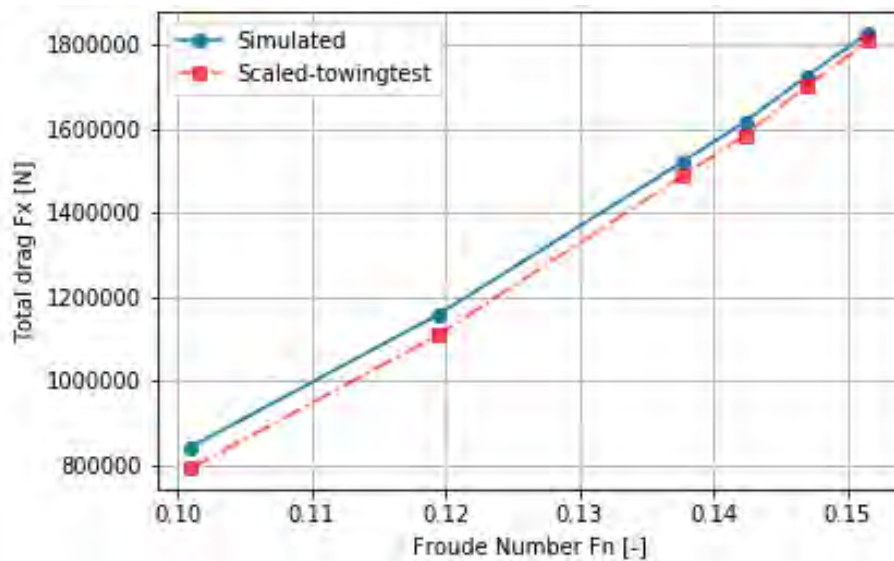
Fig.4: Speed-drag curve for the KVLCC2 in full-scale. Comparison between simulated and scaled towing tests by the *ITTC (2017)* procedure.

4. CFD Simulation results

After the validation of the CFD model, the newly developed roughness functions were incorporated into the wall function model to account for the roughness introduced by the antifouling coatings as listed in Table I. Fig.5 shows the percent increase of the total resistance of tested coatings compared to a hydrodynamics smooth ship hull. The simulation results of SPC1 and FRC have negative values, which would mean that the drags of these two cases are smaller than the smooth surface simulation. This drag reduction phenomena are due to the negative velocity shift (ΔU^+) observed from the experimental measurements from roughness function plot, Fig.2. The reason for this negative ΔU^+ is still under investigation. It is of note that the paint application was done in a laboratory setting and might have excluded environmental factors and resulted in a smoother paint application. The roughness Rt(50) of newly applied coatings commonly found on ship hulls are around 100-150 μm whereas that of the current laboratory are well below 100 μm. Hence, it is to be expected that the drag increase would have been slightly higher with a more realistic surface roughness.

The SPC1 and FRC coating reveal the better performance regarding the resistance, and HC results the highest drag penalty, followed by SPC2. However, these results contradict the measurements of the roughness parameters in Table I, where HC has the lowest Rq and Rt(50) but gives the highest drag penalty. This observation might suggest that using a single roughness parameter may not be enough to predict the performance of the antifouling coatings.
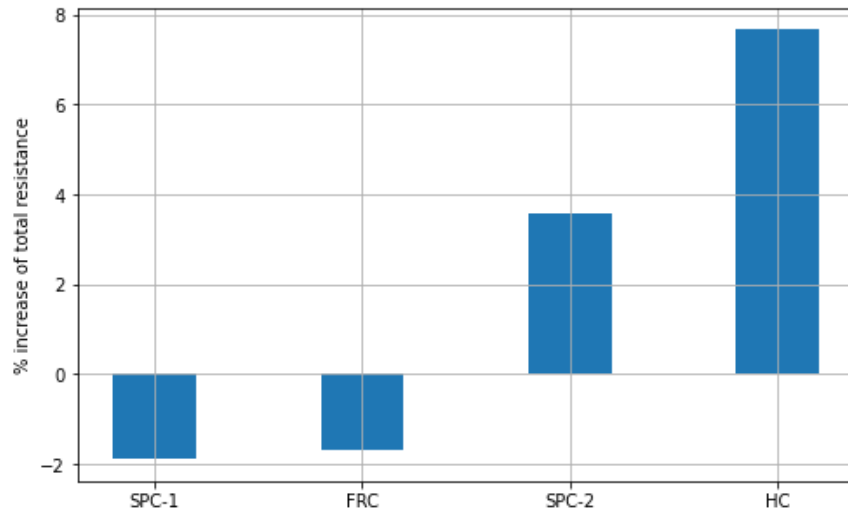
Fig.5: Estimated percentage increase in total resistance compared with smooth surface for 15.5 kn

The comparison shown in Fig.5 were for the KVLCC2 design speed of 15.5 kn. Two more velocities (14.5 and 16.5 kn) were calculated under the same condition. A higher ship velocity gives a slightly higher total resistance for all the coatings, Fig.6. However, the contribution of the frictional resistance decreases in the total resistance for higher speeds and the form resistance gets more dominant. It can also be seen that the observations from Fig.5 are valid throughout the tested speed range, indicating the consistence of the coating performance.

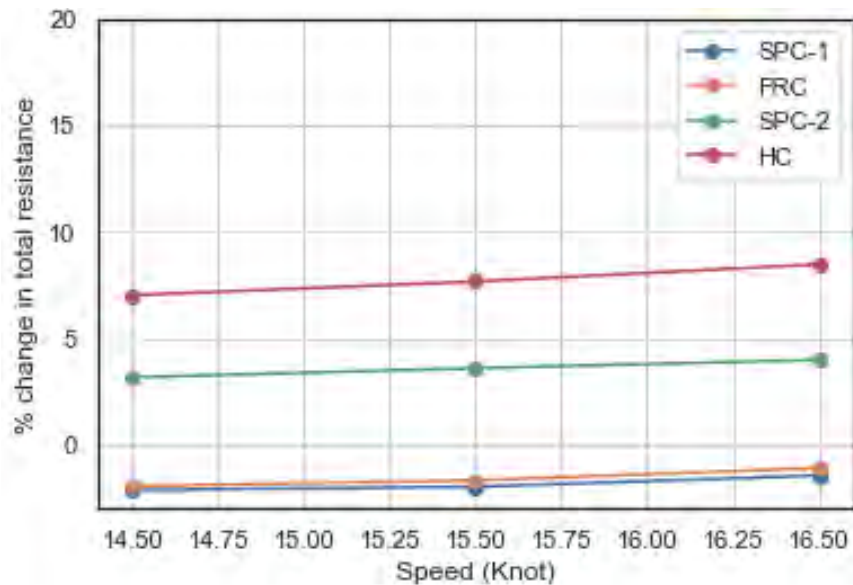Fig.6: Estimation of the percentage increase in total resistance compared with smooth surface

5. Summary

This study investigates the hydrodynamic performance of Jotun antifouling coatings on a full-scale container ship using CFD based on experimental results obtained from the University of Strathclyde. The aim is to estimate the full ship resistance caused by the antifouling coating products. Customized

roughness functions for different coatings were developed directly based on the turbulent channel experiments. The roughness functions were then implemented into the CFD code to account for the initial roughness introduced by coatings. The results show that the performance correlates with the roughness values. SPC1 and FRC have better hydrodynamic performance, while HC has the highest resistance even though it has the lowest roughness height. Further investigation will be forced on the prediction of resistance of the coatings after sea condition exposure with the slime formation and accumulation and on environmentally impacted applications with roughness higher than 100 μm.

References

ATENCIO, B.N.; CHERNORAY, V. (2019), *A resolved RANS CFD approach for drag characterization of antifouling paints,* Ocean Engineering 171, pp.519-532

CANDRIES, M.; ATLAR, M.; MESBAHI, E.; PAZOUKI, K. (2003), *The measurement of the drag characteristics of tin-free self-polishing co-polymers and fouling release coatings using a rotor apparatus,* Biofouling 19(S1), pp.27-36

CANDRIES, M.; ATLAR, M. (2005), *Experimental investigation of the turbulent boundary layer of surfaces coated with marine antifoulings,* J. Fluids Eng. 127, pp.219-232

CLAUSER, F.H. (1956), *The turbulent boundary layer,* Advances in Applied Mechanics 4, pp.1-51

DEMIREL, Y.K.; KHORASANCHI, M.; TURAN, O.; INCECIK, A.; SCHULTZ, M.P. (2014), *A CFD model for the frictional resistance prediction of antifouling coatings,* Ocean Eng. 89, pp.21-31

DEMIREL, Y.K.; TURAN, O.; INCECIK, A. (2017), *Predicting the effect of biofouling on ship resistance using CFD,* Applied Ocean Research 62, pp.100-118

HELLIO, C.; YEBRA, D. (Eds.) (2009), *Advances in marine antifouling coatings and technologies*, Elsevier

HOLM, E.; SCHULTZ, M.; HASLBECK, E.; TALBOTT, W.; FIELD, A. (2004), *Evaluation of hydrodynamic drag on experimental fouling-release surfaces, using rotating disks,* Biofouling 20(4-5), pp.219-226.

IMO (2018), *Resolution MEPC.304(72), Initial IMO Strategy on Reduction of GHG Emissions from Ships*, Int. Mar. Org., London

ITTC (2017), *ITTC - Recommended Procedures and Guidelines 7.5-02-03-01.4: 1978 ITTC Performance Prediction Method*, Int. Towing Tank Conf., https://ittc.info/downloads/quality-systems-manual/

KHOR, Y.S.; XIAO, Q. (2011), *CFD simulations of the effects of fouling and antifouling,* Ocean Eng. 38(10), pp.1065-1079

LARSSON, L.; STERN, F.; VISONNEAU, M. (Eds.) (2013), *Numerical ship hydrodynamics: An assessment of the Gothenburg 2010 workshop,* Springer Science & Business Media

LI, C.; ATLAR, M.; HAROUTUNIAN, M.; ANDERSON, C.; TURKMEN, S. (2018). *An experimental investigation into the effect of Cu2O particle size on antifouling roughness and hydrodynamic characteristics by using a turbulent flow channel,* Ocean Eng. 159, pp.481-495

ÖSTMAN, A.L.; KOUSHAN, K.; SAVIO, L. (2017), *Numerical and Experimental Investigation of Roughness Due to Different Type of Coating*, 2nd Hull Performance & Insight Conf., Ulrichshusen

SCHULTZ, M.P. (2004), *Frictional resistance of antifouling coating systems,* J. Fluids Eng. 126(6), pp.1039-1047

SCHULTZ, M.P. (2007), *Effects of coating roughness and biofouling on ship resistance and powering,* Biofouling 23(5), pp.331-341

Greening Smaller Ferries by Optimizing Operations

Soren Vinther Hansen, The Navigator, Svendborg/Denmark, svh@thenavigator.dk
Marie Lützen, University of Southern Denmark, Odense/Denmark, mlut@sdu.dk
Jan Corfixen Sørensen, University of Southern Denmark, Odense/Denmark, jcs@mmmi.sdu.dk
Niels Gorm Maly Rytter, University of Southern Denmark, Odense/Denmark, ngry@iti.sdu.dk

Abstract

A significant reduction in fuel can be achieved through operational changes, but to establish better practices, it is necessary to have equipment for evaluating the energy consumption under given circumstances and to be able to identify and evaluate energy-saving and cost-effective initiatives. Many smaller ferry companies have no tradition for documenting operations or digital performance monitoring and analyse of their energy and fuel consumption. Therefore, the ferry crew, rely mainly on their assumptions about parameters influencing the operation, and how this impact the fuel consumption. The present study shows the results of analyses of more than one year of logged data from operations of an older small island ferry. The preliminary results indicate that via digital decision support and effective decision support the ship can reduce the fuel consumption and the emissions with 10-20%.

1. Introduction

There have for many years been an increasing attention to sustainable maritime transport. The increasing focus on climate change problems have brought environmental questions and pollution prevention high on the international agenda and the International Maritime Organization (IMO), has put forward a series of measures aimed at reducing the total amount of greenhouse gas (GHG) emissions from ships. In April 2018 the International Maritime Organization, IMO, adopted an initial strategy aimed at reducing total annual GHG emissions by at least 50% by 2050 compared to the 2008 level, *IMO (2018)*.

The present study deals with green and energy efficient ferry operation. Ferry operators are as all other shipping companies interested in saving energy, not only to comply with regulation but also to reduce cost and to comply with the increasing demand for green transportation and sustainable transport from the costumers. The global ferry industry is very large, and the ferries play an essential role in transporting people, cargo and vehicles. Interferry, an organisation representing the Ferry Industry World-Wide, estimates that there are approximately 1,300 ferries over 1,000 GT (gross tons) and thousands of smaller ferries globally. These vessels transport yearly 2.1 billion passengers, 250 million vehicles and 32 million trailers. Many of these vessels are older and are therefore to be renewed and substituted by more carbon friendly vessels in the coming years. A large part of this reduction can be achieved by new and updated ship design and the introduction of new fuels or low carbon fuels, but the transition will not be fulfilled tomorrow, retrofitting and replacing older vessels with newer will take years. While this replacement process is ongoing there need to be a focus at the practical operation of the old vessels. Operating the vessels in an energy efficient way is very important for reaching the goal.

The paper presents results develop in the EU funded project Ecoprodigi, https://ecoprodigi.eu/, where eco-efficiency of shipping has been improved by introducing digitalization solutions on board island ferries in Denmark. In accordance with IMO, The Danish Government has set the course for a more climate friendly future, with a target of reducing GHG emissions by 70% by 2030 and the aim of making shipping carbon neutral. The smaller island ferries are also part of this goal. In Denmark there are 42 inland ferry routes operated by 52 vessels. The Island Ferries connect the Danish mainland to small islands of strategic importance, and their operations are supported financially by municipalities and government. The EU project involves four out of the 25 ferries.

The aim of the present study is to present the great potential for energy savings to be achieved using digital performance data and monitoring tools to optimize the operational practices on board smaller

ferries. To illustrate and highlight the potential a case study of a small Danish ferry has been chosen. The crew has a lot of knowledge about the ship, route, and the operation, but need visual and accurate information about energy consumption and good energy practices. To establish a successful system for energy efficient operation, it is necessary to have equipment for evaluating the energy consumption and to be able to identify and evaluate energy-saving and cost-effective initiatives, monitoring systems are therefore a must. Even though that the importance of monitoring and analysing the performance of the ship is well known, only a few ferries systematically collect, store, and analyse data from the operation. Furthermore, research has also demonstrated that small shipping companies, as local ferry companies often will be, lack the resources to analyse, make decisions and implement energy efficient solutions *Johnson et al. (2014), Poulsen and Johnson (2016).*

2. Ferry Operations, Digitalization and Energy Efficiency

Performance can generally be defined as the amount of useful work performed by a system compared to the time and resources used. For a ferry the performance can be defined as resources used for a given voyage. It relates to the energy consumption compared to the amount of useful work to sail and manoeuvre the vessel through the water and supplying electricity and heat to the operation of the ship and comfort of crew and passengers on board. When designing a ferry, the performance and the energy efficiency is taken into considerations through an energy-efficient hull design, optimized hotel load efficiency and focus at energy-efficient engines at the right engine layout – but awareness to the daily operation is very important and a significant reduction in fuel consumption can be achieved through changes in the operational practices, see e.g., *Jensen et al. (2018), DNV GL (2015), Eriksen et al. (2018), Viktorelius and Lundh (2019).*

2.1 Ferry Operation and voyage modes

Ferries have a unique sailing pattern that differ from the normal operational patterns of other vessel types. They usually have shorter sea passage followed by longer stay in port engaged with loading and discharging passengers, cars and trucks. The sea passage will for many ferries, especially the smaller sailing near the coast, be influenced by complex navigation in congested waters with heavy traffic. The traffic might in periods be increased by fishing or pleasure boats sailing at random crossing the route. The navigation near the coast will probably be restricted because of sailing in narrow channels or the presence of shallow water giving a low keel clearance resulting in a relatively high speed reduction. The crew is therefore busy navigating the ferry and has only limited time for voyage evaluation or optimization. Furthermore, for the crew energy efficiency is secondary to safety on board - in operations where there is limited manoeuvrability due to traffic congestion, complex navigation, low water depth or other environmental conditions, the focus is, and will always be, on safety first. Parameters that also will refrain the crew and the shipping operator from thinking greener and having an energy efficient operation will be the large focus at passenger comfort and keeping the pre-planned schedule.

A ferry sailing on a fixed route has good conditions for comparing operational parameters and thereby evaluate the level of energy efficiency. If a voyage having equal sailing distance and duration where the ship is exposed to comparable external conditions as e.g. similar wind and current, result in different energy consumption, a detailed analysis can identify reasons for the extra consumption. In order to compare voyages, it is important that the operational condition of the vessel is known. The fuel consumption for the situation where the vessel is alongside in port is very different from the consumption when it is sailing at full speed. Therefore, for reasons of comparability, the voyage must be separated into clear and comparable segments. The present study uses the definition of modes, Fig.1, presented by *Lützen et al. (2017)* and *Eriksen et al. (2018)*:

- Manoeuvring where the vessel is operated under conditions restricting the vessel's movements, such as arrival and departure from port.
- Passage where the vessel is unrestricted in its manoeuvrability and able to operate at its design speed.
- Harbour where the ship is stationary in port without using its own propulsion.

Fig.1: Modes – Harbour, Manoeuvring, Passage, *Aro et al. (2020)*

For ferries, the total voyage time is fixed due to timetables. Spending more time in one mode means that less time is available for the others. Therefore, looking at one mode in isolation will not give a true picture of the energy efficiency of the entire voyage. But the modes can be used for sub-optimisation as external conditions and operational parameters within each mode are comparable. On board ferries the separation between the modes can with advantage be geographic positions, which will give similar distances for all modes – and thereby comparable modes across more voyages.

As seen the whole operation is strongly controlled and regulated by the timetables, examining these is therefore of great importance. Rethinking schedules and timetables will open up for energy savings, an issue also mentioned by *Jensen et al. (2019)* and *Johnson and Styhre (2015)*. Changing the timetables might seem a simple solution but can in practice be very difficult as many stakeholders are involved. Keeping the time intervals but making room for a more dynamic planning can be considered as e.g. allowing shorter harbour stays in period with less passenger and cargo, to allocate more time for sea passage.

2.2 Operational data sources and monitoring

Modern ferries generate a large amount of data for a wide variety of operational parameters - navigational and engine parameters are monitored and displayed on the bridge. Even thought that data is stored in the vessel's integrated control system, it is difficult to access, and it is often not possible to export data for analysis. On board older ferries operational data is only sparsely available. Minimum information for estimating the energy efficiency will typical be:

- Navigational information as position and speed over ground available from the GPS and ECDIS
- Relative wind direction and speed from an anemometer
- Main engine RPMs and/or Power output from digital or analogue readings
- Water depth will in some vessel be measured by an echosounder, but some vessels have only access to depth information from the chart or ECDIS
- Fuel consumption measured by a flow meter though many vessels only monitor the fuel consumption by manual tank readings or by summing up bills from the weekly bunker purchases.

Other operational parameters necessary for evaluating the energy efficiency can be available on board in varying number.

To improve the performance or the energy efficiency of the ferry requires that the current energy consumption is mapped and known – then energy-saving initiatives and best practices must be identified. Therefore, various operations of the ship and the use of equipment must be carefully

examined. Monitoring systems are therefore a must. A range of commercial energy performance systems are available at the marked, e.g. Vessel Performance Solutions, www.vpsolutions.dk, Kongsberg Vessel Performance, www.kongsberg.com/digital/kognifaiecosystem/kognifai-market place/maritime/vessel-performance, Marorka Marine Energy Management, www.marorka.com, and the performance monitoring system SeaTrend, www.forcetechnology.com/en/services/onboard-decision-support-system. The problem is that these systems are mostly develop for long-distance sailing and cannot directly be used onboard working vessels or ferries. Only very few systems can handle these vessels, one of these is developed by Insatech, www.insatechmarine.com. The company's focus is on visualising data about fuel management and operation – they deliver a full package ranging from instrument installation, data collection and visualisation. BlueFlow, www.blueflow.se, has also developed an energy management package special for smaller ferries.

The biggest problem is however, for both newer and older ferries, that, even when data is monitored, it is not stored, and very few ferry companies have resources to invest, and monitoring systems are therefore seldom installed in these vessels. Many of the ferry companies having installed performance systems struggle to find time for analysis and lack more in-depth training of crew on how to convert data into systematic evaluations of energy use and optimized daily operational practices.

2.3 Parameters influencing Energy efficiency

This section considers energy savings or energy efficiency initiatives that can be considered during all modes when the ship is in operation. The description will include parameters that will influence the performance of ferries and only parameters that are easy to measure and evaluate. It is therefore not a fully thorough list of parameters to be evaluated for a detailed analysis of parameters affecting the resistance of the vessel. The external environment conditions as wind, sea and current are unchangeable and the crew must adapt to the conditions at the present time. As the route normally is short and the time relatively fixed, it will in most cases not be possible to change the navigational conditions great, but it is of most importance that the crew know the influence. The course and speed must be adjusted by increasing or decreasing the speed to the suitable level. Fouling at the hull will have a great influence at the energy consumption. The smoother the hull is the lesser the resistance will be, and thereby it will sail faster for the same power output. The draught and trim will affect the resistance. Most vessels are designed for a specific amount of cargo giving a specific draught and for a given draught there also exists a trim, that minimises the propulsion power. For a ferry with frequent arrivals and short passages the trim issue will be considered during loading, but it will normally not be a parameter for optimization due to time limitation.

During all modes a general instruction is to use the equipment most efficient. Reduce idling mode, start when needed and be aware of running equipment in most optimal load configuration. Be aware of the hotel load, turn off light, heat, and other electrical equipment when not in use.

The energy consumption in harbour is relatively low compared to the consumption in other modes, but the length of the port stay may have a big impact on the subsequent passage, where most of the energy is consumed. Minimising the time in harbour and instead using the saved time for an increase in passage time allows for a decrease in speed and thereby a lower fuel consumption and less emissions. Therefore, when analysing energy-efficiency initiative in the harbour mode, it is important not just considering directly energy saving issues but also to consider time reduction proposals.

Manoeuvring in the harbour is normally done manually and the length of the docking operation can vary greatly. The vessel is operated under conditions restricting the vessel's movements and maybe also traffic congestion. The use of engines and thrusters must be carefully considered. The on/off switching must be considered such that idling is avoided. At the same time, it is also very important that the navigator is fully confident with the situation – safety is the most important factor. Manoeuvring the vessel is both time and energy consuming and more attention to the mode can probably increase the time for passage and thereby reducing the speed and energy consumption. It is important to evaluate this in more detail for the individual vessel and route. Will a short manoeuvre running the equipment in

high load be better than a longer manoeuvre with low equipment intensity? In the first case the vessel will have more time for the passage, but will this compensate for the extra energy used for the "aggressive" manoeuvre?

During sea passage the parameters can be separated into two main topics. One regarding the engine – running the engine with optimal settings and adjust the speed to allow for "just in time" arrivals. Navigational considerations are also important for obtaining an energy efficient operation. In most ferries the voyage is pre-defined, and the same procedures have been followed for years. But is this the optimal route under all circumstances - the crew should maybe re-consider the navigation. If the vessel is passing areas with shallow water, it must also be evaluated if it is advisable to slow down the vessel in this specific area and thereby reduce the resistance. If avoiding passing these low water areas is possible a route change might be a good solution, but this must be analysed in more detail.

2.4 Importance of Crew skills and training

Monitoring systems are essential, but as it is the crew on board that operate the ship, their daily work practices play a significant role. It is important that the crew understand the basics of energy efficient operation and achieve the necessary training, which is emphasized in studies by *Banks et al. (2014), Jensen et al. (2017)* and *Hansen et al. (2020)*. Installation of monitoring equipment on board must be followed by training *Viktorelius and Lundh (2019)* and *Jensen et al. (2018)*, if the system is not intuitive to use or if the output is not meaningful for the crew, the system will not be used as expected. On board smaller ferries it will primarily be the crew themselves that will evaluate the output, and upon this plan for operational changes.

3. Case study - Exploring the energy efficiency of a small ferry - Data collection

A case study of a small Danish ferry is conducted to illustrate the great potential for energy savings to be achieved using digital performance data and operational optimization.

3.1 The ship and the route

The ferry, Fig.2, is sailing in the area south of the island Funen in Denmark, Fig.3. The trade is in between the city of Svendborg and the two smaller islands Skaroe and Drejoe. The ferry has on a normal day 8 voyages from Svendborg to Drejoe and return – which is expanded with an evening voyage Friday, Sunday and holidays. The sailing time is fixed to 75 minutes.

Name	m/f Hoejestene
IMO	9169794
Built/Yard	1997/ Tórshavnar Skipasmiðja
LOA	31.00 m
B	10.00 m
Draught	2.10 m
Service speed	11.6 kn
Engines	2 x 750 kW Volvo Penta

Fig.2: Ferry characteristics

The area is heavily trafficked by smaller leisure boats in the peak period in the summer and outside this period there is very little traffic in the area. The ferry is staying overnight at Drejoe. The Skaroe stay may in the winter season be skipped in case of no passengers to and from the island. This information is conveyed to the vessel by a telephone call.

The waters are confined with very little sea state even with high winds. The water depths are changing with very low water depths in some areas on the route. The current conditions change along the route

and is difficult to predict, due to the high dependence on the wind conditions. The magnitude of the current can vary up to 5 knots in peak periods. Between the two islands the ferry passes through a channel "Hojestene", which is very narrow, and it is difficult for two vessels to pass at the same time. The water depth is very low in this area, and the vessel experience a great influence from the shallow water effect. The current is not pronounced in this area.
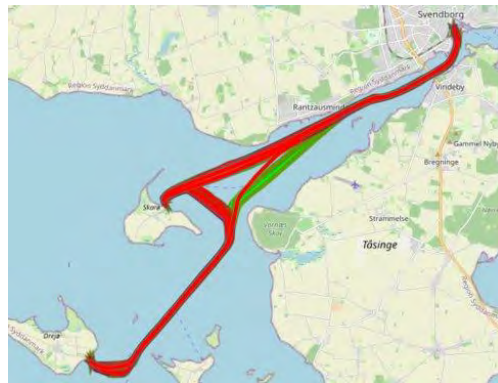

Fig.3: The Route. Svendborg – Skaroe - Drejoe

3.2 Performance data collection and visualization

The fuel consumption was not measured on board when the project was initiated. As this parameter is essential a flowmeter was installed. All other measures were identified, and an automated data logging solution was installed. Data is logged and transmitted to a cloud server where it is accessible for researchers, crew, and route leaders via a software application developed by the University of Southern Denmark, Fig.4. As the vessel is relatively old, only few parameters are possible to measure and log. The following data were found accessible and measurable on board (all logged every 30 s):

- Position (from ECDIS)
- Heading - over ground (from ECDIS)
- Speed - over ground (from ECDIS)
- Dept (echo sounder)
- Wind – direction and speed (anemometer)
- RPM from starboard and port engine (ME tachometer)
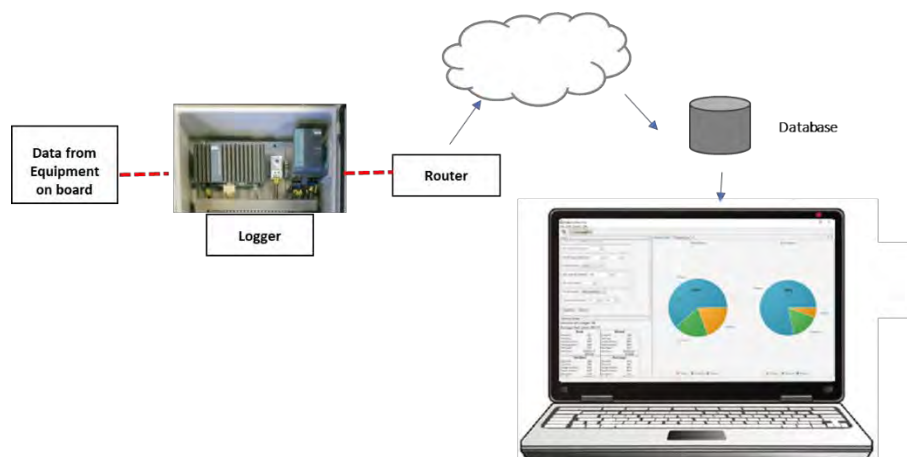- Fuel consumption starboard and port engine (flowmeter)

Fig.4: Dataflow – from equipment to computer

The current – direction and magnitude – is not measured in the area. It is possible to receive prognosis current information from meteorological institutes, but as the current is very wind dependent in the area these data must be used with caution. Current direction and magnitude can be estimated if speed through the water is measured. Unfortunately, a log is not installed onboard, only speed over ground is registered.

A software module has been developed to create transparency and insights into vessel operations and performance. This enables the user to select and filter imported data sets with respect to a given period, sailing conditions and operational modes with the purpose of viewing, or plotting operational performance for one or more variables. The system enables the officers on board or shore staff to identify the most environmentally friendly way of operating the ship. The system is not a real-time decision support system, but a system for evaluating and reflecting on voyages in order to determine best operational practices.

The presented study shows the results of analyses of more than one year of logged data from operations of the ferry.

3.3 Voyage information

The current analysis is based on data collected onboard during the whole year of 2020, from a total number of 2945 voyages. The distribution of time and fuel spent in the different modes can be seen in Fig.5. The distribution of the three modes passage, manoeuvre and harbour is respectively 56%, 11% and 34 % for the time and 79%, 13% and 9% for the fuel consumption.
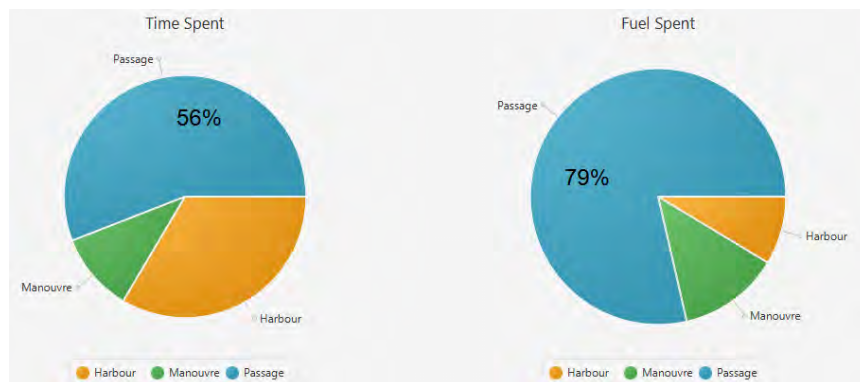
Fig.5: Time and fuel spent in different modes

Table I: Voyage information for 2020

	Voyages	Average	Minimum	Maximum
Drejoe-Skaroe-Svendborg	1313			
Fuel [litre]		90	64	129
Time [minutes]		66.5	69	67.5
Svendborg-Skaroe-Drejoe	1334			
Fuel [litre]		96	62	136
Time [minutes]		68.5	72.5	84.5
Drejoe-Svendborg	160			
Fuel [litre]		65	35	85
Time [minutes]		57.5	61	60
Svendborg-Drejoe	138			
Fuel [litre]		64	35	104
Time [minutes]		58	63.5	59

The number of individual voyages including voyages where the island Skaroe has been skipped can be seen in Table I. The average, minimum and maximum fuel consumption and time used are also shown in the table. The large variation in fuel consumption – difference between minimum and maximum - can be due to parameters that cannot be changed such as different external conditions as wind or current, and traffic congestion, but it may also be due to the way of operating the ferry, this will be analysed further in Section 4.

3.4 Challenges identified

Based on interviews and observations, onboard, the researchers identified a set of challenges with respect to operations and energy efficiency. It was seen that the ferry crew rely on their training, experience and assumptions about parameters influencing the operation, and how this impact the fuel consumption. There has been no tradition for documenting operations or monitor the effect of actions taken. The effect of wind, water depth and currents have been based on assumptions and more related to safety, passenger comfort and schedule adherence than to performance. No documentations or baselines for e.g. speed or RPM versus fuel consumption are available, and therefore there has been no link in between engine settings and consumption. The apparent difference in fuel consumption on different voyages, see Section 3.3, calls for a deeper analysis of root causes. Unfortunately, factors that may influence the performance as e.g. navigational difficulties or late departures due to a large number of cars or passengers are not registered today, therefore the analyses must be based on logged data only.

4. Case Study - Exploring the energy efficiency of a small ferry - Performance Analysis

Four different analyses have been chosen for illustration. Analyses that will provide the crew with useful information and knowledge, which can help them to evaluate and improve the performance of the ferry in the future.

The four analyses:

- Baselines - creation
- Shallow water effect on speed and fuel consumption
- Wind effect – added resistance and fuel consumption
- Time schedule analysis

All analyses are based on data logged on board the vessel during the year 2020 – a total of 2945 voyages. The visualization software described in Section 3.2 has been used to extract data for further analyses.

4.1 Baselines - Creation

Baselines for speed and engine relationship did not exist for the vessel, therefore a new set of curves for were created based on measured and logged data.

- Speed (over ground) versus fuel consumption
- RPM versus speed (over ground)
- RPM versus fuel consumption

Data filtering have been applied to eliminate influencing factors from wind and water depth (heavy sea is normally not present in the area). The resulting deep water, calm sea baseline curves can be seen in Figs.6 and 7. Here data from one year of logging has been fitted by polynomials to the best curve. Speed/fuel polynomial of degree 3, RPM/speed degree 2 and finally RPM/fuel degree 3. Fig.6, left, shows the fuel consumption as function of the speed. Right diagram in Fig.6 shows the average speed distribution for all voyages. The fuel consumption curve is dramatically steep in the operational area of about 10 kn. Meaning that just a small speed increase will result in a large fuel increase. For example, will a speed increase from 10 to 10.5 kn gives increased consumption of approximately 20%.
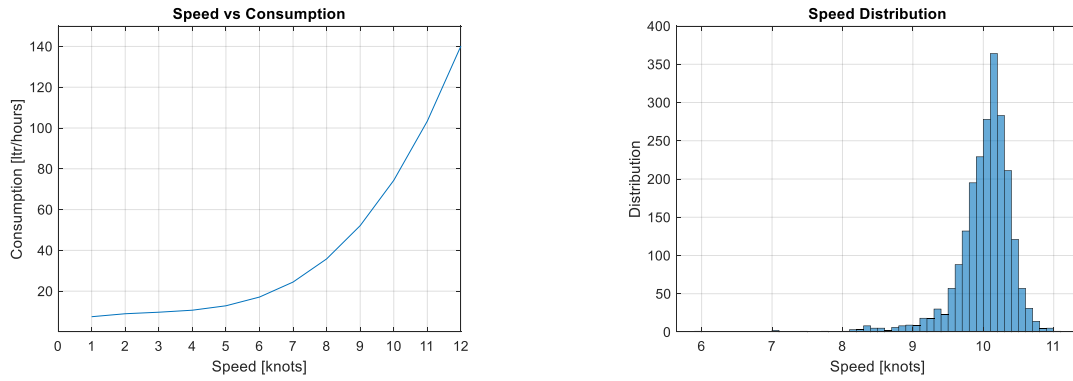
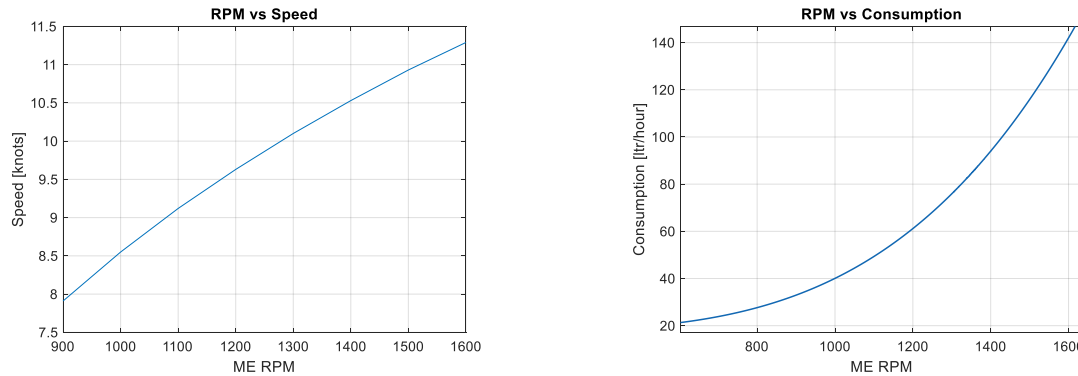Fig.6: Left: Fuel consumption versus speed. Right: Speed distribution

Fig.7: Baselines for the vessel. Left: RPM versus speed. Right: RPM versus fuel consumption

Fig.7 left and right show the RPM versus speed and fuel consumption respectively. The RPM curves will be a very useful tool for the crew on board most vessels, as it is the RPM setting that will be the input factor when they change the speed of the vessel.

4.2 Shallow water effect on speed and fuel consumption

The vessel is passing several areas where the water depth is low. The low water depth greatly influences the vessels speed for given RPM. Fig.8 shows the depth below keel and speed of the vessel when passing the "Hoejestene" channel. The figures show that passing areas with a depth between 3.5-4.5 m, the shallow water effect will result in a relatively large speed reduction.
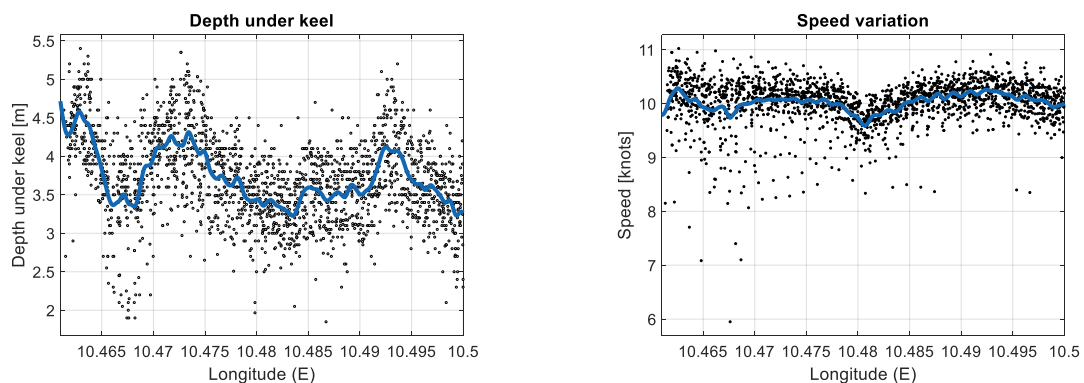
Fig.8: Left: Depth below keel, measured. Right: Vessel speed passing the channel

Fig.9: shows the speed versus the fuel consumption for varying water depths. The deep-water baseline curve is shown for comparison. It can be seen, that if RPM (and thereby the fuel consumption) is maintained as given for 10 kn, it will result in a speed reduction of about 4%, 8% and 15% for water depths of 8 m, 6 m and 4 m, respectively. If on the other hand a speed of 10 kn is maintained when

passing the channel, the increased fuel consumption will be 8%, 24%, and 70% for the same water depths.
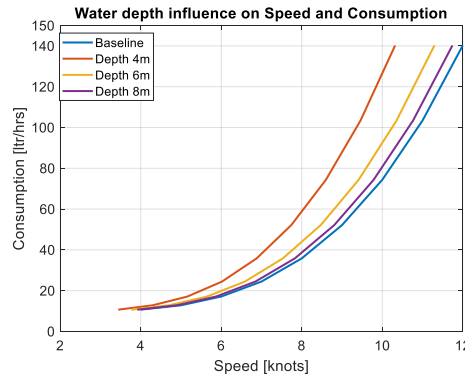
Fig.9: Fuel consumption as function of speed for various water depths

4.3. Wind effect – added resistance and fuel consumption

The axial wind force acting at the ship can be determined by:

$$R_x = \frac{1}{2}\rho_A C_x A_{VT} V_R^2 \tag{1}$$

ρ_A is the mass density of air, C_x the axial wind force coefficient, A_{VT} the projected area of the ship above the waterline and V_R the relative wind velocity. The axial wind force coefficient C_x can be determined by through model tests in wind tunnels, but in cases where these tests are not performed, the coefficient can be estimated by use of general equations. Here the empirical method suggested by *Isherwood (1973)* is used. Isherwood analyzed a number of wind tunnel tests on various ship types. Data from the tests were analysed by multiple regression techniques and was fitted to an equation for the axial wind force coefficient C_x:

$$C_x = A_0 + A_1 \frac{2(A_L + A_{SS})}{LOA^2} + A_2 \frac{2A_T}{B^2} + A_3 \frac{LOA}{B} + A_4 \frac{S}{LOA} + A_5 \frac{C}{LOA} + A_6 M \tag{2}$$

LOA is the length overall, *B* the breadth, A_L the lateral projected wind area, A_{SS} the lateral projected area of superstructure and deck cargo, A_T the transverse projected wind area, *S* the length of perimeter of lateral projection (excluding waterline and slender bodies), *C* the distance from bow to the center of lateral projected area and *M* the number of distinct groups of masts or king posts.

The constants A_0 to A_6 are derived from tests and can be found tabulated in *Isherwood (1973)*. The specific ship related constants are determined from general arrangements drawings of the vessel.

LOA	*B*	A_L	A_{SS}	A_T	*S*	*C*	*M*
35 m	10 m	170 m²	25 m²	80 m²	80 m	17 m	1

Fig.10 shows diagrams for the axial wind force coefficient and axial wind force for the ferry Hoejestene. Both values are shown as function of the relative wind direction.

The relative wind is measured by an anemometer on board the ferry Hoejestene. Fig.11 shows the distribution of the relative wind parameters, direction, and speed, for the year 2020. Left figure shows the wind for passage through the channel "Hoejestene", the right for the passage of the sound between Funen and the Island Taasinge. It can be seen that westerly winds are dominant, and that the vessel will be in the lee of land when passing the sound.
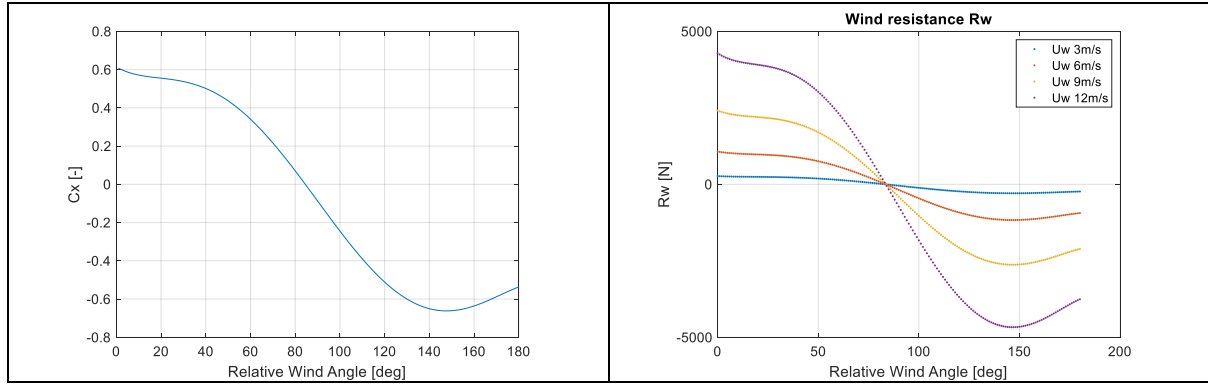
Fig.10: Left: The axial wind force coefficient. Right: The axial wind force (Hoejestene)
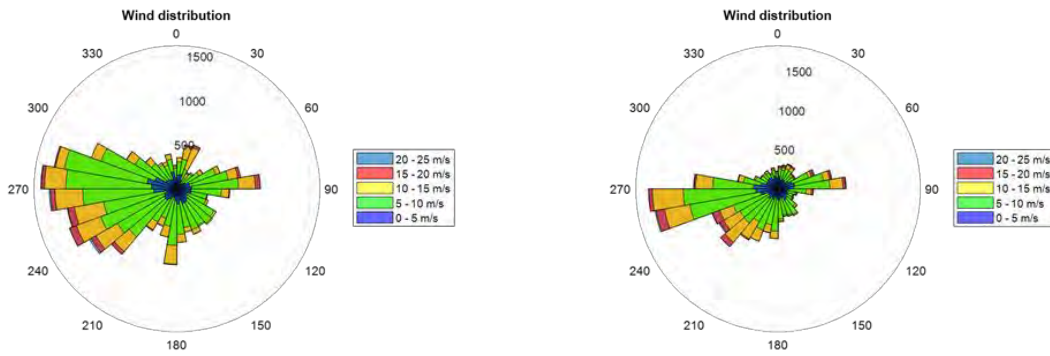
Fig.11: Wind distribution, relative wind – left channel, right sound

The extra power due to the wind resistance can be determined

$$\Delta P = R_x \cdot V \qquad (3)$$

Unfortunately, no SFOC curves are available for the engines on board but knowing the engine type and size a good estimate can be made for the extra fuel consumption due to wind. Figure 11 shows the fuel consumption as function of the vessels speed. The baseline is shown together with two examples of sailing in head wind with a measured relative wind at 6 and 12 m/s respectively. The figure shows that sailing at 10 knots and measuring a relatively wind from ahead of 12 m/s (corresponding to an absolute wind speed of 6.9 m/s ~ Beaufort 4) the fuel consumption will increase with approximate 8%. If a relative wind of 6 m/s is measured (~Beaufort 1) the increase will be approximately 3%.
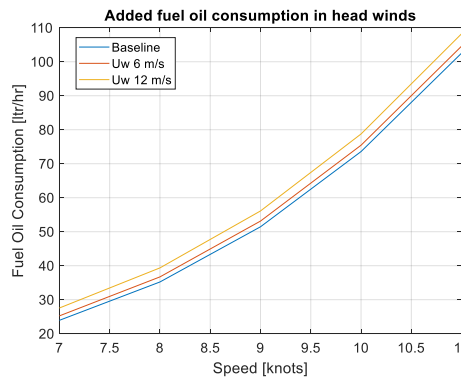
Fig.11: Fuel consumption as function of vessel speed, baseline and in head wind

59

4.4. Time schedule analysis

Analysing all voyages during 2020 shows that for voyages Drejoe-Skaroe-Svendborg (both directions) the average fuel consumption is between 90 and 96 litres and the transit time used is below 70 minutes. There can be reasons for not using the scheduled 75 minutes e.g. because of extended harbour stay due to many passengers in summer vacation. The main reason is probably that the crew onboard are not aware of the sailing condition for the whole coming voyage and therefore sail with a slightly higher speed than necessary to avoid being late for the next arrival. Today the crew does not have any instruments available that can help them to evaluate the coming voyage and thereby adjust the speed to arrival "just-in-time". Data shows that the ferry arrives about 5 minutes to early in most voyages. If these in-effective minutes are converted to sailing time – the speed of the vessel can in average be reduced from 10.2 to 9.3 knots and the fuel consumption by not less than 20%. Here the baseline curve for speed versus fuel consumption, see section 4.1, is used for estimation.

The analysis shows that if the island Skaroe is skipped, see Table 1 in section 3.3, the fuel consumption can be reduced by nearly 30%. Additionally, for these voyages the scheduled voyage time is not fully used, and the vessel will often arrive more than 10 minutes before scheduled.

6. Discussion

To improve the performance or the energy efficiency of the ferry requires that the crew has tools to help them estimate the fuel consumption and to be able to identify and evaluate energy-savings and cost-effective initiatives. The present study has shown that it is possible to provide a relative old ferry with enough information to estimate their performance. The crew did not have any information related to the fuel consumption and they relied on their assumptions about parameters influencing the operation. The study has shown that with just measuring a few data systematically, it is possible to provide the crew with valuable information.

The baseline curves for speed and engine relationship were created. These curves are of greatest importance when estimating the vessel performance. The baseline curves are very illustrative, and they give the crew information about how even smaller speed reductions can reduce the energy consumption dramatically. Sailing at shallow water at some areas of the route must be taken into account when planning the whole voyage. The shallow water analysis clearly shows that it is important to consider the speed setting through the area. The external environment conditions as wind, sea and current are unchangeable and the crew must adapt to the conditions at the present time of the voyage. As the route normally is short and the time relatively fixed, it will in most cases not be possible to change the navigational conditions much, but it is of most importance that the crew know the influence.

It must be remembered that the crew is very busy navigating the ship and has only limited time for voyage evaluation or optimisation. Furthermore, for the crew energy efficiency is secondary to safety on board - in operations where there is limited manoeuvrability due to traffic congestion and complex navigation, the focus is, and will always be, on safety first. Therefore, the above information is valuable for the crew and a great fuel reduction can be achieved by studying curves and evaluating the sailings, but to have the fully effect of the information a decision support tool would be preferable. The tool must be very simple to use – just a few inputs and outputs – like using an APP at their mobile phone.

Not having a decision support tool, the different speed settings can be very difficult for the crew to estimate and they will probably be sailing too fast, which the analysis also showed. The crew is not aware of the conditions for the coming voyage in total and therefore sail with a little higher speed than necessary to avoid being late for the next arrival. The tool can help the crew to adjust the speed to a suitable level. If this is done properly the vessel will arrive in due time and will not use unnecessary energy because of sailing too fast. The ferry has a schedule with fixed timeslots, therefore reducing the speed in some areas will also result in a necessary speed increase in others. During shallow water passages the speed must be reduced, increase during deep water passage, increased during strong head wind slowed down during tail wind etc.

Re-considering schedules is today an overlooked issue for smaller ferries and a lot of energy can be saved allowing for longer time at sea. Keeping the time intervals and making room for a more dynamic planning as e.g. shorter harbour stays in periods with less passenger and cargo allowing for a longer sea passage or even skipping voyages with only few passengers will reduce the fuel consumption significantly. Also, a smart and effective booking system may be useful, as knowing the number of passengers beforehand will give the crew good information about time required for the coming harbour stay.

Training the crew in being aware of energy consumers on board and in the use of digital performance tools can contribute to the savings. The importance of training the energy awareness and educating the crew within the subject has been emphasized by e.g. *Banks (2015), Jensen et al. (2018)* and *Hansen et al. (2020)*. Focus at energy communication is also an issue that requires training and special awareness, *Jensen et al. (2018).* Sharing knowledge and experiences is important for finding and develop new shaving initiative and keeping the crew involved and motivated.

6. Conclusions

The study has shown that digitalization of ship operations, even with very few data point, can be of great value when evaluating the performance of a ship.

The operational of a nearly 25 years old ferry with a length of 31 meter transporting a maximum of 98 passengers have be analysed and great energy savings potentials are found. The wind effect and the shallow water effect has been analysed and the importance of taking these factors into account have been illustrated.

The importance of using the available time – not coming too early – is shown. Currently, the vessel typically arrives 5 minutes too early - if these minutes are converted for sailing, the fuel consumption can be reduced by not less than 20%. The effect of having a good booking system have also been demonstrated. If there are no passengers for the middle Island "Skaroe", the arrival can be skipped, and the energy can be reduced by nearly 30%. Allowing for shorter harbor stays and converting harbor time to sailing time will be of great importance. The analysis showed that if the vessel can reduce the speed by e.g. half a knot – from 10.5 to 10 knots – the energy consumption is reduced by approximately 20%.

The study has been conducted upon data from a small ferry sailing in Danish waters, but it is assumed that the findings can be used as guidance for smaller ferries and vessels with shorter sea passages worldwide.

Acknowledgement

References

ARO, E.; RYTTER, N. G. M.; ITÄLINNA, T. (2020), *Maritime industry processes in the Baltic Sea Region: Synthesis of eco-inefficiencies and the potential of digital technologies for solving them*, ECOPRODIGI Project, https://ecoprodigi.eu/wp-content/uploads/2020/02/ECOPRODIGI-Research-Report-1-2020-final.pdf

BANKS, C.; TURAN, O.; INCECIK, A.; LAZAKIS, I; LU, R. (2014), *Seafarers' current awareness, knowledge, motivation and ideas towards low carbon-energy efficient operations*, J. Shipping Ocean Eng. 2, pp.11-20

BANKS, C. (2015), *Operational Practices to Improve Ship Energy Efficiency*, PhD Thesis, University of Strathclyde

DNV GL (2015), *Energy Management Study 2015*, Technical report, DNV GL, Hovik, www.dnv.com/maritime/publications/energy-management-study.html

ERIKSEN, S.; LÜTZEN, M.; JENSEN, J.B.; SØRENSEN, J.C., (2018), *Improving the Energy Efficiency of Ferries by Optimizing the Operational Practices*, RINA Full Scale Ship Performance Conf., London

HANSEN, E.K.; RASMUSSEN, H.B.; LÜTZEN, M. (2020), *Making shipping more carbon-friendly? Exploring ship energy efficiency management plans in legislation and practice*, Energy Research & Social Science 65, [101459]

IMO (2018), *Note by the International Maritime Organization to the UNFCCC Talanoa Dialogue*, https://unfccc.int/sites/default/files/resource/250_IMO%20submission_Talanoa%20Dialogue_April%202018.pdf

ISHERWOOD, R.M. (1973), *Wind Resistance of Merchant Ships*, RINA Transactions 16

JENSEN, S.; HANSEN, E. K.; LÜTZEN, M. (2017), *An Educational Design for Energy-efficiency Ship Handling*, Global perspectives in MET: Towards Sustainable, Green and Integrated Maritime Transport Vol 1, pp.450-459

JENSEN, J.B.; HANSEN, E.K.; LÜTZEN, M., (2019), *Optimising the Energy Efficiency of Small Ferries*, Proc. Int. Association of Maritime Univ. (IAMU), 20th Annual General Assembly, Tokyo

JENSEN, J.; LÜTZEN, M.; MIKKELSEN, L.L.; RASMUSSEN, H.B.; PEDERSEN, P.V.; SCHAMBY, P. (2018), *Energy-efficient operational training in a ship bridge simulator*, J. Clean. Prod. 171, pp.175-183

JOHNSON, H.; JOHANSSON, M.; ANDERSON, K. (2014), *Barriers to improving energy efficiency in short sea shipping: an action research case study*, J. Clean. Prod. 66

JOHNSON, H.; STYHRE, L. (2015), *Increased energy efficiency in short sea shipping through decreased time in port*, Transportation Research Part A: Policy and Practice 71, pp.167-178

LÜTZEN, M.; MIKKELSEN, L.L.; JENSEN, S.; RASMUSSEN, H.B. (2017), *Energy Efficiency of Working Vessels: A Framework*, J. Cleaner Production 143, pp.90-99

POULSEN, R.T.; JOHNSON, H. (2016), *The logic of business vs. the logic of energy management practice: understanding the choices and effects of energy consumption monitoring systems in shipping companies*, J. Clean. Prod. 112 (5), 3785e3797.

VIKTORELIUS, M.; LUNDH, M. (2019), *Energy efficiency at sea: An activity theoretical perspective on operational energy efficiency in maritime transport*, Energy Res. Soc. Sci. 52, pp.1-9

Calculating Speed Loss Due to Swell using CFD

Inno Gatin, In silico d.o.o, Zagreb/Croatia, inno.gatin@cloudtowingtank.com
David Boxall, WaveForce, Ziethen/Germany, info@waveforce.info

Abstract

When analysing the performance of a vessel in seaway, wind waves are taken into account in different ways. However, swell is usually left out of the equation. Swell can be of significant height, and wavelength that is close to the length of the vessel, and thus represents a significant source of added resistance in some cases. On the other hand, swell can be well represented with a single wave frequency, which makes it easier to model numerically. In this paper we will investigate how much speed can be lost due to swell using CFD simulations.

1. Introduction

Even though swell can have a significant impact on the performance of vessels at sea, it is often not considered when making commercial performance assessments by weather routing companies (WRC). Since these companies have become the de facto standard to measure the performance of vessels at sea, this often leads to performance claims being put forward by the characters to owners, that are inaccurate because the swell component is ignored. This is although vessels are often not warranted in swell, or where they are, that the swell factor is not calculated by the WRCs.

In time-charterparties (i.e. contracts between charterers and the shipowners regarding the charter of the vessel), vessels are described as being able to perform in defined good weather conditions. Each segment of shipping has their own usual definition of 'good weather' with tankers being the simplest: usually just a Beaufort number. Under such conditions then good weather periods are very easy to observe. With dry bulk vessels, the definition of good weather is rather more involved. The definition of "good weather" is agreed upon in the charterparty; often by reference to Douglas Sea State which is a sea state of a local sea without the influence of swell. WRCs often present just a swell height in their reports and allow themselves to consider whether swell heights above or below a certain limit are considered in or out of good weather. The trouble is how to set a threshold of swell height above which the performance is not guaranteed. According to most charterparties, any measurable swell would disqualify the conditions as good weather. This is because the effects of swell are swallowed up in the WRC methodology, but if they would be analyzed and given a value, this would change the performance speed of the vessel and in most cases reduce the claim - or possibly be the difference between there being a claim or not.

Despite this, many WRCs simply ignore the swell, *Morska et al. (2010)*. Most WRCs issue their reports based on their own methodology that is only loosely based on the warranted terms that the owners and charterers have agreed amongst themselves in the charterparty. WRCs are usually employed as a subcontractor to measure a vessel's contractual performance but instead end up monitoring the vessel on their own terms and do not follow the actual contractual terms. Any arguments on the topic of the influence of swell on the vessel performance are difficult to make because the charterers do not, in most cases, understand how the reports of WRCs have been prepared. It is not easy to establish the effect of swell on ship speed, but it is certainly possible. However, wind waves are usually defined either in terms of mentioning a specific maximum height, or by reference to the Douglas Sea State itself and are therefore easier to include in 'good weather'. This is why voyage periods of good weather where only a significant wave height is recorded are not relevant when analyzing whether the vessel performs as warranted because the swell component has been lost in the significant wave height - being a combination of wind waves and swell.

The aim of this paper is to quantify the effect the swell has on ship speed. The study is performed for two actual claims with two different drybulk vessels, a Handysize and a Capesize, where the goal is to

investigate the extent to which swell caused the claimed underperformance of the vessel. For this purpose, Computational Fluid Dynamics (CFD) is applied on this problem taking into account the nonlinear nature of the flow around the vessel and its motion in regular swell waves. Software called the Naval Hydro Pack is used for all simulations.

2. Numerical method

The Naval Hydro Pack is a CFD software based on collocated Finite Volume method which uses Level Set for interface capturing. Special discretisation techniques are employed based on the Ghost Fluid Method to guarantee high accuracy of the two-phase flow model *Vukčević et al. (2017)*.

For a simulation of a vessel in oblique regular waves, a self-propelled vessel is simulated with three degrees of freedom: heave, pitch and roll. The ship's propeller is modelled using the actuator disc model where a pressure jump is prescribed on a circular surface representing the propeller. The key feature of the algorithm is the ability to assess the undistorted propeller inflow velocity without the need to perform a separate open water calculation *Jasak et al. (2018)*. For simulations in waves, regular waves are generated in CFD using Stokes second wave theory. Waves are introduced into the CFD domain and damped out of it using implicit relaxation zones, *Jasak et al. (2015)*.

2. Approach procedure and assumptions

The approach to calculating speed loss of ships in swell is outlined here, together with some important assumptions necessary to carry out the analysis. Given that the actual geometry of the two vessels at hand is not available in the form of CAD files, a similar vessel geometry is used which is scaled to correspond to the parent geometry. The replacement CAD geometry corresponds to the publicly available Japan Bulk Carrier (JBC) hull model, due to its similar hull form and characteristics compared to the two vessels. By applying affine transformation to the JBC model, the following characteristics correspond exactly between the parent hull and the JBC CAD model:

- Displacement of the vessel,
- Inertia of the vessel,
- Overall dimensions: breadth, and draft,
- Propeller characteristics,

while small differences in length are allowed (< 0.5%). The JBC vessel has a similar stern shape and bulbous bow compared to both the Capesize and Handysize in this study. The following assumptions are posed to justify the use of another hull form for the study, rather than the geometry of the actual vessel:

1. Swell waves have wave lengths of the same order of magnitude as the length of the vessel.
2. Main vessel dimensions, mass and inertial properties are dominant parameters determining the behaviour of the vessel in these waves, rather than local details of the hull form.
3. A relative difference in speed of the transformed JBC hull is comparable to the difference in speed of the parent hull, i.e. the relative differences in resistance in calm water and in waves are comparable, even if the JBC hull form and the parent hull form will not have the same calm water resistance.

The procedure of determining the speed loss of the vessel in swell comprises the following steps:

1. Calculating the delivered shaft power P_D and RPM at minimum warranted ship speed V_{min} in calm seas,
2. Applying the RPM calculated in calm seas to swell conditions and calculating the average speed V_S achieved by the vessel.

By using this approach, where the same method is used to compute the speed in calm water and in waves, the quality of comparison is ensured since both results are obtained in comparable conditions. The only difference between the results is the swell, which is absent in the calm water simulation. The effects of ship and propeller fouling, wind, hull production imperfections and others are mitigated, and their effect does not impair the quality of the present comparison. Both the calm water and the simulation in swell assume perfectly smooth hull (hydrodynamically smooth) without imperfections, and conditions without wind. This provides a leveled ground for comparison of the two calculations. The difference in speed therefore must be a consequence of swell alone.

3. Vessel characteristics

The subject of the study are two vessels: a Capesize and an Handysize vessel. Their main particulars are shown in Table I: and Table II, respectively. The loading conditions for both vessels are selected as averages reported on the voyage segments which were the subject of charter's claims towards the owners. The tables also contain the particulars of the scaled JBC to fit the corresponding vessel's main characteristics. It can be seen that very good similarity is achieved indicating that the hull forms are similar in shape, allowing for the scaled JBC to have similar length for the same displacement.

Table III lists the swell characteristics for both vessels, including the height, period, length, and direction of the swell. The swell characteristics correspond to the actual conditions present on the claimed voyage periods of both vessels, as reported by the ship's log and hindcast data. The ships are simulated with the rudder and a propeller. Fig.**1** shows the JBC vessel with the rudder in side view.

Table I: Capesize vessel main particulars

	Original vessel	Scaled JBC
L_{WL}	282.20 m	281.00 m
B	45.00 m	45.00 m
T	7.35 m	7.35 m
∇	75 814.8 t	75 814.2 t
V_{min}	13.0 kn	N/A

Table II: Handysize vessel main particulars

	Original vessel	Scaled JBC
L_{WL}	194.00 m	193.80 m
B	32.26 m	32.26 m
T	12.48 m	12.48 m
∇	68 009.0 t	68 009.0 t
Trim	0.90 m	0.90 m
V_{min}	13.0 kn	N/A

Table III: Swell characteristics

	Capesize	Handysize
Swell height H	1.51 m	1.70 m
Swell period, T_S	9.0 s	10.0 s
Swell length, L_S	126.50 m	156.10 m
Swell direction	160°	337°
Vessel's heading	187°	293°
Effective period, T_E	6.32 s	7.85 s

Fig.1: Side view of the vessel

4. Analysis and results: Capesize vessel

In this section the results of the analysis of speed loss in swell for the Capesize vessel are presented. The simulation in calm seas is conducted with minimum warranted speed of 13 kn, while the RPM of the propeller is the unknown that is sought for. Along with RPM, the thrust, torque, thrust power and delivered power of the propeller are also calculated. Table IV: shows the results in tabular form, while Fig.2 shows images of the simulation: perspective view from the bow, from the stern, and top view of the wave field generated by the vessel, respectively.

Table IV: Results of the self-propulsion simulation in calm sea for the Capesize vessel

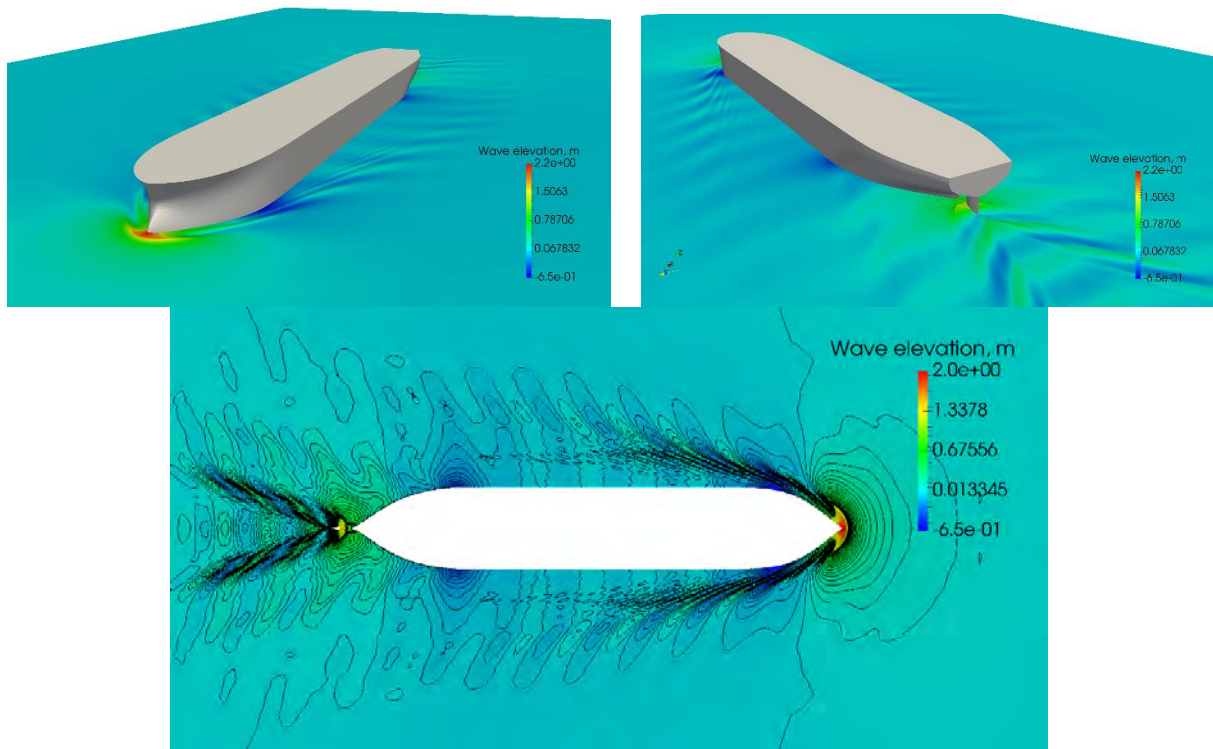|	
Propeller thrust T	859.05 kN
Propeller torque Q	895.61 kNm
Thrust power P_T	3172.8 kW
Delivered propeller power P_Q	5944.7 kW
Propeller rotation rate	63.36 rpm

Fig.2: Flow field calculated for the Capesize vessel in calm seas

As explained above, the RPM calculated in calm seas are applied to the vessel sailing in swell which was reported at the time of the voyage segment in question, shown in
Table III. For this case, the speed loss is calculated by allowing the vessel to surge in the numerical simulation, i.e. the speed of the vessel is not fixed. Initial speed of the vessel is set to 13.0 kn, and the vessel adjusts her speed with respect to the added resistance of swell.

The simulation in swell is carried out for 67.7 s of real time, which is 10.7 encounter periods of the swell. Speed loss is calculated for the time interval between 30 and 67.7 s, where the vessel has entered a regular sinusoidal pitch and heave motion, as well as speed. Fig.3 shows pitch and heave motion of the vessel, where the vessel undergoes small but significant motion oscillations. Roll motion is also shown, with very small oscillations that are insignificant.

Fig.4 shows the speed signal of the vessel in swell. Here, it is clearly visible that the vessel starts losing speed from the beginning of the simulation, until finally it settles in a regular sinusoidal

oscillation without changing the mean of speed. The average speed loss is 0.67 kn, with an oscillation of 0.08 kn around the mean value. Thus, the ship speed in swell is around 12.33 kn.
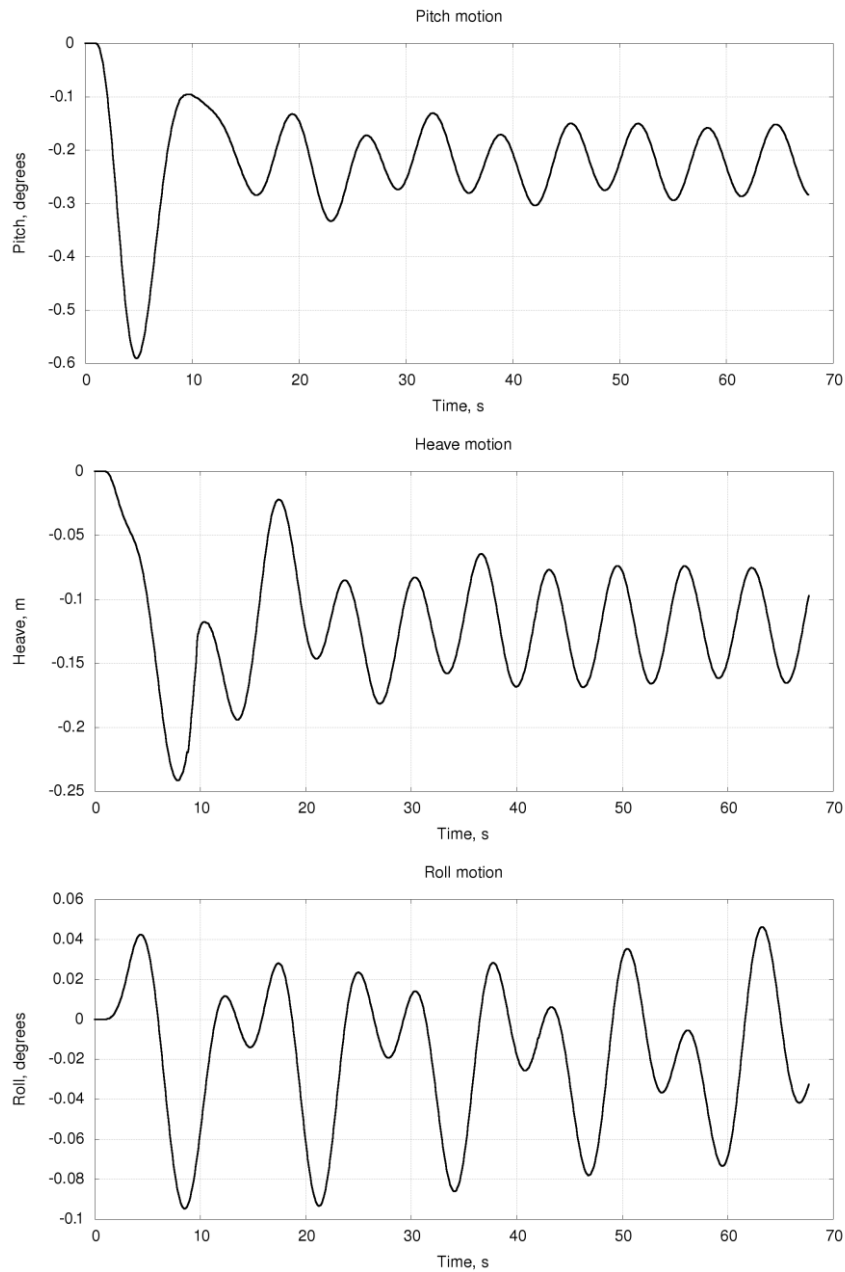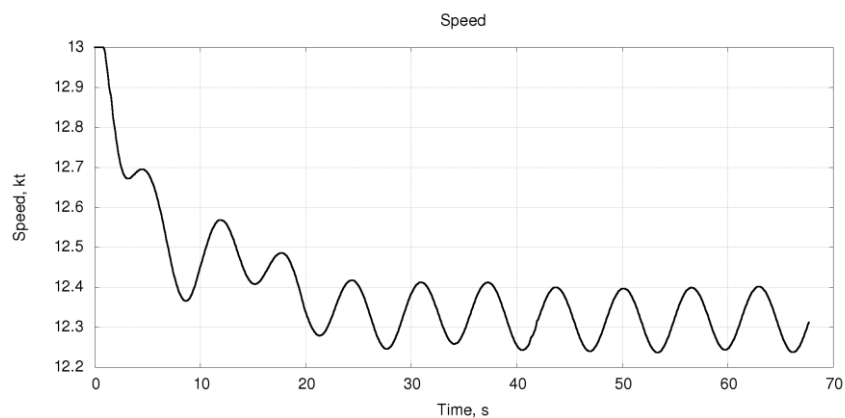
Fig.3: Motion of the Capesize vessel in swell

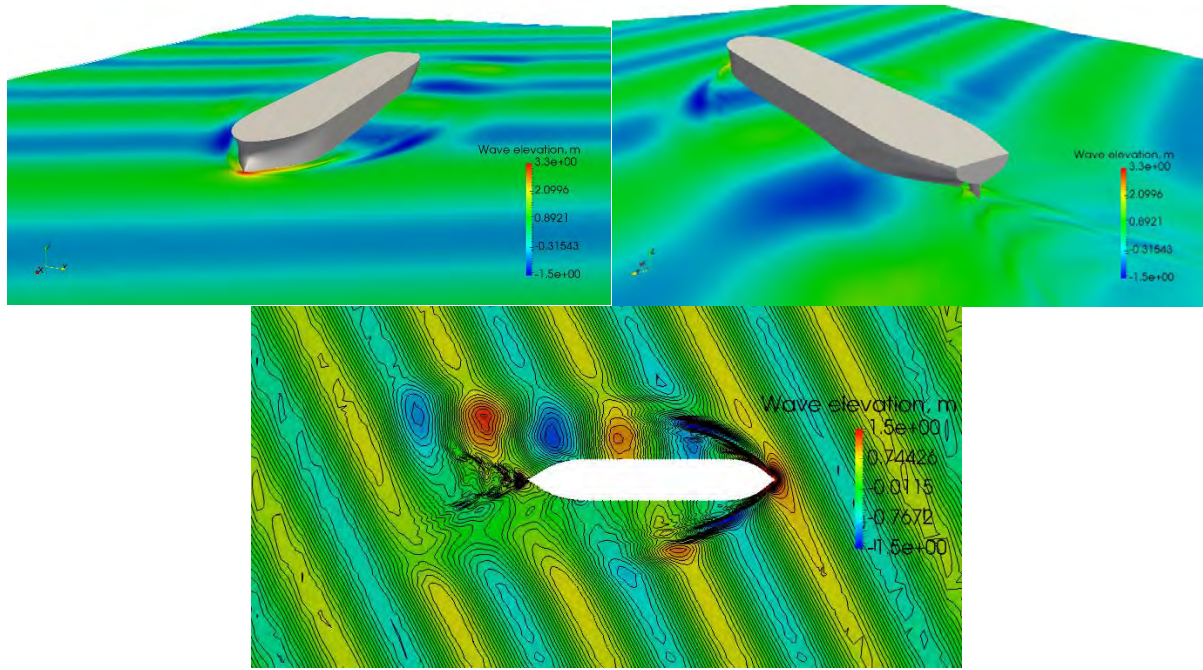Fig.4: Speed of the Capesize vessel in swell

Fig.5: Capesize vessel sailing in swell conditions

Fig.5 shows images of the vessel sailing in swell conditions, where the relation between the size of the vessel and length of the waves can be appreciated. The length of the ship is approximately equal to two wavelengths, which makes the energy transmission between the wave to the ship relatively intense. This is the reason why despite the small wave height, the swell is reducing the speed by a significant 0.67 kn.

5. Analysis and results: Handysize vessel

In this section the results of the analysis of speed loss in swell for the Handysize vessel are presented. Same as for the Capesize vessel, the simulation in calm seas is conducted with minimum warranted speed of 13 kn, while the RPM of the propeller is the unknown that is sought for. Table V shows the results in tabular form, while Fig.6 shows images of the simulation: perspective view from the bow, from the stern, and top view of the wave field generated by the vessel, respectively.

Table V: Results of the self-propulsion simulation in calm sea for the Handysize vessel

Propeller thrust T	640.1 kN
Propeller torque Q	470.4 kNm
Thrust power P_T	2587.2 kW
Delivered propeller power P_Q	5181.9 kW
Propeller rotation rate	105.2 rpm

As opposed to the approach used for the Capesize vessel for calculating speed loss in swell, where the vessel is allowed to move in the longitudinal direction in order to settle to the equilibrium speed, in this case a different approach is used, where the speed of the vessel is fixed, and three different speeds with the same imposed RPM are simulated. The reason behind this change in approach is the fact that the former approach proved to be inefficient due to a larger speed loss in this case, which caused the simulation to converge very slowly, i.e. a large amount of time would be needed for the vessel to change the speed and settle it. It is more efficient in this case to run several simulations with fixed vessel speeds, and then interpolate the tree results for the point where the average resistance is equal to average thrust generated by the propeller.
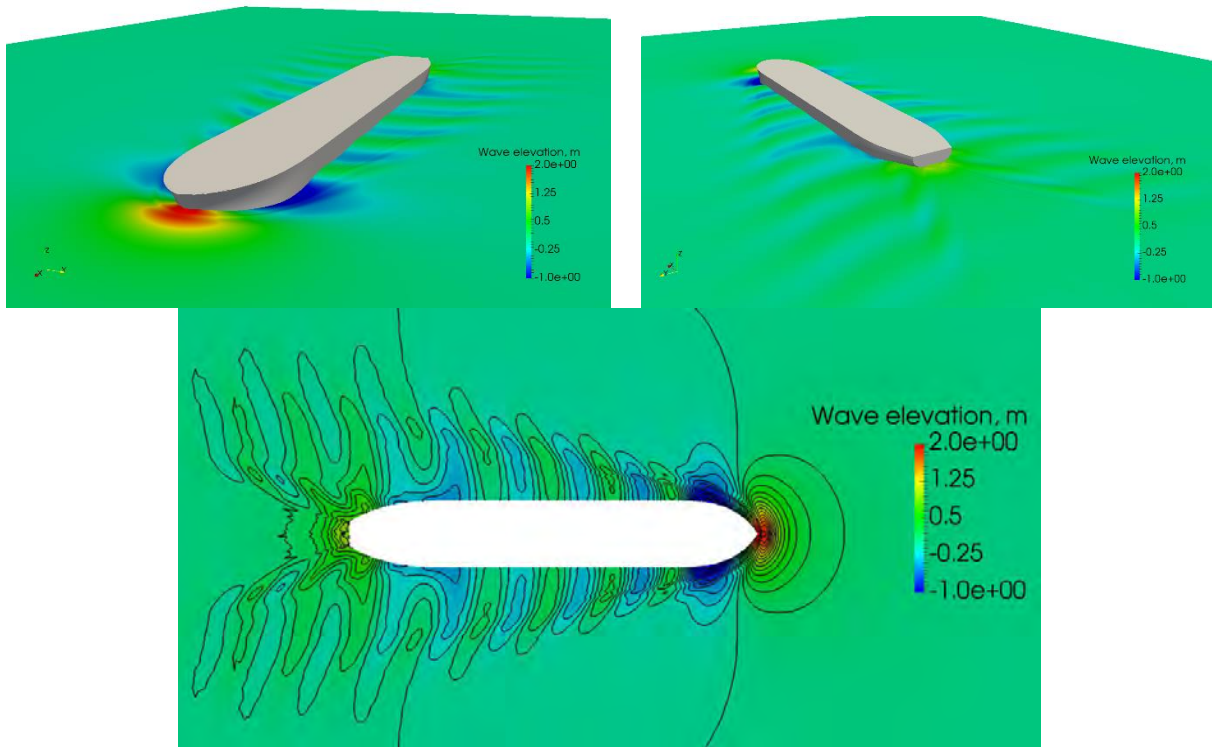
Fig.6: Flow field calculated for the Handysize vessel in calm seas

The RPM of the propeller are set to 105.18, and the vessel is simulated in swell with speeds 11, 11.5 and 12.5 kn. For the three simulations, the difference between thrust and average resistance is calculated. Based on this data, the speed at which this difference would be zero is assessed by using linear interpolation. The vessel is exposed to swell and it is allowed to pitch, roll and heave. All simulations are carried out for at least 5 encounter periods of the swell. The thrust and resistance are averaged over these 5 periods and compared.

Fig.7 shows the motion of the vessel in swell at 11.5 kn speed. The pitch and heave motion are significant, with pitch motion oscillating between -0.8° and 0.4° from trough to peak, and heave motion between -0.5 and 0.2 m. Roll shows low frequency oscillation with an amplitude of 0.6°.

Table VI shows the average resistance and thrust calculated for 11, 11.5 and 12.5 kn in swell. The difference between resistance and thrust is also shown, which needs to be zero in order for the vessel to be in longitudinal force equilibrium. A negative difference indicates that there is a deficit of thrust meaning that the vessel will reduce her speed. Using linear interpolation it is calculated that the speed of the vessel in swell is 11.15 kn, making the speed loss equal to a significant 1.85 kn.

Fig.8 shows the CFD simulation of the vessel sailing in swell, where it can be observed that the swell is larger compared to the ship comparing to the Capesize vessel simulation. In this case, the wave length is similar to ship length, producing a larger relative resistance and consequently reducing the speed by 1.85 kn.

Table VI: Average resistance and thrust in swell for different speeds for the Handysize vessel. Negative difference indicates thrust deficit (ship decelerating), and positive denotes thrust sufficit (ship accelerating).

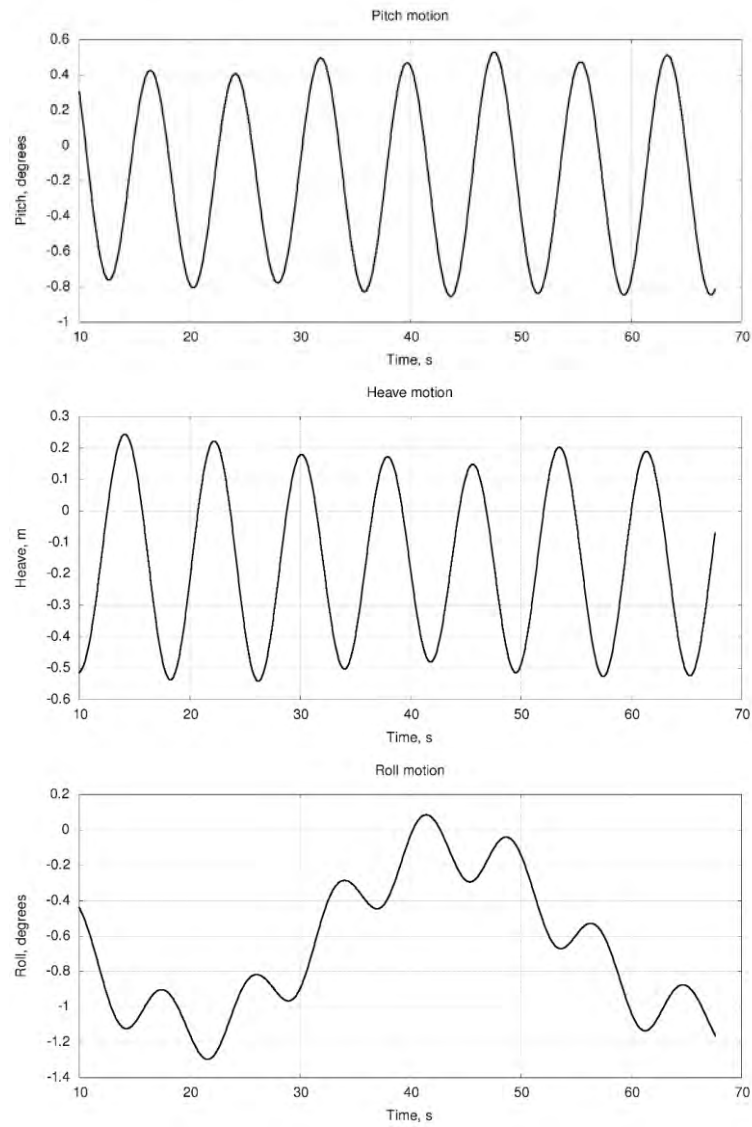| V	Resistance	Thrust	Difference
11.0 kn	743.2 kN	754.6 kN	11.4 kN
11.5 kn	750.6 kN	722.4 kN	-28.3 kN
12.5 kn	783.8 kN	659.6 kN	-123.2 kN

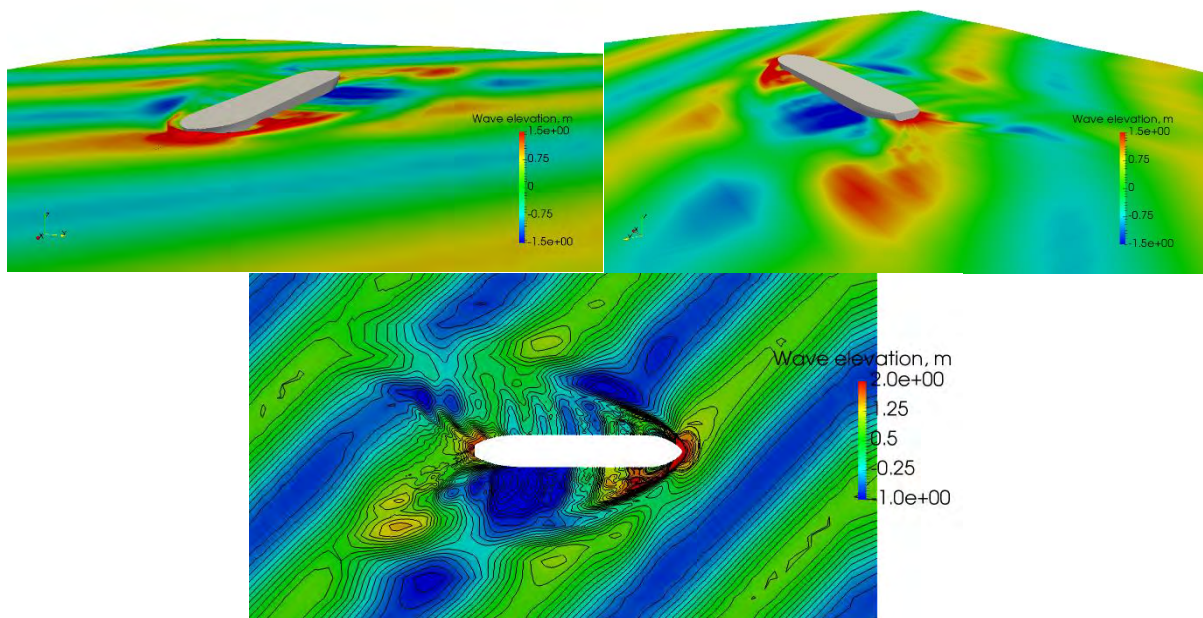Fig.7: Motion of the Handysize vessel in swell at 11.5 kn

Fig.8: Handysize vessel sailing in swell conditions

6. Conclusion

The CFD method has been applied to the problem of speed loss in swell to quantify the effect of swell on vessel performance for two vessels which were subjects of charterparty claims. In the numerical approach the two vessels were exposed to swell conditions present on the claimed voyage period, and the respective speed loss is calculated. The numerical procedure ensures that the calculated speed loss is caused only by the swell, disregarding any other phenomena that could otherwise influence the performance of the vessel, and isolating the swell effect on the performance of the vessel.

Both vessels, one Capesize and one Handysize, had a minimum warranted speed of 13 kn. The CFD study shows that the speed loss of the Capesize vessel is 0.67 kn, while for the Handysize vessel it is 1.85 kn. In both cases the speed loss surpasses the difference between the recorded ship speed and minimum warranted speed which is the main argument of both claims. This demonstrates that without swell, both vessels would have performed as warranted, i.e. with the speed above 13 kn.

The results of this study suggest that more attention needs to be given to swell when observing the performance of the vessel, especially in the event of performance claims. The influence of swell needs to be considered for the performance review to be fair to both parties, shipowners and charterers.

References

JASAK, H.; VUKČEVIĆ, V.; GATIN, I. (2015), *Numerical Simulation of Wave Loads on Static Offshore Structures*, CFD for Wind and Tidal Offshore Turbines, pp.95-105

JASAK, H.; VUKČEVIĆ, V.; GATIN, I.; LALOVIĆ, I. (2018), *CFD validation and grid sensitivity studies of full scale ship self propulsion,* Int. J. Naval Architecture and Ocean Engineering

MORSKA, A.; WIŚNIEWSKI, B.; WIELGOSZ, M.; PIOTROWSKI, T. (2010), *The problem of ship voyage evaluation by the charterer and the owners*, Scientific Journals: Maritime University of Szczecin 21(93), pp.88-97

VUKČEVIĆ, V.; JASAK, H.; GATIN, I. (2017), *Implementation of the Ghost Fluid Method for free surface flows in polyhedral Finite Volume framework*, Computers and Fluids 153, pp.1-19

High Quality Data under COVID-19 –
How to React Fast and Professionally with Remote Service

Klas Reimer, Hoppe Marine GmbH, Hamburg/Germany, k.reimer@hoppe-marine.com

Abstract

This paper provides an overview of the necessary steps from data acquisition to the provision of high-quality data via API. The continuous maintenance of the primary data sources and the validation of time series data is often underestimated. Problems are detected late and randomly and are mostly solved after a downtime period during an onboard service. To profit from the optimization potential which has a trustworthy database as precondition, a professional service on short notice is required - regardless of the ship's sailing area and position. Furthermore the travel restrictions caused by the Covid pandemic are playing an increasing role in remote maintenance. In addition to technical possibilities for creating an infrastructure in compliance with cybersecurity aspects, this paper reflects the technological trends in remote support and service in the maritime industry with respect to the autonomous operation.

1. Introduction

The interest in validated operating data, which will be provided for further worldwide usage via an API, continuously grows. In addition to the optimization potential, the need for further related information and recommendations for actions onboard, which are derived from the transferred data, also increases. Compliance with regulations and reports on emission reduction and ballast water treatment are just a few examples. In summary, for a validated data basis the possibility of access in the event of an error has become the main success factor.

For an optimized vessels operation, the access option to restore the desired state in the event of incorrect behaviour is therefore necessary. The availability of data for reporting and operational optimization can be visually compared with the tip of an iceberg. The work and process steps that have to be carried out, however, are represented visually by the much larger part of the iceberg under the waterline. If the infrastructure for remote support or remote maintenance is not available or is only created with a delay in time, the usability of data records must be decided on a case-by-case basis. By experience, the data sets with invalid signal sources cannot be taken into account for machine learning approaches of characteristic maps, or for evaluations relating to all aspects of fleet management.

2. Provide sensors and signals - Commissioning as "The Challenge before the challenge"

The database for optimization potential and automated reporting without manual input requires the automated data acquisition of nautical data, such as ship speed, rudder angles, trim and drafts. Fuel consumption, main engine power and speed as well as weather information must also be recorded, *Reimer (2020)*. The equipment with sensors as well as the acquisition and further processing of the data into a standardized and comparable database is described in detail in *ISO 19030-2 (2016)*. For systems that have been installed or expanded since 2020Q1, the "challenge" begins with the commissioning. Since then, international travel has only been possible under strict conditions.

The individual installation work during commissioning requires the knowledge of trained service personnel. Since the infrastructure for remote support can be as individual as the systems installed on board, the provision of connectivity should be defined by a central place. Even if the ship usually has a satellite connection and the crew has LTE-capable devices, this cannot and should not be a prerequisite for successful commissioning. The responsibility and sovereignty over the documentation and the software used, taking cyber-attack vectors into account, must not be randomly. The technology trend of remote maintenance, which is becoming more and more prevalent, is advancing rapidly in the onshore industry. The infrastructure and provision of a fast Internet connection for transferring software

installation packages, video calls or accessing web-hosted video tutorials, are already seen as standard on shore. In the maritime industry, this precondition for connectivity must first be created. However, since the data to be acquired by the sensor system is essential for success, a solution for commissioning must be found by trained technicians. Solution scenarios and possible uses are described in the section "Remote Service Ability".

3. Primary signals need to be validated and maintained

After successful commissioning, the system and sensor supplier is responsible for ensuring a high data quality. The continuous data maintenance with fault detection and service and spare parts planning with <u>its</u> resulting activities, are ideally part of an integrated process. Recognizing implausibility in the sensor data poses a major procedural challenge for the operator, if the manufacturer does not have access to the data. However, software providers who provide optimization solutions for fleet management do not have the in-depth required system and component know-how. The technical clarification with several involved companies often turns out to be tedious and is associated with high overhead to the worse of the operator. Until an issue had been clarified, the data records can often not be trusted until they have been solved. As an example, the white paper 2020, *Reimer (2020)* and *Harcke, 2019)* mentioned a dynamic failure of the speed through water of around 1 kn (16 kn real / 17 kn measured). For an exemplary 350 m sample container vessel with a design speed of 20 kn, this incorrect determination already results in an error in the performance determination of over 10%. This wrong value is higher than the optimization potential. Implausibility is usually not detectable by the sensor even with a self-validation, so that algorithms must be used for context validation. The more integrated and standardized the process from data acquisition to provision, the more efficiently it can be responded to. This is the only way to identify implausible data at an early stage and to take remote maintenance measures immediately or to initiate an on-board service.

4. Bidirectional Ship-to-Shore connection required - Assessing data quality mandatory when converting data into information

Fig.1: Ship-to-Shore Data Highway

The technology and the cost structure allow every ship operator to transport time series data and operational information from ship to shore. It is important to ensure that the transport is encrypted. The use cases 'remote support', in which the crew carries out the tasks on board under the guidance of a service technician, and 'remote service', which enables remote maintenance with direct system access, both require bidirectional communication. The ship-to-shore link closes the gap from data acquisition on board to availability with the option of data evaluation and maintenance contracts on shore (see image). This allows to take full responsibility from the data source to the provision of system health on shore. In general, two basic ways of communication need to be considered separately: For continuous transfer via V-SAT for 300 signals with a minute logging interval only 0.7 MB of data volume is needed per day. The V-SAT connection is characterized by the high net coverage, so that in addition to time series data, system states can also be transmitted continuously. In the opposite direction of the data highway, system and software updates as well as remote services can be carried out in short cycles between shore base and ship.

But every connection to the ship includes cyber risks. Protection against attack vectors in the area of cyber-crime requires a multi-level security concept with a focus on identity protection, access protection and integrity protection. With identity protection, the trustworthiness of the communication partners (hardware components on board the ships) is ensured in the first stage. For this purpose, each end point of communication is equipped with a private, cryptographic key. This key never leaves the de-

vices and therefore cannot be compromised. The device is only allowed to transfer data to or receive data from a cloud-based data pool if both sides have the correct keys. With access protection, a secure SSL-encrypted connection is established between the communication partners. This encrypted connection ensures that only the two communication partners can read the transmitted data in plain text. A third party cannot read the data while it is being transmitted. This is a major advantage compared to the frequently used email traffic. In the case of integrity protection, an additional step ensures that the data is completely intact and corresponds to the data that was transferred to the secure transmission channel on board. In turn, cryptographic signatures in accordance with the RFC 7519 standard are used for this purpose, https://docs.hoppe-sts.com/docs/doc2#security, FAQ STS.

5. Ensure continuous data availability - How does operation looks like?

To ensure that the service department can respond on short notice, extensive basic information is provided when using ship-to-shore. In addition to information about the connectivity status of the ships, the system status of the embedded iPCs and installed components are connected to the health monitor. The complete data transmission with the evaluation of the data quality creates the basis for more in-depth time series analyses. At this point, system notifications which represent the health status of the components on board become important. If, for example, a serial interface which provides NMEA sentences with important nautical data fails, the system notifications provide information directly in the web-based service portal. This information is actively provided before the lack of data is noticed in operation.

6. Remote service ability

In order to minimize the risk of overdue maintenance tasks caused by the Covid-19 pandemic, connectivity must be established for the After-Sales-Service. Only with this precondition the crew can receive professional support with maintenance and repair work guidance. The downtime costs of systems usually exceed the maintenance costs many times over. The expectation for fast service is increasing - so are the limiting factors for international travel activities at the moment. Customers are also used to remote maintenance from their private lives. Nobody wants to pay the travel expenses for e.g. a telecommunications technician anymore when the problem can be solved cheaper and faster by remote maintenance. But the requirements for remote service on board ships as moving objects in global operations are significantly higher. In addition to permanent data availability and connectivity in the area of remote service, the requirements of remote support are temporarily high bandwidths of >1 Mbit/s, such as those required for video telephony or the provision of larger documents or edited videos, *Harcke (2020)*. In addition to the use of the V-SAT connection, an LTE connection with up to 20 Mbit/s in coastal areas up to 25 nm away or in the port is an ideal addition.

As a consequence, the first prototype of a remote connection box was created in 2020Q4, Fig.2. In the following use cases, the internet connection near the coast is established with the help of an industrial LTE router, which offers the possibility of using several SIM cards and LTE antennas of different frequency ranges. The system establishes the remote connection, which can be actively prevented on board against unauthorized access at any time by using a hardware key, reflecting the high requirements for cyber-security. A conformity check with regards to the use of LTE technology in relation to the existing regulations and rules of the classification society DNV was also carried out.

- Use case 1: Remote support during commissioning
  The first application example is the use of the remote connection box including tablet when commissioning a newly developed sensor system in the course of a research project. Thanks to the possibility of direct communication with the crew, many preparations such as the installation of the sensors and control cabinets, as well as assistance with questions about laying around 1400 m of cable, could be carried out successfully by the crew. It was also possible to react in a time- and cost-effective manner to adjustments in the configuration of the system by means of short coordination and the exchange of edited images and voice notes. Software updates for the systems on the ship could be provided on the tablet, *Harcke and Reimer (2021)*.

Fig.2: Remote Connection Box with WiFi Extension

- Use case 2: Remote service with updating the logging configuration of high-frequency logging as well as parameter settings
  In this application, it was possible to reliably provide and install updates on the embedded iPC HOMIP from onshore. At the customer's request, the bidirectionality of the Data Hiqhway was used to integrate further signal sources into the logging in order to record high-frequency data and transmit it to shore. It is important that the updates are provided, which can be installed by the crew at a safe time via the touch display. This possibility provides cost reductions in the area of service activities for customers as well as manufacturers.

- Use case 3: Remote support with engine room call
  If the inspection with entering the ship is possible for service partners under strict conditions, the installation of a power measurement system can be carried out with the guidance of a specially trained service technician or even the crew. In the specific example, a stable data rate of 12 Mbit/s was achieved via the portable remote connection box on deck and a WiFi access point in the engine room. Video telephony and support from other service colleagues were possible in excellent quality. The video call and the provision of the information are carried out using a tablet with a safety cover. Direct use by the crew in demanding environments such as the engine room can provide encrypted data transfer, video telephony and digital access to

all system-relevant documents such as manuals and troubleshooting guides as well as video tutorials. The stable system with a set-up time of a few minutes can therefore also be converted into a permanently installed system to remain on board after successful initial use. This means that the service options can also be used after support with commissioning the system in the shipyard while the ship is in operation.

Fig.3: Remote Call from Engine Room

7. Provide data via API

The tip of the iceberg, the pursued and visible optimization potential, can be used if the data is available. The prerequisites for valid, available data mentioned in the text present the operators and suppliers with a great responsibility, which must be met professionally. In the perfect world the operators have nothing to do with this required work in order to focus on the core competence of ship management. Suppliers, who integrate the data path through to the provision of the data and thus the optimization potential, make an important contribution here.

References

HARCKE, N. (2019), *Einfluss der Datengüte auf die Optimierung des Schiffsbetriebs*, Schiff&Hafen, pp.24-26

HARCKE, N.; REIMER, K. (2020), *Digitalisierung - B ZERO: Projekt zur Entwicklung einer wachfreien Brücke*, Schiff&Hafen, pp.12-14

HARCKE, N.; REIMER, K. (2021), *Remote Service*, Schiff&Hafen

ISO 19030-2 (2016), *Ships and marine technology — Measurement of changes in hull and propeller performance - Part 2: Default method*, p.3, ISO, Geneva

REIMER, K. (2020) *How to achieve performance optimization potential considering high quality data?"*, 5th HullPIC, Hamburg

Setting the Standard for Evaluation of In-Service Technical Ship Performance

Bingjie Guo, DNV, Høvik/Norway, bingjie.guo@dnv.com
Olav Rognebakke, DNV, Høvik/Norway, Olav.Rognebakke@dnv.com
Hans Anton Tvete, DNV, Høvik/Norway, Hans.Anton.Tvete@dnv.com
Christine Adal, DNV, Høvik/Norway, Christine.Adal@dnv.com
Gaute Storhaug, DNV, Høvik/Norway, Gaute.Storhaug@dnv.com
Michael Schmidt, BW Dry Cargo, Copenhagen/Denmark, Michael.schmidt@bwdrycargo.com
Trym Bruset, Miros Group, Oslo/Norway, trym.bruset@miros-group.com
Gunnar Prytz, Miros Group, Oslo/Norway, gunnar.prytz@miros-group.com

Abstract

A technical performance index is proposed in this paper. A procedure is developed to analyze ship in-service measurements and calculate this index. Steps include data preparation use of data quality indicators, steady-state filtering and data normalization. The technical performance of a bulk carrier is evaluated following the proposed procedure. The objective is to set the standard for consistent and accurate evaluation of live technical vessel performance.

1. Introduction

The international shipping industry is responsible for transport of around 90% volume of world trade. Seaborne trade is also expected to grow in line with, or possibly outpace, the global gross domestic product (GDP) growth, *ICS (2020)*. Although shipping has much lower CO2 emissions per transport work relative to road and air transport, it still accounts for a significant share of global emissions of CO2, NOX and SOX, giving a substantial environmental footprint. The emissions from marine shipping induces approximately 60,000 deaths globally every year, *Corbett et al. (2007)*. As a result, increased scrutiny is expected to be placed upon shipping to lower environmental damaging emissions and local harmful pollutants. In April 2018, the International Maritime Organization (IMO) adopted an initial strategy on reduction of GHG emissions from ships. The strategy aims at reducing total GHG emissions from international shipping by at least 50% by 2050 as compared to 2008, *IMO (2019)*.

Both public regulators like the EU and IMO, as well as private entities, have applied several mechanisms for reporting emissions and rating performance. EU's Monitoring, Reporting and Verification (EU MRV) of CO2 emission has been mandatory for ship larger than 5000 gross tonnage (GT) at any EU ports from 1 January 2018. IMO Data Collection System on fuel consumption (IMO DCS) has been required on ships largen than 5000 GT trading globally from 1 January 2019.

IMO considers development of technical and operational energy efficiency measures for both new and existing vessels. Such indices can be instrumental to control and ensure an improved energy efficiency performance of shipping industry.

Shipping industry largely consist of shipyards/designers, shipowners, technical managers, operators, charterers and ports. All parties play an important role in the decarbonization of the shipping industry. For such energy efficiency indices to be active and effective, it is paramount that they are developed for and addressed towards the industry parties that can influence the index, i.e. be in control of the parameters that affect the energy efficiency index. The measurements and analysis done to calculate the index must ensure sufficient level of accuracy. Moreover, there must be a strong link between control and benefit to incentivize energy efficiency improvements.

IMO has made the Energy Efficiency Design Index (EEDI) mandatory, and the EEDI is developed to ensure a continuous reduction of the carbon intensity of new ships delivered. The EEDI consist of

parameters measured at main engine and aux. engines shop trials, deadweight measurement, tank tests and sea trial. All parameters are in control of the yards/designers, and these are verified and certificated by a classification society prior to delivery of a vessel. The EEDI meets all the above criteria in terms of incentive, accuracy, responsibility and control.

IMO has circulated a voluntary Energy Efficiency Operational Index (EEOI), which is proposed as an index to improve the energy efficiency of ship operation. The EEOI considers fuel oil consumption (CO_2 emission), amount of cargo transported, and distance sailed (transport work). *MEPC 75 (2020)*, introduced a mandatory Carbon Intensity Indicator (CII – e.g. Annual Efficiency Ratio [AER – grams of CO_2 per dwt·mile]) and rating scheme where all cargo and cruise ships above 5000 GT are given a rating of A to E every year. Each ship will be required to meet the CII target rating C or better. Rating thresholds will gradually become more stringent, and in line with 40% reduction target in 2030. *Klaveness (2021)* supports selecting EEOI as Climate Intensity Indicator (CII), and they argue that AER incentivizes vessels to ballast instead of cleaning the holds and take a cargo closer to the area of discharge, and AER fails at identifying carbon intensive operations.

The intention with the EEOI and AER is obviously good, but they do not meet the above-mentioned criteria for an active and effective index, as incentive, accuracy, influence and responsibility are problematic.

The annual average EEOI for a vessel is largely controlled by the charterer/commercial operator of the vessel, as the annual average EEOI is determined by the amount of cargo transported, duration of port stays, laden vs ballast distances, operating speed and thereby fuel consumed. To some extent the annual average EEOI is also influenced by weather and the state of maintenance (hull and propeller fouling, hull and propeller damages, antifouling paint etc) of the vessel. AER has the same problems.

For the shipping industry to meet the ambitious GHG emissions goals set out by IMO, it is important that all parties within the industry contribute. To ensure alignment of incentives between the parties it is important that the industry is provided with effective measures and indices directed towards the active parties.

A technical index directed towards ship owners and technical managers is needed to complement design- and operational indices. Such an index should quantify the current efficiency of the vessel based on in-service measurements. The effects of e.g. loading condition and external factors like wind, waves and current must be corrected for. A procedure to analyze in-service vessel performance measurements and to calculate a technical performance index is proposed in this paper.

Van den Boom and Hasselaar (2014) proposed power loss as Performance Indicator. In the work, the power corrected for wind resistance is divided by the power in calm water (taken from speed trial results) at the same speed, to form a 'Performance Indicator (PI)' in terms of percentage power loss. The effect of added resistance due to waves is not considered. *ISO19030 (2016)* and *GIA (2020)* define the technical Performance Index (PI) as the change in average speed loss in the reference periods(s) and the average speed loss in the evaluation period. ISO 19030 also gives one alternative index as the change in required power. The index calculation is based on data from planned measurements. All the indices can only be used to evaluate the maintenance condition and the change of ship efficiency of the selected ship. They cannot be used for ship efficiency comparison of the different ships. Moreover, they are not connected with ship emission.

In order to calculate the proposed technical index, ship fuel consumption and speed curve needs to be analyzed based on the measured data. There are mainly three different approach types for analyzing measurement data: Simple statistical approach, data-driven approach and physical model-based approach. *Bialystocki and Konovessis (2016)* proposed a statistical approach to obtain ship's fuel consumption and speed curve. The simple correction method was used. A data-driven approach to predict the propulsion power of a vessel was used by *Kim et al.(2020)*. In the study, support vector regression (SVR) is used to learn from big data obtained from onboard measurement and the National

Oceanic and Atmospheric Administration (NOAA) database. *Petersen et al. (2012)* used artificial neural networks and Gaussian processes (GP) to analyze the ship fuel efficiency based on the measured data. A more rational method to analyze power is to develop numerical models for the relevant physical processes and to correct the monitored data by projecting them to standard conditions following a procedure similar to standardized sea trial speed correction, *Liu et al. (2020)*. The physical model-based approach normally starts with the measured power, and normalizes the weather effect and water temperature effect. Some methods end up with the speed-power curve projected to calm water condition, seen in *ISO 15016 (2015); Liu et al. (2020)*. Some methods end with the change of power or speed in calm water compared with sea trial data, refer to *ISO19030 (2016), GIA (2020), Boom and Hasselaar (2014)*.

This paper develops a procedure to analyze ship measurement data following a physical model-based approach and evaluates ship technical performance of one bulk carrier by calculating the proposed technical index. The procedure is introduced first, then the case study for the bulk carrier is presented.

2. Procedure of analyzing in-service measurement data

To analyze ship technical performance using a physical model-based approach, it is necessary to have some ship design information, ship operation information and environment information. The methodology for speed performance analysis is common in sea trial tests and in-service measurements. However, there are essential differences between the two kinds of analysis. The operation condition during sea trial is well controlled and acceptance limits enforced for wind, current and waves. The measurement noise is reduced to a minimum and the measured data is reliable. The measured in-service performance is often polluted by both ship operation and environmental conditions, which leads to a necessary data filtering process as part of the analysis, *van den Boom and Hasselaar (2014), Liu et al. (2020)*. Moreover, there is sufficient detailed information on ship geometry available, and all the necessary sensors are installed for the sea trial. This is not practical for in-service measurement, *Liu et al. (2020)*. Therefore, when setting standard for evaluating ship technical performance based on in-service measurement, it is not straightforward to apply normal sea trial analysis. Cases where some ship geometry information or measured information are missing should be considered.
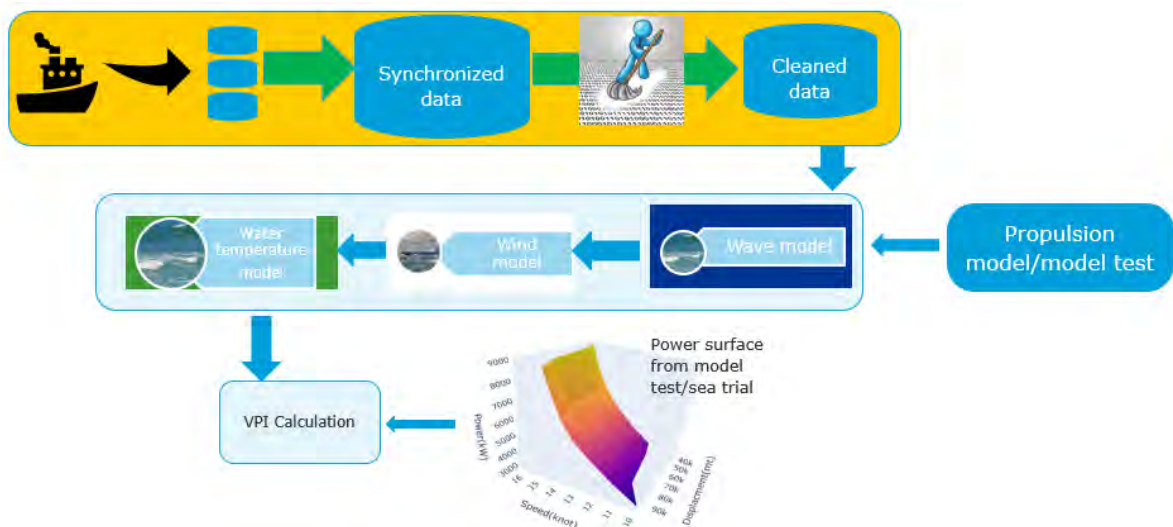

Fig.1: Procedure for analyzing ship technical performance based on in-service measurements

The procedure for analyzing in-service measurement data and calculating the proposed technical performance index is illustrated in Fig.1. The procedure includes three main steps (indicated by three rows in Fig.1): measurement data preparation; normalizing the effect of weather and calculating technical performance index. The measured data from different sensors is synchronized and cleaned prior to analysis using physical model-based approach. Normalization is used to correct for the effects of

wave, wind and water temperature based on the corresponding physical models and ship propulsion efficiency. Finally, the normalized speed-power curves are utilized for calculating the proposed technical performance index. The following sections give a more detailed description of the three steps.

3. Preparation of measured in-service data

Accurate prediction of vessel speed-power curves requires monitoring and recording of key parameters such as ship power, ship speed, ship loading condition and weather information. Different sensor systems will be used for measuring key parameters, and their sampling frequency could be different. Re-sampling and synchronization may be required.

In the proposed method, the effect of water depth is not corrected for and the measured data in shallow water is removed.

The model for normalizing weather effect is following resistance and thrust identity method (RTIM), *Liu et al. (2020)*, which assumes that the ship total resistance is represented by a linear superposition of calm water resistance and added resistance components due to disturbance. Periods with ship acceleration and maneuvering should be removed from the dataset, since a more advanced model is needed to analyze speed-power curve given those conditions. It is beneficial to remove harsh weather periods as well. A cut-off criterion should be based on balancing the amount of remaining data with the uncertainty in predictions in strong wind or high waves. Weather filtering is not investigated in this paper.

Measured data can be filtered through a physical or mathematical approach. The physical approach filters out noise by setting limits based on physical phenomena, which is easy to understand. However, the limit could be dependent on ship type, ship size or ship location. A mathematical approach purely based on data has no limit to ship type or ship size. However, physical effects that are not corrected for included in a parametrization will appear as noise, which cannot be removed using a pure mathematical approach. One example is the effect of limited water depth.

Liu et al. (2020) filter the data according to acceleration, rate of course change, primary seaway direction and difference between speed through water (STW) and GPS speed. *van den Boom and Hasselaar (2014)* filter data by double checking the measured speed through water with speed estimated based on propeller torque and RPM. *Kim et al. (2020)* filter the data based on ship speed, and vessel speeds less than 6 knots were omitted. ISO19030 requires the data to be filtered according to Chauvenet's criterion first, then filtered further by setting threshold values for standard error of mean for ship RPM, ship speed through water, speed over ground and rudder angle.

Steady state detection (SSD) algorithms have been investigated in many industry applications. SSD can be used to detect windows or intervals when a process is operating in a steady state. *Kelly and Hedengren (2013)* summarized the previous work in the area of SSD and analyzed the limitations and challenges of each method. They proposed an SSD algorithm that is based on time window and utilizes the Student's t test to approximately determine a probability of being at steady state for each window. *Dalheim and Steen (2020)* argued that this method is sensitive to the window length. The shorter window will have low probability of stationarity and the longer window with multiple non-stationary intervals could end as stationary interval. They proposed a new method to identify steady state parts of time series data using a sliding window, which is adopted in this paper.

3.1 Steady state selection

To avoid including data collected during periods of acceleration, a steady state selection method was implemented based on *Dalheim and Steen (2020)*. The method evaluates the piecewise steadiness of a time series signal based on a moving window approach and is suited for signals that are close to constant in time for the desired time interval. Once the steady state periods have been identified, the entire data set is filtered prior to averaging. An outline of the method follows. For a more detailed

overview the reader is referred to *Dalheim and Steen (2020).*

The method assumes that the behavior of the signal can be modelled by a deterministic linear model, expressed as:

$$z_t = b_0 + b_1 t + a_t \tag{1}$$

$b_1 t + b_0$ is the linear model inside a time window with time parameter t. a_t is a zero mean white noise with constant variance. The linear slope b_1 can be estimated with least squares method. The standard derivation $\hat{\sigma}_{b_1}$ of the estimated linear slope b_1 can be calculated according to:

$$\hat{\sigma}_{b_1} = \sqrt{\frac{\sum_{t=1}^{n}(z_t - \hat{z}_t)^2}{(n-2)\sum_{t=1}^{n}(t-\bar{t})^2}} = \sqrt{\frac{\sum_{t=1}^{n}(z_t - \hat{b}_1 t - \hat{b}_0)^2}{(n-2)\sum_{t=1}^{n}(t-\bar{t})^2}} \tag{2}$$

n is the total number of samples in each window. A two-tailed t-test on $\hat{b}_1$, using $t_1 = \frac{\hat{b}_1}{\hat{\sigma}_{b_1}}$, is used to evaluate whether the slope is significantly different from zero, indicating a period of transition, or a window of non-steady-state signal. Since the slope can be positive or negative, we compare the absolute value with the t-value for the required window size and acceptance parameter alpha, $|t_1| < t(alpha, n-2)$. If the check fails, all the samples in the window will be marked unsteady ($s_t = 0$), otherwise they will be marked as steady ($s_t = 1$).The steady state probability is calculated according to the arithmetic average of s_t for each sample point. A proportionality constant is used for accepting/rejecting individual points based their steady state probability; essentially dictating if the proportion of moving windows containing the point in question are accepted. In the application of this method, the length of the time windows, confidence level of Students' t-distribution and proportion for accepting the sample point as steady state are adjustable.

3.2 Parameter selection and configuration

For the purposes of the calculation of the technical performance index the parameter selected for steady state filtering is the ship's RPM. This signal is practically a piecewise constant function within the accepted conditions for water depth and ship speed, and as such is ideally suited for the algorithm.

The algorithmic parameters needed are the size of the sliding window, the t-test confidence level as well as the proportionality test for the acceptance of each point. Due to the steady nature of the RPM signal, the t-test confidence level was set to 0.001, however depending on the choice of parameter and level of noise.

The sliding window size should be chosen with consideration to two things: the sampling frequency of the parameters and the desired averaging period. The averaging period was chosen to be 1 hour, and the sampling rate of the various parameters was synchronized to 1 minute. In general, the sliding window size should be smaller than the averaging period, but large enough to contain sufficient data to reduce the impact of signal noise. The prototype developed used a window size of 45.

The proportionality parameter used for accepting each point based on their steady state probability has significant impact towards the lower and higher extreme values: a proportion lower than 20% of accepted windows will allow more points closer to transitory periods, and a value higher than 90% risks rejecting points in otherwise steady states under the influence of signal noise. The developed prototype uses a proportionality requirement of 50%.

3.3 Averaging

Following steady state selection, the accepted subset of measurements can be averaged to a desired interval. The presented prototype uses data sampled with 1-minute frequency and averages to 1-hour

intervals, and this data can be used for larger timescale analysis such as daily, weekly, monthly, quarterly etc.

For each 1-hour interval there are two cases that should be taken into consideration following the steady state selection procedure described.

Case 1 is if there is too much data either missing or rejected by the algorithm within one interval. A minimum requirement for number of accepted data points within each interval is recommended, set in the presented prototype to 30 points out of 60.

Case 2 is when an interval contains data from more than one steady state with different values, such as at the start and end of periods of acceleration. In this case the average will be weighted between the desired averages for the two steady states and should not be included. A simple elimination procedure to avoid this is to use the steady state t-test described above on the data for each interval, considering potentially missing data following the steady state selection.

4. Normalizing (correcting) the effects of weather

For a ship owner, it is of interest to know the ship performance in an ideal condition, without the disturbance of wind and waves. There are several established methods for normalizing the effect of weather, *ITTC (2017), ISO19030 (2016), ISO15016 (2015), Liu et al. (2020), Orihara and Tsujimoto (2018).* There are some commonalities in all the methods. They all adopt the 'Direct power method' to calculate the change of power with estimated added resistance. The open water propeller curves are utilized to calculate propeller efficiency, and propeller thrust coefficient K_T and torque coefficient K_Q are assumed to be parabolic functions to the propeller advance ratio J. However, the open water propeller curves are not always available. Thus, two new methods of normalizing the weather effects are developed based on the information that are typically available for a ship owner. The difference of the two methods will be compared in the case study later.
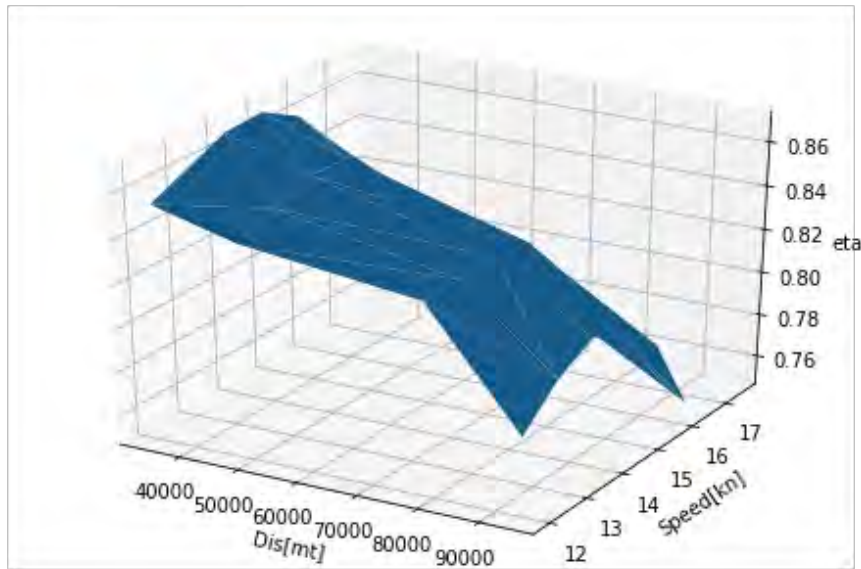

Fig.2: Ship efficiency at different loading conditions and speeds from model test

Normally ship owner has a ship self-propulsion model test report, but this rarely includes all the main parameters of the propeller such as propeller diameter, number of blades, area ratio and pitch. The first method of normalizing the weather effect is based on the self-propulsion model test report. Typically, four different loading conditions are tested: normal ballast, heavy ballast, design full loading condition and scantling full loading condition. Based on the model test results, ship efficiency at different loading conditions and speeds can be derived, and one example is shown in Fig.2. The ship total efficiency η includes ship open water efficiency η_0, relative rotative efficiency η_R and ship

hull efficiency η_H. The ship total efficiency η at different time step can be obtained by B-spline interpolation on the ship displacement (Dis) and ship speed through water V_W.

The correction power ΔP_D due to the weather effect can be calculated according to Eq.(3):

$$\Delta P_D = \frac{R_{add} \cdot V_W}{\eta} \qquad (3)$$

R_{add} is the added resistance due to weather, which should include added resistance due to waves, added resistance due to wind and the change of resistance due to water temperature. The corrected power P_{D_cor} is calculated as:

$$P_{D\_cor} = P_{D\_s} - \Delta P_D \qquad (4)$$

P_{D_s} is the in-service delivered power, which can be calculated with the measured shaft power and the transmission efficiency. The influence of weather on ship propulsion efficiency is not considered in this method, and the effect of this assumption will be discussed in the case study.

When propeller main parameters are also available, more advanced method is investigated to consider the change of propeller efficiency due to weather influence. In this method, the open water propeller efficiency needs to be estimated. Wageningen B-series polynomials express the thrust and torque coefficients in terms of the blade number, pitch-diameter ratio, blade area ratio and advance coefficient, which is derived from open water characteristics of 120 B-series propeller model tested at the Netherlands Ship Model Basin in Wageningen, *Bernitsas et al. (1981), Carlton (2008)*. The propeller models used in the model test are very old. However, the derived polynomials were optimistic for the old propellers, since propeller roughness and the cavitation effect were not considered. According to authors' knowledge, Wageningen B-series polynomials can approximately estimate the propeller efficiency of the existing propellers. Therefore, the propeller thrust coefficient K_T and torque coefficient K_Q at different advance ratio J are calculated with Wageningen B-series polynomials. Fig.3 shows an example. The K_T, K_Q and load factor of propeller $\tau = \frac{K_T}{J^2}$ at different advance ratio J are saved as tables for interpolation. For later reference, these are denoted K_T-J curve, K_Q-J curve, and τ-J curve.
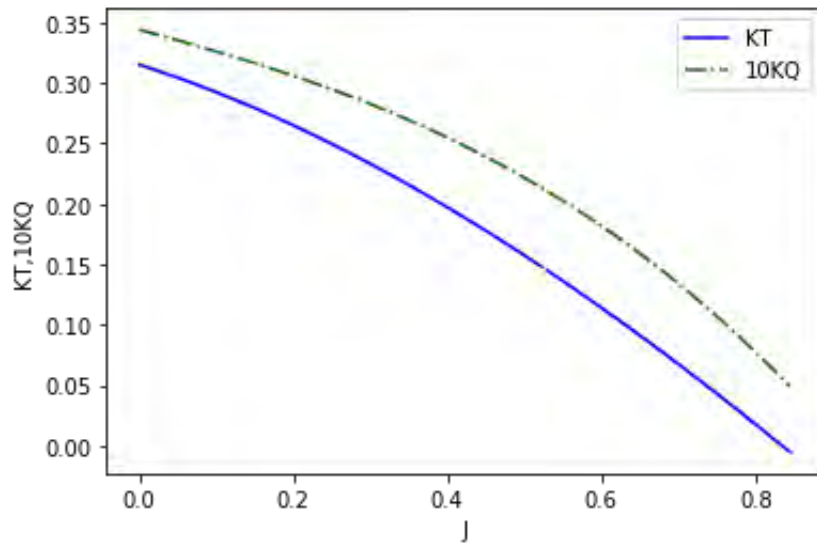

Fig.3: Propeller thrust coefficient K_T and torque coefficient K_Q at different advance ratio J calculated with Wageningen B-series polynomials

The in-service propeller torque coefficient K_{Q_s} can be calculated according to Eq.(5).

$$K_{Q\_s} = P_{D\_s} \cdot \eta_{R\_s}/(2\pi\rho n^3 D^5) \tag{5}$$

The relative rotative efficiency in service η_{R_s} is obtained by B-spline interpolation on the model test results with ship displacements and speeds. ρ is water density. n is shaft speed, and D is propeller diameter.

The in-service advance ratio J_s is obtained by linear interpolation on the open water K_Q-J curve with in-service propeller torque coefficient K_{Q_s}.

$$J_s = Interp_{K_Q-J}(K_{Q\_s}) \tag{6}$$

Where the open-water K_Q-J curve is calculated with Wageningen B-series polynomials. Since the measured speed and wake fraction have large uncertainties, the speed of flow through the propeller is calculated according to:

$$V_a = J_s nD \tag{7}$$

The in-service thrust coefficient K_T can be derived by linear interpolation on the open-water K_T-J curve with J_s.

$$K_{T\_s} = Interp_{K_T-J}(J_s) \tag{8}$$

The in-service open water propeller efficiency η_{0_s} can be calculated as:

$$\eta_{0\_s} = \frac{J_s}{2\pi}\frac{K_{T\_s}}{K_{Q\_s}} \tag{9}$$

Then the in-service propulsion efficiency η_s can be obtained as:

$$\eta_s = \eta_{0\_s}\eta_{R\_s}\eta_{H\_s} \tag{10}$$

η_{H_s} is the ship hull efficiency, which is calculated with $\eta_{H\_s} = \frac{1-t}{1-w}$. The thrust deduction t and wake fraction w are also obtained with by B-spline interpolation on the model test results at different displacements and ship speeds.

The in-service load factor of the propeller τ_s can be obtained as:

$$\tau_s = \frac{K_{T\_s}}{J_s^2} \tag{11}$$

The total ship resistance R_s is equal to propeller thrust, which can be calculated according to:

$$R_s = \tau_s(1-t)(1-w)^2\rho_s V_w^2 D^2 \tag{12}$$

The corrected total ship resistance $R_{s,cor}$ is calculated by subtracting the estimated added resistance due to weather from R_s:

$$R_{s,cor} = R_s - R_{add} \tag{13}$$

The corrected propeller load factor $\tau_{s,cor}$ can be calculated according to

$$\tau_{s,cor} = R_{s,cor}(1-t)(1-w)^2\rho_s V_w^2 D^2 \tag{14}$$

The corrected propeller advance ratio $J_{s,cor}$ can be calculated by interpolating the τ-J curve with $\tau_{s,cor}$. The corrected thrust coefficient $K_{T\_s,cor}$ and corrected torque coefficient $K_{Q\_s,cor}$ can be obtained by interpolating the K_T-J curve and K_Q-J curve with $J_{s,cor}$.

The corrected propeller open water efficiency $\eta_{0\_s,cor}$ can be obtained:

$$\eta_{0\_s,cor} = \frac{J_{s,cor}}{2\pi} \frac{K_{T\_s,cor}}{K_{Q\_s,cor}} \tag{15}$$

The corrected propeller efficiency $\eta_{s,cor}$ is calculated as:

$$\eta_{s,cor} = \eta_{0\_s,cor}\eta_{R\_s}\eta_{H\_s} \tag{16}$$

It is assumed that the relative rotative efficiency and ship hull efficiency are not influenced by added resistance due to weather. The corrected shaft speed n_{cor} can be obtained according to Eq.(17).

$$n_{cor} = V_a/(J_{s,cor}D) \tag{17}$$

V_a is the the water speed through the propeller, which is calculated with Eq.(7). The correction power ΔP_D due to the weather effect can be calculated according to Eq.(18):

$$\Delta P_D = \frac{R_{add} \cdot V_W}{\eta_{s,cor}} + P_D(1 - \frac{\eta_s}{\eta_{s,cor}}) \tag{18}$$

The corrected delivered power P_{D_cor} can be obtained:

$$P_{D\_cor} = P_{D\_S} - \Delta P_D \tag{19}$$

In the second normalization method, the effect of added resistance due to wave and wind should be corrected first according to Eqs.(5)-(19). With the corrected delivered power P_{D_cor} and corrected shaft speed n_{cor}, the effect of water temperature and water density should be corrected following the same procedure using Eqs.(5)-(19). The evaluation of added resistance due to wave, wind and water temperature is discussed in the following subsections.

4.1 Added resistance due to waves

Added resistance in a sea state is normally calculated by integrating the Added Resistance Operator (ARO) with the wave spectrum in an actual sea state. The ARO is the Quadratic Transfer Function (QTF) of the mean force along the longitudinal axis of the ship.

There are mainly four groups of methods for obtaining the ARO of added resistance in regular waves: experimental methods, Computational Fluid Dynamics (CFD) simulations, theoretical methods based on potential flow and empirical formulas, *ITTC (2018)*. The first two requires detailed hull geometries. Experimental results are often considered as providing 'true' values, although there are measurement uncertainties, especially in short waves, *Larsson et al. (2010), Guo and Steen (2011)*. Model tests in oblique wave conditions must be performed in an ocean basin, which makes the tests more expensive. CFD simulations have been verified to predict ship added resistance with high accuracy, *Sadat-Hosseini et al. (2013), Ozdemir and Barlas (2017)*. However, CFD is still time consuming and expensive. Some theoretical methods based on potential flow can also predict added resistance due to waves with acceptable accuracy, *ITTC (2018), Kim et al. (2017)*. However, most of them also need the detailed ship geometry, which is not available for ship owners.

The empirical formulas only take some main ship parameters as input and can be used at low cost. Although they cannot capture the effect of detailed geometry on added resistance due to waves, some

of them can give reasonable results in the given limited ranges. *MARIN (2016)* developed STAWAVE formulas based on an extensive database of added resistance due to waves measured by MARIN. These formulas are accepted for predicting added resistance by *ISO 15016 (2015), ISO19030 (2016)* and *ITTC (2017)*. STAWAVE-1 is limited to sea states where ship heave and pitch motion can be neglected. The influence of ship motions and ship forward speed on added resistance are considered in STAWAVE-2. The application of STAWAVE-1 and -2 is limited to waves in the bow sector (less than ±45° off the bow). The measured data with waves from outside the bow sector has to be dropped if STAWAVE methods are used to predict ship added resistance due to waves.

Liu and Papanikolaou (2016) derived a new empirical formula based on experimental data of different hull forms, which could be used for different ship forward speeds in head sea. They extended the formula to arbitrary wave heading in *Liu and Papanikolaou (2020)*. This method is adopted here. The added resistance in irregular sea is calculated with

$$\bar{R}_{awireg} = 2 \int_0^\infty S(\omega) \frac{R_{AW}(\omega)}{\zeta_a^2} d\omega \tag{20}$$

$S(\omega)$ is the wave spectrum. A JONSWAP spectrum is implemented, which can be expressed as:

$$S_J(\omega) = A_\gamma S_{PM}(\omega) \gamma^{\exp\left(-0.5\left(\frac{\omega-\omega_p}{\sigma\omega_p}\right)^2\right)} \tag{21}$$

γ is the peak enhancement, $A_\gamma = 1 - 0.287\ln(\gamma)$, σ is the spectral width parameter. $S_{PM}(\omega)$ is Pierson-Moskowitz spectrum, which can be written as:

$$S_{PM}(\omega) = \frac{5}{16} H_S^2 \omega_p^4 \omega^{-5} \exp\left(-\frac{5}{4}\left(\frac{\omega}{\omega_p}\right)^{-4}\right) \tag{22}$$

$\omega_p = \frac{2\pi}{T_p}$, T_p is wave peak period. H_S is significant wave height. ω is wave frequency. More details can be found in DNV Recommended Practice C205.

The added resistance due to waves is dependent on wave direction, wave peak period, significant wave height and ship speed. It will take a long time to calculate the added resistance using Eq.(20)-(22) at each sample data. Random forest algorithm is adopted to model the added resistance in irregular sea with unit significant wave height at different wave directions, wave peak periods and ship speeds. The sample data used for Random forest algorithm is calculated with Eq.(20). According to *Taskar and Andersen (2021)*, changing the peak enhancement factor in JONSWAP spectrum did not show much influence on the added resistance. It is sufficient to use a single wave spectrum for the combination of wind sea and swell sea with $\gamma = 1$ for the computation of added resistance in waves. The samples are calculated with a single wave spectrum with $\gamma = 1$. The effect of significant wave height will be handled when the normalization is performed.
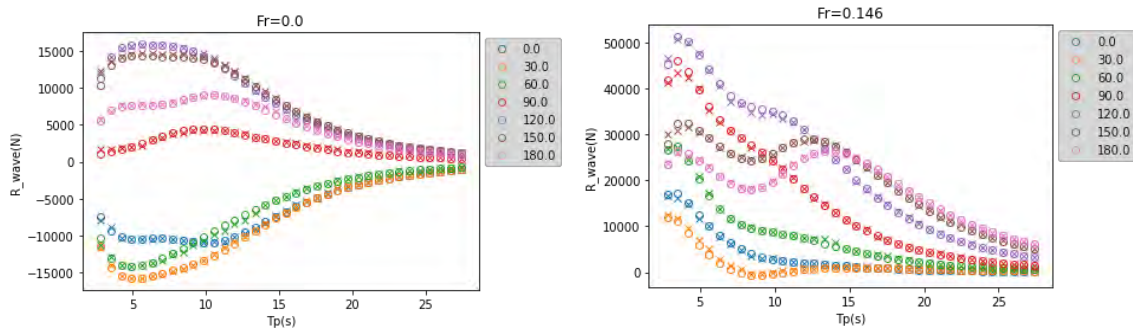

Fig.4: The comparison of added resistance from Random forest algorithm (shown with 'x') and added resistance from theoretical calculation (shown with 'o') at different directions (Left: the comparison at Fr = 0; Right: the comparison at Fr = 0.146)

The verification of the Random forest algorithm is shown in Fig.4. The comparisons confirm that the Random forest algorithm is a fair approximation of the theoretical model.

4.2 Added resistance due to wind

Added resistance due to wind is calculated according to

$$R_{wind} = \frac{1}{2}C_X(\theta_{rel})\rho_{air}V_{wrel}^2 - \frac{1}{2}C_X(\theta_0)\rho_{air}V_G^2 \qquad (23)$$

ρ_{air} is air density and V_{wrel} is relative wind speed. The calculation of relative wind speed is done according to *ISO15016 (2015)*. V_G is the ship speed over ground. $C_X(\theta_{rel})$ is longitudinal wind coefficient at relative wind direction θ_{rel}. $C_X(\theta_0)$ is longitudinal wind coefficient in head wind. The wind coefficient is evaluated with regression formula proposed by *Fujiwara et al. (2005, 2006),* which is also recommended by *ISO15016 (2015)* and *ITTC (2017).*

4.3 Added resistance due to water temperature and water density

The predictions done for speed power trials are usually based on a temperature of 15°C and water density of 1026 kg/m³. To compare the in-service performance with the design condition, the effect of water temperature and water density is corrected for according to *ISO15016 (2015).*

The added resistance due to water temperature and water density is calculated from

$$R_{AS} = R_{T0}(\frac{\rho_S}{\rho_{S0}} - 1) - R_F(\frac{C_{F0}}{C_F} - 1) \qquad (24)$$

Where R_{T0}, ρ_{S0} and C_{F0} are the total resistance, water density and frictional resistance coefficient at the reference water temperature and water density. R_F, C_F and ρ_S are the frictional resistance, frictional resistance coefficient and water density at the actual water temperature and water density. The frictional coefficients C_{F0} and C_F are calculated according to the ITTC'57 formula. Most of the time the in-service loading condition would be different from the loading conditions in sea trial, so that the resistance curve is not readily available. Therefore, the total resistance at reference water temperature and density R_{T0} is calculated as:

$$R_{T0} = (1 + k)C_{F0} + C_W \qquad (25)$$

Where the form factor k is calculated according to the *Holtrop (1984)* method. It is assumed that wave making resistance C_W is not influenced by water temperature and density, and it is calculated based on the measurement.

5. Proposed technical performance index

After the effects of weather (wind, wave, water temperature) is corrected, the measured in-service data is available for evaluating a proposed vessel technical index (VTI)*,* which is defined as:

$$VTI = EEDI \cdot \frac{P_E}{P_{E_{ref}}} = \frac{Power*SFC*FC}{Deadweight*speed} \cdot \frac{P_E}{P_{E_{ref}}} \qquad (26)$$

EEDI is the ship design index by IMO. $P_E = R_s V$ is the effective power in service, which is corrected to calm water condition:

$$P_E = P_{D\_cor}\eta_{0\_s,cor}\eta_{R\_s}\eta_{H\_s} \qquad (27)$$

$P_{E_{ref}} = R_{ref}V$ is the reference effective power at the corresponding ship speed, which is derived

from sea trial data.

The ratio $\frac{P_E}{P_{E_{ref}}}$ is used to indicate the ship hull and propeller condition in operation. The ship hull and propeller roughness will increase this ratio value, and the ship owner can decide when to take corrective measures based on this value. It should be noted that the speed range cannot be too large in the calculation of this ratio, since this ratio is equivalent to the ratio of ship resistance coefficient and ship resistance coefficient is dependent on ship speed. The difference of ship resistance coefficients at different speeds cannot be neglected if the ship speed range is too large. The total ship resistance coefficients from model test report can be used as a reference to choose the reasonable ship speed range in the analysis. EEDI is used as baseline for comparison with other ships.

6. Case study

A bulk carrier, Table I, was chosen as case study to calculate the VTI index following the proposed procedure. The measured in-service data includes four voyages, Fig.5.

Table I: Ship main parameters

Lpp	225.10 m
Breadth	32.26 m
Design Draft	12.20 m
Design Displace Volume	76535 m^3
Ballast Displace Volume	47173 m^3

Voyage 1:
Dates: 2020-02-10 – 2020-02-25
Displacement: 37.700 mt

Voyage 2:
Dates: 2020-04-22 – 2020-05-07
Displacement: 37.600 mt

Voyage 3:
Dates: 2020-05-13 – 2020-05-21
Displacement: 84.600 mt

Voyage 4:
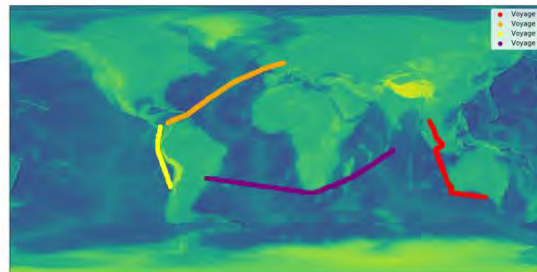Dates: 2020-07-15 – 2020-08-13
Displacement: 80.058 mt

Fig.5: The travel dates, displacements, and routes of four different voyages

Table II: The measured parameter used for data analysis

|	Parameters	Unit	Method 1	Method2
1	Speed Through Water	knot	x	x
2	Speed Over Ground	knot	x	x
3	Course Over Ground	Deg.	x	x
4	Time	Dates	x	x
5	Vessel Heading	Deg.	x	x
6	Shaft Power	kW	x	x
7	Shaft Revolutions	rpm		x
8	Relative Wind Speed	m/s	x	x
9	Relative Wind Direction	Deg.	x	x
10	Wave Height	m	x	x
11	Wave Direction	Deg.	x	x
12	Wave Period	s	x	x
13	Water Depth	m	x	x
14	Water Temperature	°C	x	x

The measured parameters used for two types of data analysis are given in Table II. The water temperature for the studied ship is not measured directly during the operation but retrieved from Copernicus database, https://marine.copernicus.eu. All the parameters are synchronized at 1-minute frequency.

The measured data is first filtered according to water depth, and only measurements in deep sea are used for further analysis. The measurement data with low measurement quality indicators is also excluded before the dynamical window method is used to select steady state time window and remove ship acceleration/deceleration periods. The steady state selection and 1-hour averaging are performed following the procedure given in Section 3. The raw data and selected data of the measured shaft speed, shaft power and ship speed through water during four different voyages are illustrated in Fig.6. In the application of dynamical windows, the confidence level α of Student's t-distribution is 0.01, the length of time window is 45 min. The threshold value for accepting each sample as steady is set to be 0.5.
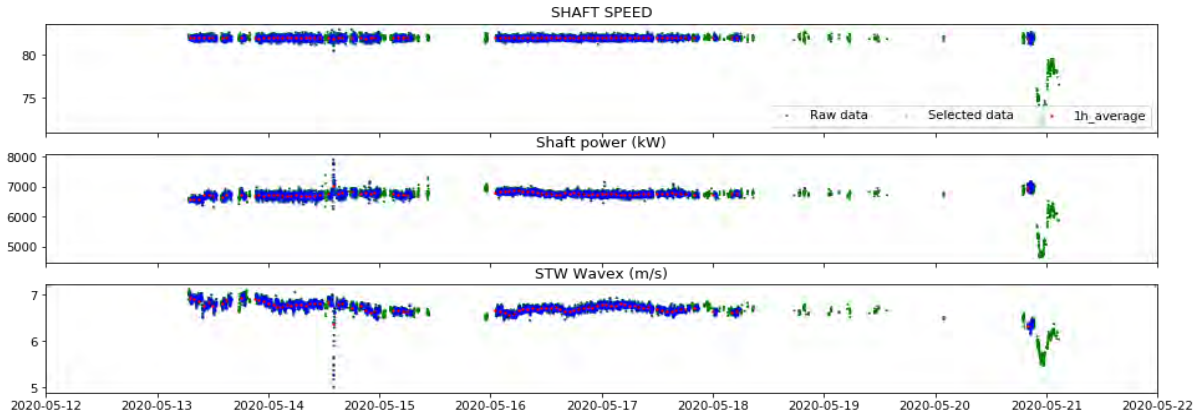
The results show that the dynamic window method can remove the acceleration/deceleration periods very well. The transition periods of shaft speed are removed, and the change of the ship speed is due to the weather disturbance.
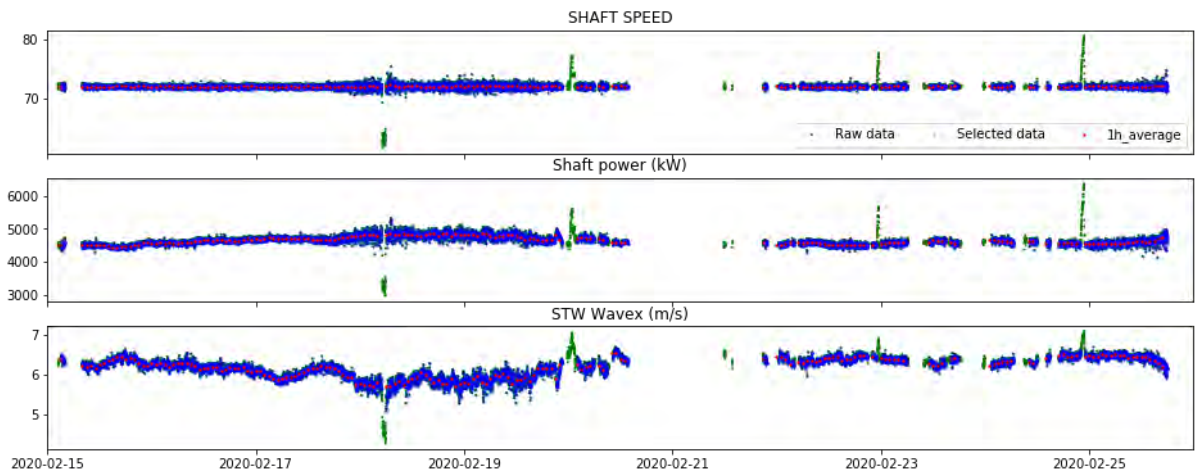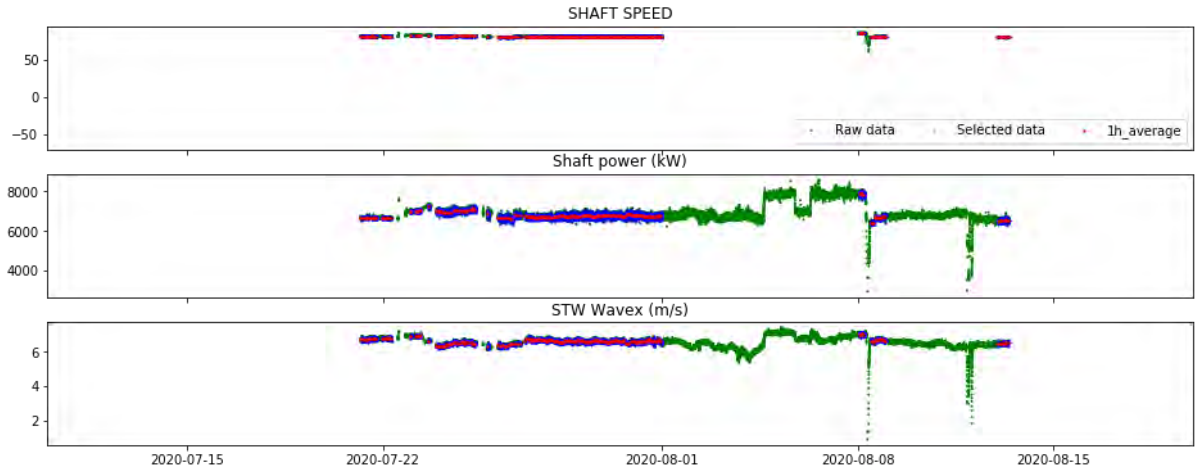

(a) Voyage 1
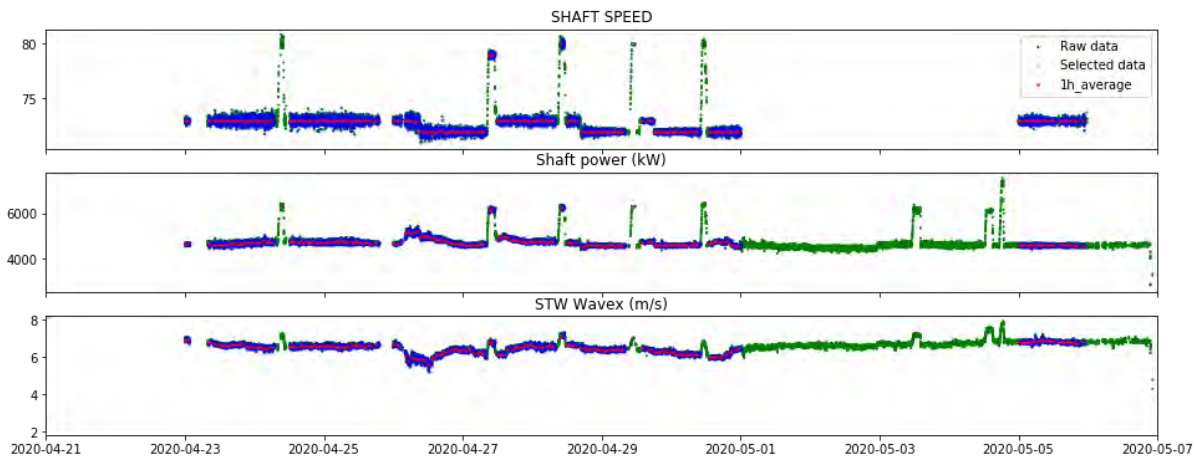
(b) Voyage 2

(c) Voyage 3

(d) Voyage 4

Fig.6: The comparison of raw data and the selected data of four different voyages ('Raw data' represents the raw measured data with filter on measured power range and measured data quality; 'Selected data' shows the selected data using the dynamical time window; '1h_average' gives the one hour mean value for analysis)

With the selected 1-hour mean value, correction of weather disturbance and water temperature effect is performed with the two different methods that are discussed in Section 4. The corrected power as a function of ship speed through water is illustrated in Fig.7. 'Shaft power (kW)' gives the measured shaft power. 'Simple Corrected power (kW)' is the corrected ship shaft power using the first normalization method, given by Eq.(3)-(4). 'Propeller Corrected power (kW)' represents the corrected ship shaft power using the second normalization method, given by Eq.(5)-(19). 'Speed/power curve' shows the speed-power curve derived from sea trial data, which is obtained by interpolating shaft power as a function of speed and the given loading condition. 'Speed/power curve_admiral' and 'Speed/power curve_surf' are the power-speed curves derived from sea trial data using admiral method and scaled wetted surface area method. In the calculation, the first step is to find the one loading condition in the sea trial report that is closest to the real ship loading condition. The power-speed curve at selected loading condition is used as a basis for further calculation. The admiral method calculates power according to

$$P = P_{sea-trial}\left(\frac{\nabla}{\nabla_{sea-trial}}\right)^{2/3} \tag{28}$$

∇ is the displacement of the ship, $\nabla_{sea-trial}$ is the displacement in the sea trial report that is closest to ship displacement ∇. For the scaled wetted surface area method, the power is calculated with

$$P = P_{sea-trial}\frac{S}{S_{sea-trial}} \tag{29}$$

90

S is the ship wetted surface area and $S_{sea-trial}$ is the wetted surface that is corresponding to $\nabla_{sea-trial}$ in (28).

The results show that 'power-speed curve' is very close to 'Speed/power curve_suf' in all four different voyages, which indicates that it is reasonable to derive the reference power from sea trial data using interpolation.

Since the measured data is selected based on fixed RPM, the shaft power decreases with the increase of ship speed. This is because of weather. The added resistance due to weather reduces ship speed and increases the output shaft power. The power corrected with both normalization methods increases with the increase of ship speed. The corrected power with Eqs.(5)-(19) gives lower value than that with Eqs.(3)-(4). This is expected, since Eq.(19) considers the change of propeller efficiency due to waves, while Eq.(4) does not. The power with Eqs.(5)-(19) has larger scatter, which could be partly due to that the propeller model introduces some uncertainty. This needs further investigation.
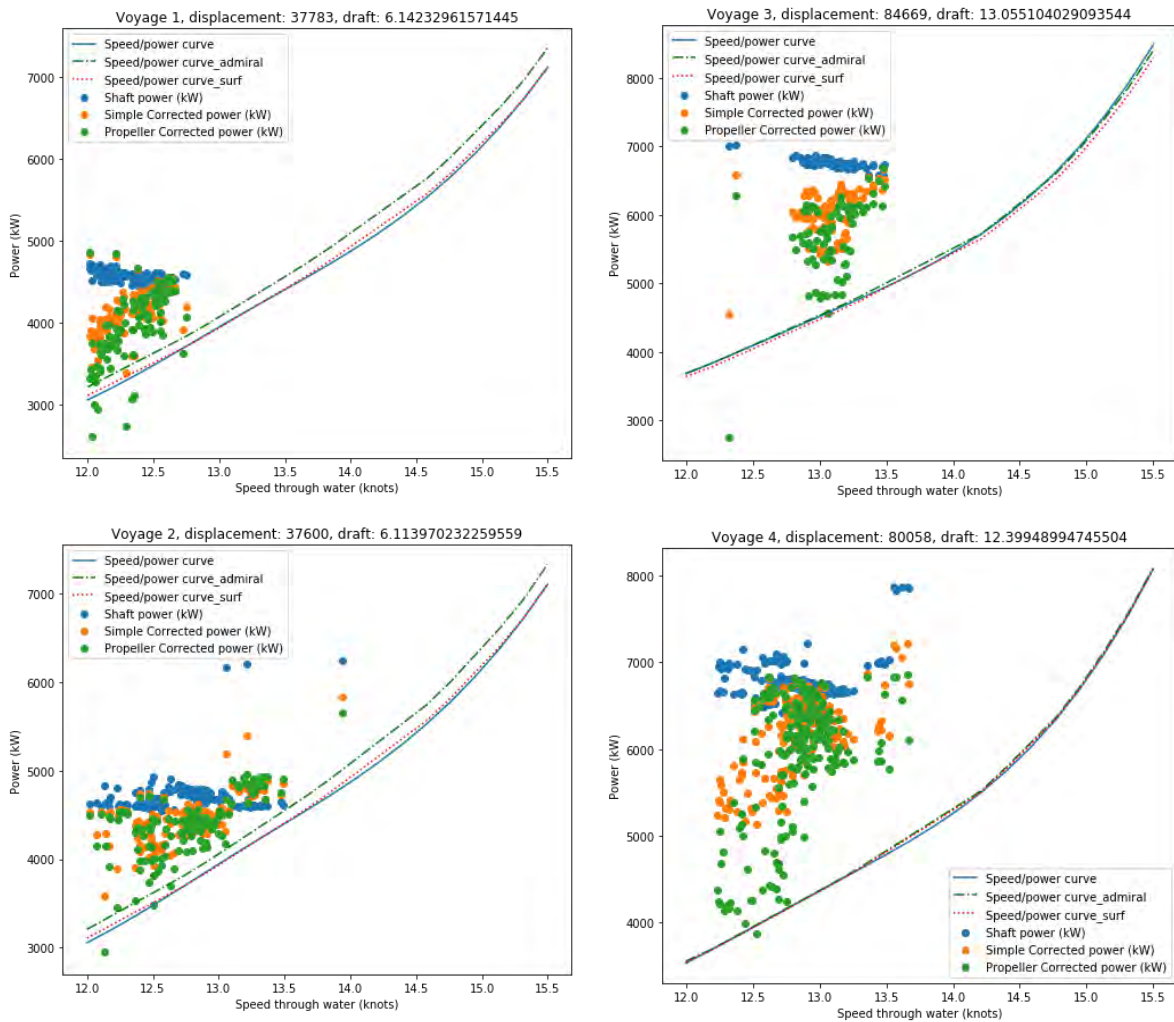

Fig.7: Ship shaft power vs ship speed through water using the two different normalization methods

The ratio $\frac{P_E}{P_{E_{ref}}} = \frac{VTI}{EEDI}$ at four different voyages is illustrated in Fig.8. 'VTI/EEDI' is the power ratio of effective power calculated directly from measured power to reference power. The weather and water temperature effects are not corrected. 'Cor_VTI/EEDI_Simple' represents the ratio of effective power corrected with Eqs.(3)-(4) to the reference power. 'Cor_VTI/EEDI_Propeller' gives the ratio of effective power corrected with Eqs.(5)-(19) to the reference power. The ship stayed in port for long

time between voyage 3 and voyage 4. Thus, the results in voyage 4 is analyzed separately. The power ratio trend is also given in Fig.8. The results show that the ship roughness increases approximately linearly at the first three voyages. Roughness effect increases faster in voyage 4 after long time stay in port.
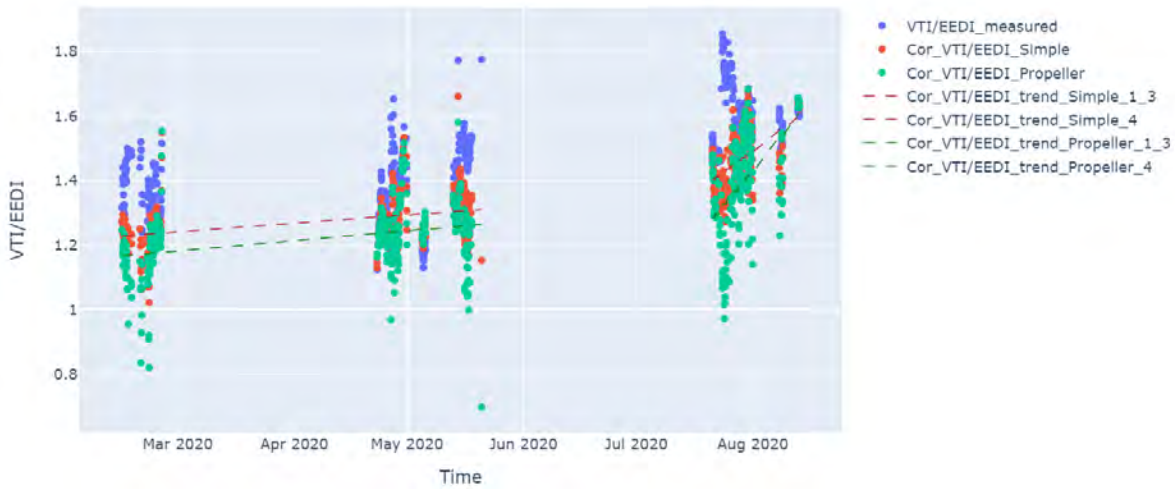

Fig.8: The change of Power ratio with time

7. Conclusions

A technical performance index is proposed in this paper, which can be used to check the ship hull and propeller condition. EEDI value is included as a coefficient in the index to make the index comparable amongst different ships. Moreover, a procedure is developed to analyze ship in-service measurements and calculate this index.

The technical performance of a bulk carrier is evaluated following the proposed procedure. The measured data used for analysis includes ship speed through water, shaft power, shaft speed, wind and wave information. The water temperature is derived from the Copernicus database. All the measured data is synchronized at 1-minute frequency. The measured data is first filtered based on water depth and measurement quality indicators. Then the dynamical window method is used to remove ship acceleration/deceleration periods. Finally, the clean data is averaged on 1-hour interval for the weather normalization.

The effects of wave and wind on ship power are first corrected for. Then the effect of water temperature and water density is corrected to get speed power curves in standard calm water condition with water temperature of 15°C and water density of 1026 kg/m^3. Two different normalization methods are tested. The results show that both normalization methods can capture a reasonable relationship between the shaft power and speed. The correction power is larger when propeller model is used in the normalization, since the effect of weather on propeller efficiency is considered in this method. The results of this method have larger scatter, which needs further investigation.

After normalizing for the weather effect, the correlation between power and ship speed seems reasonable. The technical performance index can capture the change of ship hull and propeller condition, which indicates that the proposed procedure for analyzing ship technical performance is very promising.

There is still scatter in the corrected power speed data. More study on the data preparation and weather normalization should be performed. 1-hour data is averaged for the analysis, and the effect of time window length should also be studied further. Analyzing ship engine and propeller efficiency based on in-service data will be the next topics.

References

BERNITSAS, M.M.; RAY, D.; KINLEY, P. (1981), K_T, K_Q *and Efficiency Curves for the Wageningen B-Series Propellers*, Dept. of Naval Architecture and Marine Engineering, University of Michigan

BIALYSTOCKI, N.; KONOVESSIS, D. (2016), *On the estimation of ship's fuel consumption and speed curve: a statistical approach*. J. Ocean Eng. Sci. 1 (2), pp.157-166

CARLTON, J., (2008), *Marine Propellers and Propulsion,* Butterworth-Heinemann.

CORBETT, J.J.; WINEBRAKE, J.J.; GREEN, E.H.; KASIBHATLA, P.; EYRING, V.; LAUER, A. (2007), *Mortality from Ship Emissions: A Global Assessment*, Env. Sci. Tech. 41, pp.8512-8518

DALHEIM, Ø.; STEEN, S. (2020), *A computationally efficient method for identification of steady state in time series data from ship monitoring*, J. Ocean Engineering and Science 5, pp.333-345

FUJIWARA, T.; UENO, M.; IKEDA, Y. (2005), *A new estimation method of wind forces and moments acting on ships on the basis of physical component models*, J. Japan Soc Naval Architects Ocean Eng. 2, pp.243-255

FUJIWARA, T.; UENO, M.; IKEDA, Y. (2006), *Cruising performance of a large passenger ship in heavy sea*, 16th Int. Offshore and Polar Eng. Conf., San Francisco

GIA (2020), *Protocol for validation of performance of Energy Efficiency Technologies (EETs)*

GUO, B.J., STEEN, S. (2011), *Evaluation of added resistance of KVLCC2 in short waves*, J. Hydrodynamics, Ser. B 23/6, pp.709-722

ICS (2020), *Shipping and World Trade: World Seaborne Trade,* Int. Chamber of Shipping, https://www.ics-shipping.org/shipping-fact/shipping-and-world-trade-world-seaborne-trade/

IMO (2009), *Guidelines for Voluntary Use of the Ship Energy Efficiency Operational Indicator (EEOI),* https://gmn.imo.org/wp-content/uploads/2017/05/Circ-684-EEOI-Guidelines.pdf

IMO (2019), *Low carbon shipping and air pollution control*, http://www.imo.org/en/MediaCentre/HotTopics/GHG/Pages/default.aspx

ISO (2015), *ISO 15016: Ships and marine technology — Guidelines for the assessment of speed and power performance by analysis of speed trial data*, Int. Standard Org., Geneva

ISO (2016), *ISO 19030: Ships and marine technology — Measurement of changes in hull and propeller performance,* Int. Standard Org., Geneva

ITTC (2017), *Procedures and guidelines. Preparation, Conduct and Analysis of Speed/Power Trials.* 7.5-02.-07-02.1., Revision 05, International Towing Tank Conference

ITTC (2018), *Calculation of the weather factor fw for decrease of ship speed in wind and waves*, Seakeeping committee of the 29th International Towing Tank Conference

KELLY, J.D.; HEDENGREN, J.D. (2013), *A steady-state detection (SSD) algorithm to detect non-stationary drifts in processes,* J. Process Control 23, pp.326-331

KIM, M.; HIZIR, O.; TURAN, O.; DAYA, S.; INCECIK, A. (2017), *Estimation of added resistance and ship speed loss in a seaway*, Ocean Engineering 141, pp.465-476

KIM, D.; LEE, S.; LEE, J. (2020), *Data-driven prediction of vessel propulsion power using support vector regression with onboard measurement and ocean data,* Sensors 20 (6)

KLAVENESS (2021), *Selecting the right Climate Intensity Indicator (CII) to move shipping towards IMO's 2030/2050 decarbonization targets,* SFI Smart Maritime WEBINAR

LARSSON, L.; STERN, F.; VISONNEAU, M. (2010), *Gothenburg 2010 - A workshop on Numerical Ship Hydrodynamics*, Report, Gothenburg, http://www.gothenburg2010.org/

LIU, S.; LOH, M.; LEOW, W.; CHEN, H.; SHANG, B.; PAPANIKOLAOU, A. (2020), *Rational processing of monitored ship voyage data for improved operation*, Applied Ocean Research 104

LIU, S.K.; PAPANIKOLAOU, A. (2016), *Fast approach to the estimation of the added resistance of ships in head waves*, Ocean Engineering, pp.211-225

LIU, S.; PAPANIKOLAOU, A. (2020), *Regression analysis of experimental data for added resistance in waves of arbitrary heading and development of a semi-empirical formula*, Ocean Engineering

ORIHARA, H., TSUJIMOTO, M. (2018), *Performance prediction of full-scale ship and analysis by means of on-board monitoring. Part 2: Validation of full-scale performance predictions in actual seas,* J. Mar. Sci. Technol. 23 (4), pp.782-801

OZDEMIR, Y.H.; BARLAS, B. (2017), *Numerical study of ship motions and added resistance in regular incident waves of KVLCC2 model*, Int. J. Naval Architecture and Ocean Eng. 9, pp.149-159

PARKER, S.; RAUCCI, C.; SMITH, T.; LAFFINEUR, L. (2015), *Understanding the Energy Efficiency Operational Indicator: An empirical analysis of ships from the Royal Belgian Shipowners' Association, Executive Summary,* Royal Belgian Shipowner's Association

PETERSEN, J.P.; JACOBSEN, D.J.; WINTHER, O. (2012), *Statistical modelling for ship propulsion efficiency*, J. Mar. Sci. Technol. 17, pp.30-39

SADAT-HOSSEINI, H.; WU, P.C.; CARRICA, P.M.; KIM, H.; TODA, Y.; STERN, F. (2013), *CFD verification and validation of added resistance and motions of KVLCC2 with fixed and free surge in short and long head waves*, Ocean Engineering 59, pp.240-273

TASKAR, B.; ANDERSEN, P. (2021), *Comparison of added resistance methods using digital twin and full-scale data*, Ocean Engineering 229

TVETE, H.A.; GUO, B.; LIANG, Q.; BRINKS, H. (2020), *A Modelling System for Power Consumption of Marine traffic*, 39th Int. Conf. Ocean, Offshore and Arctic Eng. OMAE2020-18651

VAN DEN BOOM, H.J.; HASSELAAR, T.W. (2014), *Ship speed-power performance assessment,* SNAME Maritime Convention, Houston

HullMASTER – An Interactive Tool to Calculate Economic and Societal Costs and Benefits of Ship Hull Maintenance

Dinis Reis Oliveira, Chalmers University of Technology, Gothenburg/Sweden, dinis@chalmers.se
Maria Lagerström, Chalmers Univ. of Technology, Gothenburg/Sweden, maria.lagerstrom@chalmers.se
Lena Granhag, Chalmers Univ. of Technology, Gothenburg/Sweden, lena.granhag@chalmers.se
Sofia Werner, SSPA Sweden AB, Gothenburg/Sweden, sofia.werner@sspa.se
Ann Larsson, University of Gothenburg, Gothenburg/Sweden, ann.larsson@marine.gu.se
Erik Ytreberg, Chalmers University of Technology, Gothenburg/Sweden, erik.ytreberg@chalmers.se

Abstract

Through cross-disciplinary research a novel interactive tool has been developed, HullMASTER, which enables shipowners, operators, and authorities in the Baltic Sea region to make evidence-based decisions on strategies and policies related to ship hull maintenance. This novel tool is deployed as a standalone app (source code in MATLAB). Modelling is based on cost-effective approximate prediction methods (Granville method), as well as on empirical fouling data. Validation of HullMASTER predictions for hull-and-propeller performance shows ~80% agreement against nearly 40 vessel-years of performance data (fleet of 9 vessels). Further, three types of hull coating were compared in a demonstration case: a copper-based antifouling coating, a biocide-free foul-release coating, and an inert abrasion-resistant coating. In this demonstration, the foul-release coating is shown to be the most sustainable alternative for a 10,000-DWT cargo ship in terms of pressure on the environment and health. These societal savings are aligned with potential economic savings for the shipping operator.

1. Introduction

Shipowners and operators are well aware of the economic importance of well-maintained underwater hull and propeller surfaces for vessel energy efficiency (Adland et al., 2018). However, dry-docking decisions may currently lack independent and objective evidence in the selection of a fouling-control strategy for a given vessel, *Safinah Group (2020),* while having economic consequences for the following 2-5 years of vessel operation or even longer in some cases, *Bebić et al. (2018)*. Maintenance strategies include selecting from different coating types, for example between conventional biocidal copper-based coatings and biocide-free alternatives, frequency of docking, frequency of in-water cleaning, and hull pretreatments (full blasting or spot blasting). The optimal answer depends on ship size, speed, activity profile, salinity etc. A knowledge gap is identified on how to support operators in making these decisions. Consequences of sub-optimal decisions are beyond sheer economics, with hull maintenance being a low-hanging fruit for decreasing shipping's pressure on climate, human health, and marine water quality, *Wan et al. (2018), Ytreberg et al. (2021)*.

In a cross-disciplinary research effort, Chalmers University of Technology, together with SSPA Sweden AB and University of Gothenburg, has developed an interactive tool – HullMASTER, Hull MAintenance STrategies for Emission Reduction – to equip shipowners, operators and other stakeholders with evidence on economic and environmental cost-and-benefit of different ship hull maintenance strategies. The tool is freely available as a standalone executable Windows-based program, Fig.1, in which the user specifies main vessel particulars, engine and fuel details, as well as route details. The user is then able to customize their hull maintenance strategies, i.e. scenarios for type of coating, surface preparation in dry dock, dry-docking frequency, and in-water hull cleaning frequency, and compare scenarios in terms of both economic and environmental performance. The environmental impact includes both emissions to air from burning fuel and emissions to water from antifouling paint's biocide release. This paper focuses mainly on the validation of the hull performance aspect. To assess the different strategies, the tool includes models for fouling growth rate, hull roughness as an effect of fouling and maintenance, and finally the effect on propulsion power consumption. The current scope of the tool is restricted to vessels operating exclusively in the Baltic Sea region, but the authors envision future extension of the tool to include other marine regions worldwide.

In the current paper, the principles behind development of HullMASTER as a decision-support tool are presented and discussed, including validation against hull-and-propeller performance data (nine vessels, nearly 40 vessel-years) and a demonstration case (one vessel).
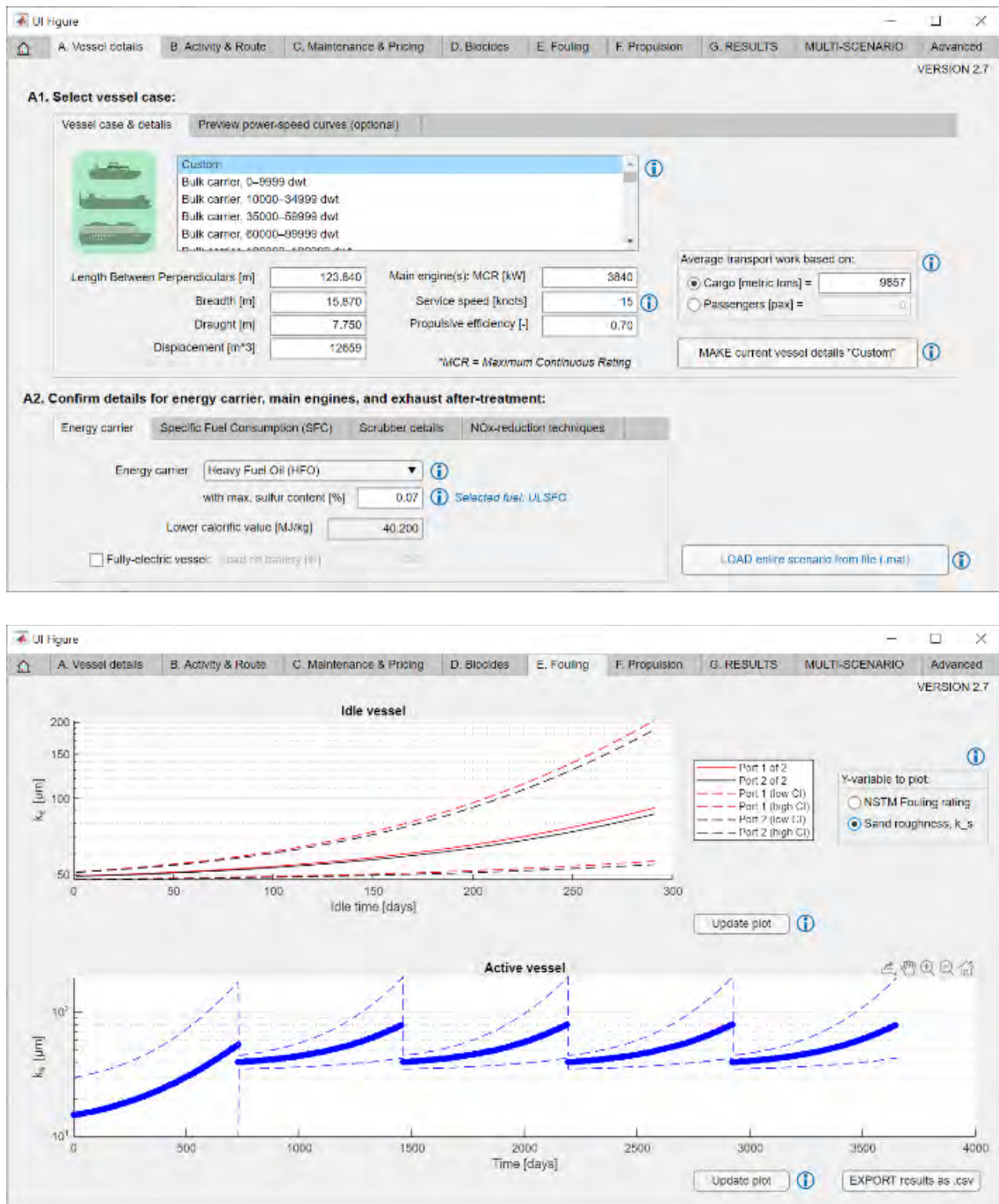

Fig.1: HullMASTER's user interface, a free-license standalone Windows executable for calculating the economic and societal cost of biofouling and fouling control.

2. Materials and Methods

2.1. Fouling growth model

How quickly biofouling is established and growing on a hull surface depends on many parameters. In this study, a model for fouling growth is developed for the Baltic Sea and Skagerrak Sea (North Sea) accounting for the type of coating, seawater salinity, fouling pressure and idling time.

Uzun *et al. (2019)* fitted Gaussian curves to the time-series of fouling growth at different locations, each for Equatorial and Mediterranean waters. In the present study, data from previous idle-panel studies in the Baltic Sea region are complemented with new data for several types of coatings, as described below, and data are also fitted using Gaussian curves, which helps easily define the severity of fouling accumulated over time for a given location, as exemplified in Fig.2. The US Navy's Naval Ships' Technical Manual (NSTM) fouling rating is chosen, as this has been previously correlated to propulsive penalties via determination of an equivalent hydraulic sand-grain roughness height, k_s, *Demirel et al. (2017), Schultz (2007), Uzun et al. (2019)*, i.e. the height of sand grains that leads to the same frictional penalty as a given hull condition. The NSTM fouling rating is reported in a 0-100 scale, where 0 is a clean coating (k_s ~30 µm) and 100 represents a heavily fouled surface, with all types of fouling present (k_s ~10,000 µm, according to *Schultz (2007)*). It is noted that NSTM fouling rating and k_s are correlated exponentially, as detailed below, Eq.(1).
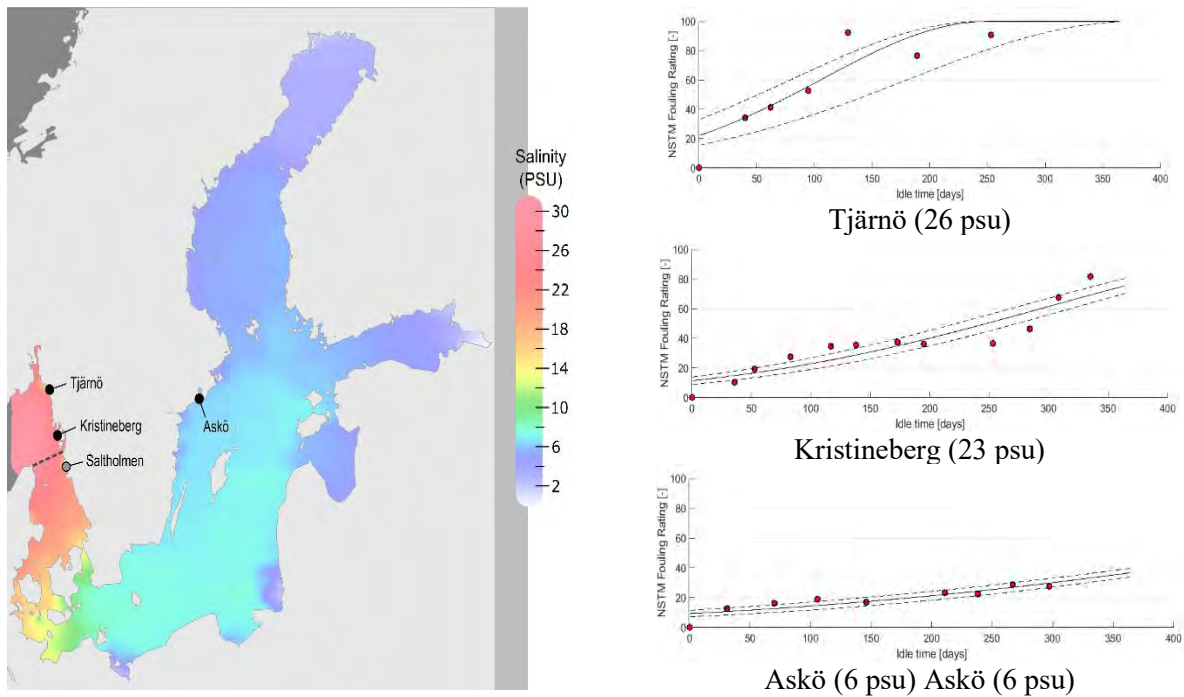

Fig.2: Location of marine field stations and respective fouling pressure an inert coating. Gaussian curves are fitted to sampled fouling rating datapoints. Ongoing data collection is obtained from Tjärnö, Kristineberg and Askö. Data from Saltholmen (Gothenburg, Sweden) is obtained from *Oliveira and Granhag (2020)* and currently used for modelling antifouling and foul-release coatings (not shown). Salinity data originates from *IMR (2012)*. The map is produced in Ocean Data View, *Schlitzer (2018)*.

In previous studies conducted in the Baltic Sea region, panels with area ~100-200 cm² and coated with different types of hull paints were submerged at sea to determine the performance of fouling-control coatings and in-water maintenance events, *Oliveira and Granhag (2020)*, as well as fouling pressure, *Wrange et al. (2020)*, i.e. the severity of fouling developed on inert surfaces submerged at sea for a given period of time. Similarly, in the current study, panels are submerged at three different locations, Tjärnö and Kristineberg on the West coast of Sweden (salinity 23-26 psu) and Askö on the East coast (~6 psu, Fig.2), bearing three types of coating: conventional biocidal copper-based antifouling, biocide-free foul-release, and an inert coating. Fouling data is fitted using Gaussian curves, *Uzun et al. (2019)*, resampled at all time steps available, and linearly interpolated between 4 available geographical locations: Tjärnö (26 psu), Kristineberg (23 psu), Saltholmen (19 psu), *Oliveira and Granhag (2020)*, and Askö (6 psu). Salinity is currently the best predictor for fouling pressure in the Baltic Sea region, *Wrange et al. (2020)*. Given the currently low number of geographical locations, Fig.2, preliminary analysis has shown a linear interpolation to be the most reasonable approach to account for salinity effect on fouling pressure. Finally, fouling is assumed to only settle and develop (grow) when a vessel

is idle, following the same approach as in *Uzun et al. (2019)*. Effects of seasonality are not addressed explicitly in HullMASTER, meaning that e.g. high fouling growth rates in the summer cannot be exactly timed by the user. Still, the average effect of seasons in fouling growth is included implicitly in the results, as panel data ranges both summer and winter seasons.

2.2. Hull roughness condition

Hull roughness condition is expressed as hydraulic sand-grain roughness height, k_s. Roughness is assumed to build up within a dry-docking interval, i.e. the period between two dry-dockings, from an initial coating roughness height to a hull condition where fouling has a predominant effect. Hydraulic sand-grain roughness height, k_s, is not the same as Average Hull Rougness (AHR): the latter is the physical peak-to-valley height, whereas the former is a hydrodynamically-determined value, *Oliveira et al. (2020)*.

Initial coating roughness height is assumed in HullMASTER according to values presented in Table I, where initial coating condition is the smoothest for a foul-release coating after full-grit blasting (as low as 0 μm, i.e. hydraulically smooth) and increases for other coating types and touch-up coating maintenance. The highest initial roughness is obtained for "Light cleaning", *Leer-Andersen (2018)*, i.e. an imperfectly in-water-cleaned hull surface, assumed to correspond to the case of reactive cleaning on calcareous forms of fouling, with e.g. barnacle baseplates remaining after the cleaning, Table I.

Table I: Equivalent hydraulic sand grain roughness height ks values for initial coating roughness, converted from power or frictional penalties given in cited sources, using the method detailed in *Oliveira et al. (2020)*. IWHC = in-water hull cleaning.

Initial condition	k_s [μm], Lower bound	k_s [μm], Average	k_s [μm], Upper bound	Source, coatings and treatments
Full grit blasting: foul-release coating	0	15	30	Jotun Silicone: Seaquantum, *Leer-Andersen (2018)* foul-release, normal application, *Yeginbayeva and Atlar (2018)*
Full grit blasting: polishing antifouling and inert coating	30	40	60	Jotun: Antifouling Seaforce 60, *Leer-Andersen (2018)*, linear polishing polymer, normal application, *Yeginbayeva and Atlar (2018)*
Touch-up: foul-release coating	35	40	45	Foul-release, mimicked hull roughness, *Yeginbayeva and Atlar (2018)*
Touch-up: polishing antifouling and inert coating	30	65	150	Jotun: Rough antifouling Seaforce 60, and flaked paint, *Leer-Andersen (2018)*, linear polishing polymer, mimicked hull roughness, *Yeginbayeva and Atlar (2018)*
Proactive IWHC, negligible wear	same as out-docking	same as out-docking	same as out-docking	Currently assuming no further coating deterioration
Proactive IWHC, moderate wear	50	80	150	High pressure cleaning, *Leer-Andersen (2018)*
Reactive IWHC, high wear	70	150	300	Light cleaning, *Leer-Andersen (2018)*

Adding to this initial coating roughness height, hull roughness due to fouling is modelled based on data from *Schultz (2007)*, using a fitted curve (correlation coefficient $R^2 = 0.96$):

$$k_{s,fouling} = 46.927 \times e^{\,0.056614 \times (NSTM\ fouling\ rating)} \tag{1}$$

2.3. Modelling of powering penalty

Hydraulic sand-roughness height, k_s (not to be confused with AHR), is translated into propulsion penalties using a flat-plate similarity-law scaling method, *Granville (1958)* method. According to the current version of the Granville method, *Demirel et al. (2017), Schultz (2007)*, the flat-plate Kármán-Schoenherr friction line is offset by $+\Delta U^+ \kappa [\log(10)]^{-1}$ along the Reynolds axis (Reynolds number based on vessel speed and length), where ΔU^+ is the roughness function at a given roughness Reynolds number, i.e. based on roughness height and viscous length scale, *Demirel et al. (2014)*. The method relies on iterative estimation of the hull's average roughness Reynolds number k_s^+ (and the respective ΔU^+ value) for a given sand roughness height k_s [μm], vessel speed V, and waterline length L_{WL}, until results converge to ship-scale Reynolds number, as described in more detail and validated elsewhere, *Demirel et al. (2017), Oliveira et al. (2018), Song et al. (2021)*.

The Granville method allows calculation of towing resistance penalty due to hull roughness, ΔR in kN. This change in towing resistance is currently translated to shaft power penalty, ΔP in kW, assuming negligible effect of hull roughness on propulsive efficiency η_D, *Oliveira et al. (2020)*:

$$\Delta P = \frac{\Delta R(k_s) \times V}{\eta_D} \tag{2}$$

2.4. Validation of hull-and-propeller performance predictions

Data contributions were kindly made by four collaborating shipping operators in the RoRo and RoPax segments (Roll-on/Roll-off Cargo and Vehicle/Passengers, respectively), consisting of auto-logged or voyage performance data for nine vessels, or a total of nearly 40 vessel-years, Table II:. From Table II:, it is important to retain that reported data varied across the fleet in regards to availability and reliability of primary parameters speed through water (e.g. unreliable STW for vessels A and B, so speed over ground SOG is used as a proxy) and delivered power (e.g. shaft torque meters unavailable on vessels C and I, so fuel consumption FC is used for deriving a proxy). Unavailable secondary parameters also presented challenges for most of the vessels (D-I). Further, the source of curves for baseline power-speed performance spans from simple empirical methods, based on vessel main particulars, *Holtrop and Mennen (1982)*, to detailed model test and sea trials, representing conditions close to those observed during vessel operation. Vessel performance data is further filtered for vessel displacement within 5% of reference displacement value (in metric tons) and vessel speed is then corrected using the Admiralty formula, *ISO (2016)*, and filtered to the speed range of the reference baseline power-speed curves. Finally, wind, rudder angle and depth data, or else estimated by the crew onboard (except for vessels D, E and F, 'Other': wind data sourced from land-based weather stations located within 2 nautical miles) was used for filtering out rough weather datapoints (wind speed > 7.9 m/s, or Beaufort > 4), shallow water effects, and changes in course, *ISO (2016)*. Finally, data logging frequency corresponded to 10-min averages and standard error (vessels A, B and C, which "can be useful for analysis" according to ISO, 2016), ISO 19030 part 2-compliant data-logging frequency (vessels D, E and F) or ISO 19030 part 3-compliant data-logging frequency (vessels G, H and I).

In regard to coating systems applied during dry-docking maintenance, some vessels had been recently retrofitted with a different coating type ("→" indicates coating retrofit):

- Vessel A: antifouling polishing coating (AF) → abrasion resistant coating (inert)
- Vessel B: antifouling polishing coating (AF) → hybrid foul-release (hybrid FR)
- Vessel C: antifouling polishing coating (AF) → copper-free polishing coating
- Vessel D: antifouling polishing coating (AF) (no retrofit)
- Vessel E: antifouling polishing coating (AF) (no retrofit)
- Vessel F: antifouling polishing coating (AF) (no retrofit)

- Vessel G: antifouling polishing coating (AF) (no retrofit)
- Vessel H: antifouling polishing coating (AF) → hybrid foul-release (hybrid FR)
- Vessel I: silicone foul-release coating (FR) (no data prior to retrofit), with hull water pressure washing every subsequent dry-docking (no hull blasting),

where antifouling polishing coatings are conventional biocidal coating containing copper(I) oxide and zinc oxide (among other booster biocides), silicone foul-release coatings are biocide-free coatings, and hybrid foul-release coatings contain a booster biocide, in this case copper pyrithione at ≤10% w/w. Since there is currently no available field panel data for the latter hybrid coatings, hull performance is compared to the closest coating type available in HullMASTER, i.e. a biocide-free foul-release coating.

Table II: Vessel performance parameters, autologged or manually logged as voyage reports. Data for vessel I is from *Kowalski (2020)*, who kindly shared raw data to validate HullMASTER.

Vessel	Area of opera-tion	Primary parameters			Secondary parameters				Data size and rate	baseline power--speed curve
		Speed [kn]	P [kW]	FC [kg/h or L/h]	Wind speed [m/s], dir. [°] (or Bft)	Rudder angle [°]	Sea depth [m]	Draft and Trim[m]		
A 190-m RoRo Cargo	Kattegat Sea and North Sea	SOG	+	(L/h)	+	+	+	+	5.2 years @ 10-min A±SE	Model test
B 190-m RoRo Cargo	Kattegat Sea and North Sea	SOG	+	(L/h)	+	+	+	+	5.3 years @ 10-min A±SE	Model test
C 180-m RoRo Cargo	Baltic Proper	SOG	N/A	L/h	+	+	+	+	4.5 years @ 10-min A±SE	Sea trial
D 100-m RoPax	Danish Straits	SOG	+	(L/h)	Other	N/A	N/A	N/A	1.5 years @ Every 15 s	Sea trial
E 95-m RoPax	Danish Straits	SOG	+	(L/h)	Other	Azimuth	N/A	N/A	1.8 years @ Every 15 s	Model + Sea trial
F 95-m RoPax	Danish Straits	SOG	+	(L/h)	Other	Azimuth	N/A	N/A	2.3 years @ Every 15 s	Model + Sea trial
G 220-m RoPax	Kattegat Sea and Danish Straits	STW	+	(L/h)	+	N/A	+	Only trim	3.5 years @ Every minute	Model test
H 230-m RoPax	Kattegat Sea and Danish Straits	STW	+	(L/h)	+	N/A	+	Only trim	3.5 years @ Every minute	Empirical
I 140-m RoPax	Baltic Proper	SOG	N/A	kg/h	BF	N/A	N/A	+	11.8 years @ Each sea passage (2 day⁻¹)	Empirical

Legend: + variable available and included in the analysis, () variable available but excluded from the analysis, SOG – speed over ground, STW – speed through water, Other – from sources external to the vessel (oceanographic and land-based weather data), Azimuth – thruster azimuth angle used instead of rudder angle, P – shaft power, FC – fuel consumption, BF – Beaufort scale, A±SE – average ± standard error, N/A – not available.

Finally, for the current validation purposes, percentage powering penalties relative to smooth hull condition, P_{diff}, defined as:

$$P_{diff}[\%] = \frac{P_{rough\,hull} - P_{smooth\,hull}}{P_{smooth\,hull}} \times 100 = \frac{\Delta P}{P_{smooth\,hull}} \times 100 \qquad (3)$$

are used in validating HullMASTER predictions against measured performance (in-service data).

2.5. Emission factors and Pricing

Emissions to the atmosphere are modelled according to methods presented in IMO's 4th greenhouse gas study, *IMO (2020)*, for calculating specific fuel oil consumption and emission of greenhouse gases and air pollutants, per ton of fuel or per engine break power, as applicable for each substance.

Regarding emissions to the marine environment, copper and zinc release rates from a biocidal polishing antifouling coating are currently modelled as a function of salinity, for each of immersion periods 0-14 days and 14-56 days separately, *Lagerström (2020),* paint product: Micron Superior), and with time decay based on time-resolved release rate data, *Valkirs et al. (2003)*.

Dry-docking and in-water hull cleaning prices are derived from multiple sources (local operators and a shipyard, as well as previous studies, *Bebić et al. (2018), Hansen (2013)*, bunker costs are estimated for Ultra-Low Sulfur Fuel Oil (ULSFO) based on historic data in the period 2014-2020, *DNV GL (2020), Ship & Bunker (2020)*.

Besides economic costs for operators, societal costs are also accounted for, based on willingness-to-pay surveys on citizens living in the Baltic Sea region, among other damage-cost estimates, for impacts on human health, climate, marine eutrophication, and marine ecotoxicity, *Nordhaus (2017), Noring (2014), Noring et al. (2016), Ytreberg et al. (2021)*.

3. Results and Discussion

3.1. Model validation

Validation scenarios are detailed according to maintenance and operation of nine vessels, Table III. Scenario details concern maintenance interval, average cruising speed, typical idle/active profile, and salinity in visited ports. Additionally, HullMASTER accounts for type of dry-dock maintenance, coating, one-off idle periods (exceptions from schedule), and in-water cleaning events (if any).

Table III: Vessel maintenance, activity, and route details for validation of HullMASTER

Vessel	Average dry-docking interval [years]	Average speed [knots]	Typical idle period [days]	Typical active period [days]	idle time	Seawater salinity range [psu]
A	2.0	19.0	0.72	1.28	36%	19 – 22
B	2.0	19.0	0.72	1.28	36%	19 – 22
C	2.8	21.5	0.31	0.69	31%	2 – 14
D	2.0	10.5	0.54	0.46, with shorter 10-min stops and 20-min trips	69%	12 – 13
E	2.0	10.5	0.009	0.011	45%	12 – 13
F	2.0	10.5	0.009	0.011	45%	12 – 13
G	3.0	17.5	0.42	0.58	42%	14 – 19
H	3.0	17.5	0.42	0.58	42%	14 – 19
I	1.9	14.0	0.23	0.27	46%	5 – 9

Dry-docking intervals are comparable across the fleet (2-3 years). Differences are observed in average speed (10-22 kn) and idle time (30-70%), which are relevant in testing HullMASTER in different operational profiles. However, vessel speed and idling time are moderately correlated ($R^2 = 0.57$), i.e. a higher average speed tends to co-occur with shorter total idling, so it is not possible to separate these two factors in respect to fouling growth. In modeling fouling growth, HullMASTER accounts solely for total idling time, route and maintenance details, whereas vessel speed is only accounted in further translating a hull roughness condition into powering penalty (Granville method).

Examples of time series for percentage powering penalties P_{diff} are shown in Fig. for vessels A, B and I, respectively. Dry-dockings are marked by vertical solid blue lines and in-water hull cleaning events are marked by vertical dashed blue lines.
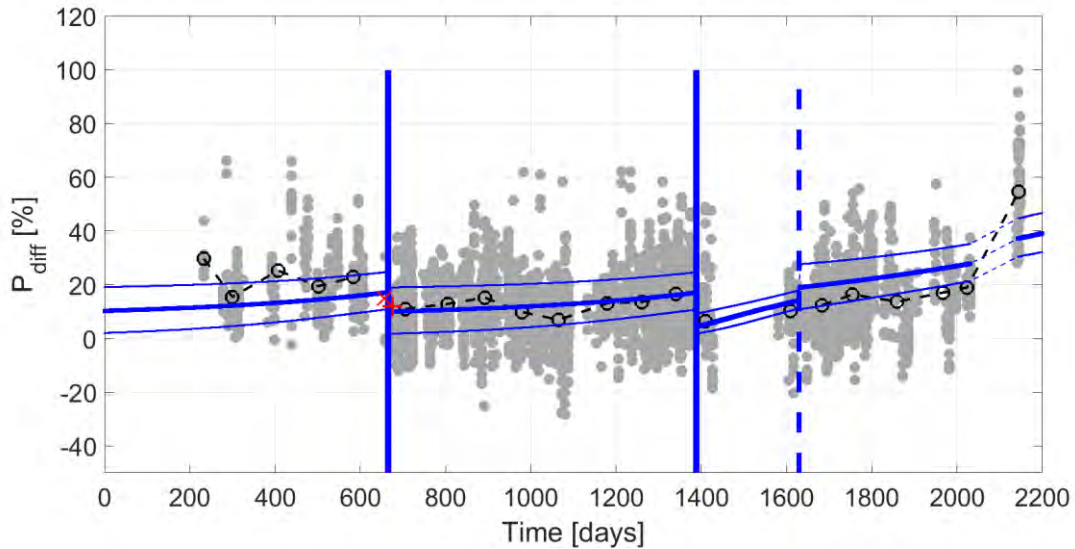

Fig.3: Hull-and-propeller performance: vessel A (190-m RoRo, coatings: AF – AF – Inert). Vertical lines indicate dry-dockings (solid) or in-water cleaning events (dashed). Legend: —— HullMASTER (average and 95% confidence intervals), ---o--- 3-month averages obtained from filtered vessel performance data (•).
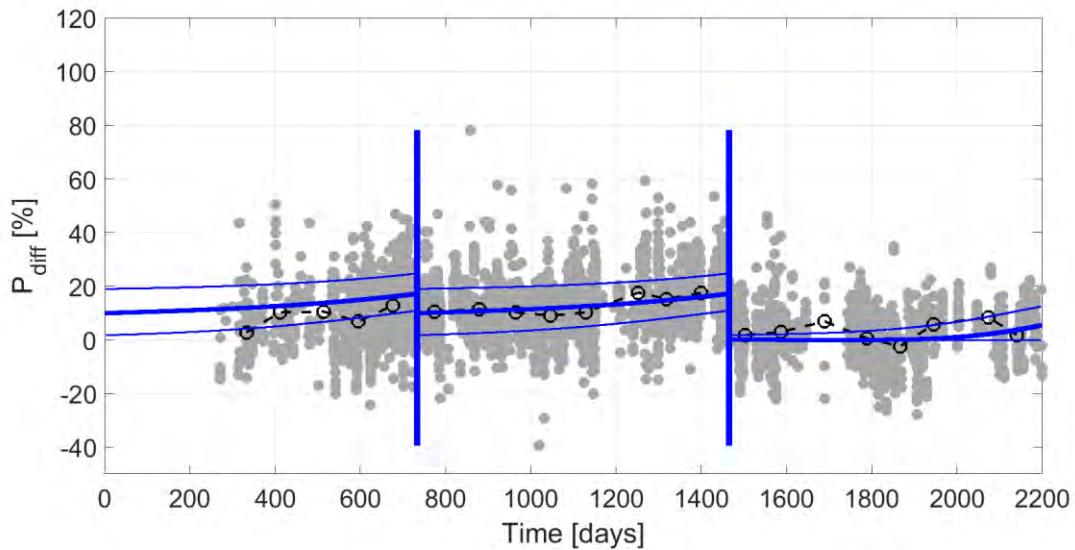

Fig.4: Hull-and-propeller performance: vessel B (190-m RoRo, coatings: AF – AF – hybrid FR). Vertical lines indicate dry-dockings (solid) or in-water cleaning events (dashed). Legend: —— HullMASTER (average and 95% confidence intervals), ---o--- 3-month averages obtained from filtered vessel performance data (•).
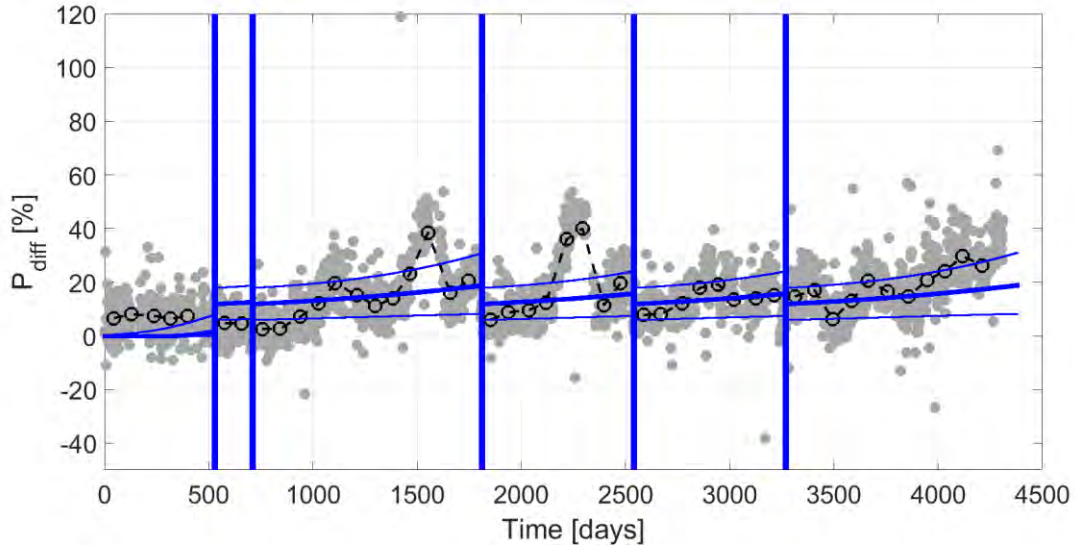
Fig.5: Hull-and-propeller performance: vessel I (140-m RoPax, silicone FR coating). Original data reported in Kowalski (2020). Vertical lines indicate dry-dockings (solid) or in-water cleaning events (dashed). Legend: —— HullMASTER (average and 95% confidence intervals), ---o--- 3-month averages obtained from filtered vessel performance data (∘).

For vessel A, Fig.3, it is observed that 3-month moving average values (---o---) fall almost entirely within the 95%-confidence prediction intervals from HullMASTER (——), except for the last period. Uncertainties in HullMASTER prediction include uncertainties in initial roughness height, Table I, replicate variability in idle panel data (quadruplicates), embedded seasonal variability, and interpolation uncertainty in fouling data. In the first 2 dry-docking intervals, an antifouling coating with initial touch-up condition applies. In the first dry-docking event, power penalty estimates based on in-docking inspection of NSTM fouling rating (X, Granville method) and peak-to-valley hull roughness survey on the out-docking vessel (+, Townsin's formula, *ITTC (2014)*) are also in close agreement with performance predicted by HullMASTER. Upon the second dry-docking, vessel A was retrofitted with an inert abrasion resistant coating, with no fouling control properties. Out-docking performance initially improved compared to previous homologous out-docking period, from 11% → 6%, this being due to full sandblasting of the hull down to bare steel on the second dry-docking. However, performance rapidly deteriorated for this inert coating, as shown by both measured and predicted performance. A single in-water cleaning event seems to have granted no significant improvement in performance. Towards the end, a prolonged idle period of ~4 months is qualitatively captured in predictions from HullMASTER, even though predictions are somewhat lower, Fig.3.

For vessel B (Fig.4), the first 2 dry-docking intervals are identical to those of vessel A, as expected since these two vessels are sister vessels operating in the same route. Good agreement between measured and predicted penalties is also found here. Vessel B was retrofitted with a hybrid foul-release coating in the second dry-docking, following full sandblasting, which resulted in a drastic decrease in out-docking powering penalty compared to previous homologous out-docking period, 11% → 2%, with sustained low powering penalty of ~5% throughout the last dry-docking interval. Such low values of measured penalties agree well with a lower penalty and slow deterioration in performance predicted by HullMASTER for a foul-release coating, on this specific vessel and route, Fig.4, even though the actual coating was not a biocide-free but instead a hybrid foul-release coating.

Long-term performance of a foul-release coating has been tested on vessel I for a total of nearly 12 years, Fig.5, during which the coating was only maintained by hull water pressure washing at each of the five dry-dockings, according to the original study, *Kowalski (2020)*. Measured performance seems to suggest a typical saw-shaped curve for propulsion penalties, where dry-docking events contribute to bringing propulsive penalties down (on average). For vessel I, HullMASTER closely follows these

trends, except in the first dry-docking interval where HullMASTER seems to underestimate propulsive penalty for the newly applied foul-release coating. However, confounding factors, such as varying engine performance (shaft power is estimated here based on fuel consumption, as a proxy), might still be affecting measured performance for vessel I, as seen by unexplained peaks at $t = 1550$ and 2295 days. Still, on average, there seems to be good agreement with predicted penalties.

Results for all nine vessels are shown in Fig.6, as 3-month averages before/after maintenance events. In this plot, powering penalties predicted by HullMASTER are plotted against measured performance. Plotted dashed line corresponds to an ideal 100% agreement between predicted and measured penalties. Agreement between predicted and measured propulsive penalties, i.e. overlapping 95% confidence intervals, is observed in 34 out of 43 control points, meaning that there is no statistical difference between HullMASTER predictions and measured performance in ~80% of the current validation cases. A higher amount of detail and improved models may be required to increase prediction success rate. Nevertheless, an 80% agreement with measured performance provides sufficient assurance to conduct a demonstration case on possible future application of HullMASTER.
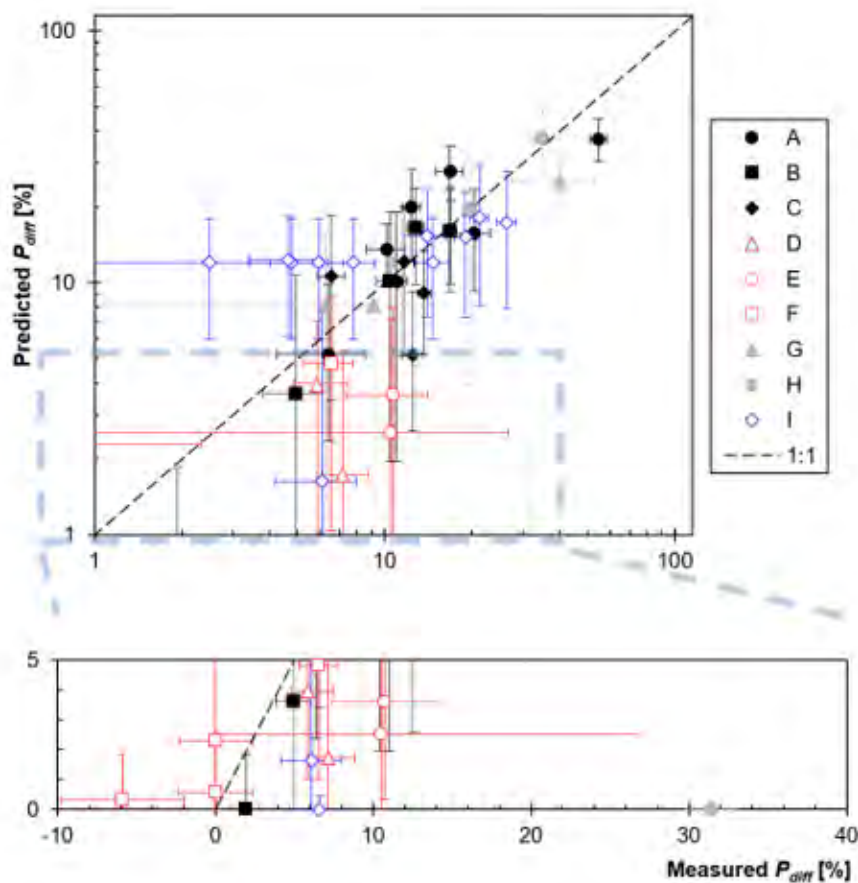

Fig.6: Validation of HullMASTER's predicted hull-and-propeller performance against measured performance ($R^2 = 0.56$, with statistically significant slope: p-value $= 10^{-8} < 0.05$). Y-axis error bars represent HullMASTER uncertainties, including uncertainties in initial roughness height, replicate variability in idle panel data, and seasonal variability. On the x-axis, error bars correspond to 95% confidence intervals for 3-month onboard performance data (filtered data).

3.2. Demonstration case: 10,000 DWT General Cargo Ship

For a demonstration case, a general cargo ship is selected, since dry cargo vessels are the single largest contributor to biocide emissions from antifouling coatings (copper and zinc) in the Baltic Sea region, while being among the top three emitters of CO_2 in the region, after RoPax and tankers (HELCOM,

2019). A 10,000-DWT vessel (wetted surface area ~3330 m^2) was selected based on median engine power and country of domicile, control or registration around the Baltic Sea, *IHS Markit (2020)*.

Three scenarios are defined as summarized in Tabke IV. Scenario 0 is a baseline, or business-as-usual scenario (BAU) for an antifouling biocidal polishing coating, with initial full-blasting of the hull, and touch-up of the coating every other docking, *Gundermann and Dirksen (2016)*. Dry-docking interval is 2 years, with full re-blasting of the hull down to steel every 4 years (i.e. every other docking). Scenario 1 is a foul-release biocide-free coating, also with initial full-blasting of the hull, and touch-up of the coating on every subsequent dry-docking. Dry-docking interval is also 2 years, but full re-blasting occurs only every 10 years for this foul-release coating, *Kowalski (2020)*. Finally, Scenario 2 is an inert biocide-free abrasion-resistant coating, also with initial full-blasting of the hull, and touch-up of the coating on every subsequent dry-docking. Dry-docking interval is again 2 years, with full re-blasting every 10 years, similar to the foul-release coating. However, for this inert coating, in-water hull cleaning is required, being automatically triggered according to criteria adapted from US Navy, *Naval Sea Systems Command (2006)*, in this case whenever confidence intervals for NSTM fouling rating reach a maximum fr_{NSTM} of 40 (small calcareous fouling).

Table IV: Scenarios used in HullMASTER demonstration case (10,000 DWT General Cargo Ship). BAU – business-as-usual, IWHC – in-water hull cleaning.

Scenario	Coating	Lifetime	First dry-docking	Subsequent dry-dockings	Dry-docking frequency	IWHC
Scenario 0 Baseline, BAU	antifouling	4 years	Full grit blasting	Touch-up	2 years	None
Scenario 1 Biocide-free	foul-release	10 years				None
Scenario 2 Biocide-free	inert	10 years				US Navy criteria

For the current demonstration purposes, the vessel operates a pendulum route between Kiel and Gothenburg (14-19 psu), at an average cruising speed of 12 knots, and idle/active cycle of 0.53/0.8 days, i.e. a percentage idle time of 40%.

In Fig.7, the simulation process is illustrated for a foul-release coating (Scenario 1) in converting fouling data from panel studies to propulsion penalties on an active vessel. Raw data for NSTM fouling rating versus idle time is linearly interpolated for local port salinity and Gaussian curves are fitted to salinity-interpolated datapoints (lines in Fig.7a), including 95%-confidence intervals for uncertainties due to replicate variability in idle panel data, and seasonal variability. Then, accounting for idling periods, over which fouling develops according to Fig.7a, and periods of vessel transit, when fouling settlement is halted, an estimate of fouling growth is obtained for the active vessel over time, resetting on each dry-docking event, i.e. every 2 years (Fig.7b). This fouling rating curve for the active vessel, where a maximum NSTM fouling rating of ~20 corresponds to advanced slime, is then converted to equivalent roughness height (Fig.7c), according to Eq.(1) and initial coating roughness estimates, Table I. Finally, using Granville method, powering penalties, Fig.7d, are estimated based on vessel details and hull roughness height k_s versus time, Fig.7c, here with a maximum ~15% penalty relative to a smooth hull, Fig.7d.

Hull surface-related operator costs (Fig.8) are calculated based on powering penalties, dry-docking costs related to hull coating maintenance and in-water hull cleaning costs, as plotted in Fig.8 for all three scenarios (results presented in €$_{2020}$). In this line plot, it is observed that the foul-release coating (Scenario 1) is initially more expensive (on average), due to higher investment on the first application, but it becomes more cost-effective than the inert coating (Scenario 2) within the first year, and breaks even with the BAU antifouling coating (Scenario 0, Baseline) within 3 months after the first

touch-up. Also, the expected lifetime of coating systems will affect average annual costs, where foul-release (Scenario 1) and inert coatings (Scenario 2) have a longer expected lifetime, Fig.8., i.e. less frequent full sandblasting. However, uncertainties need to be further addressed, as discussed at end of this section.

Annual hull surface-related societal costs, i.e. costs related to emissions resulting from hull roughness penalties (difference to a smooth hull) and antifouling biocide emissions, and cost differences between scenarios, are presented in Figs.9 and 10, respectively, including 95% confidence intervals to enable assessment of results' significance.

a)

Activity and maintenance profile

b)

$k_s = f$ (*coating condition, NSTM fouling rating*)
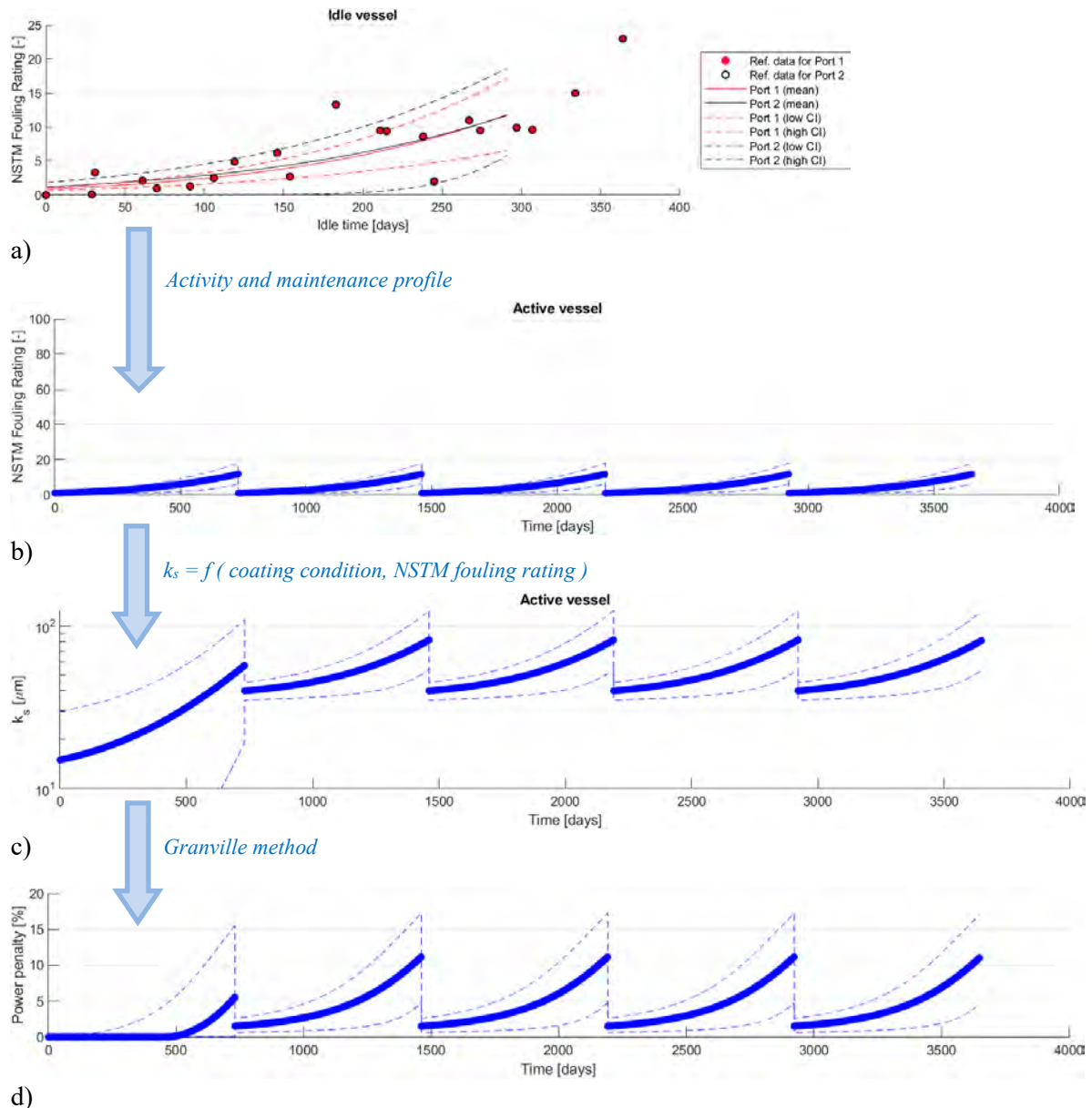
c)

Granville method

d)

Fig.7: From hull fouling to powering penalty on a 10,000 DWT General Cargo Ship: a) NSTM fouling rating for idle conditions; b) NSTM fouling rating for active vessel; c) equivalent sand roughness height; d) percentage power penalty, P_{diff}. Results are for a foul-release coating, which has an initial equivalent roughness height k_s in the range 0 to 30 μm (full grit blasting of the hull).
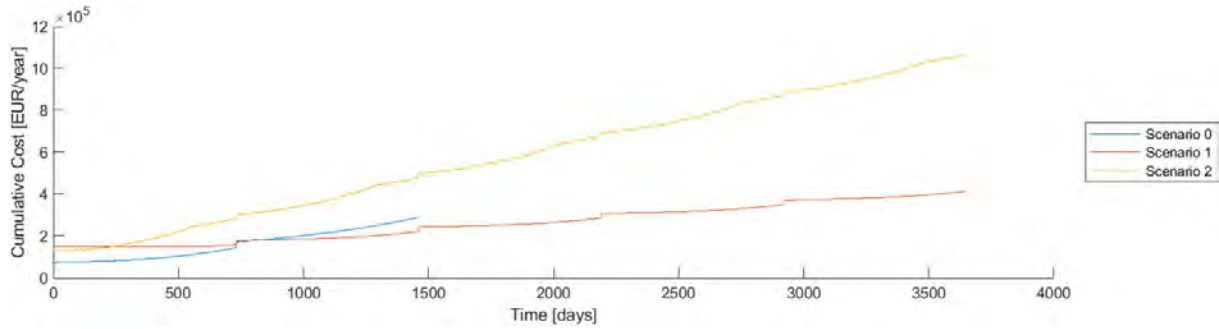
Fig.8: Time series for hull surface-related average costs for operators, including hull maintenance and roughness-related bunker expenses (430 $€_{2020}$/ton ULSFO): Scenario 0 – antifouling biocidal coating; Scenario 1 – foul-release coating; Scenario 2 – inert coating with in-water cleaning. Scenario 0 (biocidal antifouling) has a shorter lifetime of 4 years: docking cycle is assumed to repeat thereafter.
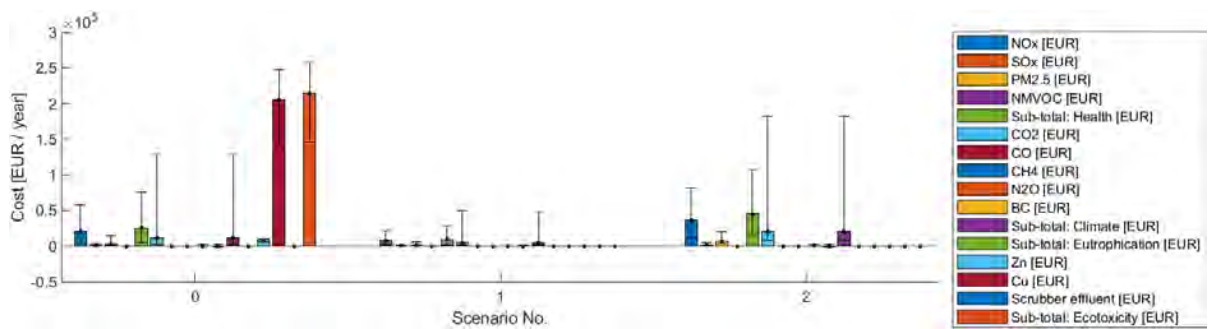
a)
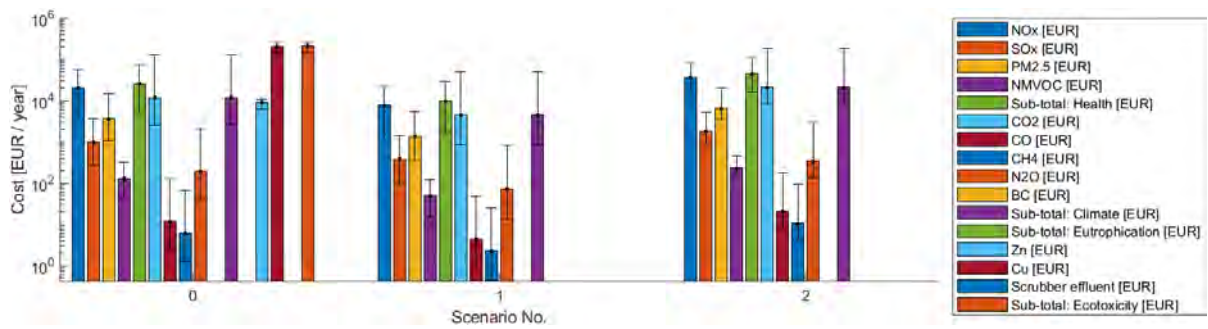
b)

Fig.9: Hull surface-related societal costs [$€_{2020}$/year] to health, climate, eutrophication and ecotoxicity, a) linear scale and b) logarithmic scale. Scenario 0 – antifouling biocidal coating; Scenario 1 – foul-release coating; Scenario 2 – inert coating with in-water cleaning.
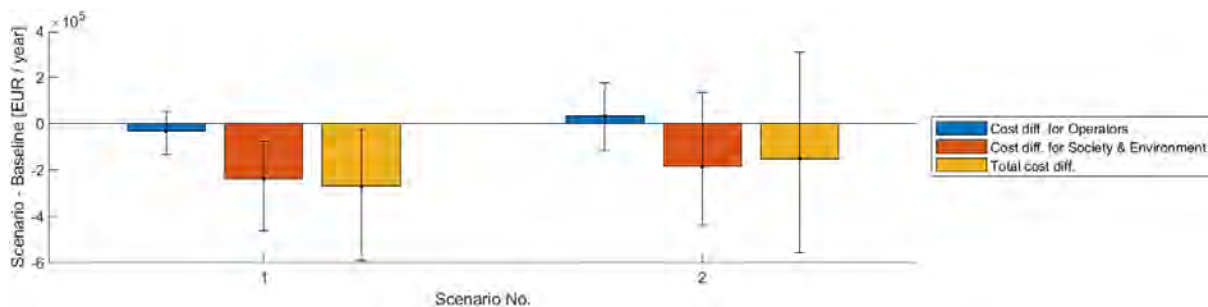

Fig.10: Hull surface-related annual cost difference for operators and society, as well as total cost (society + operators), calculated as difference to baseline Scenario 0 (antifouling biocidal coating), where Scenario 1 is a foul-release coating, and Scenario 2 is an inert coating with in-water cleaning.

From Fig.9, it can be concluded that the main societal issue with BAU antifouling biocidal coatings, for this specific vessel and route, deals with marine ecotoxicity, where damage costs are at ~145-260 thousand €$_{2020}$/year, resulting from emission of ~100 kg Cu and ~20 kg of Zn on an annual basis. This marine-ecotoxicity cost is followed by pressures on climate due to hull roughness-related bunker penalties and consequent CO_2-equivalent emissions, at ~2.5-130 thousand €$_{2020}$/year, and pressure on human health due to other air emissions, at ~5-76 thousand €$_{2020}$/year. Since the purpose of this tools is to compare different scenarios, the focus is on difference in cost rather than the total cost. Pressures on climate and human health relate only to the fuel consumption allocated to hull roughness penalty, so the total air emissions would be higher, including other resistant components (wave-making, smooth viscous resistance, wind, weather). Still, the single largest impact of selecting a BAU antifouling coating, for this specific vessel and route, is the pressure of biocide release on the marine environment, i.e. chemical pollution.

Since biocide emissions are null for Scenarios 1 and 2, these scenarios have zero impact on marine ecotoxicity, Fig.9. Also, air emissions are lower for Scenario 1 compared to Scenario 0, due to improved performance of the foul-release coating, but increase slightly for Scenario 2, due to faster fouling growth rates on the inert coating and the selected in-water cleaning scheme. On the latter, it is noted that in-water cleaning, which is triggered in this example based on an NSTM fouling rating of 40 (small calcareous fouling), is performed at a rate of 1 cleaning per dry-docking interval, more precisely ~ every 18 months, with room for further increase in frequency, depending on constraints related to economics and logistics.

Finally, cost comparisons can be drawn referring to Fig.10. According to these results, Scenario 1 significantly reduces the burden of hull condition and fouling-control strategies on society, as compared to Scenario 0, by ~75-460 thousand €$_{2020}$ in annual savings, while resulting in mean savings for shipping operators at ~30 thousand €$_{2020}$ / year. However, confidence interval for the latter economic results still includes zero, meaning that uncertainties are larger than the differences between scenarios. Thus, retrofitting this vessel from a biocidal antifouling to a foul-release coating would bring about significant savings for society, with marginal gains for shipping operators. Both societal and economic interests seem to be aligned, as mean results are both below zero, Fig.10, Scenario 1.

For Scenario 2, the mean result for the operator is above zero, meaning an economic loss for the operator, although a null cost difference is still within uncertainty. In this scenario, confidence interval for societal cost difference also spans across zero, meaning arguable gains for society. In this case, there seems to be a misalignment between economics (operator) and societal values, as mean cost difference results have opposite signs. However, results must be interpreted with caution, considering large uncertainties involved. The latter are due to uncertainties in fouling growth modeling, as discussed before, but also in pricing estimates.

From the above validation and demonstration, HullMASTER is suggested as a valuable tool in evidence-based comparison of fouling-control strategies, duly acknowledging uncertainties in available data and pricing of economic and societal components. Future work is required in further reducing model uncertainties and developing model corrections that account for vessel speed, namely adjusting fouling growth and biocide release rates to hydrodynamic conditions, as well as further taking seawater temperature and pH into account. Finally, future extension of the tool to include other marine regions worldwide, as well as development of metrics and a valuation framework for biosecurity (transport of non-native invasive species), are all seen as mid-term goals.

References

ADLAND, R.; CARIOU, P.; JIA, H.; WOLFF, F.C. (2018), *The energy efficiency effects of periodic ship hull cleaning,* J. Cleaner Production 178, pp.1-13

BEBIĆ, D.; STAZIC, L.; MISURA, A.; KOMAR, I. (2018), *EDD – Economic Benefit Analysis of Extending Dry Docking Interval*, Trans. Maritime Science 7/02, pp.164–173

DEMIREL, Y.K.; KHORASANCHI, M.; TURAN, O.; INCECIK, A.; SCHULTZ, M.P. (2014), *A CFD model for the frictional resistance prediction of antifouling coatings*, Ocean Eng. 89, pp.21-31

DEMIREL, Y.K.; TURAN, O.; INCECIK, A. (2017), *Predicting the effect of biofouling on ship resistance using CFD,* Applied Ocean Research 62, pp.100-118

DNV GL (2020), *Current price development oil and gas*, https://www.dnvgl.com/maritime/lng/current-price-development-oil-and-gas.html

GRANVILLE, P.S. (1958), *The frictional resistance and turbulent boundary layer of rough surfaces*, J. Ship Research 2/04, pp.52–74

GUNDERMANN, D.; DIRKSEN, T. (2016), *A Statistical Study of Propulsion Performance of Ships and the Effect of Dry Dockings, Hull Cleanings and Propeller Polishes on Performance*, 1st Hull Performance & Insight Conf.(HullPIC), Pavone

HANSEN, K.F.S. (2013), *Analysis of estimations, quotations and actual costs related to dry-docking,* Master thesis, Vestfold University College

HELCOM (2019), *Discharges to the sea from Baltic Sea shipping in 2006 - 2018*, pp.23–26

HOLTROP, J.; MENNEN, G.G.J. (1982), *An approximate power prediction method,* Int. Shipb. Progress 29, pp.166-170

IHS Markit (2020), *Sea-web Ships: detailed records on 200,000+ ships of 100 GT and above, updated nightly*, https://maritime.ihs.com/

IMO (2020), *Reduction of GHG emissions from ships - Fourth IMO GHG Study 2020 - Final Report.* MEPC 75/7/15, https://doi.org/10.1017/CBO9781107415324.004

IMR (2012), *Baltic Sea - Temperature and salinity observation collection,* Inst. Marine Research, V1.1. 10.12770/993571FA-CDAF-4B5F-BE7E-DB9A88CA6D8C

ISO (2016), *ISO 19030:2016 - Ships and marine technology - Measurement of changes in hull and propeller performance*, ISO/TC 8/SC 2 http://www.iso.org/iso/home/store/catalogue_tc/catalogue_detail.htm?csnumber=63774

ITTC (2014), *Recommended Procedures and Guidelines - 1978 ITTC performance prediction method 7.5-02-03-01.4* (Revision 03)

KOWALSKI, A. (2020), *The impact of the underwater hull anti-fouling silicone coating on a ferry's fuel consumption*, J. Marine Science and Eng. 8(2)

LAGERSTRÖM, M. et al. (2020), *Antifouling paints leach copper in excess – study of metal release rates and efficacy along a salinity gradient*, Water Research 186

LEER-ANDERSEN, M. (2018), *Slutrapport för "Ytfriktionsdatabas för maritima sektorn"*

[RE40147243-02-00-A]

NAVAL SEA SYSTEMS COMMAND (2006), Chapter 081 – *Water-borne underwater hull cleaning of Navy ships*, In *Naval Ship's Technical Manual*

NORDHAUS, W.D. (2017), *Revisiting the social cost of carbon,* Proc. National Academy of Sciences of the United States of America 114(7), pp.1518-1523

NORING, M. (2014), *Valuing ecosystem services: linking ecology and policy,* PhD thesis, KTH Royal Institute of Technology School

NORING, M.; HÅKANSSON, C.; DAHLGREN, E. (2016), *Valuation of ecotoxicological impacts from tributyltin based on a quantitative environmental assessment framework*, Ambio 45(1), pp.120-129

OLIVEIRA, D.R.; GRANHAG, L. (2020), *Ship hull in-water cleaning and its effects on fouling-control coatings*, Biofouling 36(3), pp.332-350

OLIVEIRA, D.R.; GRANHAG, L.; LARSSON, L. (2020), *A novel indicator for ship hull and propeller performance: Examples from two shipping segments*, Ocean Eng. 205

OLIVEIRA, D.R.; LARSSON, A.I.; GRANHAG, L. (2018), *Effect of ship hull form on the resistance penalty from biofouling,* Biofouling 34(3), pp.262-272

SAFINAH GROUP (2020), *Biofouling in Commercial Shipping: The Importance of Ship-Specific Functional Specifications*, www.safinah-group.com

SCHLITZER, R. (2018), *Ocean Data View*, odv.awi.de

SCHULTZ, M.P. (2007), *Effects of coating roughness and biofouling on ship resistance and powering.* Biofouling 23(5–6), pp.331-341

SHIP & BUNKER (2020), *Rotterdam Bunker Prices*, https://shipandbunker.com/prices/emea/nwe/nl-rtm-rotterdam

SONG, S.; RAVENNA, R.; DAI, S.; MUSCAT-FENECH, C.D.; TANI, G.; DEMIREL, Y.K.; ATLAR, M.; DAY, S.; INCECIK, A. (2021), *Experimental investigation on the effect of heterogeneous hull roughness on ship resistance,* Ocean Engineering

UZUN, D.; DEMIREL, Y.K.; CORADDU, A.; TURAN, O. (2019), *Time-dependent biofouling growth model for predicting the effects of biofouling on ship resistance and powering*, Ocean Engineering 191

VALKIRS, A.O.; SELIGMAN, P.F.; HASLBECK, E.; CASO, J.S. (2003), *Measurement of copper release rates from antifouling paint under laboratory and in situ conditions*: *Implications for loading estimation to marine water bodies*, Marine Pollution Bulletin 46(6), pp.763-779

WAN, Z.; EL MAKHLOUFI, A.; CHEN, Y.; TANG, J. (2018), *Decarbonizing the international shipping industry: Solutions and policy recommendations*, Marine Pollution Bulletin 126, pp.428-435

WRANGE, A.L.; BARBOZA, F.R.; FERREIRA, J.; ERIKSSON-WIKLUND, A. K.; YTREBERG, E.; JONSSON, P.R.; WATERMANN, B.; DAHLSTRÖM, M. (2020), *Monitoring biofouling as a management tool for reducing toxic antifouling practices in the Baltic Sea*, J. Environmental Management 264

YEGINBAYEVA, I.A.; ATLAR, M. (2018), *An experimental investigation into the surface and*

hydrodynamic characteristics of marine coatings with mimicked hull roughness ranges, Biofouling 34(9), pp.1001-1019

YTREBERG, E.; ÅSTRÖM, S.; FRIDELL, E. (2021), V*aluating environmental impacts from ship emissions – The marine perspective*, J. Environmental Management 282

Accurate Speed Through Water Measurements Enable Accurate Vessel Performance Management

Vemund Svanes Bertelsen, Miros Mocean, Asker/Norway, vsb@miros-group.com
Trym Bruset, Miros Mocean, Asker/Norway, tb@miros-group.com
Rune Gangeskar, Miros Mocean, Asker/Norway, rg@miros-group.com
Gunnar Prytz, Miros Mocean, Asker/Norway, gp@miros-group.com
Michael Schmidt, Copenhagen Commercial Platform, Copenhagen/Denmark, ms@ccp-platform.com

Abstract

Identifying the true performance of vessels and documenting the effect of new technologies to improve that performance requires accurate data related to vessel propulsion, vessel operation and the weather surrounding the vessel. It has been particularly challenging to get hold of accurate speed-through-water data, and without this parameter, obtaining accurate insight into vessel performance is not possible. However, recent technology advances have significantly improved the accuracy of speed-through-water data. This paper will discuss how the availability of accurate speed-through-water data combined with a set of other parameters can be used to estimate the actual performance of a vessel. This insight can also be used to identify the effect of various measures to improve vessel efficiency and to optimize how the vessels are operated. Ultimately, this is a powerful technology targeting the present large focus on sustainability and reduced emissions within the shipping industry.

1. Introduction

The shipping industry is a key part of the modern global infrastructure. It is also a main piece of the foundation for the world economy and offers the cheapest mode of transportation per ton of goods. On the downside, shipping also contributes to a significant amount of the global air pollution of substances such as sulfur dioxide, nitrogen oxide and particulates as well as to global emissions of carbon dioxide. It is therefore crucially important to find ways to reduce the energy consumption and the associated emissions from the shipping industry.

Ship designers and builders, ship owners and operators and ship charterers (as well as regulators and the global community in general) are all interested in improving ship performance, i.e. making sure that ships have an optimal transportation efficiency. There is a multitude of both emerging and mature technologies targeting this challenge. Such solutions include new types of hull and propeller designs, new coatings, improved engines and powertrain components as well as various types of sails, rotors, air lubrication systems, hull cleaning methods etc. In addition to this there are many initiatives focusing more on the operational side of shipping, including speed reduction, improved route and logistics planning strategies etc.

Before continuing, let us for a moment consider an analogy: A ship has some similarities with a factory where a certain amount of input factors is used to produce a certain amount of output factors or products. The efficiency of a factory can be measured in how good it is at using the input factors to produce the output factors. For a ship, the efficiency can be measured in how good it is at transporting a certain amount of cargo over some distance. The key inputs would be the fuel and the cargo, and the output would be the resulting speed of the vessel. In practice there are many more input factors related to the vessel condition (e.g. hull fouling), the vessel configuration (e.g. trim and ballasting) and the weather conditions (e.g. waves, wind and current). Still, the speed of a vessel can be seen as a measure of the output or transport efficiency of a vessel at a given input of fuel, cargo, weather, trim etc.

Taking the factory analogy a step further, it seems obvious that any attempt at optimizing the production of a factory requires accurate data on both inputs and outputs. Without knowing exactly how many components come off the assembly line, it is hard to specify the return on an investment in optimization. It would also be difficult to quantify the improvement resulting from a change of the production process.

Modern factories and factory automation systems are therefore highly instrumented, providing a lot of accurate data to facilitate monitoring and optimization of the production process.

However, the analogy between a factory and a ship often fails when it comes to the availability of accurate ship data throughout the chain from input factors to output factors. There is a wide range of instrumentation and methods in use and the accuracy can vary widely from poor to good. Coriolis mass flow meters measure the fuel oil consumption by the various engines while shaft power meters measure the propulsion power generated by the engines. The displacement or cargo weight can be measured by a variety of sensors and systems or can even be manually assessed based on the load lines on the vessel hull. Also, the trim configuration of the vessel can often be measured.

There are however some crucial parameters that have low accuracy in many, if not most, cases. The weather conditions affect the vessel performance to a great extent. Often, the wave information is manually assessed by the crew or based on weather models. Manually assessed data will typically contain significant inaccuracies whereas model data is based on coarse grids with limited accuracy. The wind speed and direction is measured by various types of anemometers, but the flow of air can be influenced by the vessel itself, and care has to be taken to correct the measurements taken at the sensor height to a more vessel-relevant reference height of, say, 10 m. Finally, the most important measure of the vessel output, the Speed Through Water (STW), is often measured with poor accuracy or estimated with fairly low accuracy based on GPS data and forecast models with coarse grids.

Measurements of ocean surface current from moving vessels by traditional underwater (in-situ) instrumentation are associated with numerous challenges. STW data from such underwater speed-logs is heavily influenced by noise and offsets, where many of these effects are due to disturbances generated by the vessel itself, *Antola et al. (2017), Baur (2016), Bos (2016), Fritz (2016)*.

Accurate and reliable STW and wave measurements based on radar technology have recently been made available from Miros, *Gangeskar (2018,2019)*. This has the potential to significantly push modern vessel performance management towards greater insights while also offering a possibility to utilize accurate STW data operationally in real-time.

A further aspect is that many vessel performance optimization initiatives are based on noon data, i.e., with one data point per 24 hours. This data point might be the average over this period (e.g. the fuel consumption) or the value observed at some point in time, typically at the end of the period (e.g. wave height). All these parameters are likely to vary significantly during the 24 hours and the result of using noon data can be that the resulting analysis is not accurate enough.

The crucial data point STW, which is the vessel speed relative to the water, is equal to the Speed Over Ground (SOG) when there is no ocean surface current present. SOG is easily measured by means of a GPS receiver. STW can be derived from SOG and ocean surface current models, but accuracy is then limited by the model. STW, however, has not been accurately measured until recently, *Gangeskar (2019)*. There are quite strong and complex surface current patterns all over the world's oceans. Studies have shown that although models can indicate how these patterns behave, they are based on coarse grids and are unable to accurately predict the current at a specific location at a specific time. Without accurate data on STW, it is not possible to accurately determine the performance of a vessel. Consequently, the lack of accurate STW data leads to challenges related to the following topics:

- Evaluation of hull and propeller designs
- Evaluation of hull coating efficiency related to friction and anti-fouling properties
- Evaluation of the efficiency of hull and propeller cleaning procedures
- Vessel performance estimations at a specific vessel speed, draft, trim and weather state
- Evaluation of performance relative to contractual agreements (claims)
- Accurate and reliable voyage optimization
- Speed optimization

The situation is similar for ocean waves, where neither manually assessed nor model-based wave heights, directions and periods are accurate enough to provide detailed insight into vessel performance. The weather (ocean waves, ocean currents and wind) therefore has a significant impact on ship performance. On top of this comes effects induced by the water temperature, water salinity and the water depth. The vessel needs to spend energy to counter the forces inflicted by the environments. In some situations, it might also gain some energy from the environment.

With accurate STW data it is possible to investigate in detail how the various input factors influence the efficiency of a vessel. In a given situation, the STW (i.e. the transport efficiency) depends on the influences of the vessel state and the sea state. With accurate wind, wave and current/STW data, the added power (or resistance) coming from these influences can be estimated via a process called weather normalization. A set of well-known methods can be applied for this purpose (e.g. *ISO-15016-2015*). When subtracting the main influencing factors from the environment, the focus can then be shifted to the vessel. The main vessel factors influencing performance are the hull and propeller performance. With the appropriate instrumentation (e.g. mass flow meters and shaft power meters) it is possible to separate the two effects.

Based on the above it would be possible to assess the performance of a vessel continuously and compare it with the ideal condition, i.e. when the vessel was new, or with other vessels. There are numerous baseline indices developed already, e.g. EEDI (Energy Efficiency Design Index) and EEXI (Energy Efficiency Existing Index), which may be relevant in such a context.

This paper presents a description of an instrumentation system that provides reliable wave, current and STW measurements, based on an X-band radar. Furthermore, a full system taking into account all the main data points for vessel performance management is outlined. Finally, the paper will investigate the sensitivity of a vessel performance indicator to inaccuracies in the significant wave height and STW data.

2. Measuring waves, currents and STW based on imaging X-band radar

There have been significant improvements within radar-based sea state measurements recently *Gangeskar (2017,2018a,2019), Gangeskar et al. (2018)*. The latest solutions in radar-based sea state measurements can measure both ocean waves and ocean currents accurately under widely varying conditions and with high availability and reliability.

The Miros Wavex solution bases its measurements on radar images covering local areas of interest, in a distance of a couple of hundred meters in front of the vessel. Fig.1 illustrates how configurable measurement areas can be extracted from polar radar images for wave, current and STW measurements. The images are processed using dedicated algorithms to obtain real-time wave spectra, integrated wave parameters, surface current vectors and STW data, *Gangeskar et al. (2018), Prytz et al. (2019)*. During the recent years, considerable works have been carried out to improve data quality under various conditions, and to test and verify the high measurement accuracy provided by Wavex, *Gangeskar (2017, 2018a,b,c, 2021), Prytz et al. (2019), Svanes Bertelsen et al. (2020)*.

Specialized DNV type-approved hardware is connected to the analog video signal output from a marine navigation X-band radar to obtain digitized images. Digitized images can also be acquired directly from radars with digital data output (Internet Protocol radars). In addition, Wavex utilizes certain radar image meta-data from a GPS and a gyro compass. For further details on the basic components of a Wavex system on a moving vessel, refer to *Prytz et al. (2019)* and *Svanes Bertelsen et al. (2020)*.
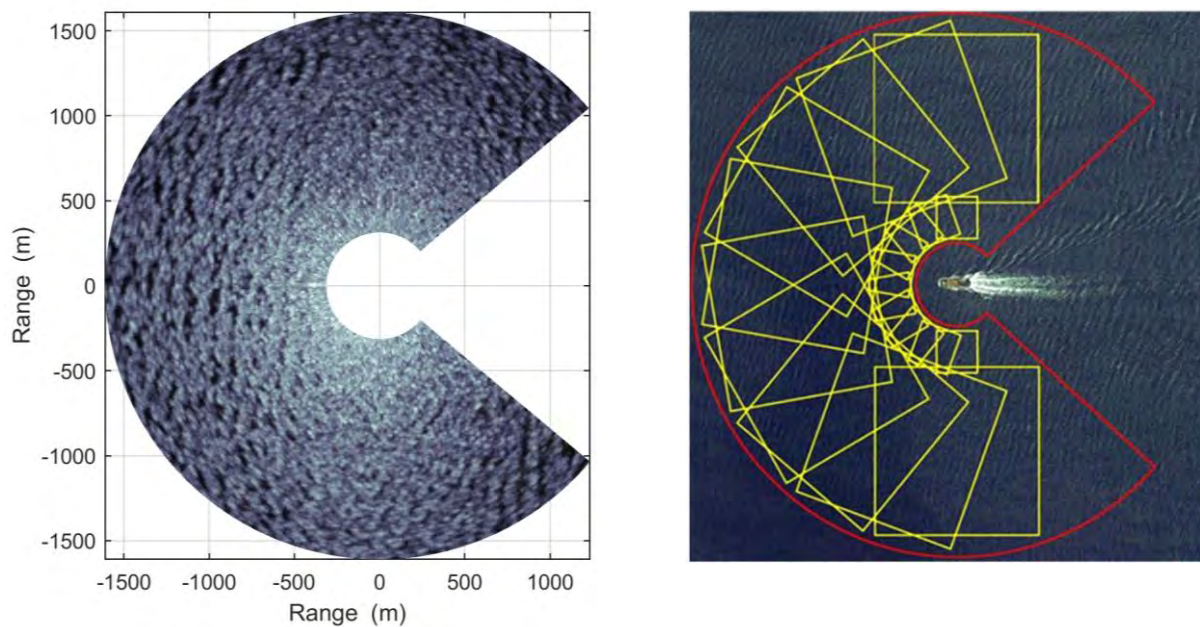
Fig.1: How measurement areas can be extracted from a polar radar image

3. A system for vessel performance management

When working with vessel performance management, it is important to determine what level of accuracy is required. A high level of insight will require accurate data with a high resolution in time combined with extensive knowledge about the involved processes from input factors to output factors. Using noon data with typically one data point per parameter per 24 h might be ok for some more superficial investigations, but to make significant advances there is a need to get data with resolution down to minutes or even lower. A further crucial point which is sometimes forgotten is the need to have a technology platform supporting an easy flow of real-time information from end to end, supporting efficient automatic and manual handling of data.

In practice there is a need to combine equipment and systems from many suppliers as there is no solution that fits all purposes or that can handle everything. With the use of modern technology, it is now easier than ever to integrate systems together and share information in a robust manner. In this way, a joint effort between suppliers of the various bits and pieces necessary for vessel performance management can be readily achieved. An example of such a system for vessel performance management is shown in Fig.2, where the Miros Mocean IoT system is used to collect a set of key data points which can be used by the system or be transferred to third-party systems either onboard or onshore. In other situations, the data flow might be reversed, the third-party systems might collect some of the data points and transfer these to the Miros Mocean system, either onboard or onshore.

4. Data analysis

This section contains an initial investigation of the sensitivity of a vessel performance analysis to the accuracy of some of the key the input parameters. The primary objective is to illustrate how data accuracy influences what level of vessel performance accuracy can be achieved.

4.1. Inaccuracies associated with various types of data and data sources

Svanes Bertelsen et al. (2020) presented results from comparisons of measured data and model data from four voyages made by a dry bulk carrier. The measured data was collected using a Miros Wavex system to collect accurate wave, current and STW data and a traditional speed-log to collect current and STW data.
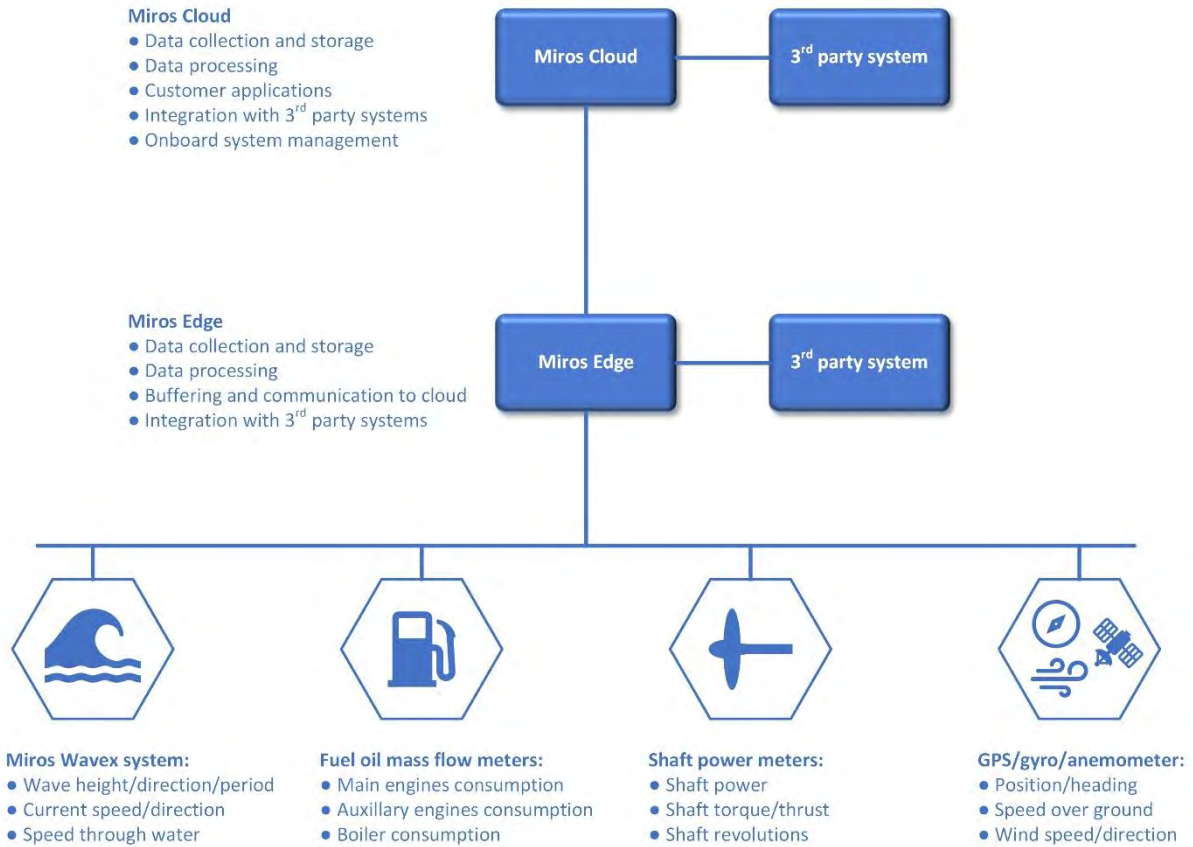
Miros Cloud
- Data collection and storage
- Data processing
- Customer applications
- Integration with 3rd party systems
- Onboard system management

Miros Edge
- Data collection and storage
- Data processing
- Buffering and communication to cloud
- Integration with 3rd party systems

| Miros Cloud | 3rd party system |

| Miros Edge | 3rd party system |

Miros Wavex system:
- Wave height/direction/period
- Current speed/direction
- Speed through water

Fuel oil mass flow meters:
- Main engines consumption
- Auxillary engines consumption
- Boiler consumption

Shaft power meters:
- Shaft power
- Shaft torque/thrust
- Shaft revolutions

GPS/gyro/anemometer:
- Position/heading
- Speed over ground
- Wind speed/direction

Fig.2: A vessel performance management system centered around the Miros Mocean IoT system. In this case, the Miros Mocean system collects data from many sources and can distribute this to other systems, either onboard or onshore. In other scenarios, the 3rd party systems might collect some (or all) the data points and distribute these to the Miros Mocean system. In this way, a high level of flexibility and adaptability is achieved, with easy collaboration with other stakeholders.

When comparing the measured current data from the Miros Wavex system and the speed-log, the resulting RMS deviation was found to be 0.47 m/s (0.91 kn) whereas the mean deviation was -0.43 m/s (0.84 kn).

Similarly, when comparing the measured wave height data from the Miros Wavex system with the model data, the resulting RMS deviation was 0.47 m and the mean deviation was 0.17 m. The model data had a time resolution of 6 hours and had a limited spatial resolution in the order of tens of kilometers. The measured data was averaged over the same time span to facilitate the statistical comparison.

It is possible to perform a simple but realistic sensitivity analysis of how sea state data accuracy will affect a vessel performance analysis by defining a vessel performance indicator (VPI) as follows:

$$VPI = \frac{measured\ power}{reference\ power}$$

Based on data from tank tests and sea trial, a cubic spline interpolation allows the expression of reference power for any combination of speed through water and displacement within certain bounds. Interpolated level curves from the surface, along with recorded points for the BW RYE vessel are shown in Fig.3.
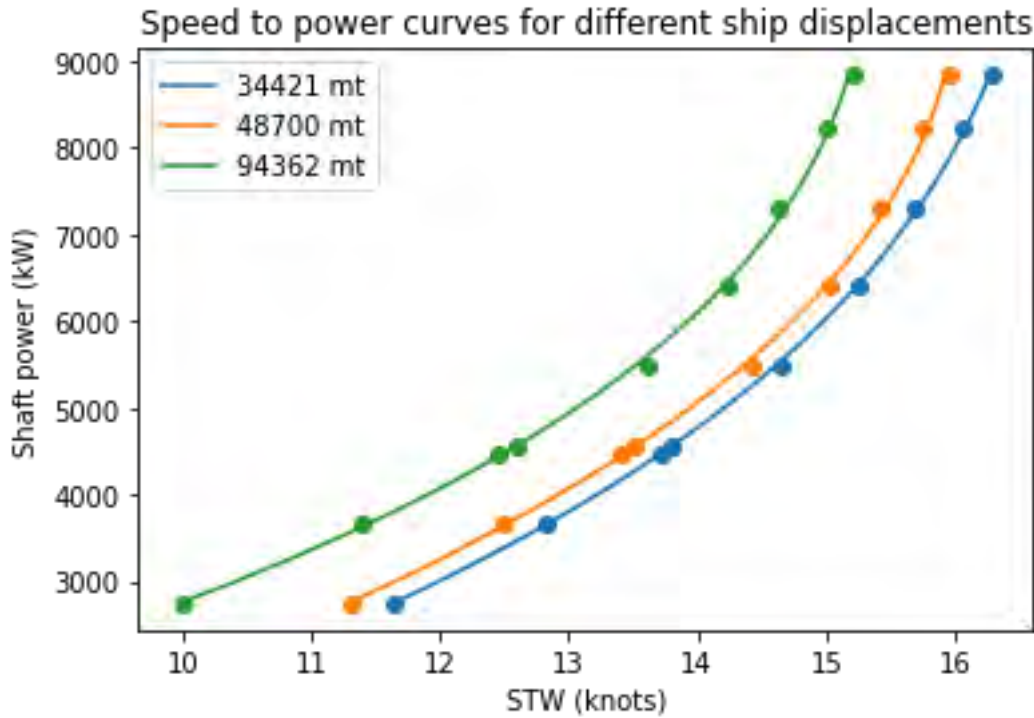
Fig.3: Reference power curves for different displacements as functions of STW. Scattered points represent tank test/sea trial data.

From the above, a value for VPI = 1 would make vessel performance identical to the vessel design or newbuilt condition. A VPI > 1 means that the performance of the vessel is lower than when the vessel was newbuilt, due to fouling or other types of degradation effects. A VPI < 1 could be possible if means to improve performance has been applied, e.g. a more optimal propeller, sails or a hull coating providing less friction.

Weather has a significant effect on the VPI (i.e. bad weather typically requires the vessel to use more power to keep the same speed). The VPI was therefore normalized for weather to eliminate the weather effects as much as possible. Inaccuracies in the input parameters will have an influence on the accuracy of the VPI. The focus in this investigation was on the influence of the accuracy of the significant wave height and the STW parameters. For significant wave height, the analysis was performed with the following five different datasets:

- The measured data from the Miros Wavex
- Two adjusted datasets with constant offsets of -0.2 m and 0.2 m
- Two adjusted datasets with constant offsets of -0.5 m and 0.5 m

The rationale behind the dataset with an offset of 0.2 m is that the specified accuracy of wave height for the Miros system is ± 0.2 m. Based on *Svanes Bertelsen et al. (2020)*, a constant offset of 0.5 m was selected to illustrate the inaccuracy that can be expected from using model data. A similar inaccuracy or worse can be expected when relying on manually assessed noon data.

For STW, the analysis was performed with the following five different datasets:

- The measured data from the Miros Wavex
- Two adjusted datasets with constant offsets of -0.05 m/s (-0.1 kn) and 0.05 m/s (0.1 kn)
- Two adjusted datasets with constant offsets of -0.4 m/s (-0.8 kn) and 0.4 m/s (0.8 kn)

The verified, in-operation accuracy of current and STW for the Miros system is ± 0.05 m/s (± 0.1 kn).

Based on *Svanes Bertelsen et al. (2020)*, a constant offset of 0.4 m/s (0.8 kn) was selected to illustrate the in-operation accuracy of a speed-log. A similar inaccuracy or worse can be expected when relying on model data, which often fails to describe the current conditions accurately in time and space, as described by *Gangeskar et al. (2018)*.

4.2. Data preparation process

Before doing the analysis, the data went through a data preparation process consisting of filtering, synchronization and averaging. This was done to simplify the analysis process and to ensure that only valid, high quality data was used. The data preparation process is outlined in Fig.4 and is described further below.

Fig.4: Data preparation process

The raw data was logged from several onboard sensors. The Miros Wavex system was used to measure the significant wave height and the STW. Data was also collected from the vessel speedlog, anemometer, shaft power meter, GPS and gyro. The water temperature was not measured directly, but retrieved from the Copernicus database (https://marine.copernicus.eu/). The water depth data was obtained from the GEBCO gridded bathymetric dataset (https://www.gebco.net), a global terrain model for ocean and land, providing elevation data, in meters, on a 15 arc-second interval grid.

Each data parameter was filtered based on the criteria specified in Table I:

Table I: Data filtering specification

Parameter	Unit	Filter values
Shaft power	kW	[2745, 8839]
Water depth	m	[70, ∞>
Water temperature	°C	[0, 31>
Wave parameters	m, s, °	Data validated by the automatic data quality control
STW	m/s	

The shaft power filtration was chosen based on the available range in the speed-power curves coming from the vessel tank tests and sea trial, Fig.3. Only values within this range would be selected for the vessel performance analysis.

The water depth filter was set to only allow data from locations where the water depth was more than 70 m to eliminate possible shallow-water effects that could distort the analysis. 70 m was selected to make sure that the ISO-15016-2015 water depth requirement was fulfilled with some margin in all loading conditions.

The water temperature requirement was also based on the procedures outlined in ISO-15016-2015.

The significant wave height and STW parameters from the Miros Wavex went through the system's automated data validation and quality control process to ensure that only good quality data was used in the analysis. For the speed-log data, there was no data quality parameters available.

After the filtering, the data was synchronized to get the timestamps (the timestamps were slightly different since the data was measured by different types of equipment and systems. The parameters were therefore resampled to make sure that all parameters had the same timestamps with 1-minute resolution. The resampling method used was a simple arithmetic mean for magnitudinal parameters

(significant wave height, wind speed, shaft power, STW, etc.),| and a slightly more involved angular mean for angular parameters (peak wave direction, wind direction, vessel heading etc.).

A steady-state selection procedure, *Dalheim and Steen (2020)*, was carried out to determine the one-hour windows where the ship RPM was practically constant to exclude data obtained during transitional periods. The data was then averaged over these one-hour windows using the same averaging methodology as the data synchronization step. The averaged, steady-state data was then ready to be used in the subsequent vessel performance analysis.

4.3. Weather normalization

Weather normalization is about eliminating the effect of the weather on the energy consumption of a vessel. There are many weather-related properties that have an impact on vessel performance, such was ocean waves, ocean current, wind, water temperature and salinity.

In this paper, the data was normalized for the influences of wind, waves, water temperature and water density. The added resistance due to waves was estimated using the results from *Liu and Papanikolaou (2016)*. Further details on the weather normalization procedures used can be found in *Guo et al. (2021)*.

Weather normalization is not an exact science as the models involved can only be expected to describe the weather effects to some degree of accuracy. However, these are well-known models utilized for vessel performance investigations and are therefore relevant in this study.

4.3. Impact of inaccurate measurements on the VPI

The VPI serves as a real-time indicator of the performance of the vessel, normalized for weather. The weather normalization is necessary because weather has a large impact on the performance of a vessel. The influence of the weather blurs the influence from the vessel (e.g. hull degradation) and make it impossible to determine whether a certain performance degradation is due to the weather or the vessel itself, or alternatively, which portions of the deviation from the ideal condition can be described to either the weather or the vessel. The following figures show a calculation of the VPI, along with plots of VPI calculated with constant offsets in STW and significant wave height for data collected during 2 voyages of the vessel BW RYE. Voyage I was a ballast voyage between Singapore and Australia in February 2020 whereas Voyage II was a laden voyage from the Panama Canal to Chile in May 2020.
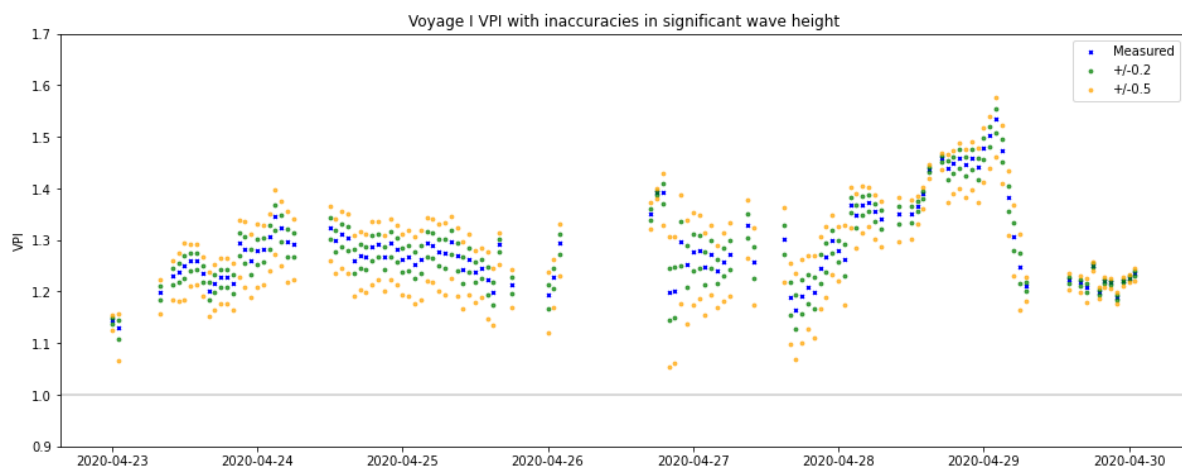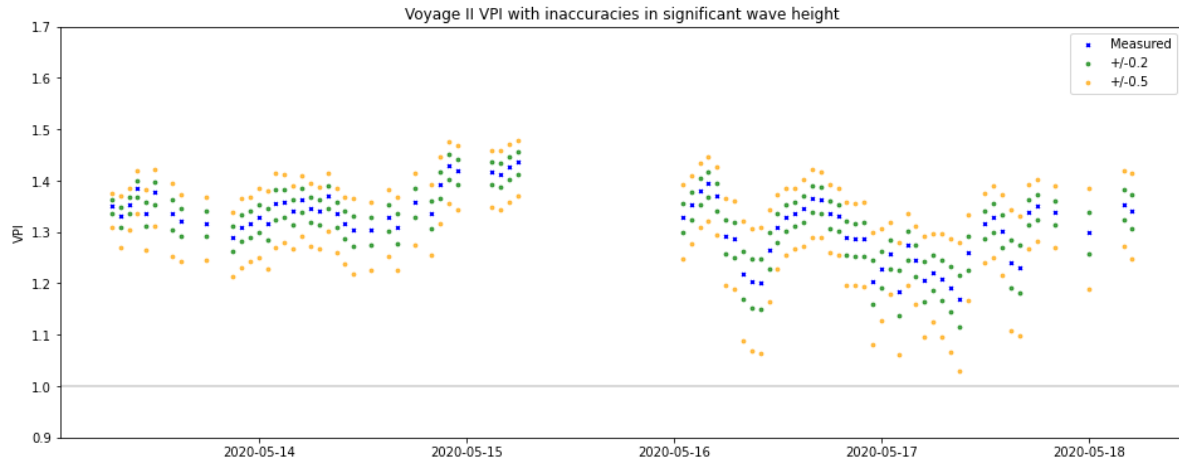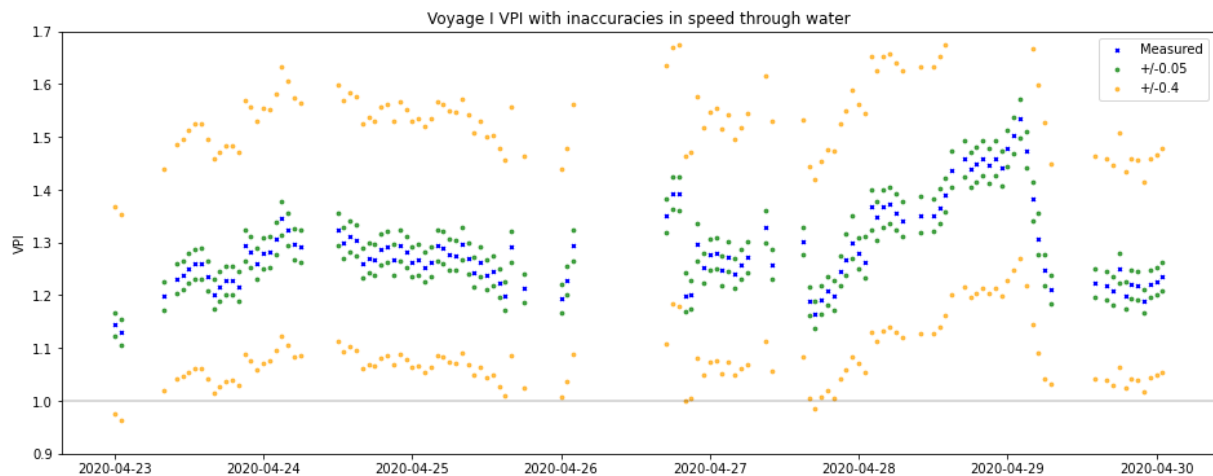

Fig.5: VPI calculation of Voyage I in ballast condition, demonstrating the impact of an offset in significant wave height. The blue dots show the VPI based on the measured values, the green dots show the VPI calculated with a significant wave height of ±0.2 m and the orange dots show the VPI calculated with a significant wave height of ±0.5 m. The grey line at VPI=1 represents the reference performance of the vessel in perfect weather (from tank tests and sea trial data).

Figs.5 and 6 show how the calculated VPI varies with inaccuracies in the significant wave height parameter, where the inaccuracies are modelled as constant offsets, both in the positive and negative direction. The impact on the VPI of changes to the accuracy of the significant wave height is noticeable. By analyzing the VPI time series, it can be found that an offset of ±0.2 m in the significant wave height leads to an average offset of 2.6% in the VPI, whereas an offset of ±0.5 m leads to an average offset of 6.5% in the VPI.

Fig.6: VPI calculation of Voyage II in loaded condition, demonstrating the impact of an offset in significant wave height. The blue dots show the VPI based on the measured values, the green dots show the VPI calculated with a significant wave height of ± 0.2 m and the orange dots show the VPI calculated with a significant wave height of ± 0.5 m. The grey line at VPI=1 represents the reference performance of the vessel in perfect weather (from tank tests and sea trial data).

Figs.7 and 8 demonstrate how the calculated VPI varies with inaccuracies in the STW parameter, where the inaccuracies are modelled as constant offsets, both in the positive and negative direction. The impact on the VPI to inaccuracies in the STW appears to be significantly larger than for inaccuracies in significant wave height. An analysis of the VPI time series shows that an offset of ±0.05 m/s (±0.1 kn) in the STW leads to an average offset of 2.8% in the VPI, whereas an offset of ±0.4 m/s (±0.8 kn) leads to an average offset of 23% in the VPI.

Fig.7: VPI calculation of a Voyage I in ballast condition, demonstrating the impact of an offset in STW. The blue dots show the VPI based on the measured values, the green dots show the VPI calculated with an STW ± 0.05 m/s (±0.1 kn) and the orange dots show the VPI calculated with an STW of ± 0.4 m/s. (±0.8 kn) The grey line at VPI=1 represents the reference performance of the vessel in perfect weather (from tank tests and sea trial data).
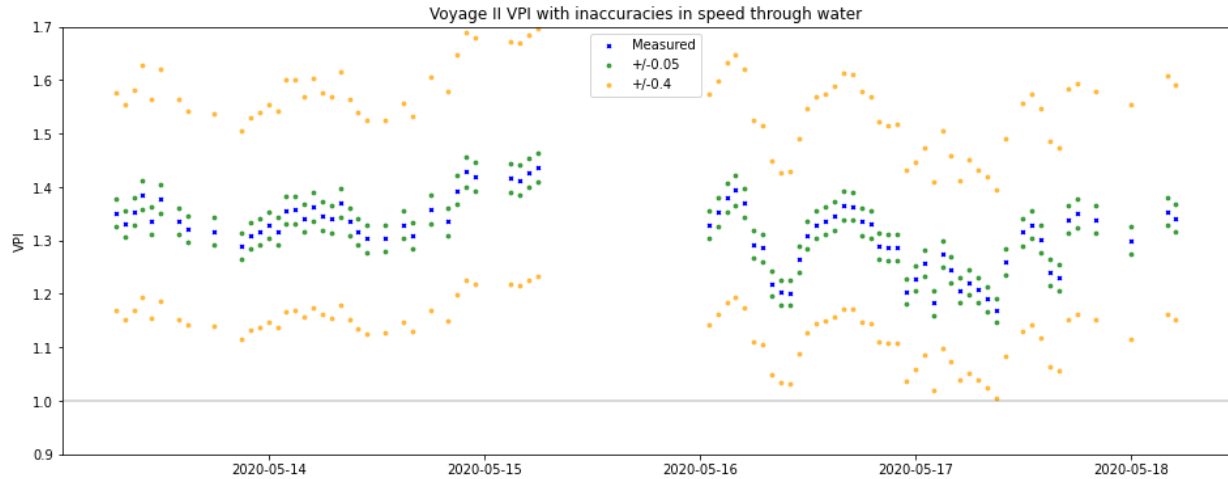
Fig.8: VPI calculation of Voyage II in loaded condition, demonstrating the impact of an offset in STW. The blue dots show the VPI based on the measured values, the green dots show the VPI calculated with an STW ± 0.05 m/s (±0.1 kn) and the orange dots show the VPI calculated with an STW of ± 0.4 m/s (±0.8 kn). The grey line at VPI=1 represents the reference performance of the vessel in perfect weather (from tank tests and sea trial data).

5. Discussion

Further analysis using data from more journeys will have to be done in order to investigate the sensitivity of the VPI further, but the analysis presented above gives a clear indication of how important data accuracy is, particularly for STW. The scenarios used here have been quite simple, since only one parameter at a time was assigned an offset error. In practice, also wave period and wave direction are used by the weather normalization methods, and these parameters will also have a certain inaccuracy, leading to inaccuracies in the VPI. Thus, it is likely that the inaccuracies related to waves are larger in practice than what is reported here.

Measured data can have both constant offsets and noise so the analysis of just the offset part is too simple to get the full picture. The different types of errors might also have different implications depending on how the data is intended to be used. Finally, it should also be investigated further how the various inaccuracies add up.

6. Conclusion

Weather conditions have a significant influence on the in-operation performance of a vessel. This paper has investigated how the accuracy of a vessel performance analysis depends on the accuracy of the two key input parameters significant wave height and STW. The investigation was partly motivated from the fact that more accurate measurement technologies have become available recently, so it was of interest to see to what extent this is important for modern vessel performance management.

To accommodate the analysis, a VPI index was defined as the ratio of the measured power and the reference power based on sea trial and tank test data. It was found that while the VPI is quite sensitive to realistic inaccuracies in the significant wave height data, it is far more sensitive to realistic inaccuracies in the STW parameter. From this it can be concluded that the accuracy gap between traditional methods and the best available instrumentation solutions is significantly greater for STW than for significant wave height and other wave parameters. For the voyages analyzed in this paper, accurate STW data was shown to lead to an uncertainty in the VPI of ±2.8 % while data from traditional methods would lead to an uncertainty of ±23 %. This clearly shows the large impact of inaccuracies in STW data and the importance of using sufficient accurate technologies to measure this parameter.

Thus, inaccurate STW data has a very large influence on the accuracy of the VPI. Consequently, the practical implication is that an accurate, in-operation quantification of technical vessel performance is difficult or even impossible to obtain without very accurate STW data as exemplified by the Miros Wavex system.

References

ANTOLA, M.; SOLONEN, A.; PYÖRRE, J. (2017), *Notorious speed through water,* 2nd HullPIC, Ulrichshusen, pp.156-165

BAUR, M. (2016), *Acquisition and integration of meaningful performance data on board - challenges and experiences,* 1st HullPIC, Pavone, pp.230-238

BOS, M. (2016), *How MetOcean data can improve accuracy and reliability of vessel performance estimates*, 1st HullPIC, Pavone, pp.106-114

FRITZ, F. (2016), *Practical experiences with vessel performance management and hull condition monitoring*, 1st HullPIC, Pavone, pp.128-136

GANGESKAR, R. (2017), *Automatically calibrated wave spectra by the Miros Wavex system – Accuracy verified*, Miros AS, Asker

GANGESKAR, R.; PRYTZ, G.; SVANES BERTELSEN, V. (2018), *On-Board Real-Time Wave & Current Measurements for Decision Support*, 3rd HullPIC, Redworth, pp.223-233

GANGESKAR, R. (2018a), *Verifying High-Accuracy Ocean Surface Current Measurements by X-Band Radar for Fixed and Moving Installations*, IEEE Trans. Geosci. Remote Sens. 56/8, pp.4845-4855

GANGESKAR, R. (2018b), *Ocean Surface Current Measurement by the Miros Wavex System*, Miros AS, Asker

GANGESKAR, R. (2018c), *Surface Current Measurements from Moving Vessels by Wavex – Verified*, Miros AS, Asker

GANGESKAR, R. (2019), *Measuring the speed through water by Wavex®,* Miros AS, Asker

GANGESKAR, R. (2021), *Automatic Radar Data Quality Control – Applying Deep Learning, AI to Ocean Wave, Current Measurements*, Sea Technology 62/2, pp.23-27

GUO, B.; ROGNEBAKKE, O.; TVETE, H.A.; ADAL, C.; STORHAUG, G.; SCHMIDT, M.; BRUSET, T.; PRYTZ, G. (2021), *Setting the standard for evaluation of in-service technical ship performance,* 6th HullPIC, pp.88-105

ISO-15016-2015: *Ships and marine technology — Guidelines for the assessment of speed and power performance by analysis of speed trial data*, Int. Standard Org., Geneva

LIU, S.; PAPANIKOLAOU, A., (2020), *Regression analysis of experimental data for added resistance in waves of arbitrary heading and development of a semi-empirical formula*, Ocean Engineering

PRYTZ, G.; GANGESKAR, R.; SVANES BERTELSEN, V. (2019), *Distributing Real-Time Measurements of Speed Through Water from Ship to Shore*, 4th HullPIC, Gubbio, pp.114-127

SVANES BERTELSEN, V.; GANGESKAR, R.; PRYTZ, G.; SCHMIDT, M. (2020), *Accurate Voyage Sea State and Weather Measurements Improve Performance-Based Vessel Management*, 5th HullPIC,

Hamburg, pp. 157-171

DALHEIM, Ø. Ø; STEEN, S. (2020), *A computationally efficient method for identification of steady state in time series data from ship monitoring,* J. Ocean Engineering and Science 5/4, pp.333-345

Using Publicly Available Data to Assess Hull and Propeller Performance

Cedric Deymier, Wärtsilä Voyage, Paris/France, cedric.deymier@wartsila.com
Matti Antola, Wärtsilä Voyage, Helsinki/Finland, matti.antola@wartsila.com
Daniel Schmode, Wärtsilä Voyage, Hamburg/Germany, daniel.schmode@wartsila.com

Abstract

Vessel performance solutions often require high frequency data to be collected on the ships, including flowmeter data. The data collection comes at a high cost and requires long implementation projects due to the lack of industrial standards regarding digital technologies and protocols in the maritime industry. Flowmeters also create an extra risk as the whole system relies on their accuracy which requires regular calibrations and maintenance. In this paper we demonstrate how vessel performance can be measured using voyage reports from the crew or from automatic voyage reporting systems. This solution does not require the installation of any data logging hardware onboard the ship. We will focus on creating a speed fuel consumption model using only publicly available data and vessel noon reports for fuel consumption.

1. Introduction

Leg performance analysis objective is to explain the various factors that influence the fuel consumption of a vessel during a voyage. The main ones will be weather conditions but other factors such as hull condition, draft or engine usage will have an impact. Correlating the influence of each of these factors with the fuel consumption of the ship is a statistical exercise that usually requires very good quality and high frequency data as an input. Each vessel being unique in terms of hull performance and systems, performing this statistical analysis on every vessel is highly cost and time consuming.

The alternative we suggest is to use noon to noon voyage report data (aggregated data for short voyages), in order to perform this performance analysis. The basis for this work relies on the low frequency to high frequency modeling solution already presented, *Antola et al. (2017)*.

In the following, we present a vessel performance analysis over 12 months performed using noon reported data from a real vessel. We will fusion this data with high frequency navigational and environmental condition data from AIS and weather hindcasts. This enables us to create a model that will infer the high frequency live fuel consumption of the ship in any environmental conditions. To validate the model, we will check how accurate the fuel consumption prediction is against the past reported data from the vessel. Finally, we will go through some valuable applications of this methodology, like analyzing the changes in the hull and propeller performance of the vessel over time.

2. Gathering multiple sources of data

2.1. Ship characteristics

Ship characteristics can be obtained from various online databases or shared by the shipowner. In most cases, data can be found from public data sources. Main dimensions needed are vessel main dimensions, vessel type, and information about the expected draft range.

2.2. AIS data

Automatic Identification System (AIS) data can be obtained from providers that store and sell the data from all vessels. Data from AIS is usually not as good quality as an onboard logger would provide. In this study we want to check what is the difference between AIS reported SOG and data collected onboard the vessel in order also to evaluate the relevance of using AIS data as an input.

The input provided by AIS data is:

- Vessel Maritime Mobile Service Identity (MMSI).
- Navigation status: E.g., "at anchor", "under way using engine(s)", "not under command", etc.
- Rate of turn: right or left, from 0 to 720 degrees per minute
- Speed over ground: 0.1-knot (0.19 km/h)
- Longitude: to 0.0001 arcminutes
- Latitude: to 0.0001 arcminutes
- Course over ground: relative to true north to 0.1°
- True heading: 0 to 359°
- True bearing at own position: 0 to 359°
- UTC seconds: The seconds field of the UTC time when these data were generated. A complete timestamp is not present.

This data is shared every 2 to 10 s by the vessel, which is considered high frequency in the case of the modeling we want to create. Data intervals up to 5 minutes would be acceptable.

AIS data can sometimes be missing due to a lack of satellite coverage of the vessel, leading to gaps in the database. Some geographical locations are more prone to showing missing data, such as SE Asia due to an overload of vessels transmitting at the same time.
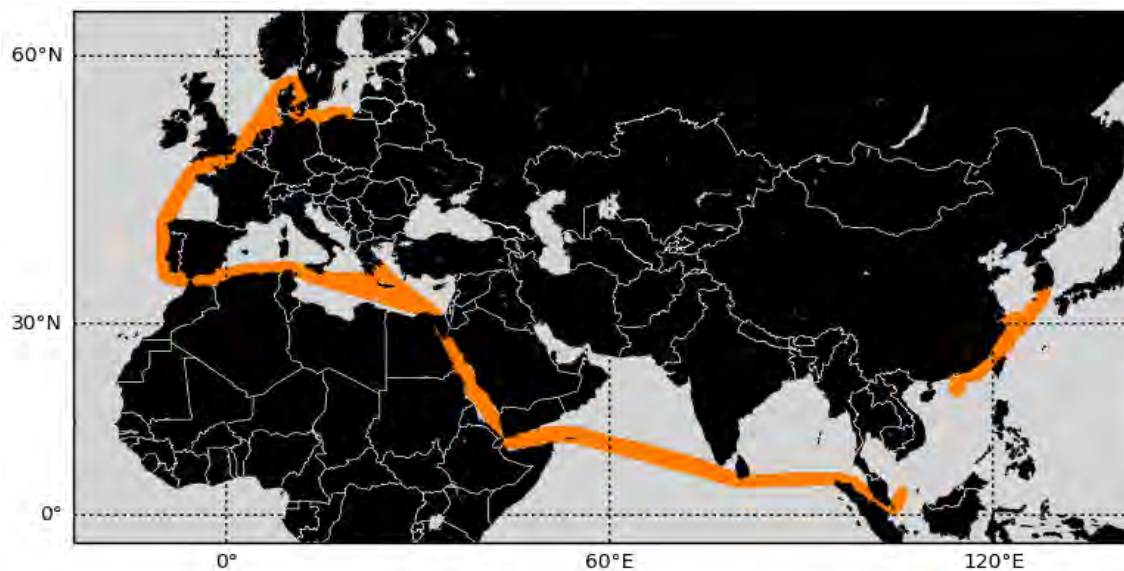
Fig.1: Vessel route over one year based on AIS location data

2.3. Weather hindcast data

Environmental conditions in high frequency are also needed as an input to our model in order to evaluate the impact of waves, wind and current on the fuel consumption of the vessel. We use hindcast data obtained from weather providers. Hindcast data includes extra observational data that was time-delayed and therefore not available to the original forecast run. This means that hindcast data is more accurate than archived forecast data. The resolution and frequency depend on the model used. In our study we use the NOAA GFS model and we query the weather conditions based on the location of the vessel according to AIS data.

2.4. Vessel noon reports

The only input provided by the ship is draft and the fuel consumption for propulsion and for service power by noon to noon period or by (short) leg, with corresponding start and end time In this study

we use data from a vessel with one main engine for propulsion and auxiliary engines for service power.

The needed data must be shared by the shipowner. However, this does not require any additional workload from them as this reporting is already needed for EU-MRV or IMO DCS regulations. Most operators use digital tools to create those reports already, making it simple to extract and reuse.
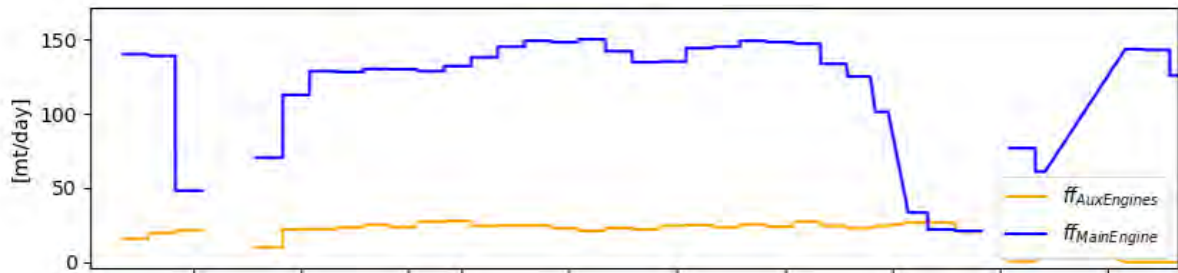

Fig.2: Reported daily average fuel consumption from noon reports

3. Model creation and validation

3.1. Checking input data

Once all needed data has been collected and merged, it is interesting to check if the noon reported data and the AIS data show some inconsistencies.

One way to investigate this is to plot the average SOG over each leg according to AIS data and compare to the noon reported data. We can observe on the following graph that several legs show major inconsistencies and should be excluded from our analysis.
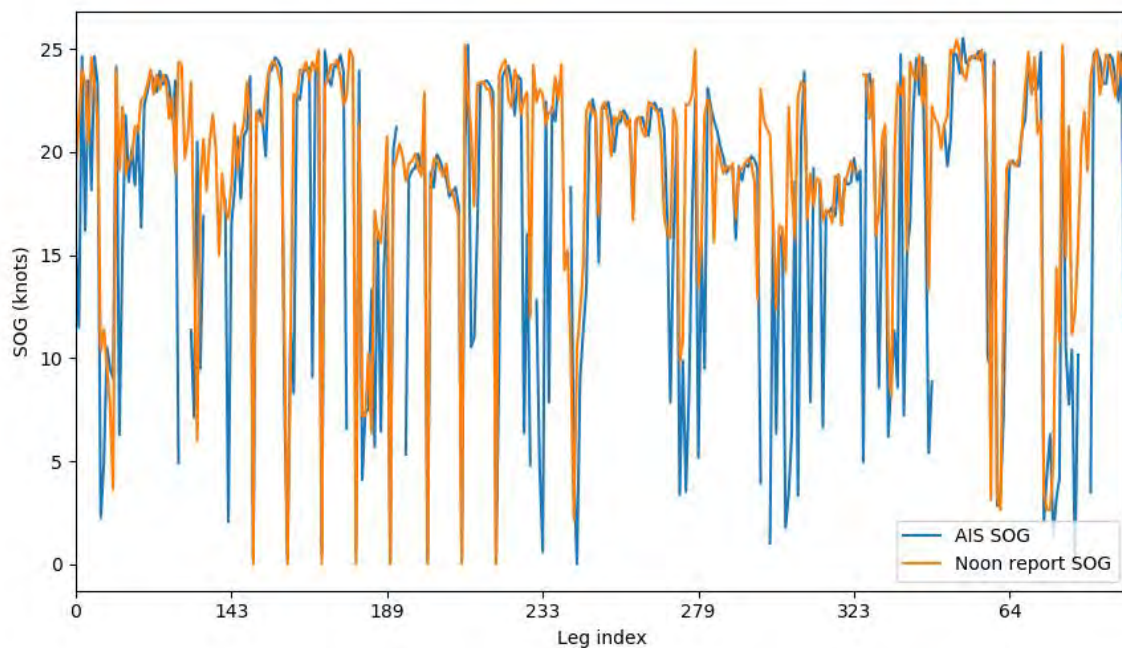
Fig.3: AIS vs Noon reported SOG

After looking into the data quality, we make the choice to remove all legs where the difference between AIS data and noon report data for the SOG is more than 2 knots in absolute value. This leaves us with more than 200 legs, which is enough to create the model and removes a lot of inaccuracies from the input data. The result is visible in Fig.4.
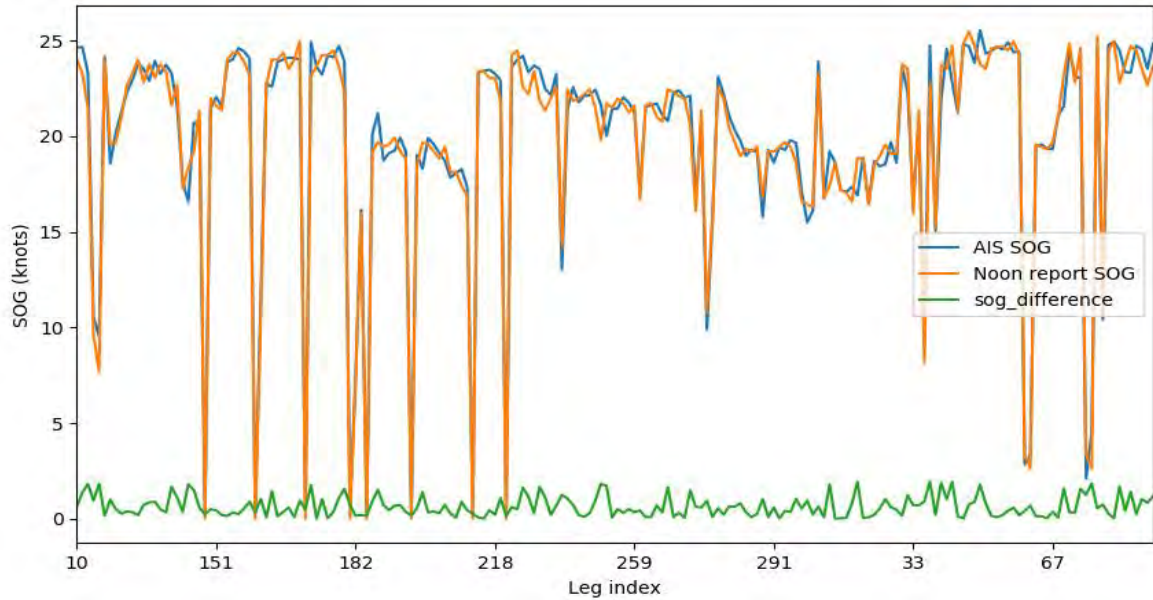
Fig.4: Effect of removing all legs with non-consistent reported SOG (difference > 2 kn on average)

A second check we perform is looking into the average fuel consumption per nm reported by the vessel against the one we calculate using AIS data. This helps to identify potential gaps in the data where the distance performed by the vessel is incorrect due to a lack of AIS data.

3.2. Model creation

Antola et al. (2017) presented a sensor fusion model that used speed over ground, forecast data, and average fuel flow from noon reporting. We will refer to this model as fuel flow model (FFM). In the following we will verify if the FFM can predict the fuel consumption of the vessel using AIS and weather hindcast data as an input. We provide this data as an input to the FFM model. The model takes around one month of data to learn from the input data and improve its predictions.

3.3. Model validation

In order to validate the model, we plot the speed fuel curve of the vessel based on noon reported data and the modeled fuel consumption. The result shows a less scattered curve with less noise at lower speeds compared to the values reported by hand. Some of the outliers in the noon reports might be some reporting human errors. The modeling is not impacted by those errors. Note that the remaining scatter in the modelled data is caused by varying draft and weather. Scatter caused by misreporting is significantly reduced.

Finally, the fuel consumption can be normalized by excluding the impact of environmental conditions, Fig.5. The green curve represents the calm sea fuel consumption of the vessel. Changes along time of this curve are one way to track the evolution of hull and propeller performance of the vessel.

4. Model applications

4.1. Hull & propeller performance change

Having modelled the efficiency of the vessel in calm sea conditions makes it possible to assess the changes in the performance of the vessel along time. As input data is fuel flow and speed only the hull and propeller and engine performance can be monitored. One possible improvement would be to use power data in order to be able to monitor only hull and propeller performance.
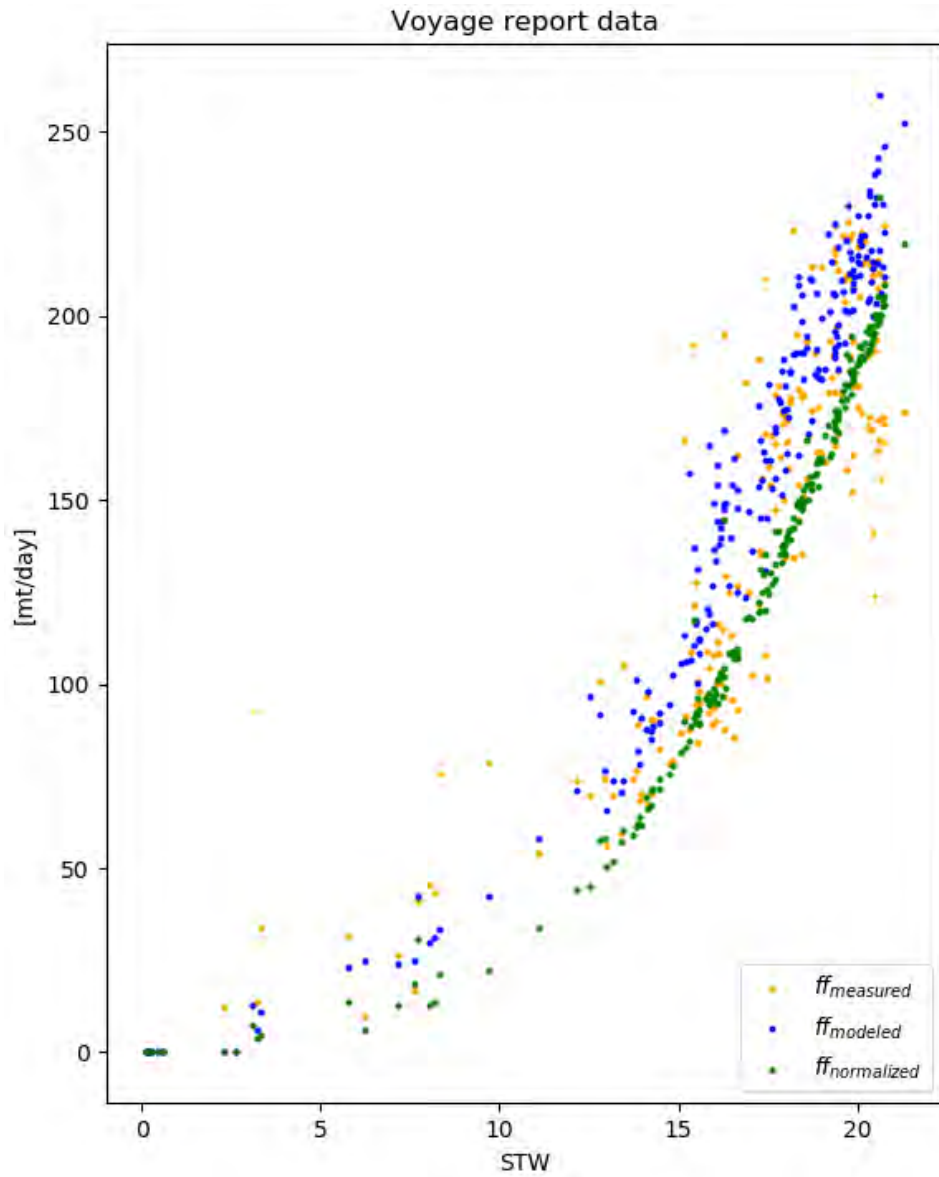
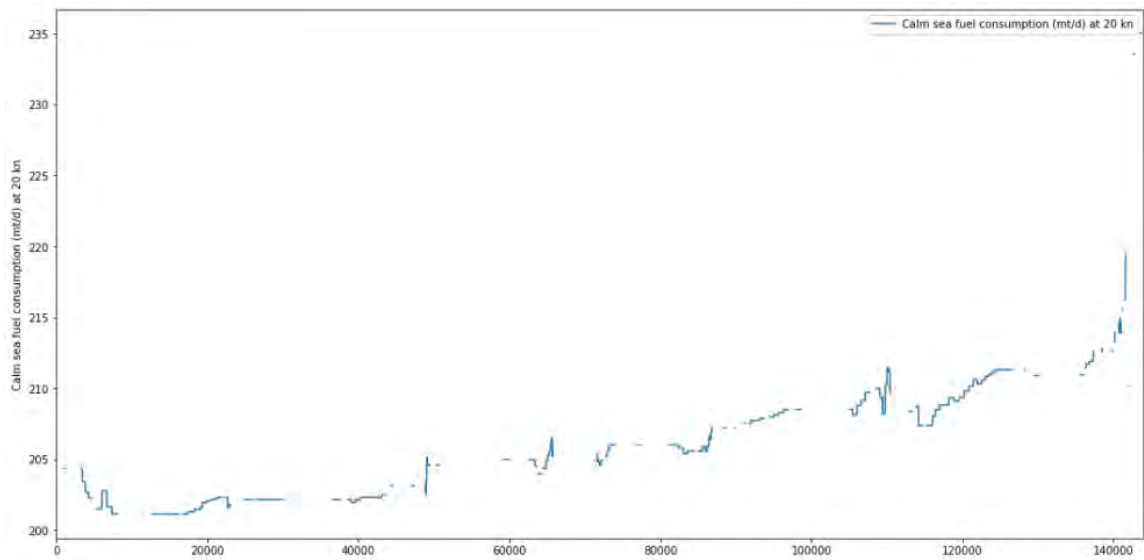Fig.5: Modeled and noon reported fuel consumption over speed

Fig.6: Calm sea power at 20 kn evolution over time

The main application of this feature is to monitor the changes in performance following sea changes, dry docks, paint applications, or the installation of an energy reduction device onboard the ship, Fig.6.

4.2. Speed variations and weather conditions impact

FFM model provides good inputs to assess how a previous voyage was executed. In fact, it is possible to model what would have been the optimum speed and fuel consumption of the vessel according to the executed route and weather conditions.

First step is to assess the speed profile of the voyage, looking into speed or power variations. Those changes should be avoided in order to perform a minimum fuel consumption in a just-in-time arrival context. In case we observe such variations, the FFM model allows to calculate how much fuel was overconsumed and what is the margin of improvement for the vessel.

The impact of weather conditions on the fuel consumption of the vessel can also be calculated from the model. This feature provides a possibility to assess when did the weather create some overconsumption and to what extent. The crew can use this knowledge to improve its weather routing for each specific vessel. This kind of benchmarking can be displayed as in Fig.7, where the crew can review the voyage performance and understand how to improve on the next voyage.
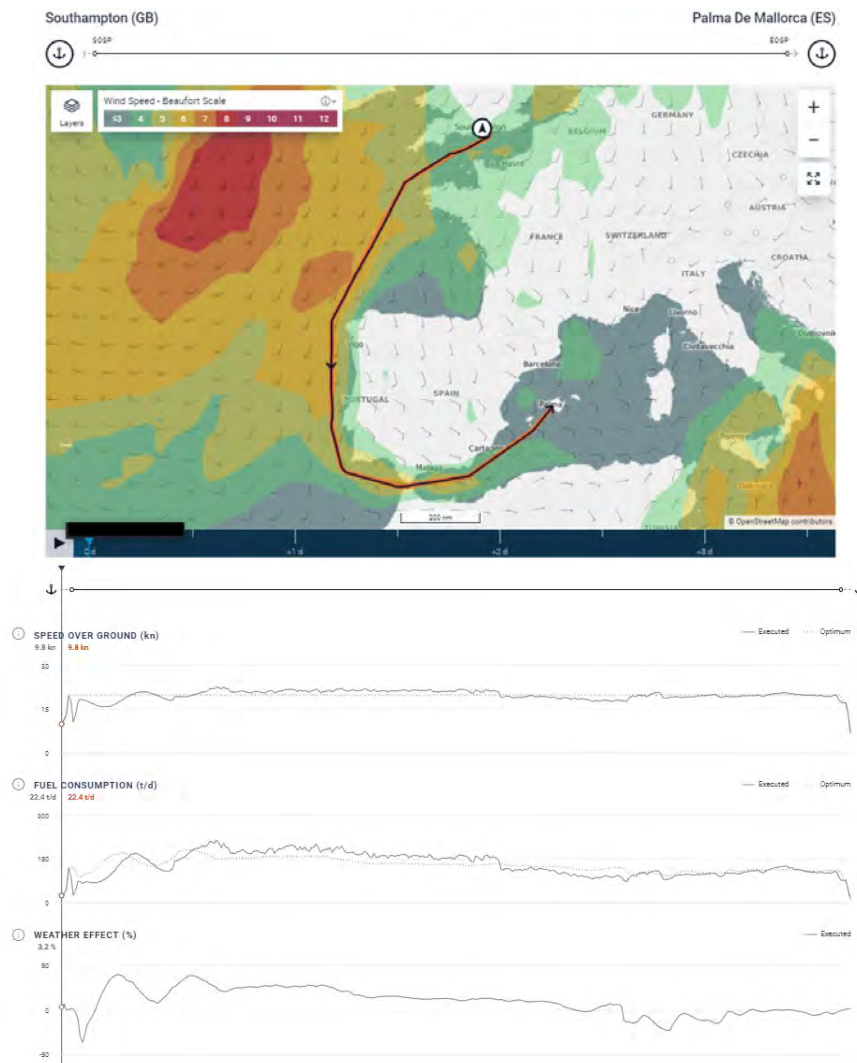
Fig.7: Impact of weather on a given route along time

4.3. Fuel planning for next voyage

The fitted model can be used to predict the fuel consumption of the vessel in any weather conditions. It can replace empirical speed loss tables used in weather routing today. It is also possible to simulate the cost of using a given vessel in a sea area based on average weather forecasts per season. This applies well to a ferry operator for example.
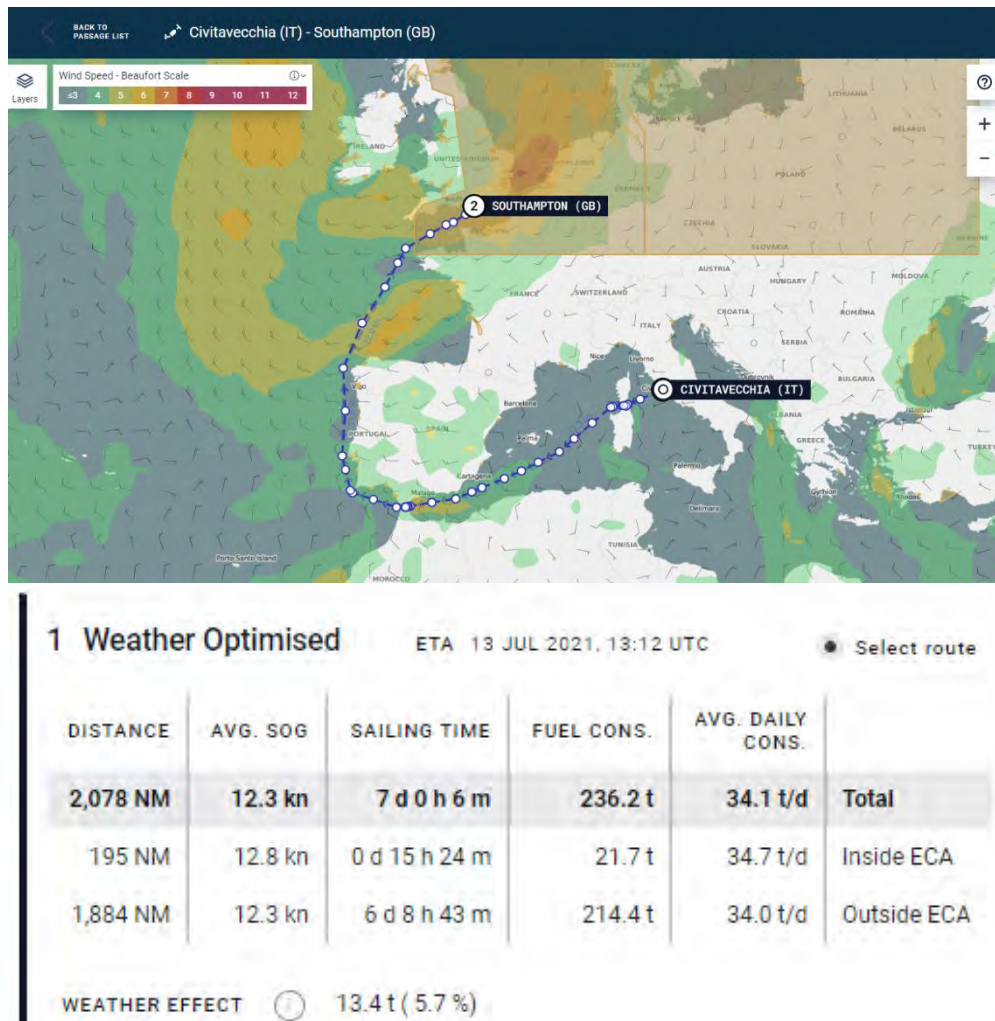

Fig.8: Example of passage planning using FFM model

5. Conclusions and outlook

We verified that using AIS data and weather hindcasts as inputs to the FFM (fuel flow model) presented by *Antola et al. (2017)* is possible and assessed the performance and applications of the model with such inputs.

The model successfully captures the behavior of the ship and impact of the weather conditions and draft on its performance. An important data cleaning and filtering work is needed prior to using the data. Despite this effort, AIS data seems not reliable enough to reach the full potential of the model when compared to other studies such as presented by *Schmode and Antola (2020)*.

Navigational data logged in high frequency by using existing navigational equipment is a more reliable data source to feed the FFD model. This is the way the Wärtsilä Fleet Operations Solutions system works, and this approach has proven to be robust and reliable. FFD model is then used to benchmark past voyages performance and accurately plan the most optimal routes for future voyages.

Hull fouling analysis and quality-check of fuel consumption reporting is also performed automatically.

References

ANTOLA, M.; SOLONEN, A.; STABOULIS, S. (2017), *The Art of Scarcity: Combining High-Frequency Data with Noon Reports in Ship Modelling*, HullPIC'17, Ulrichshusen, pp.118-123

SCHMODE, D. (2017), *Influence of Noise and Bias on the Uncertainty of Data-Based Hull Performance Prediction*, HullPIC'17, Ulrichshusen, pp.19-24

SCHMODE, D.; ANTOLA, M. (2020) *Fusion of High-Frequency Navigational Data and Noon-Reported Data to Predict Hull Condition*, HullPIC'20, Hamburg, pp.189-197

Using Unsupervised Machine Learning for Building Ship Performance Reference Model

Wojciech Górski, Enamor Ltd., Gdynia/Poland, wojciech.gorski@enamor.pl
Jerzy Michniewicz, Enamor Ltd., Gdynia/Poland, jerzy.michniewicz@enamor.pl
Agnieszka Szlendak, Enamor Ltd., Gdynia/Poland, agnieszka.szlendak@enamor.pl

Abstract

Ship performance evaluation in most cases is based on a reference model. Reference model describes ship performance in conditions which define base for performance evaluation. Usually the reference model describes new, clean ship in calm weather and deep waters. Comparing current ship performance to its reference, one can evaluate performance drop e.g. due to ship and propeller fouling. Traditionally the model has a form of speed-power curves obtained in a course of towing tank tests at ship design stage. More often modern computational techniques such as CFD are employed for this purpose. Both methods however require reliable resources and considerable efforts to provide data suitable for reference model preparation. Within the presented study the method of reference model preparation based on data collected during ship operation is examined. Method employs various machine learning algorithms. It starts with unsupervised data clustering in order to detect most common operational patterns. Each cluster is evaluated with respect to outliers and preprocessed in order to get consistent input for further analyses. After data cleaning separate local reference model is built for each cluster. General reference model allowing for performance evaluation in different operational conditions is prepared by automatic selection of relevant local model enriched with appropriate smoothing algorithms. Entire process is realized with minimal user input and does not require additional information (model tests or CFD results) except data collected during ship operation. Method has been validated against operational data obtained prior to and following the ship cleaning events for various ship types. Promising results allowed the application in SeaPerformer where it become a valuable tool for ship performance assessment in case standard data sources for building reference model are unavailable.

1. Introduction

The vessel, being a complex system described by various data can be now closely analysed and evaluated. Especially with modern technologies enabling to gather signals from the machine almost in real-time. Now since we are able to present, via data collection and visualization, how the ship is operating at any given moment, we could also be able to create and use references for performance evaluation. And that brings us countless benefits, especially for more economical and environmentally conscious vessel operation.

2. Importance of reference model

Reference models prove to be very useful when observing and evaluating a ship's performance. Their role is to present the best results under the defined conditions that the ship can achieve. And this allows for comparison between actual and desirable performance.

There are a few methods for creating ship reference models. E.g. at the vessel's design stage by conducting measurements in the model basin, or by carrying out numerical calculations using CFD method. Useful are also reports from sea trials created shortly after the ship is built and leaves the shipyard - that is when during tests it can achieve the best results which are then recorded and set as its reference model.

The main problem with those approaches is that there are not many varied tests undertaken and they do not cover the whole spectrum of conditions under which the ship may be sailing. This way we get for example one reference model for fixed water depth and wind speed and directions with no universal

information on how to shift the model when any of those change during exploitation.

This lack of data can lead to misleading results with insufficient accuracy when comparing reference models to observed ship's results. In an ideal situation, we should be able to see when the vessel is losing its efficiency, but with models too general we cannot be sure whether it is the case of actual failing or of model misrepresentation.

Our first approach was to shift the existing reference model's curve in order for it to better suit the data, Fig.1. We used our collected data points, filtered them with regards to the environmental conditions, and tried to fit the model to their shape.
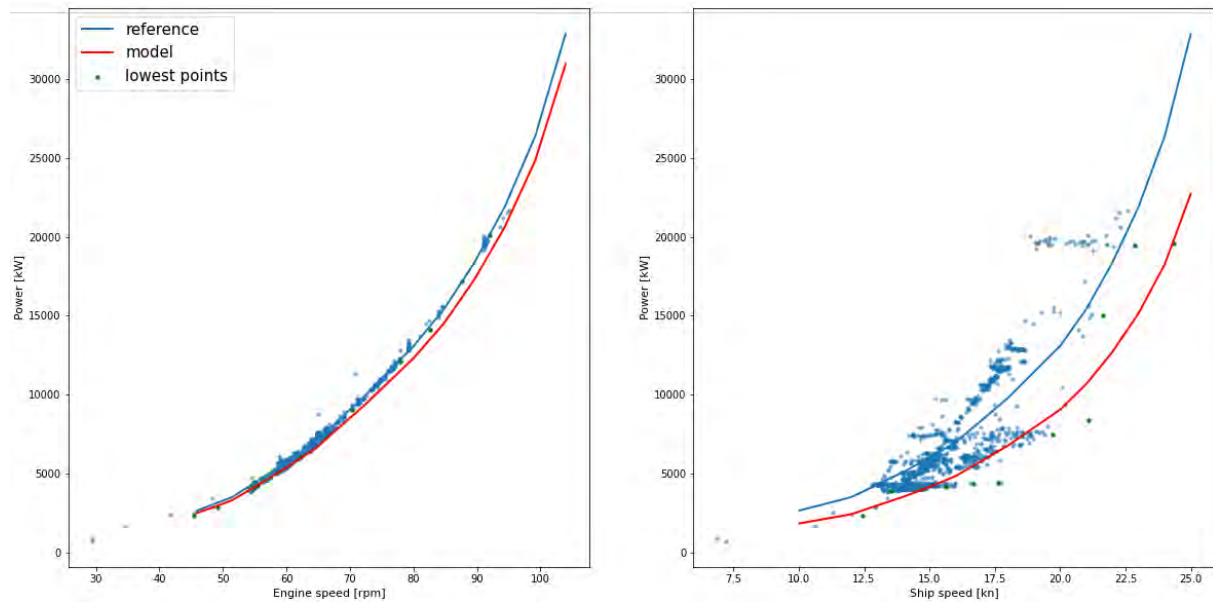
Fig.1: First approach – Shifting reference model's curves

The biggest challenge at this stage was the quality of data points. During our work, we noticed that vessel speed measurements have way more noise and outliers than engine speed measurements. Thus why for our research we focused on the latter.
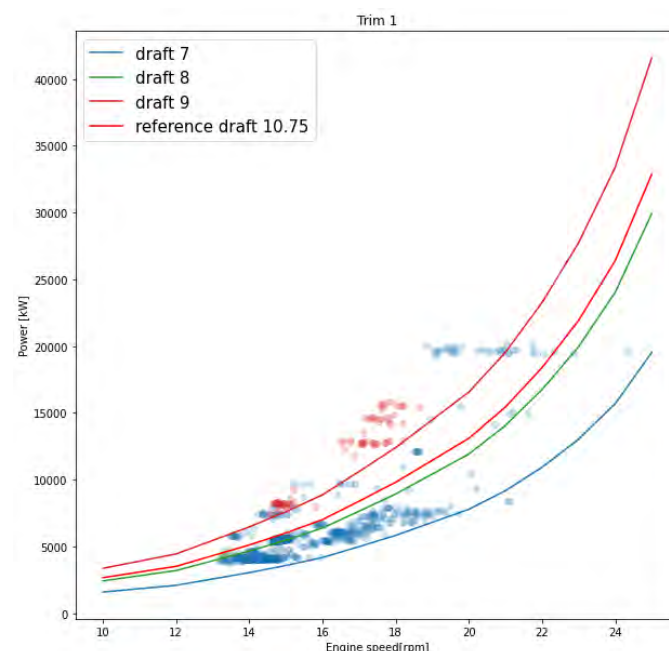
Fig.2: Curves for drafts

We hoped to spot dependencies with how our curve shifts depending on trim and draft it is being adjusted to. As presented in Fig.2, unfortunately, it was not the case – models for drafts selected for particular trim do not fall in a logical sequence. Even though these results turned out to be inconclusive, the experiment brought us to another, main idea of this paper.

3. Motivation and method

Difficulties faced in traditional approach to model preparation and importance of reference model in performance analyses influenced our research direction. The team aimed at the development of the method enabling the creation of the reference model with the use of data collected onboard. It was assumed that the user shall not be engaged in the process as far as possible.

Building the reference model starts with the definition of the time period of vessel operation. Selection of the period is arbitrary – it is up to the user to select a period which shall be considered as the reference. Although there are no formal contraindications in the selection of reference periods, some general guidelines shall be considered:

- Ship performance in reference period shall be consistent i.e. selection of period in which performance changes substantially (either due to maintenance procedures e.g. hull cleaning or due to natural process e.g. fouling) shall be avoided. The reference model is built of local models each defined for different draft and trim. Each of the local models shall describe the same vessel performance,
- Both periods of "good" (new ship, ship after cleaning) or "bad" performance (vessel with heavy fouling) can be used as long as not mixed within one reference period. Although both options are feasible, interpretation of results will be different since relative performance is presented,
- Periods of continuous operation in bad weather and/or shallow waters shall be avoided. Periods of operation in weather and bathymetry conditions that may affect vessel performance will be removed. In case these are prevailing conditions of operation final dataset after filtering may be insufficient for the purpose of building the model,
- Operational conditions of the vessel in the reference period shall be representative of the general operational pattern. In case the vessel in reference period operates in unique conditions which are not used in other periods of operation such reference period, although formally correct, is not useful.

Once the reference period is selected, underlying data are processed in order to build a reference model. The first phase of processing consists of environmental and bathymetry filtering. Any data point which was recorded in bad weather conditions or in shallow waters will be removed from the dataset. Filtering conditions depend on the vessel's operational characteristics and are stored as a part of ship settings.
An essential part of model preparation comprises of identification of the frequently used operational conditions. The process is commonly denoted as grouping or clustering. This machine learning technique results in the identification of data points of similar features. Thanks to the similitude revealed in the clustering process data points belonging to one cluster can be described by a common model and used for performance evaluation.

There are more than ten different clustering algorithms practically used in machine learning problems and implemented in software packages such as scikit-learn, *Pedregosa et al. (2011)*. Therefore an essential part of this study was the determination of the most suitable one. The selection of the appropriate algorithm was performed in two stages. At first general features of the algorithms were evaluated with respect to the unique properties of the reference model identification task. Secondly, initially selected algorithms were exercised with vessel data in order to confirm their robustness and to tune the algorithm's parameters in order to achieve desirable performance irrespectively of the input data. Algorithm fine-tuning was an essential part of ensuring method interoperability i.e. ability to work properly with data belonging to vessels of different types, sizes, and operational characteristics without a need of user intervention.

Let us first discuss the general features of clustering algorithms and describe an intuition behind the initial selection. The following criteria were analysed with this respect:

- Flexibility in selecting clustering features i.e. ability to cope with different sizes of feature array,
- Efficiency i.e. providing a reasonable time of computations for moderately large data sets,
- Scalability i.e. ability to work with datasets of different sizes and ranges,
- Compatibility of algorithm parameters with model identification problem.

Clustering features i.e. dataset variables used to identify similitude among groups were identified as an important factor in searching for favourable clustering algorithm Although ship draught and trim were considered as mandatory parameters it was observed that some algorithms perform weakly with relatively small feature array. On the other hand, for some other algorithms, it was relatively complicated to modify implementation in order to use a larger feature array.

Initial tests with real ship operation data allowed us to identify that size of the dataset varies in the range of a couple of thousands up to about one hundred thousand data points. Already lower boundary posed efficiency problems (resulting in an unacceptable time of computations) for some algorithms while the upper limit revealed that additional methods for optimizing execution time were necessary. In order to cope effectively with large datasets, a random sampling technique was implemented. A fixed number of data points were selected at random which allowed preserving features of the problem and greatly reduce computational effort at the same time.

Resampling dataset to the fixed size allowed overcoming the scalability challenge but the problem of ship-specific ranges of feature array variables needed to be solved. Analysed features (e.g. draft and trim) vary in ranges specific to a particular ship and as a result, clustering algorithm parameters needed to be modified when executed for a different vessel. An obvious solution was to implement normalization on features array. However, due to its computational effort, algorithms that perform well without it were preferred.

Finally, clustering algorithms were analysed with respect to their input parameters and ability to cope with complicated cluster boundaries. Data visualization revealed that clusters in the draft–trim space form centroid-like shapes, often unsymmetrical and skewed. Adding dimensions to feature arrays makes the problem even more non-linear. Another limiting factor in the selection of clustering method stemmed from the inability to determine the cluster number a priori which is the mandatory parameter for some clustering algorithms. Therefore, among a dozen of popular clustering methods, only a few could be implemented. The most widely described clustering algorithm – k-means, Fig.3 (left), was rejected due to difficulty in handling non-linear boundaries and a need of defining a number of clusters as the input parameter. The latter problem can be solved by multiple runs of algorithms with different cluster numbers and the application of clustering quality measures. However, the inability to cope with non-linear divisions among clusters makes k-means incompatible with the analysed problem. A similar problem with non-linear boundaries was identified for the spectral clustering method, Fig.3 (right).
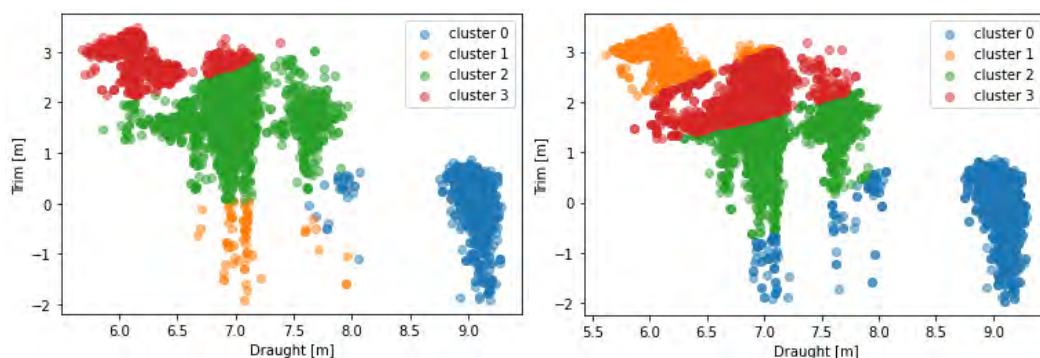

Fig.3: K-means (left) and spectral (right) fail to handle non-linear boundaries

Hierarchical clustering was another group of algorithms tested in a conjunction with ship conditions identification problems. Although different linkage types were exercised (including average, complete, and ward) none of them performed well. In the case of complete and average linkage types, artificial boundaries were observed while algorithm based on ward type of linkage was difficult to adjust. Set of parameters that resulted in fair clustering for a dataset of one vessel resulted in inappropriate clustering for another vessel. Ward linkage-type was found very sensitive for a number of data points in the dataset and required manual tuning for each case.

Another interesting alternative was the implementation of density-based clustering algorithms such as DBSCAN and OPTICS. The latter is a generalization of a more established DBSCAN algorithm. OPTICS allows for relaxation of DBSAN's density parameters thus was believed to be applicable for vessels of different types and sizes. The initial results were very optimistic. Clusters of vessel operational parameters were clearly identified with just a few cases where cluster identification was doubtful, Fig.4 (left). Despite very promising initial results algorithm validation on different vessels' datasets was not successful. Although different sets of OPTICS parameters were exercised it was not possible to find a universal one that results in proper clustering for different vessels or even in the case of different operation periods of the same vessel. An example of poor OPTICS clustering, Fig.4 (right) exhibits a tendency of excluding a major part of the dataset (identified as outliers and enclosed in cluster -1). This example was obtained by application of the same algorithm parameter as in the successful case.
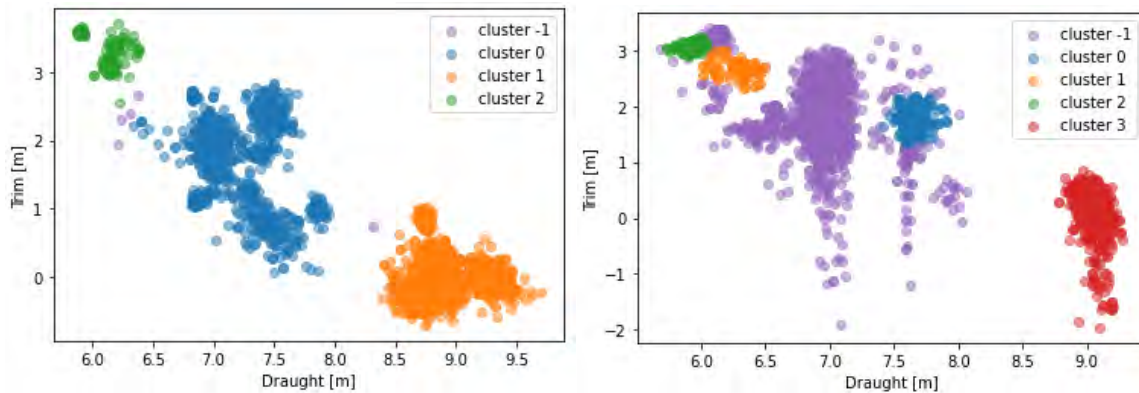

Fig.4: Successful (left) and poor (right) implementation of OPTICS clustering algorithm

Despite unfavourable results of OPTICS algorithm validation, density-based clustering was considered as the most capable as far as the identification of non-linear boundaries. Therefore, further studies were undertaken to implement DBSAN algorithm. The major difficulty was in defining the appropriate value of the algorithm's density parameter. The universal value which allows for clustering data of different ships was not found therefore another approach was implemented to allow automatic (unsupervised) clustering. Different density parameter values, within a given range, were subsequently used in order to perform clustering. Each case quality of clustering was evaluated and clusters that received the highest score were selected as the result. Few clustering quality measures were evaluated, i.e. silhouette, *Rousseeuw (1987), Calinski-Harabasz (1974),* and Davies-Bouldin, *Thomas et al.* (*2013*).

None of these single measures were found universally applicable, Fig.5. Therefore, for the purpose of selection of the optimum value of density parameter, a combined quality measure was employed. Scores obtained with Calinski-Harabasz and Davies-Bouldin were averaged and used as the final quality criteria.
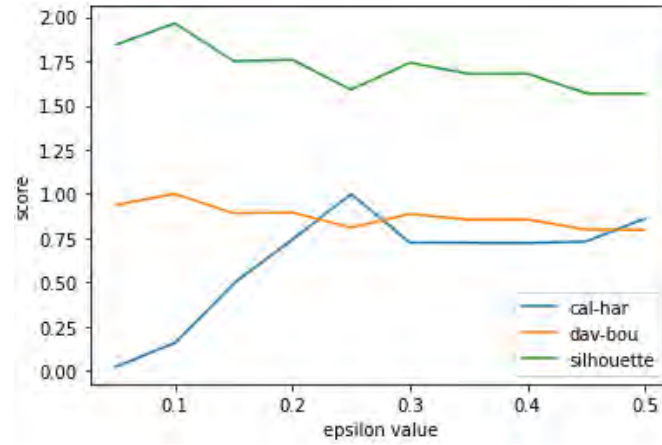
Fig.5: Clustering evaluation according to different scoring methods

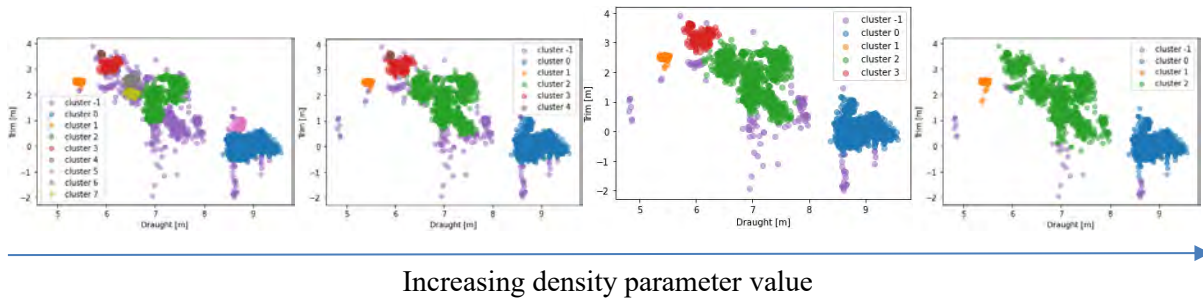

Increasing density parameter value

Fig.6: Clustering results for different density parameter (optimum enlarged)

Density value determines the level of detail of our clustering, Fig.6. It states the distance at which points can still be classified to the same group. That being said, we can see that with a small density value there are more separate clusters while with the bigger values those merge into wider and more general. Both of those extreme cases are unfortunate, because a bigger number of aggregation may lead to unnecessary computations while too small a number can make our model not precise enough.

Application of DBSCAN algorithm with adjustable density parameter according to combined quality measure has been proven to work efficiently with datasets obtained for different vessels, Fig.7. It can be observed that the algorithm is able to detect outliers (cluster -1) which is an important feature for analyses of highly scattered data.

As soon as clusters are properly identified, a reference model for each group can be prepared. It has been decided to define linear models although performance data (especially main engine power vs ship speed or engine rpm) exhibit highly non-linear character. The linearization method is not described within the present paper. However, interested readers may refer to *Journée and Meijers (1980)*.

In order to match each test data point with the corresponding reference model, certain mapping between points and models is required. As the clustering method does not provide any explicit way for the reassessment of arbitrary points belonging to certain clusters, the only traces of the performed clustering are reference points flagged with relevant cluster numbers. Therefore, we needed an alternative way to classify test points.
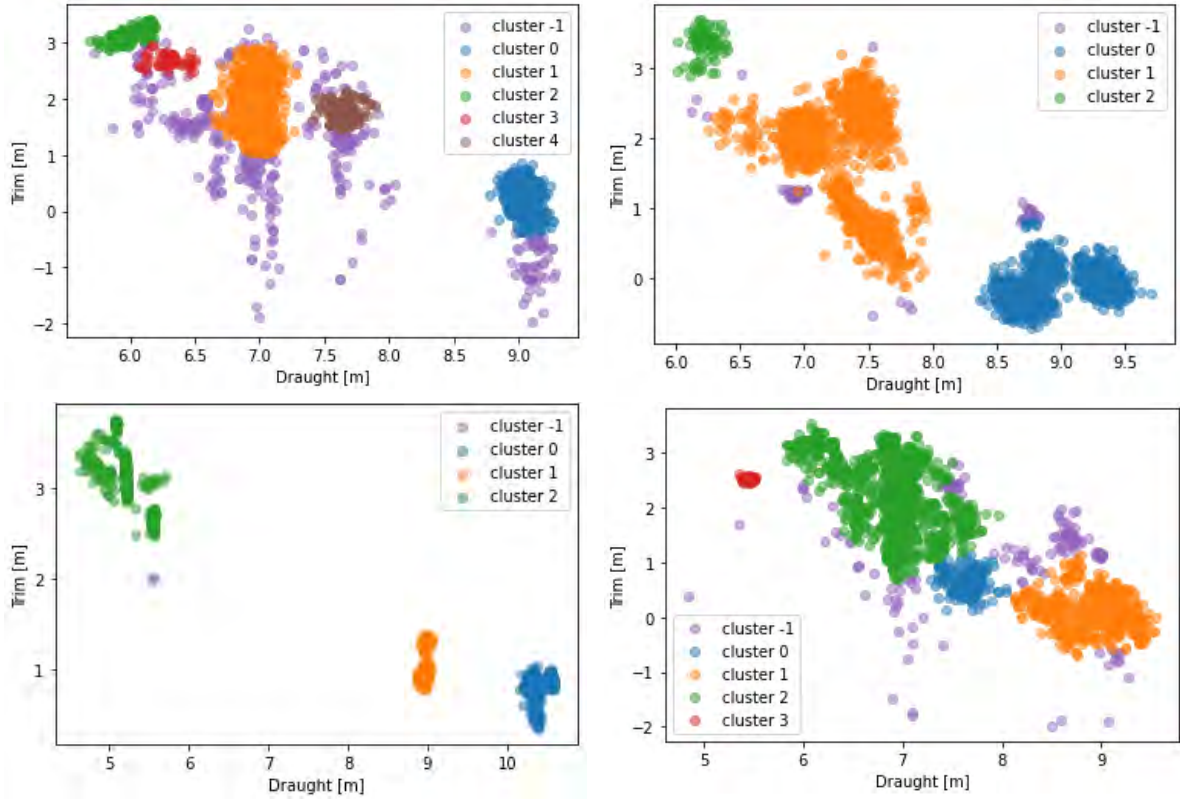
Fig.7: Successful implementation of DBSCAN clustering algorithms

We have decided on a geometrical approach to describe and store the boundaries of each cluster. Draught and trim were chosen as basic attributes of loading conditions to form a two-dimensional space. Each identified cluster in this space is wrapped around using alpha shape to formulate its boundaries as a polygon. The polygon definition in turn allows examining any test point's belonging to a cluster, in terms of two mentioned attributes.

Although the alpha shape proved both its usability and reliability, computational performance tests revealed unacceptably long execution time in case of more than about 50 points in a cluster. Hence, few different approaches were taken to hollow up the point cloud and reduce it to the most important points close to the boundary, which illustrate orange points, Fig.8.
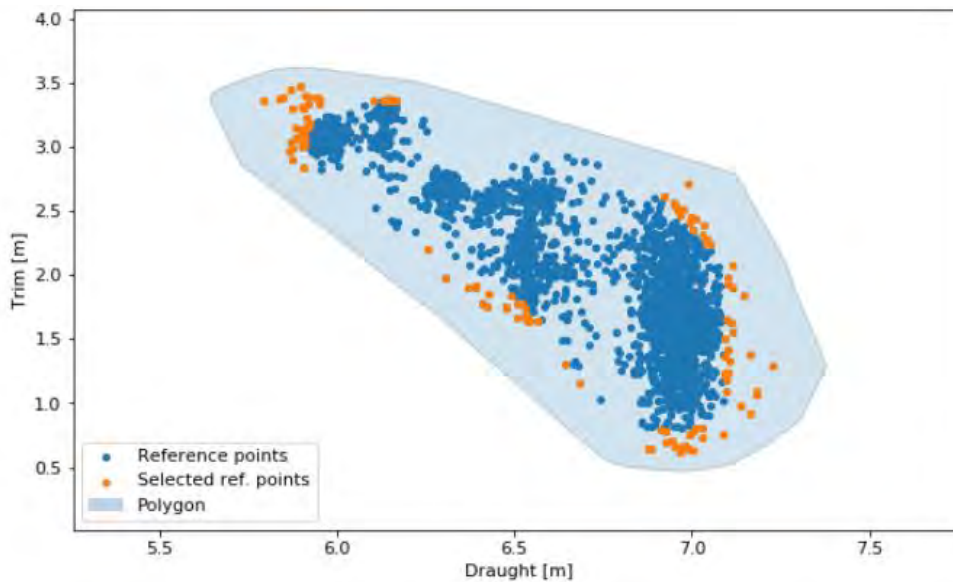
Fig.8: Polygon representation of a single cluster based on reference points

138

It may happen that two or more polygons are overlapped at a certain place. Potential conflicts between polygons are solved one by one. The overlapping part of each polygon is then cut off and the polygon is being redefined.

4. Application of models

Having defined the limits of validity for each cluster, operational points of test period are classified into certain clusters. Fig.9 demonstrates reference-period (dark) points wrapped into polygons and the mapping of test-period (light) points to clusters.
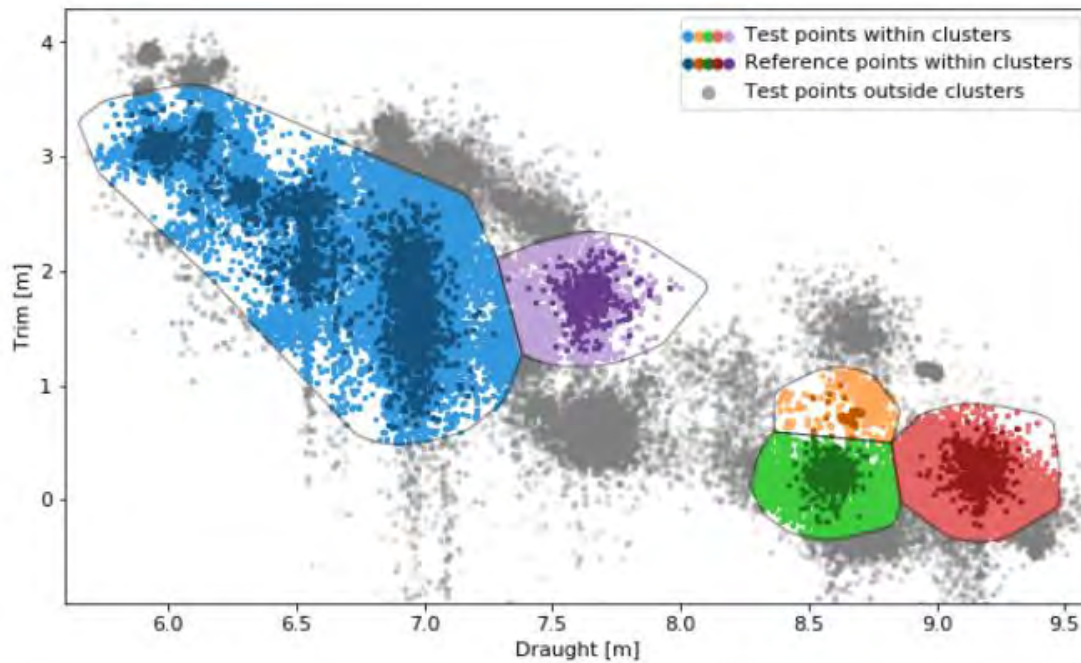
Fig.9: Identified polygons overlayed over operational points in test period

According to the operational complexity of the chosen reference period, some part of test points falls into specific, coloured clusters. While the outstanding observations (in grey) remain unclassified and are not subject to further performance assessment.

Once the test period points were classified according to their adherent polygons, appropriate model can be matched allowing for the calculation of a performance indicator. Power increase KPI has been selected as the performance measure. It has been defined as:

$$Power_{KPI} = \frac{Power_{in\ operation} - Power_{acc.\ to\ model}}{Power_{acc.\ to\ model}}$$

$Power_{in\ operation}$ – is power measured during vessel operation in test period
$Power_{acc.\ to\ model}$ – is power according to reference model defined for same operational conditions

In order to assess vessel performance changes, obtained KPI shall be plotted against time of operation. However, in order to make the time trend meaningful, data cleaning must be applied. KPI data exhibit significant scatter due to limited credibility of collected data and deficiencies of methods for environmental impact filtering and correction. Data cleaning has been implemented in two phases. First gross outliers are removed with the use of the Z-Score filter, https://www.geeksforgeeks.org/z-score-for-outlier-detection-python/. The final shape of the time trend is obtained with the use of smoothing techniques. Locally Weighted Scatterplot and Spline, https://pypi.org/project/tsmoothie/, smoothers proved to be well fitted for the analysed problem. Smoothing allows for filtering short-term performance disturbances which make the long-term trend more pronounced and visible.

5. Implementation of the model for performance analyses

The method for automatic (unsupervised) determination of reference model developed by Enamor and described here has been implemented as ship performance evaluation tool in SeaPerformer™ system. It proved to be useful in cases when design data (results of model tests, CFD calculations, sea trials results. Etc.) are not available or are incomplete. It is suitable for the evaluation of vessel performance changes in time especially due to hull fouling. The method has been implemented as the time trend and therefore enables to:

- capture current and historical vessel performance with respect to the reference model,
- detect significant changes in vessel performance e.g. due to accelerated fouling development caused by long port stay,
- predict how vessel performance would change in time assuming that operational pattern will not change,
- effectively assess hull maintenance treatment procedures (hull cleaning, re-coating) in short and mid-terms, i.e. what is an immediate performance gain after the completion of maintenance procedure and how long the resulting performance improvement is visible.
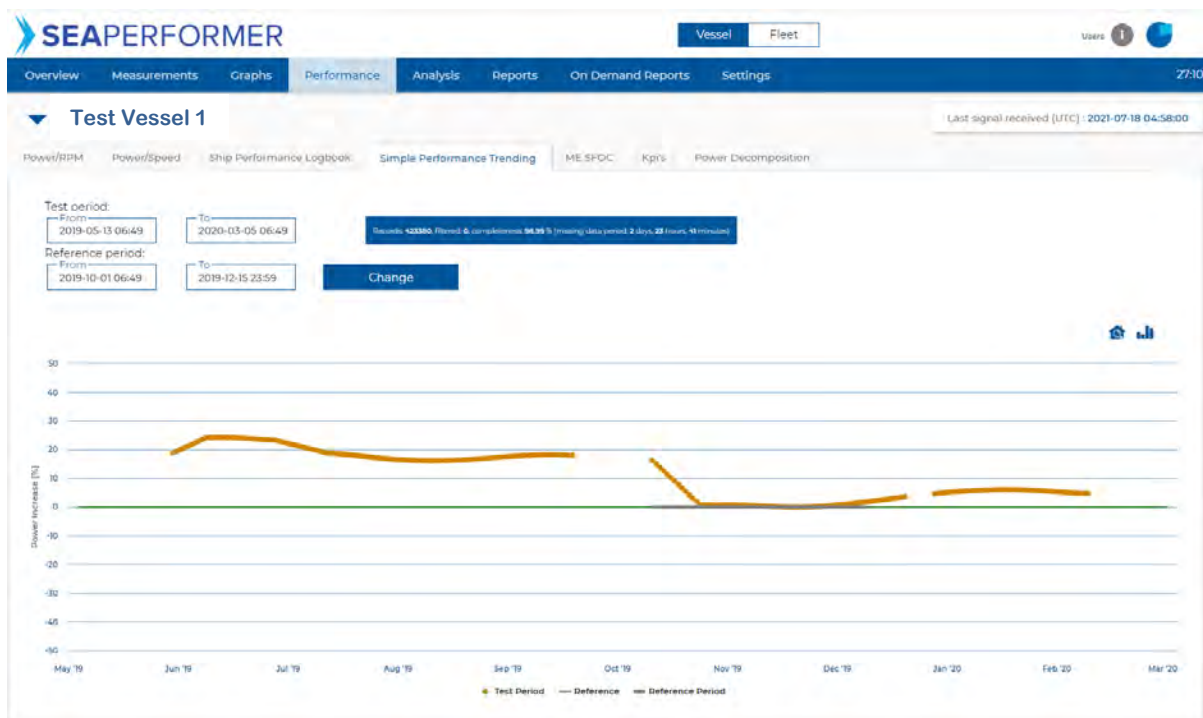

Fig. 10: Performance time trend

An example of vessel performance analysis is presented in Fig.10. Test period covers operation prior vessel dry docking and few months following the hull cleaning performed in October 2019. Reference model was created over the period after hull cleaning (approximately 6 weeks) and was implemented for performance analysis. In the period preceding dry-docking vessel suffered due to hull fouling which resulted in ~20% power increase (and similar fuel over-consumption) in comparison to reference period. Comparison of performance gain allows for evaluation of hull cleaning effectiveness. Observation of the performance trend after the hull cleaning allows for assessment of performance durability. Although some fluctuation of trend in entire test period can be observed the implemented method allows for clear identification of performance changes. Trend fluctuations reveals limited applicability of data cleaning methods which will be addressed in future works.

6. Future development

Works on the method presented in this paper will be continued. Data preparation algorithms will be optimized in order to reduce computation time. At present, building the time trend for a period of 12 months of vessel operation takes approximately 2 minutes. Execution time can be greatly reduced by precomputing partial data each time a new data set is transferred from the vessel to the cloud. Partial results will be stored and retrieved when a time trend is created.

Data scatter will be reduced by the application of updated environmental correction methods. The most important, with respect to this, is the wave correction algorithm. Currently used methods tend to overestimate correction thus lead to inconsistent results. Furthermore, a model quality assessment will be developed. In some cases, especially in the case of clusters build on a small number of points, least-square linear regression tends to create unreliable models. Proper identification of erratic models will allow for their rejection and, in consequence, reduce the scatter of the time trend.

7. Conclusion

Unsupervised machine learning algorithms were successfully implemented for the problem of model identification. The elaborated method allows for automatic identification of frequent vessel operational conditions and the creation of local models. These models are used for the evaluation of ship performance which can be practically used for planning and evaluating maintenance procedures allowing reduction of vessel operational costs and environmental impact.

Acknowledgements

References

CALINSKI, T.; HARABASZ, J. (1974), *A dendrite method for cluster analysis*, Communications in Statistics 3/1, pp.1-27

JOURNÉE, J.M.J.; MEIJERS, J.H.C. (1980), *Ship routeing for optimum performance,* TU Delft

PEDREGOSA, F.; VAROQUAUX, G.; GRAMFORT, A.; MICHEL, V.; THIRION, B.; GRISEL, O.; BLONDEL, M.; PRETTENHOFER, P.; WEISS, R.; DUBOURG, V.; VANDERPLAS, J.; PASSOS, A.; COURNAPEAU, D.; BRUCHER, M.; PERROT, M.; DUCHESNAY, E. (2011), *Scikit-learn: Machine Learning in Python,* J. Machine Learning Research 12, pp.2825-2830, https://www.jmlr.org/papers/volume12/pedregosa11a/pedregosa11a.pdf

ROUSSEEUW, P. J. (1987), *Silhouettes: a graphical aid to the interpretation and validation of cluster analysis*, J. Computational and Applied Mathematics 20, pp.53-65

THOMAS, J.C.R.; PEÑAS, M.S.; MORA, M. *(2013), New version of Davies-Bouldin index for clustering validation based on cylindrical distance,* 32nd Int. Conf. Chilean Computer Science Society (SCCC), pp.49-53

Historical Position Measurement Validation and Correction using AIS Data - An Account from a Larger Shipping Company

Angelos Ikonomakis, Maersk R&D, Copenhagen/Denmark, angelos.ikonomakis@maersk.com
Jesper Dietz, Maersk Line Fleet Performance, Copenhagen/Denmark, jesper.dietz@maersk.com
Klaus Kähler Holst, Maersk R&D, Copenhagen/Denmark, klaus.holst@maersk.com
Ulrik Dam Nielsen, Technical University of Denmark, Copenhagen/Denmark, udn@mek.dtu.dk
Roberto Galeazzi, Technical University of Denmark, Copenhagen/Denmark, rg@elektro.dtu.dk

Abstract

Accurate position measurements are extremely valuable in the shipping industry for various reasons such as safety (collision avoidance), fuel saving (weather identification), punctuality (route prediction), etc. Although GNSS (Global Navigation Satellite System) receivers installed on-board the ships are proven to be highly accurate, the data collection process may occasionally be problematic, mainly due to the complexity of the measurements and the decimal precision that is required. Data was collected from 3 years of operations of 228 Maersk Line container vessels and an analysis reveals that there is a substantial amount (≈ 20%) of historical position measurements sent to shore that does not reflect reality. With this study, the authors initially identify the source of the faulty logged position measurements, then they categorize them into segments and finally they apply an interpolation methodology in order to validate and correct them by using AIS (Automatic Identification System) data.

1. Introduction

1.1. Background and motivation

Satellite navigation is a very important asset in modern positioning systems of the shipping industry and is the only system that can provide a ship's absolute position relative to the geocentric coordinate system, *Chang et al. (2020)*. Consequently, shipping companies should be extremely cautious on taking good care of their navigation systems in order to avoid losing coordinates data. There are many internal processes that rely on good quality position measurements. The most critical is safety. To name a few safety related processes, there is collision avoidance, *Hu et al. (2007)*, motion prediction in ports, *Johansen and Fossen (2016)* and accuracy in warships, *Núñez et al. (2017)*. Apart from safety, a strong incentive for the shipping companies is fuel saving. The operating cost of a ship is mainly influenced by bunker fuel and lubricating oil prices which consist of 50–60% of the total ship operating cost, *Perera and Guedes Soares (2017)*. By improving the precision in position measurements, voyage planning and weather routing could be made more accurate therefore less fuel would be consumed.

The most frequent measurement loss/modification effects of GNSS (Global Navigation Satellite System) antennas are jamming and spoofing. Jamming is a kind of white noise interference, causing loss of accuracy and potentially loss of positioning, *Morong et al. (2019)*. Spoofing is an intelligent form of interference which fools the GNSS receiver into computing a wrong location, *Psiaki and Humphreys (2016)*. Besides the above, there in another issue that has been recently identified by the authors which refers to the posterior modification/loss of the position data after the signal has successfully arrived at the GNSS receiver. Apparently, for a position data point to reach the shore (shipping company's data center) it travels through a long path which varies depending on the ship type. This path might transform the format of the position data point several times before reaching the company's data center at shore.

The current paper intents to initiate an open dialogue over this issue. Firstly, it describes the posterior position measurements path (after the signal has being received from the GNSS antenna) through the data recording system of the ship, leading to shore. This path is proven to be malefcent for the position measurements in ~20% of the vessels tested in this study. Given that the data analyzed is large enough to represent a statistically significant sample, it is assumed that the percentage is not dataset-specific but a global standard. There are claims of choosing AIS position data over owned measurements on

mathematical model of high precision due to low trust on the latter. This is unreasonable given that sometimes, AIS receives satellite coordinates from the same GNSS antenna as the data monitoring and recording system of the ships. In a second phase, the paper introduces ways of identifying and correcting faulty historical position observations by implementing an interpolation methodology.

1.2. State-of-the-art

Various researchers in the past have proposed solutions for jamming, *Gao et al. (2016), Medina et al. (2019),* and spoofing, *Akos (2012), Broumandan et al. (2012), Schmidt et al. (2016), Fukuda et al. (2021)* which correspond to the most frequent a priori data loss in navigation systems (a priori refers to the moment before a position data point reaches the GNSS receiver). Others like *Liang et al. (2019)* explored the issue by building the missing trajectory using a Random Forest model to identify missing data and a LSTM(Long Short-Term Memory)-based supervised learning method for trajectory reconstruction. *Ryu et al. (2016)* focus on improving the accuracy of the position data by integrating INS(Inertial Navigation System) measurements using an EKF (Extended Kalman Filter) and an UKF (Unscented Kalman Filter). As far as we know, no previous research has investigated the a posteriori data loss/modification of position measurements (after the data has reached the receiver).

1.3. Objectives

The first asset of this paper is the description of the the data processing steps that the position measurements go through before reaching the ships's data center. Secondly, the introduction of the interpolation methodology algorithm sets the structural basis for solving the problem of a posteriori data loss/modification.

2. Data

The study includes data recordings from 228 container ships collected over a three-years period (2017-2020) during operations in the majority of the world's larger oceans. The data is divided into two categories, Table I; the CAMS dataset which consists of ~25 million rows of sensor data recordings stored in the company's database, and the AIS dataset which is sourced from two external providers consisting of ~50 million rows of data.

Table I: Type, description, frequency, value range and units for CAMS and AIS datasets

Type	Description	Sampling Time	Range	Median	Unit
CAMS	Time	10 mins	01/01/2017–22/02/2020	-	[UTC]
	ImoNo	10 mins	228 unique vessels	-	[-]
	Latitude	10 mins	−49–61	25.0247	[°]
	Longitude	10 mins	−180–180	23.7328	[°]
	SOG	10 mins	0–26	12.6	[kn]
AIS	Time	Uneven	01/01/2017–22/02/2020	-	[UTC]
	ImoNo	Uneven	228 unique vessels	-	[-]
	Latitude	Uneven	−50–61	32.1264	[°]
	Longitude	Uneven	−180–180	9.9188	[°]
	SOG	Uneven	0–25	12.3	[kn]
	COG	Uneven	0–360	188	[°]

Here, we should note that the reason of sourcing and merging the AIS dataset from two providers was to get as many valid points as possible to maximize the average frequency. So the final AIS dataset consists of three measurements types (i) terrestrial, (ii) satellite, and (iii) dynamic. In terrestrial, the data is broadcast on a common international VHF frequency. In satellite, the data is received through the satellite navigation network. Finally, for heavy traffic regions such as the "South China Sea" or the

"English Channel" AIS signals collide resulting in position detection failures and inaccurate reporting. Dynamic type measurements solve this issue.

3. Problem Formulation

3.2. Problem Source

GNSS (Global Navigation Satellite System) is the standard generic term for satellite navigation systems that provide automated geo-spatial position with global coverage. The term includes the GPS (US), GLONASS (Russia), Galileo (EU), Beidou (China) and other regional systems like QZSS (Japan) and IRNSS or NavIC (India). GNSS is a term used worldwide and its advantage to having access to multiple satellite networks is accuracy, redundancy and availability at all times. Satellite systems do rarely fail, because if one fails GNSS receivers will pick up signals from another network, *Heukelman (2018), Venezia (2015)*.

The position signal that reaches the GNSS receiver is transformed into a so-called NMEA (National Marine Electronics Association) sentence. NMEA is a standard data format supported by all GNSS manufacturers. Particularly, the NMEA sentence is in printable ASCII form and may include information such as time, position, speed, water depth, etc., *NMEA (2021)*. An example of a NMEA sentence is:

$$\$GPGGA, 181908.00, 3404.7041778, N, 07044.3966270,$$
$$W, 4, 13, 1.00, 495.144, M, 29.200, M, 0.10, 0000^*40$$

All NMEA sentences start with the \$ character, and each data field is separated by a comma. GP stands for GPS position (e.g GL would denote GLONASS). The next value 181908.00 is the timestamp (UTC time in hours, minutes and seconds) followed by 3404.7041778 the latitude in the DDMM.MMMMM format. Here we should mention that decimal places are variable. N denotes north latitude. 07044.3966270 is the longitude again in DDDMM.MMMMM format and W denotes west longitude, *Gakstatter (2015)*. The rest of the values will not be explained because they are irrelevant for the purpose of this paper.

The NMEA sentence, apart from traveling to shore through internal systems, it is also received from the AIS transceiver. AIS stands for Automatic Identification System and is an automatic tracking system that is used by vessel traffic services (VTS) supplementing the marine radar for collision avoidance. AIS transceivers can be tracked by AIS base stations located along coast lines or, when out of range of terrestrial networks, through a growing number of satellites, *Contributors (2021)*. According to the literature, AIS transmission rate is relative to ship's speed and range from 5 to 180 s, *ITU (2014)*.

In order for the data deriving from multiple sensors to be monitored and stored, Maersk is using a data processing system called the ADC (Auto Data Collector) which is the source from where the data is sent to shore. Within ADC there is a system called CAMS (Control Alarm Monitoring System). CAMS is responsible to connect the sensors, normalize and convert each data point, aggregate into either 1 second or 10 minutes and later log it and transmit it towards multiple internal services. Whenever there is good internet connection, ADC sends the 10-minute aggregates to shore. Depending on the vessel class, CAMS is bought from a list of manufacturers, each with distinct characteristics. The main characteristic that distinguishes them is the encoding/decoding memory format. They are either 32-bit or 64-bit. In some unique cases, the memory format is even lower, accepting only 6-digit numbers. The memory format of ADC is 64-bit. While converting among memory formats, sometimes data quality is degraded up to a few kilometers away. Location closer to the Equator are more sensitive due to the oval shape of the earth and need to have at least 4 valid degree decimal points to get ≤10 m error precision. Limiting the memory format to 6-digit numbers, it automatically increases the error to ≤100 m. Fig.1 illustrates the path a data point follows before reaching the shipping company's data center.
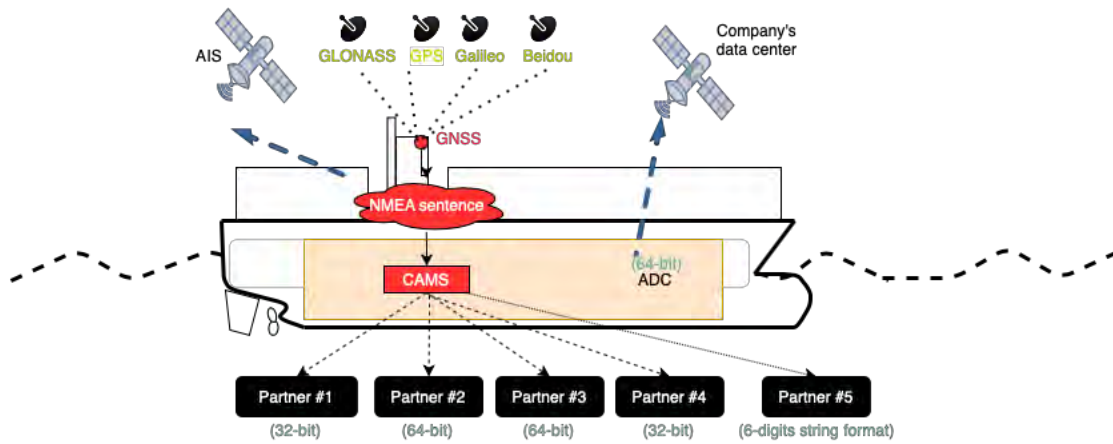
Fig.1: Position measurement path on board a vessel before reaching shore

Before we decompose the various sources that degrade the position data, we should first have a look at how the position data looks like in a big dataset like the one used in this study. Fig.2 shows the coordinates registered from 228 container ships during 3 years of operation (2017-2020). It is evident in the map that there are multiple measurements registered in locations away from a common vessel's trajectory.

Fig.2: Position measurements of 228 container ships during 3 years of operation (2017-2020)

A whole range of different sources degrading the ship's position data have been identified. The most prominent are:

- N/E issue: It refers to when the longitude values do not turn to negative when the vessel crosses the prime meridian towards the western hemisphere. As a result, location measurements get packed on the upper right quadrant of the map where both longitude and latitude values are positive. Fig.3 illustrates the registered trajectory of a vessel with a CAMS system experiencing such a problem. The issue is present in classes where Partner #2 and #3 CAMS systems are installed.

- Zig-Zag issue: It refers to when either longitude or latitude values go beyond 0.599999. In this case, the next step is 1.000000 based on the logic that 1 degree is made up of 60 minutes. That is obviously not true, as it should simply be 0.600000, followed by 0.600001. Every time this happens, we see a "jump" of 0.4 degrees of either latitude or longitude, which relates to ~40 km of error. Fig.4 illustrates the location of the vessel on the right part with a zoomed version

on bottom right to have a clearer view of the zig-zagging effect. On the left there is a data table that indicates the "jumps" in red color. Here, we should mention that the previous source "N/E issue" is also visible. The issue is present again in classes where Partner #2 and #3 CAMS systems are installed.
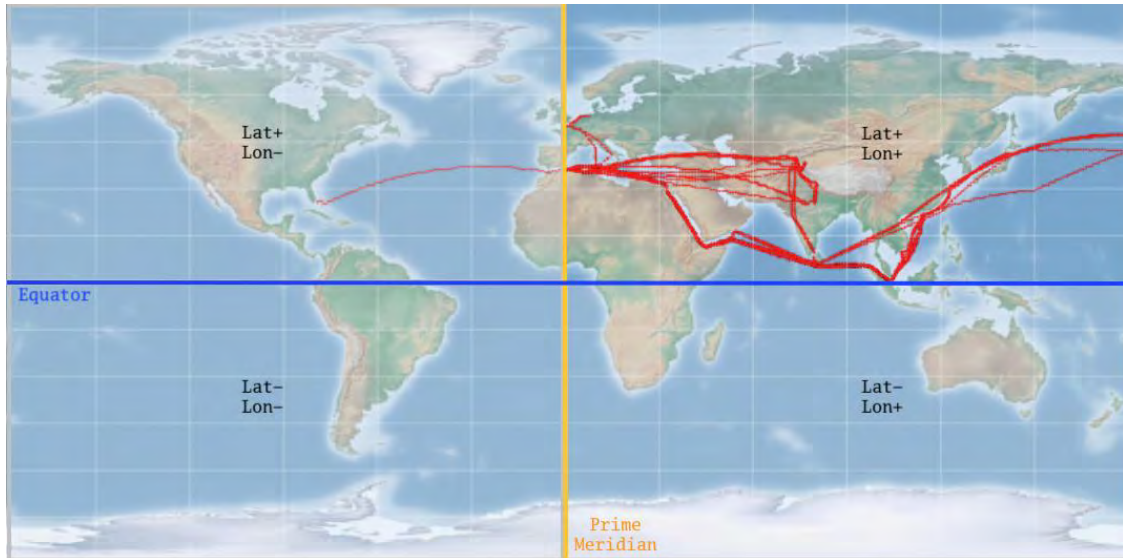

Fig.3: Registered trajectory of a vessel with "N/E issue".

Timestamp	7: Position Latitude [DD]	5: Position Longitude [DD]
2020-05-22 04:00:00	7,087135	76,308050
2020-05-22 04:10:00	7,074442	76,337243
2020-05-22 04:20:00	7,063569	76,366003
2020-05-22 04:30:00	7,052612	76,395564
2020-05-22 04:40:00	7,041450	76,425406
2020-05-22 04:50:00	7,030998	76,454078
2020-05-22 05:00:00	7,020308	76,483448
2020-05-22 05:10:00	7,009499	76,513218
2020-05-22 05:20:00	6,598878	76,541891
2020-05-22 05:30:00	6,587945	76,570984
2020-05-22 05:40:00	6,576370	77,000341
2020-05-22 05:50:00	6,564854	77,028670
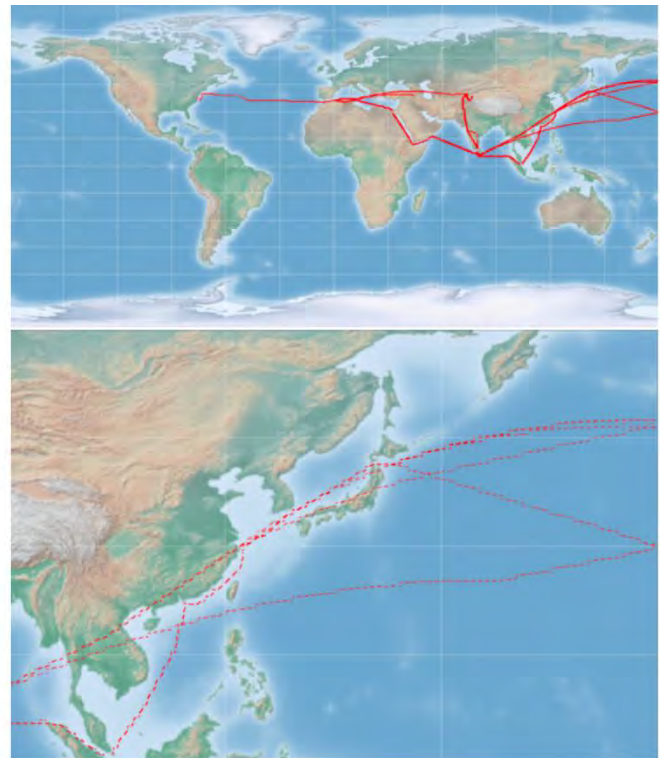
Fig.4: Vessel with "zig-zag issue" on stored position data. Data table (left) indicating the "jumps" in red color. Map and zoomed detail (right)

- <u>Scatter issue:</u> It refers to when there are plenty of random iterations of either longitude or latitude scattered around the globe away from the regular vessel's trajectory. Fig.5 illustrates the registered trajectory of the vessel with "scatter issue". Source "N/E issue" is again visible in this vessel's trajectory. The issue is present in vessel classes where Partner #2 CAMS system is installed.

146

Fig.5: Registered trajectory of a vessel with "scatter issue"

Fig.6: Registered trajectory of a vessel with "drift issue"

- Drift issue: It refers to when parts of the vessel's trajectory are shifted a few degrees towards either East/West or North/South affecting both longitude and latitude values. Fig.6 illustrates the registered trajectory of the vessel with "drift issue". Source "N/E issue" is again on top, given that the vessels are using the same CAMS system. The issue is present again in classes where Partner #2 CAMS system is installed.

- Frozen issue: It refers to when either longitude or latitude values are frozen to 0 degrees. Fig.7 illustrates the registered trajectory of the vessel with "frozen issue". The issue is present in classes where Partner #4 CAMS system is installed.

- Bit-rate issue: Besides the visible issues that were described and showed on the above maps, Partners #1, #4 and #5 experience the bit-rate conversion degradation on the position data as shown in Fig.1. Given that this is an issue which should also be solved, we sum up 6 issues in total.

Fig.7: Registered trajectory of a vessel with "frozen issue"

In the next subsection, we introduce the indicators built to identify faulty position measurements in the whole dataset.

3.3. Validation Indicators

We know from *Gakstatter (2015)* that SOG (Speed Over Ground) is included in the NMEA sentence which means that the SOG is computed using internal estimation processes by the navigation devices. We also know that AIS and CAMS systems record values of SOG from -10 to 50 knots (with 99.9% of our dataset being positive values). On top of that, SOG is registered with a single decimal point which makes it less vulnerable to accidental measurement degradation (averaging, bit-rate conversion, etc.). Taking into account the previous statements and due to speed's physical relationship with position, SOG makes an ideal measurement for comparison purposes. Thus, if we compute the distance a vessel has traveled between consecutive data logging/transmission (10 minutes between one another) with two different methodologies (one using the position measurements and one using the SOG) the two outputs should theoretically match. Based on that we use the following distance deviation indicators to validate our assumption.

$$D^c = d_p^c - d_s^c \qquad (1)$$
$$D^a = d_p^a - d_s^a \qquad (2)$$

Eqs.(1) and (2) describe how the distance deviation indicators D^c and D^a are composed. The super-scripts $\{c\}$ and $\{a\}$ stand for CAMS and AIS, respectively. On the right part of the equations, the sub-scripts $\{p\}$ and $\{s\}$ denote the two distance calculation methodologies using position measurements and SOG, respectively. In short, in Eq.(1) we use CAMS data to compute the distance deviation D^c which is calculated by subtracting the distance between consecutive coordinates using the SOG methodology d_s^c from the same distance using the position measurements methodology d_p^c. In Eq.(2) we have the same computation, but by using the AIS data.

For the position measurement methodology, the shortest route between two points on a sphere is along an arc of a great circle. A great circle is a circle drawn on the surface of the sphere, centered on the same point as the sphere and having the same radius. An example is the equator of the Earth. Two points P and Q divide the great circle they lie on into two arcs. The shorter of these arcs gives the shortest path between the two points. Fig.8 depicts the distance between P and Q in red color.
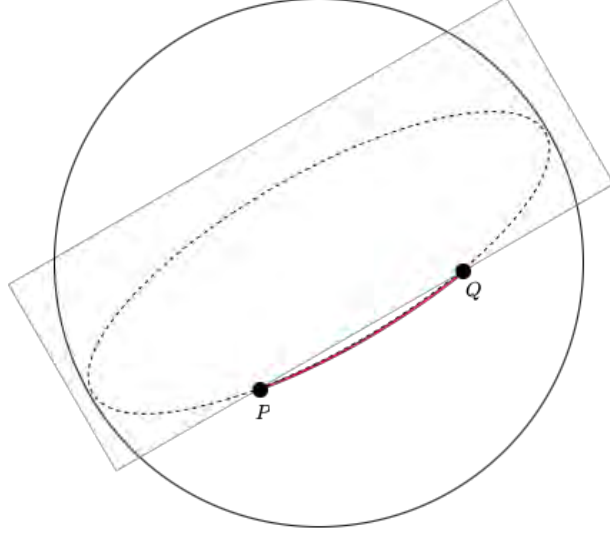
Fig.8: Arc denoting the path from point P to point Q on great circle

P and Q are points with latitudes ϕ_1 and ϕ_2 and longitudes λ_1 and λ_2, such that $P = (\phi_1, \lambda_1)$ and $Q = (\phi_2, \lambda_2)$. Given the earth's radius, the distances d_p^c and d_p^a can be computed using the following Eq.(3).

$$\text{haversin}\left(\frac{d_p}{R}\right) = \text{haversin}(\phi_2 - \phi_1) + \cos\phi_1\cos\phi_2 \text{ haversin } (\lambda_2 - \lambda_1) \qquad (3)$$

where haversine is defined by

$$\text{haversin}(y) = \sin^2\left(\frac{y}{2}\right) \qquad (4)$$

For the SOG methodology, the travelled distance is computed as the integral of the SOG within the time period of 10 minutes. At this point, we should clear out a few assumptions before we move on.

Assumption 1: The vessels are equipped with an AIS Class A receiver providing asynchronous measurements of vessel position (ϕ, λ), SOG U and COG ψ. The position measurement in the North and East directions is affected by zero mean white Gaussian noise with variance σ_p^2, i.e. $w_\phi \sim \mathcal{N}(0, \sigma_p^2)$ and $w_\lambda \sim \mathcal{N}(0, \sigma_p^2)$. The SOG measurement is affected by zero mean white Gaussian noise with variance σ_s^2, i.e. $w_U \sim \mathcal{N}(0, \sigma_s^2)$. The COG measurement is affected by zero mean white Gaussian noise with variance σ_c^2, i.e. $w_\psi \sim \mathcal{N}(0, \sigma_c^2)$. It is further assumed that the noise sources w_ϕ, w_λ, w_U and w_ψ are uncorrelated among each other.

Assumption 2: Earth is a perfect sphere with radius $R = 6378.2$km.

After having introduced that both D^c and D^a are the main indicators of this study, there is a third one utilized as a safety indicator. That is d_p^b denoting the distance between AIS and CAMS coordinates. The subscript $\{p\}$ indicates the position measurement methodology and the superscript $\{b\}$ stands for "between".

Figs.9 and 10 show the IQRs of both D^c and D^a indicators categorized by encoded ship names V_{imo} and classes V_{class}. Each of the 228 boxes represent the IQR of either D^c and D^a of each ship of the dataset. The boxes are categorized by ship class showing in different color. The grey dots represent data outliers for values outside 99.3% of the distribution. Fig.11 represents the CAMS dataset.
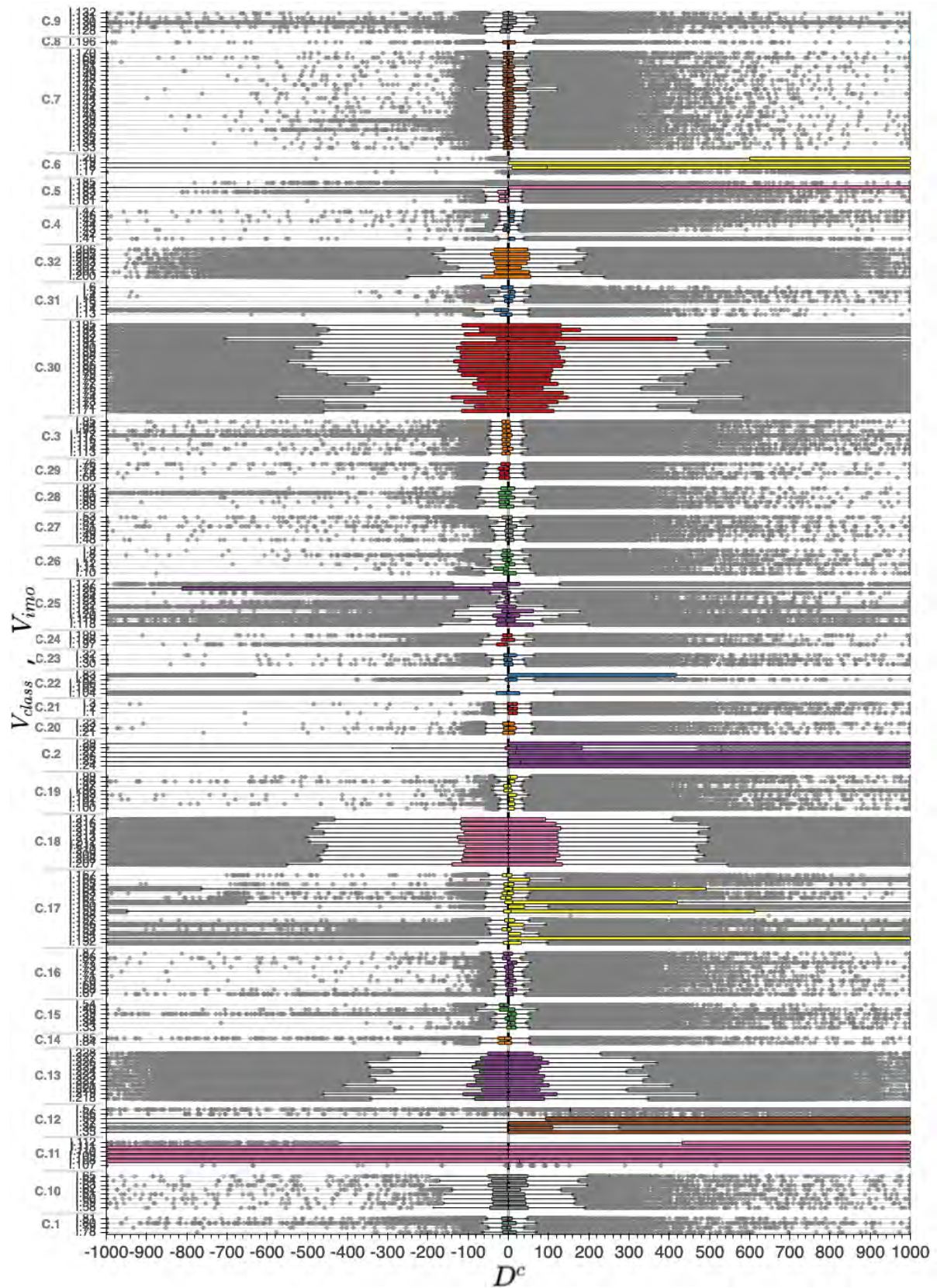
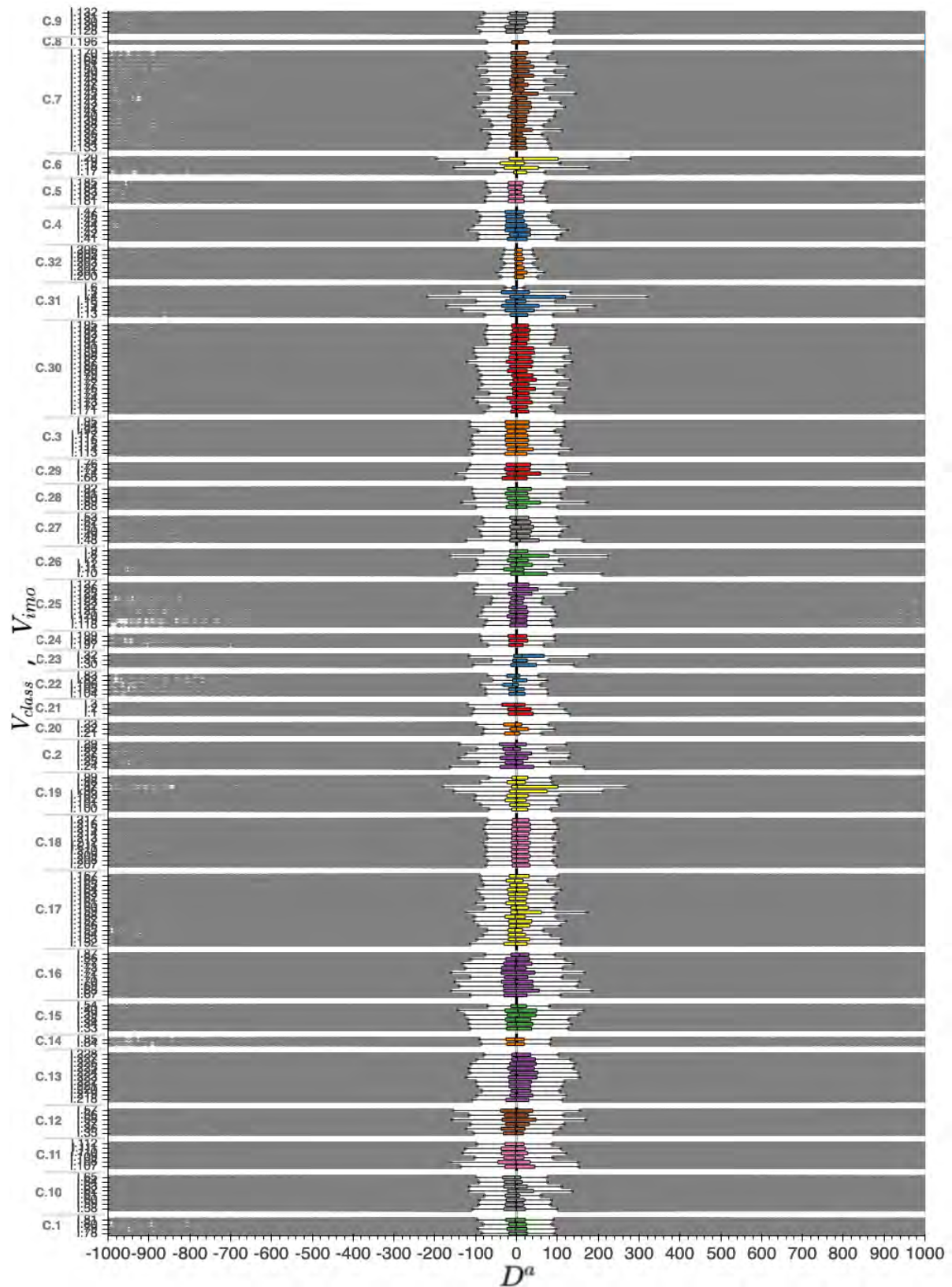Fig.9: CAMS distance deviation D^c per vessel, categorized by class

Fig.10: AIS distance deviation D^a per vessel, categorized by class

Starting from Fig.9 and having in mind the above remarks, it is evident from the boxplots of classes such as C.7, C.3, C.16 which have ships with very narrow boxplots and with mean values close to 0, that these are the ships with good quality position CAMS measurements on the data base. Classes like C.32, C.30, C.19, C.13 and C.10 with medium size boxplots close to the 300 m threshold (ref. Remark 2) are questionable and need further investigation. Finally, position measurements from classes like C.6, C.2, C.17 (only a few ships), C.12 and C.11 are clearly problematic and need replacement. In Fig.10 it is a fact that there are no big issues in the AIS dataset. Unfortunately, this does not mean that we can blindly replace the faulty CAMS measurements with AIS mainly due to the fact that the data logging in AIS is not registered in even time intervals like in CAMS.

To sum up and create an overview of how the CAMS vs. AIS measurements look like on the dataset of this study, the requirements for a ship's position measurements to be of good quality are the following:

Remark 1: The mean value of $D^{c,a}$ distribution should be close to 0 m with small variance.

Remark 2: Based on internal company research and considering the results from the boxplots in Figs.9 and 10, we decided that the IQR (interquartile range) of the $D^{c,a}$ of each ship should not exceed 300 m, given that IQR represents the 50% of the distribution.

4. Methodology

4.2. Position measurements conversion models

Geodetic position coordinates are measured in degrees. As previously mentioned, degrees close to the equator are longer in meters than those close to the poles. That makes any potential usage of the degree unit problematic for various reasons. In order to avoid plausible errors, the geodetic coordinates (ϕ, λ) must be converted into geocentric (Cartesian) coordinates (X, Y) and then after any modification they are turned back to geodetic again. Before showing the methodology, it is important to start with notation.

a, b, e = semi-major axis, semi-minor axis, eccentricity of reference ellipsoid
X, Y, Z = Cartesian geocentric coordinates
λ, φ, h = geodetic longitude, geodetic latitude, geodetic height

The coordinate transformation from geocentric to geodetic is given by, *Vermeille (2002)*

$$\begin{aligned} X &= (h + n)\cos\varphi\cos\lambda \\ Y &= (h + n)\cos\varphi\sin\lambda \\ Z &= (h + n - e^2 n)\sin\varphi \end{aligned} \tag{5}$$

where:

$$n = \frac{a}{\sqrt{1 - e^2\sin^2\varphi}} \tag{6}$$

To transform back geocentric coordinates to geodetic coordinates, given that (X, Y, Z) is known, first we should compute the value of k and D by the following sequence of formulae:

$$p = \frac{X^2 + Y^2}{a^2}$$

$$q = \frac{1 - e^2}{a^2}Z^2$$

$$r = \frac{p + q - e^4}{6}$$

$$s = e^4\frac{pq}{4r^3}$$

$$t = \sqrt[3]{1 + s + \sqrt{s(2 + s)}} \tag{7}$$

$$u = r\left(1 + t + \frac{1}{t}\right)$$

$$v = \sqrt{u^2 + e^4q}$$

$$w = e^2\frac{u + v - q}{2v}$$

$$k = \sqrt{u + v + w^2} - w$$

$$D = \frac{k\sqrt{X^2 + Y^2}}{k + e^2}$$

Next, we compute the geodetic coordinates λ, ϕ and h by:

$$\lambda = 2\arctan\frac{Y}{X + \sqrt{X^2 + Y^2}}$$

$$\varphi = 2\arctan\frac{Z}{D + \sqrt{D^2 + Z^2}} \tag{8}$$

$$h = \frac{k + e^2 - 1}{k}\sqrt{D^2 + Z^2}$$

The computations in this paper were carried out with $a = 6378137$ m and $e = 0.081819191$.

4.3. Interpolation Methodology

We called this algorithm the interpolation methodology because it underlines the main function used to replace the missing vessel trajectories. The scope here is to make a versatile and customizable algorithm which will provide a robust solution with a potential to scale up in the future. Additionally, it should be possible to run in batch, meaning on datasets with multiple ships of similar characteristics. The algorithm starts by creating a vessel subset from each dataset, one for CAMS such that $vsl^c \subseteq CAMS$ and one for AIS such that $vsl^a \subseteq AIS$. Focusing on vsl^a the algorithm starts by converting the geodetic-to-geocentric coordinates as described in subsection 4.1. Next, it creates a feature which is the time difference in hours between consecutive timestamps of the vsl^a subset. This feature combined with a minimum threshold of 10 h is used in the next step, where vsl^a is dynamically split into sub-segments. The split functionality is applied in order to avoid interpolation when the time distance between consecutive available AIS measurements is greater than 10 h. In such cases, this trajectory gap is left uncorrected in order to avoid interpolation over land. Fig.11 illustrates an example. The threshold's number has been chosen after a series of tests for optimal algorithm performance. A smaller number creates a lot of splits of short scaled sub-segments resulting to a greater amount of missing values. This step can be further improved by invoking a physical system that uses the course over ground to approximate the location in such long gaps.
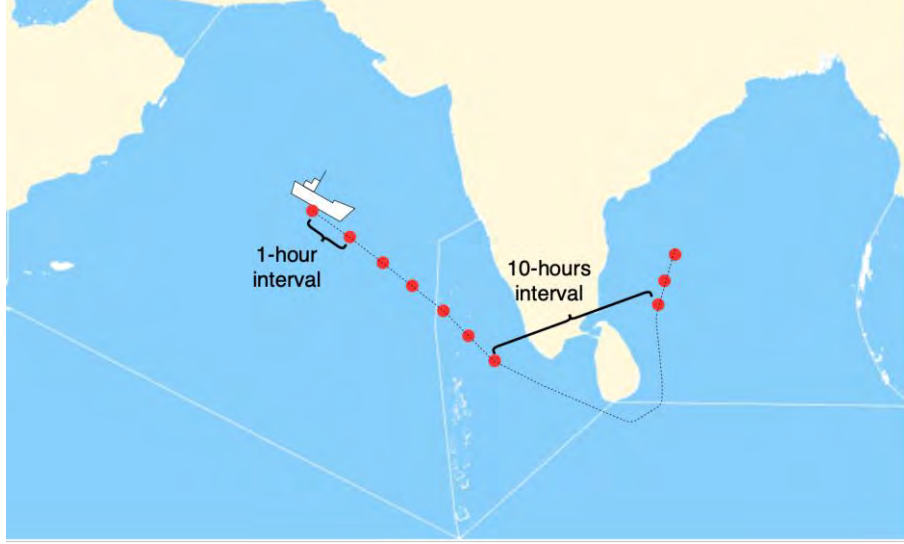
Fig.11: Example of AIS coordinates with a gap ≥10 h on the measurements. Red dots indicate the measurements and the black dashed line is considered to be the real trajectory of the vessel.

After the split is over, each sub-segment is initially up-sampled to a 10-minute interval frequency similar to that of vsl^c and then linearly interpolated using the deterministic methodology of polynomial interpolation for time-series data described by, *Lepot et al. (2017)*. Then all sub-segments have been concatenated to form a vessel's dataset where the reverse procedure of geocentric-to-geodetic has been applied as described in subsection 4.1. Last step before creating the validation indicators D^c, D^a and the safety indicator d_p^b was to merge vsl^c with vsl_{new}^a. Algorithm 1 sums up the methodology step-by-step as described above including the rule for defining which of the two (AIS or CAMS) coordinates are the more accurate for the current vessel. For easier interpretation, Fig.12 illustrates the algorithm up to the point where the rule is applied in line 21.

Apart from the two remarks from subsection 3.2 which have defined an initial step on how to validate the position measurements of a vessel, we have also created a simple rule based on a series of trials and errors:

$$P(\phi, \lambda) = \begin{cases} CAMS, & \tilde{d}_p^b < 1000m \quad \& \quad IQR(D^a) > IQR(D^c) \\ AIS, & \left(\tilde{d}_p^b < 1000m \quad \& \quad IQR(D^a) \leq IQR(D^c)\right) \quad \| \quad \left(\tilde{d}_p^b \geq 1000m\right) \end{cases} \tag{9}$$

The rule is generally sufficient to produce good results. In short, the equation clarifies that the final position measurement of the historical dataset of one vessel can be drawn directly from the CAMS dataset if $\tilde{d}_p^b < 1000$ m and $IQR(D^a) > IQR(D^c)$. In the contrary, when $\tilde{d}_p^b < 1000$ m and $IQR(D^a) \leq IQR(D^c)$ or $\tilde{d}_p^b \geq 1000$ m then the final dataset encloses position measurement processed in even time intervals derived from the interpolation.

154

Algorithm 1: Interpolation methodology algorithm

input : Two datasets, one with CAMS and one with AIS positioning measurements both including data from 228 container vessels

output: One dataset with both CAMS and AIS-corrected positioning measurements including D^c, D^a and d_p^b validation indicators

1 foreach *vessel in CAMS* **do**
2 $vsl^c \subseteq$ CAMS
3 $vsl^a \subseteq$ AIS
4   GeodeticToGeocentric(vsl^a)
5   diff $\leftarrow$ MeasureTimeDiff(vsl^a)
6 $vsl_{lst}^a \leftarrow [vsl_1^a, vsl_2^a, \dots, vsl_n^a], \quad n \in \mathbb{Z}^+$
7   **foreach** vsl_j^a *in* vsl_{lst}^a *where* $j \in \mathbb{Z}^+$ **do**
8   UpSample(vsl_j^a)
9   LinearInterpolation (vsl_j^a)
10 $vsl_{new}^a \leftarrow$ Concatenate (vsl_{lst}^a)
11   **end**
12   GeocentricToGeodetic(vsl_{new}^a)
13 $vsl^{c,a} \leftarrow vsl^c \bowtie vsl_{new}^a$
14 $d_p^c \leftarrow$ GreatCircleMethodology($vsl^{c,a}$)
15 $d_p^a \leftarrow$ GreatCircleMethodology($vsl^{c,a}$)
16 $d_s^c \leftarrow$ DifferentialSOGMethodology($vsl^{c,a}$)
17 $d_s^c \leftarrow$ DifferentialSOGMethodology($vsl^{c,a}$)
18 $D^c \leftarrow d_p^c - d_s^c$
19 $D^a \leftarrow d_p^a - d_s^a$
20 $d_p^b \leftarrow$ GreatCircleMethodology($vsl^{c,a}$)
21   **if** $\tilde{d}_p^b < 1000m$ *and* IQR(D^a)$>$ IQR(D^c) **then**
22   prefer CAMS over AIS positioning measurements
23   **else if** $\tilde{d}_p^b < 1000m$ *and* IQR(D^a)$<$ IQR(D^c) **then**
24   prefer AIS over CAMS positioning measurements
25   **else if** $\tilde{d}_p^b > 1000m$ **then**
26   prefer AIS over CAMS positioning measurements
27   **end**
28 end
---

5. Results

Overall, the interpolation methodology obtained sufficiently good results. According to Algorithm 1's output, 18.4% of the fleet on the examined dataset of 228 vessels have been identified as faulty. This accounts for 19.2% of the dataset's total position measurements. The slight percentage difference occurs due to the variation in the number of measurement points from the different vessels. Some of them contribute with a few days of data while others contribute with as much as up to 36 months.

To get a better look we start from the vessel with the most degrading sources combined, as mentioned in sub-section 3.1. In Fig.6 we examined the "drift issue". That specific ship apart from drifting it was also zig-zaging and losing the values where either longitude or latitude were negative ("N/E issue"). Not to mention the frozen coordinates where the equator crosses the prime meridian (0,0) right below Nigeria in Africa. The output of Algorithm 1's output, for this vessel can be seen in yellow-colored points of Fig.13. In this case, the rule from equation (9) decided to pick AIS even-spaced estimates over CAMS.
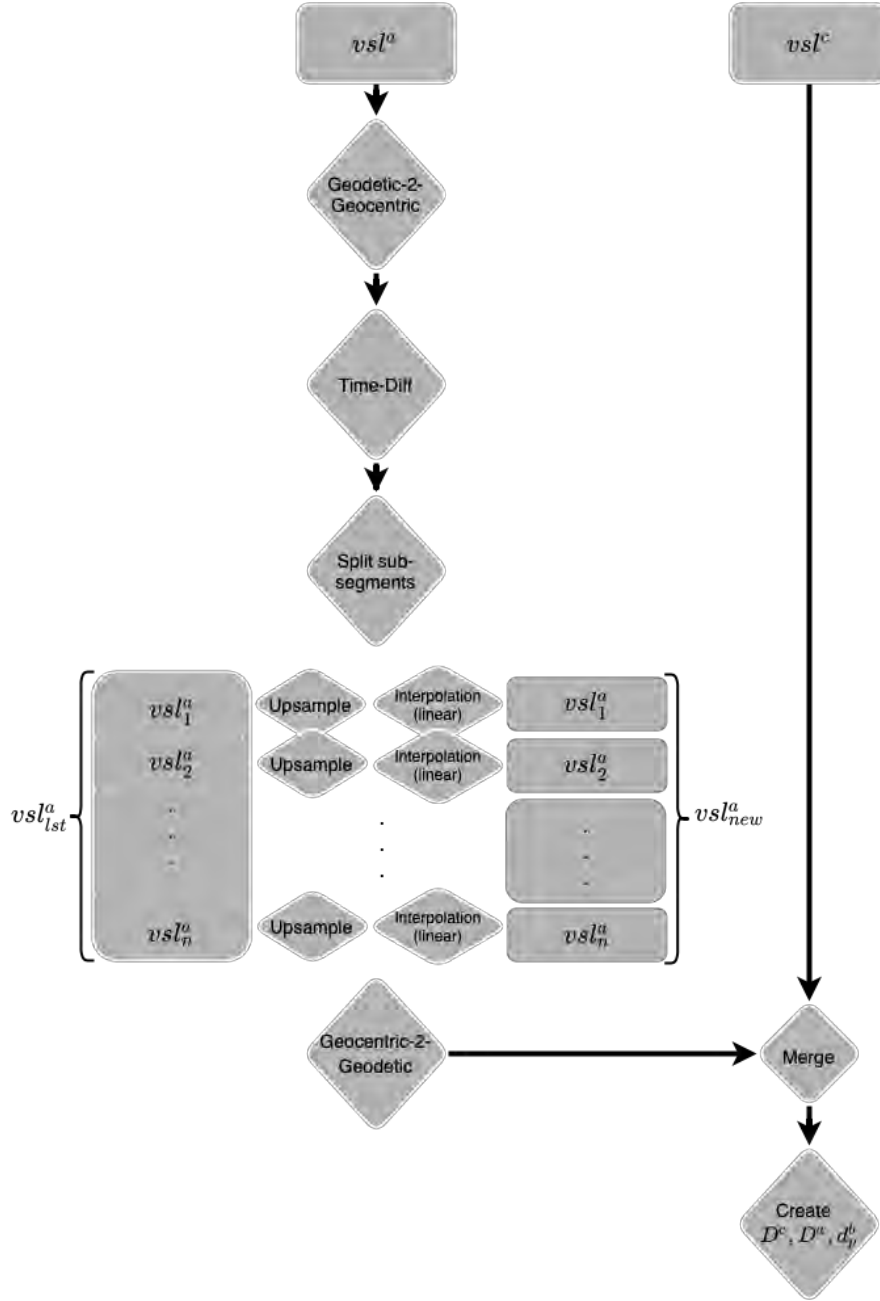
Fig.12: Flow chart of the interpolation methodology

With a glimpse at the map of Fig.13, it is clear that the yellow points eliminate all degrading sources mentioned for that vessel. Here, we should note that the pure AIS coordinates as sourced from the external provider were missing by 64% when they merged with the CAMS dataset vsl^c. The interpolation methodology decreased the missing value percentage to $< 0.1\%$.

In the next examined ship, Algorithm 1 chose CAMS over even-spaced AIS estimates when deciding on the best quality coordinates. In fact, if we compare the boxplots (referring to each ship's D^c and D^a IQRs) from Figs.9 and 10 of vessel I.48 in class C.27, D^c's boxplot is narrower than that of D^a which confirms the second scale of the rule in Eq.(9).

Fig.13: Trajectory of vessel I.36 from class C.12. Red points refer to the CAMS registered coordinates and yellow refer to even-spaced AIS estimates of the interpolation methodology.

In Fig.14 we have the vessel's trajectory both in CAMS and in AIS even-spaced estimates. Note that in the AIS even-spaced coordinates, the effect of land interpolants mentioned in Fig.11 is visible when the vessel is crossing the Gulf of Oman, despite the minimum threshold splitting of 10 h. In this case, the time difference was smaller than 10 h. Luckily for this case, CAMS measurements were chosen over AIS estimates.

Fig.14: Trajectory of vessel I.48 from class C.27. Red points refer to the CAMS registered coordinates and yellow refer to even-spaced AIS estimates of the interpolation methodology.

In line with the acquired knowledge from applying alternative algorithms (Linear/Non-linear Kalman Filter) during the process of building the interpolation methodology, it can be concluded that if we create a hybrid model invoking a state-space model into the interpolation methodology it will bring optimal results in historical data validation and correction. Additionally, it will form the fundamentals to build a real-time model that can validate and correct position measurements right before the data has been recorded into the ship's database. In the next sub-sections, two vessels were chosen to evaluate the results of the methodology.

157

6. Summary and Conclusions

This paper has been conducted to tackle the a posteriori data loss/modification of position measurements which refers to the posterior modification/loss of the position data after the signal has successfully arrived at the GNSS receiver.

We categorized the faulty measurements into 6 groups; (i) the "N/E issue", (ii) the "zig-zag issue", (iii) the "scatter issue", (iv) the "drift issue", (v) the "frozen issue" and finally (vi) the "bit-rate issue". Some groups are visible in ships with different CAMS installed where others are only visible in CAMS from specific providers.

Further, we created 3 validation indicators with which someone can identify if a ship carries faulty measurements in a specified time range. These validators are designed to be used in batch processing and not in individual data points.

Lastly, we have proposed an algorithm/methodology for correcting the faulty measurements by reversing to the raw state right in the beginning of their path from the GNSS receiver to the company's data center. The methodology used interpolation as its main ingredient. According to the evaluation of the methodology, it achieved sufficiently good results mainly due to its highly customizable algorithm.

6.2. Future Work

Various processes can be improved to achieve better results. The main proposal is to use a hybrid methodology which will combine both interpolation and a state-space model into it. More specifically:

- In cases where there is more than 10 h gap between consecutive AIS coordinates, the interpolation methodology leaves the trajectory gap uncorrected. This can be improved by invoking a physical system that uses the COG to approximate the location in such long gaps.
- We could extend the validation in per-month or per-day state. Right now, the validation refers to the IQR of the data from the whole time that the ship has operated. Apparently, this is not a fair judgement because many CAMS systems have been fixed and after that they register good quality data. Unfortunately, the proposed validators are built for batch corrections and not for individual data points.
- We could use a state-space model directly into the CAMS position measurements in real-time. Unfortunately, for the time being, both COG and compass true heading measurements from CAMS are missing most of the times (72% and 28%, respectively). Additionally, some ships have frozen or faulty position measurements for long periods of time - say up to 6 months. So the use of AIS data is unavoidable, if those problems are not solved.
- We could develop a data-driven/automatic identification of when a signal falls into one of the 6 identified categories. Subsequently, the correction algorithm could then use this information (e.g. with an identified frozen signal in CAMS, we can use AIS measurements to initiate a state-space model until CAMS gets unfrozen).

References

AKOS, D.M. (2012), *Who's Afraid of the Spoofer? GPS/GNSS Spoofing Detection via Automatic Gain Control (AGC),* J. Institute of Navigation 59(4), pp.281-90

BROUMANDAN, A.; JAFARNIA-JAHROMI, A.; DEHGHANIAN, V.; NIELSEN, J.; LACHAPELLE, G. (2012), *GNSS Spoofing Detection in Handheld Receivers Based on Signal Spatial Correlation,* IEEE/ION Proc. PLANS, pp.479-487

CHANG, L.; NIU, X.; LIU, T. (2020), *GNSS/IMU/ODO/Lidar-Slam Integrated Navigation System Using IMU/ODO Pre-Integration,* Sensors 20(17), p.4702

FUKUDA, G.; HATTA, D.; GUO, X.L.; KUBO, N. (2021), *Performance Evaluation of IMU and DVL Integration in Marine Navigation,* Sensors 21(4), p.1056

GAKSTATTER, E. (2015) *What Exactly Is GPS NMEA Data?,* GPS World, https://www.gpsworld.com/what-exactly-is-gps-nmea-data/

GAO, G.X.; SGAMMINI, M.; LU, M.Q.; KUBO, N. (2016), *Protecting GNSS Receivers from Jamming and Interference,* Proc. IEEE 104(6), pp.1327-1338

HEUKELMAN, C. (2018), *About UGPS Vs GNSS - What Engineers Need to Know for Their Designs,* Semiconductor Store, https://www.semiconductorstore.com/blog/2018/GPS-vs-GNSS-What-Engineers-Need-To-Know-For-Their-Design-Symmetry-Blog/3083

HU, S.P.; FANG, Q.G. ; XIA, H.B. ; XI, Y.T. (2007), *Formal Safety Assessment Based on Relative Risks Model in Ship Navigation,* Reliability Engineering & System Safety 92(3): 369-377

ITU (2014), *M.1371: Technical Characteristics for an Automatic Identification System Using Time-Division Multiple Access in the Vhf Maritime Mobile Band*, International Telecommunication Union, https://www.itu.int/dms_pubrec/itu-r/rec/m/R-REC-M.1371-5-201402-I!!PDF-E.pdf

JOHANSEN, T.A.; FOSSEN, T.I. (2016), *The Exogenous Kalman Filter (XKF),* Int. J. Control 90(2), pp.161-167

LEPOT, M.; AUBIN, J.B.; CLEMENS, F.H. (2017), *Interpolation in Time Series: An Introductive Overview of Existing Methods, Their Performance Criteria and Uncertainty Assessment,* Water 9(10), pp.796

LIANG, M.H.; LIU, R.W.; ZHONG, Q.R.; LIU, J.X. (2019), *Neural Network-Based Automatic Reconstruction of Missing Vessel Trajectory Data*, IEEE Int. Conf. Big Data Analysis, pp.426-430

MEDINA, D.; LASS, C.; PEREZ MARCOS, E.; ZIEBOLD, R.; CLOSAS, P.; GARCIA, J. (2019), *On GNSS Jamming Threat from the Maritime Navigation Perspective,* 22nd IEEE Int. Conf. Information Fusion, pp.1-7

MORONG, T.; PURIČER, P.; KOVÁŘ, P. (2019), *Study of the GNSS Jamming in Real Environment,* Int. J. Electronics and Telecommunications 65(1), pp.65-70

NMEA (2021), *NMEA-0183 Standard,* National Marine Electronics Association, https://www.nmea.org/content/STANDARDS/NMEA_0183_Standard

NÚÑEZ, J.M.; ARAÚJO, M.G.; GARCIA-TUÑÓN, I. (2017), *Real-Time Telemetry System for Monitoring Motion of Ships Based on Inertial Sensors,* Sensors 17(5), p.948

PERERA, L.; GUEDES SOARES, C. (2017), *Weather Routing and Safe Ship Handling in the Future of Shipping,* Ocean Eng. 130, pp.684-695

PSIAKI, M.L.; HUMPHREYS, T.E. (2016), *GNSS Spoofing and Detection,* Proc. IEEE 104(6), pp.1258-1270

RYU, J.H.; GANKHUYAG, G.; CHONG, K.T. (2016), *Navigation System Heading and Position Accuracy Improvement Through GPS and INS Data Fusion,* J. Sensors

SCHMIDT, D.; RADKE, K.; SEYIT, C.; ERNEST, F.; REN, M. (2016), *A Survey and Analysis of the GNSS Spoofing Threat and Countermeasures,* ACM Computing Surveys (CSUR) 48(4), pp.1-31

VENEZIA, M. (2015), *What Is the Difference Between GNSS and GPS?,* Semiconductor Store, https://www.semiconductorstore.com/blog/2015/What-is-the-Difference-Between-GNSS-and-GPS/1550

VERMEILLE, H. (2002), *Direct Transformation from Geocentric Coordinates to Geodetic Coordinates,* J. Geodesy 76(8), pp.451-454

Improving True Lies –
Creating Sophisticated Baselines out of Woefully Little

Richard Marioth, Idealship, Itzehoe/Germany, rm@idealship.de
Piyush Raj, AlphaOri, Singapore, piyush@alphaori.sg

Abstract

The draught & speed band of a sea trial is often so narrow, that only small fragments of the vessel's operation can be compared to it. Still, it has become common practice by Vessel Performance Analysts to say: "We use sea trials as our baselines." A true lie, as extensive extrapolation of the baselines is required to cover the actual vessel operation band. Many approaches use only Naval Architecture principles or pure data science for the baseline creation. This paper describes a hybrid approach.

1. Introduction

1.1. The need for a baseline and the available data

When one wants to analyse hull & propeller performance developments over time one needs a baseline. A model where the measured operation is held against, which stands for the expected performance. The difference between the expected performance and the observed performance is described through a performance indicator, such as the percentage Speed Loss, *ISO (2016)*, Power Percentage, Added Resistance or similar.

It is beneficial, when the reference model is available as soon as a vessel starts to feed operational data into an analytics system as the ship operator can directly see, where the vessel is compared to her reference and take actions accordingly. Most important is however that the model describes the hull & propeller performance accurately.

The one and predominantly only set of curves describing vessels propulsion performance a ship operator has available right away is the speed test of the sea trial. Every vessel that is built needs to prove that her propulsion performance is as good as it was stated in the building contract. For this purpose and to understand the power/speed/rpm relations the yard conducts a speed trial, where the vessel is tested at one or several main engine loads. A sea trial gives typically 2 to 5 measurements at the time when the vessel was built.

Usually, one loading condition is tested and a calibration factor between the model basin curve and the measured and corrected Speed & Consumption values is determined. In case more than one speed power curve was given by the model basin the percentage difference is used to calibrate the curves. In this way the vessels design speed point, so the contract design speed and propulsion power at design draught, can be proven regardless of the sea trial draught condition.

Speed Test diagrams often show 3 curves (Ballast, Design and Scantling condition), but not always. We analysed available information from a sample of 100 sea trial (Speed Trial) documents. Fig.1 shows how many different sailing conditions were given in the documents. Little less than half of them had three separate curves (Ballast, Design and Scantling). Many documents had only one curve available, that is woefully little data to develop an accurate model. This study describes how additional data was used to improve the situation substantially.
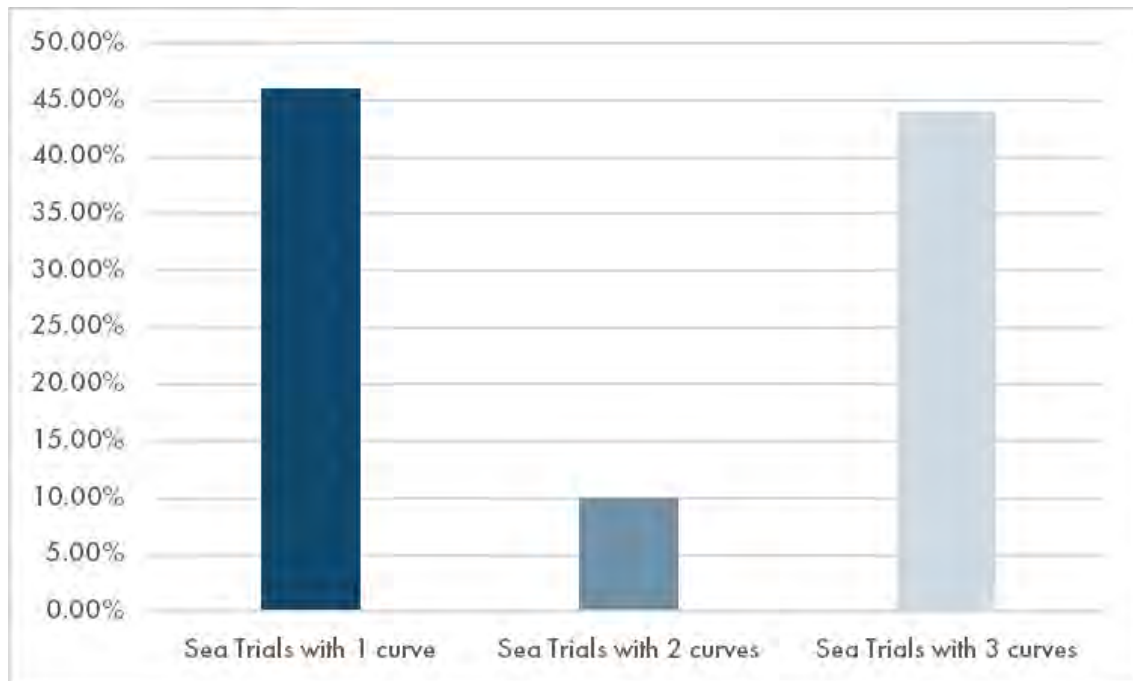
Fig.1: Available information at a sample of 100 sea trial documents

1.2. Modelling options

By definition, a model is an estimate of the reality. Besides the above-mentioned speed tests, there are several ways how one can obtain a speed-power model. The methods differ with the type of information that is used, and the resources needed to create it. Typical approaches are:

a. Model only based on Speed Test (Sea Trial):
Such approaches use the Speed Test measurements to create a model. The main advantage is that this can be done quickly, and the modelled curves of the given draughts are close to the optimum performance of the vessel, as the hull and propeller(s) were most likely in a good shape back when the Sea Trial was conducted. The main disadvantage is that the range of the sea trial measurements is often very narrow, so that one can only analyse a small band of data. More details to this modelling approach can be found in chapter 2.1.

b. Models based on the measured values
Such approaches are mostly used when one receives sufficient information from the vessel, i.e. high-frequency data. Using suitable filters, advanced data analytics and appropriate mathematical fitting models, this method can provide good estimates. The main advantage is that the modelled performance will reflect current performance of the vessel fairly well. The main disadvantage is that one needs to collect sufficient data before one can achieve this. Further details about this modelling approach are given in chapter 2.2.

c. Model based on computation of fluid dynamics (CFD)
Numerical simulations on a 3D hull shape of the vessel are used to compute the resistance. The main advantage of this methodology is that one can determine the hull performance in any sailing condition. The model is wider as off-design conditions and different trims can be simulated, *Krapp and Bertram (2016)*. The disadvantage is that creating a proper hull shape and studying its hydrodynamics via CFD can be labour intensive. It pays off well for trim studies of large container vessels, which are using a lot of fuel, but not necessarily for smaller vessels. Finally, using CFD technics correctly, one can get very good reference models for vessels, but the quality of results seems to depend significantly on the chosen CFD experts and service provider, *Tsarsitalidis and Rossopoulos (2018)*.

d. <u>Models based on extensive tests within the model basins</u>
These models require larger investments when the vessel is built. The model basin supplies their prognosis for additional off-design and low-speed conditions. In this way one obtains a model covering most common sailing conditions. The advantage is a more reliable model, though the quality of scaling factors in off-design conditions might be a challenge. The disadvantage is the high costs of the towing tank time.

Fig.2 qualitatively compares the modelling approaches. The modelling approaches are assumed to be working well (green bullets) and having challenges (yellow/orange bullets) in different fields.

	Accuracy	Coverage	Availability at System entry	Show optimum Performance	Costs
A. Models based on Sea Trials	🟡	🟠	🟢	🟢	🟢
B. Models based on measurements	🟢	🟢	🔴	🟠	🟢
C. Models based on CFD	🟢	🟢	🟢	🟡	🟠
D. Models based on Towing Tank	🟢	🟢	🟢	🟢	🔴

Fig.2: Comparison of modelling approaches

Within this study, CFD based or towing tank-based approaches are not analysed further. Reasons are required effort and (limited) available vessel design data in our applications. An approach was chosen, that uses the little data that exists upon system entry and uses it in the starting phase until sufficient high-frequency data is available to verify and correct the model. Fig.3 shows a qualitative judgement of the developed hybrid approach.

	Accuracy	Coverage	Availability at System entry	Show optimum Performance	Costs
E. Hybrid Approach (A & B)	🟢	🟢	🟢	🟢	🟢

Fig.3: Hybrid modelling approach

In the following section, an example method of model creation is described when models are created only based on Speed Test or only based on the measured values.

2. Typical power model creation

2.1. Power models based on Sea Trials

Many service providers for hull performance analytics state that they are creating their speed-consumption models based on the available sea trial information. Then only through interpolations and extrapolation a model covering the whole operation profile of the vessel can be created. Fig.4 shows how this may work, when the sea trial curves cover a wide speed range and Ballast, Design and scantling curves are given.

The approaches can give somewhat useful models when sufficient information is available within the sea trial documents and the vessels are predominantly sailing in Ballast or Scantling conditions. The methods may use linear interpolation or the admiralty formula between the draughts and polynomial extrapolation methods for speeds. For container vessels, this can lead to particularly inaccurate models, *Krapp and Bertram (2016)*. The method fails even more, when the available information is too limited (e.g. only 1 curve given). Using linear or polynomial methods to extrapolate more than 90% of the vessel operation only through a small set of known data will likely lead to very inaccurate models.
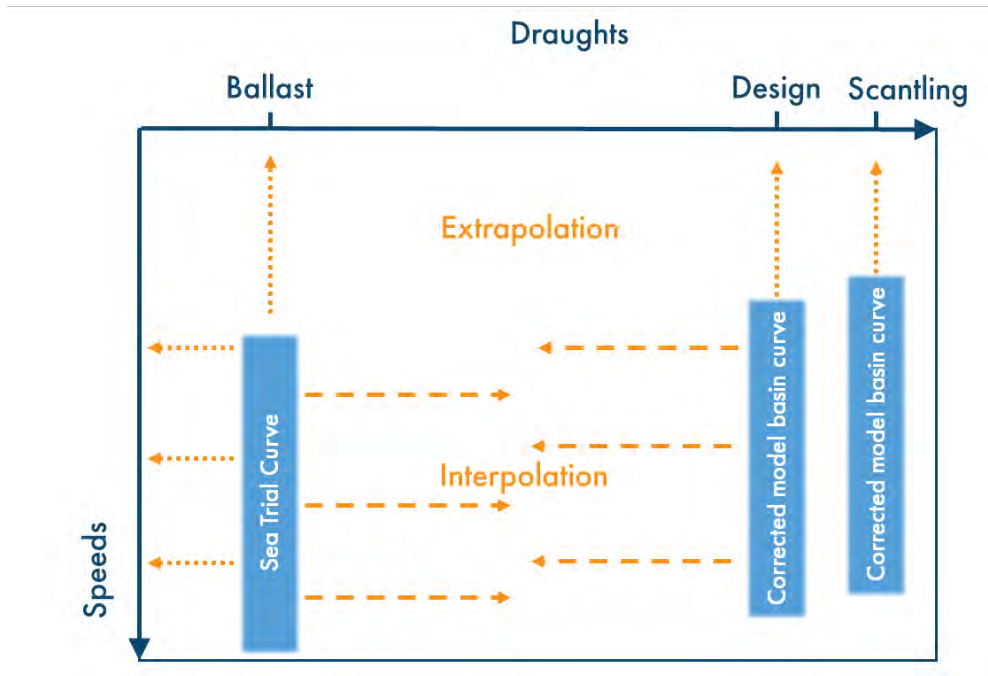
Fig.4: Interpolation/Extrapolation of model curves Speed Trial (3 curves)

2.2. Power models based on mathematical methods

Mathematical curve fitting approaches that create a best fit curve based on the measured speed-power data have become more popular over the last decade. The quality of these models is sufficient when high-frequency data is used, which is collected by data loggers and is combined with weather data, available from third party or obtained from vessels.

The high-frequency data usually includes information on other parameters such as location, GPS speed, telegraph position, RPM, anemometer data, etc. They can be used to include several layers of validation and filtering. The filters help in removing noise, such as variations due to wind speed. Some data logging systems also have wave and current information recorded which can help in improving the filtration scheme. If such data is not available, then hindcast weather information can be used.

A mathematical curve is determined for each draught, which goes through the data in the best way. One can use a function like, *Boutillier et al. (2015)*:

$$Consumption = \beta \cdot Speed^{\alpha}$$

The parameters of the curve (here e.g. β and α) are determined based on the data. An example is shown in Fig.5. It can help to separate curves for say each Beaufort (BF) scale or even a current calm weather curve by normalizing them.

In this way, one obtains quickly power curves that reflect the current performance of the vessel fairly well. Putting a certain margin upon such curves gives a decent charter party contract curve.

A main disadvantage of pure mathematical approaches is that the model only covers experienced sailing conditions of a vessel. Such models may not accurately predict in newly encountered conditions simply because the models have no experience data to do so, *Bertram (2014)*.

For certain vessel types like Bulker and Tanker vessels the sailing condition often does not change over longer periods. This, combined with fouling impacts, can lead to models that do not reflect the performance differences between the sailing conditions correctly.
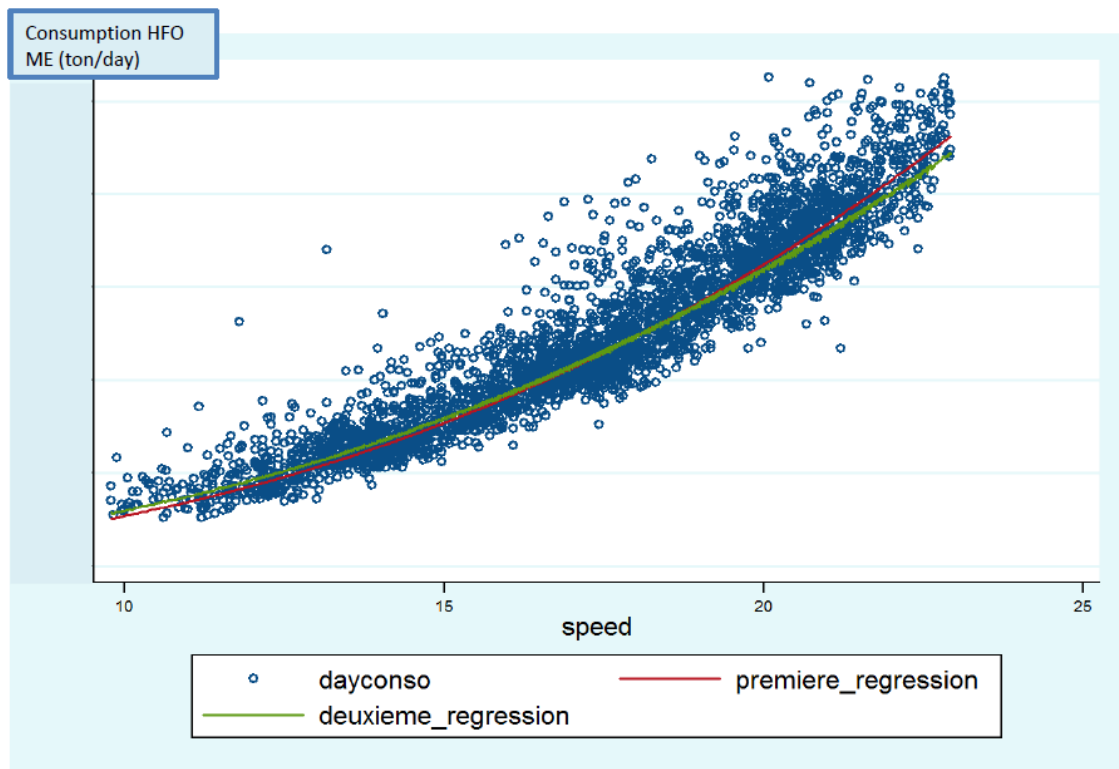
Fig.5: Consumption vs. speed mathematical model fit, *Boutillier et al. (2015)*

Another disadvantage of these approaches is that a clear indication of the "optimum performance" can only be given after a dry docking. Hence data logging systems need to be in place for fairly long periods (length between drydocks) to develop understanding of the optimal performance of a vessel.

3.   Hybrid Model – Initial Model creation

3.1 Overview of approach

The goal of the developed modelling approach is to use physical principles of naval architecture to analyse an individual vessel's sea trials and make reasonable extrapolations. The methodology selection depends on the available information. It is assumed that at least the General Arrangement plan, a displacement table and some general information about the propeller are available. The methodology estimates a power model which covers Ballast, Design and Scantling condition over a wide speed range. A draught extrapolation is required when the sea trial has only 1 or 2 of these curves available. Additional draught conditions can be added when the model is compared to high-frequency data.

3.2 Analysis of the Sea Trial

The following is read from the Sea Trial document:

1.   The corrected Speed vs. Power curves
2.   The Speed, RPM & Power measurements

Some sea trials cover only the actual measurements. The sea trial curve is then often just a mathematical curve between the measurement points. For the sample analysis, this was the case for ~15% of the documents. To bring all sea trials to the same base, one needs to run an ISO 15016 correction on the data in such cases.

3.3 Propulsion efficiency

Physically the required propulsion power is described as:

$$P_D = \frac{R_T \cdot v_s}{\eta_D} \qquad (1)$$

with R_T = Total vessel resistance, hull resistance determined in chapter 3.4
        v_s = vessel speed through water
        η_D = propulsive efficiency

The propulsive efficiency is defined as:

$$\eta_D = \eta_H \cdot \eta_R \cdot \eta_O = \frac{(1-t)}{(1-w)} \cdot \eta_R \cdot \eta_O \qquad (2)$$

The individual factors are derived by:

- η_R (relative rotative efficiency): Values are between 0.99…1.05 for single-screw vessels, *Krüger (2017);* due to lack of information, we set $\eta_R = 1 \rightarrow Q = Q_0$.
- η_O (propeller open-water efficiency): Is read from the digitized open water propeller diagram. If this is not available, the propeller geometry parameters are used to create an open-water propeller model of the Wageningen B-Series Propeller, *Bernitsas et al. (1981)*. The sea trial measurements (RPM, Speed, Power) give then an indication of the open-water efficiency at sea trial condition. The open-water propulsion efficiency of all other conditions can be determined through K_T-identity, when speed and resistance are given, or K_Q-identity, when speed and power are given.
- *t* (Thrust deduction factor): Determined through estimation formulas, *Schneekluth and Bertram (1998)*.
- *w* (wake fraction): Determined by estimation formulas, *Schneekluth and Bertram (1998),* over the whole speed and draught range and calibrated based on the sea trial measurements condition at design speed and using the open-water propeller diagram.

3.4 Hull Resistance

The total resistance coefficient c_T, excluding weather impacts, is calculated for the sea trial condition. This value is then decomposed to the viscous resistance coefficient c_F, the wind resistance coeffiicent c_W, the correction factor c_A and the residual resistance c_R. c_F gets calculated through the ITTC 1957 formula and c_A is estimated through the standard formula, *Hollenbach (1997)*. With this the residual resistance can be calculated for the sea trial:
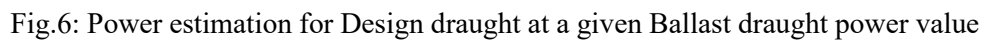
$$c_{R_{SeaTrial}} = c_{T_{SeaTrial}} - \frac{0.075}{(Log(Re)-2)^2} - c_A - c_W \qquad (3)$$

3.4.1. Draught extrapolation

The residual resistance value of the Sea Trial speed power curve is the basis to determine the residual resistance coefficient for other sailing conditions were no speed-power curves are available. An overview of the process for this is shown in Fig.6. The central element of the approach is that the residual resistance of non-sea trial conditions is estimated by the typical value difference of the different sailing conditions. For instance, when the residual resistance coefficient for Ballast condition is given, the values for Design and Scantling can be computed by:

$$c_{R-Design} = c_{R-Ballast} \cdot \left(1 + Change\%_{Design}\right) \qquad (4)$$
$$c_{R-Scantling} = c_{R-Ballast} \cdot \left(1 + Change\%_{Scantling}\right) \qquad (5)$$

Fig.6: Power estimation for Design draught at a given Ballast draught power value

The CR% change factors are retrieved by an empirical method, which uses standard series methods, *Hollenbach (1997),* and enriches them with the information from available sea trials, where sufficient information, i. e. three power curves were available. The resistance coefficients are to a certain amount depending on speed. It was chosen to use the "Design Speed Point" as the general reference to compute $Change\%_{Design}$, but allow individual changes over speed in the review mechanism.

3.4.2. Speed extrapolation

Another requirement to the power model is, that it covers an extensive speed vs. power range. To run the vessel efficiently, operators may need to execute voyages with super slow steaming at 10% of MCR power with speeds as low as 9 kn speed ($F_n \approx 0.08$). Most low-speed extrapolation methodologies use a cubic speed power relation to extrapolate. Some vessel performance analytics companies use machine learning based approaches to correct for this, e.g. *Hympendahl et al. (2018)*. No matter which method one choses, generally the accuracy with which one can predict low power values is limited.

Fig.7: Low speed extrapolation of c_R coefficients using cubic parametric splines

In order to give ship operators a fair indication of the lower speed power values the developed methodology extrapolates the residual resistance coefficient over the Froude number. The residual resistance for three Froude numbers is estimated through an empirical model and a cubic parametric spline function is used to connect the points, Fig.7. The empirical model is based on curve comparisons with valid high frequency data. Findings of this empirical model were that the residual resistance generally seems to increase at lower speeds, particularly for vessels with a high block coefficient. Detaching flow effects and a bigger hydrodynamic mass could be the reason for this.

4. Hybrid Model – Review mechanism

When one ensures its validity, high-frequency data allows to create accurate models, *Reimer (2020)*. Having high-quality sensors and a scheme of ensuring the validity in place, one gets measurements which can be used to correct and calibrate the initial model.

As mentioned above, pure mathematical models would only describe the current performance of the vessel, including fouling and aging effects. The goal of the hybrid model developed here is that it describes the optimum (sea trial) performance of the vessel in holistic and accurate manner.

4.1. Data selection and preparation

It is important to select a data period where the hull performance was steady and where a wide operational band is covered. Preferably data after a dry docking should be used, whereas data with long idle periods should be avoided. It is not important for the model review that the data is recent.

The measurements need to be filtered to remove points with unstable operating conditions. Using such filters, a significant number of the data may get excluded, but this is often necessary to remove any bias. The remaining data gets corrected for the weather impact, either through high frequency weather data from ship, which is averaged on a 3-hours base or hindcast weather data from a weather company. Fig.8 gives an overview of the process.
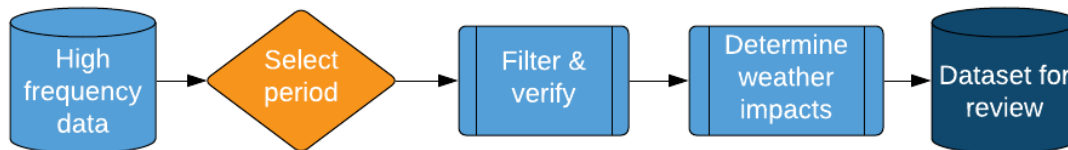

Fig.8: Filter process for model review

4.2. Review mechanism

The initially created model is held against the filtered and corrected operational data. As a major part of the hull and propeller model is derived through empirical formulas, its accuracy is limited by the quality of the empirical models. The review mechanism improves the accuracy of the models estimates and in a further process also the empirical model. However, the sea trial curves are assumed to be correct, and they are usually not changed but only visually inspected. The review mechanism has its limits, a few assumptions remain:

- The thrust deduction factor t is not reviewed as there is in most cases no thrust meter available to distinguish between thrust and resistance.
- The relative rotative efficiency η_R and the open-water characteristics are not changed. Only the wake fraction is taken as a variable.

A slightly modified admiralty formula is used to account for smaller draught differences between the model and reference curves. In case significant performance change is evident within the data, additional loading conditions can be added and reviewed separately.

At the review mechanism a mathematical best fit approach is used to create a calibrated curve of graphs for reference. Using the measurements, the shape of the power over speed, power over RPM and wake fraction over speed curves are assessed for each loading condition. An overview of the review process is given in Fig.9.
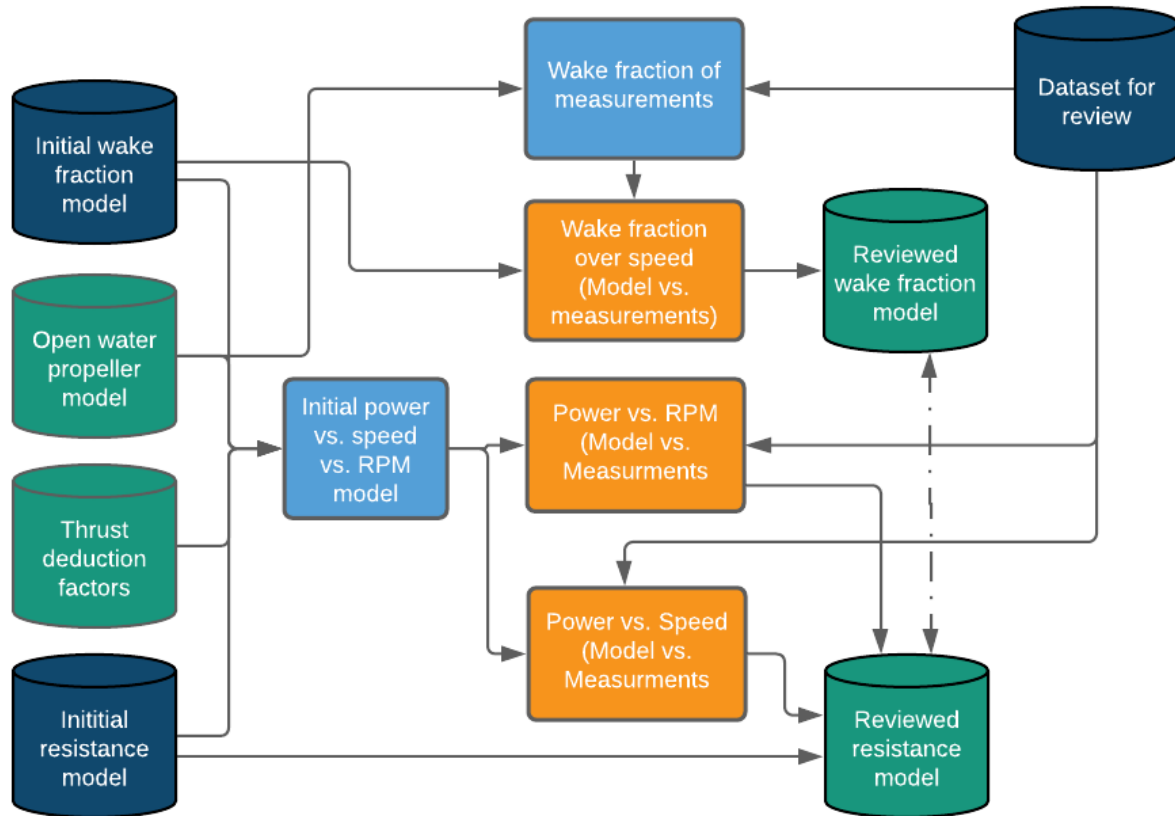

Fig.9: Review process of the generalized power model

A curve comparison allows to assess, where and how a change is needed. Using not only the power vs. speed assessment, but also the power vs. rpm curves allows to determine where the propeller operation point is different than estimated. This is partly corrected via a change of the modelled wake fraction slope over speed. In a second step the estimated resistance parameters are analysed further. As the values are interacting, i.e. the propeller operation point is dependent of the wake fraction and the resistance, the review process is iterative.

4.3 Final model

To derive the final model, it is assumed that the fouling impact in percentage of power is similar over the speed range. The final model is close to a minimum curve of the corrected measurements. An example for a container vessel curve in one of the Laden conditions is shown in Fig.10. The difference of the curve to the measurements is due to fouling and other environmental impacts which are yet not taken care of by the weather correction models. Future work may include improvements in this field.

The generalized power model (power vs. RPM vs. Speed model) is derived from a resistance model and a model of the propellers open water efficiency in the background. The advantages of this approach as compared to two-dimensional speed-power models that do not cover RPM, are:

- Measured Power and corresponding RPM can be cross-validated.
- More accurate assessment of weather and fouling impacts as the impact on propulsion efficiency is considered. Note: Any additional resistance causes a drop of propulsion efficiency, which is not modelled when one estimates: $\eta_D \approx 0.7 \approx const.$

- When converted from "clean hull" to "current performance" model, proper RPM and Power predictions can be derived.

Overall a more accurate prediction of RPM and power can be given through cross-validation.
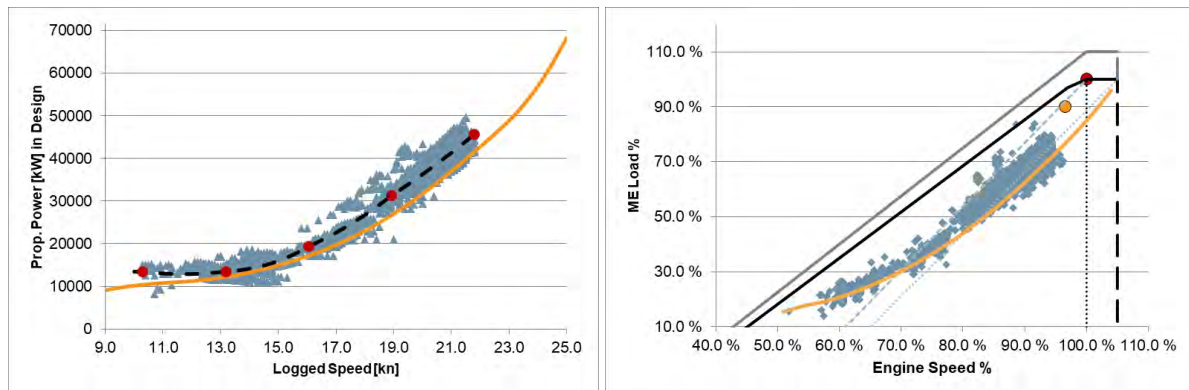

Fig.10: Left: Orange curve - Optimum modelled curve; Black curve with red markers - Calibrated best fit; Grey points – High frequency observations. Right: Main Engine Diagram with modelled propeller curve (orange)

5. Summary

In order to assess the vessel's capabilities a ship operator needs an accurate hull and propeller model for clean hull conditions. The modelling approach described in the paper achieves this by verifying an initial model, based on sea trials and empirical models from naval architecture, with valid high-frequency vessel measurements. The approach is hybrid as typically sea trial data, standard series methods and vessels operational data is used.

The hull and propeller are modelled separately to account for the interaction of the propeller and the hull when resistance changes. By this, the theoretical achievable power and RPM can be estimated and, via calibration to the current fouling condition, the vessels RPM and power can be predicted for the current vessel operation condition.

References

BERNITSAS, M.D.; RAY, D.; KINLEY, P. (1981), *KT, KQ and Efficiency Curves for the Wageningen B-Series Propellers*, Univ of Michigan, Ann Arbor

BERTRAM, V. (2014), *Trim optimization – Don't blind me with science*, The Naval Architect July/August, pp.66-68

BOUTILLIER, J.B.; MALLEK, S.; GERARD, L. (2015), *Vessel Consumption Models*, Ship Efficiency Conf., Hamburg, https://www.stg-online.org/veranstaltungen/Ship_Efficiency_2015.html

HOLLENBACH, K.U. (1997), *Contribution to the Estimation of Resistance and Propulsion of Single- and Twin-Screw-Vessels in the Preliminary Design*, PhD thesis, University of Hamburg

HYMPENDAHL, O.; GUNDERMANN, D.; SCHMODE. (2018), *Hull Performance Prediction beyond ISO 19030*, 3rd HullPIC Conf., Redworth

KRAPP, A.; BERTRAM, V. (2016), *Hull Performance Analysis – Aspects of Speed-Power Reference Curves*, 1st HullPIC Conf., Castello di Pavone

KRÜGER, S. (2017), *Grundlagen der Propulsion*, lecture notes, TU Hamburg

REIMER, K. (2020), *How to Achieve Performance Optimization Potential Considering High-Quality Data,* 5th HullPIC Conf., Hamburg

SCHNEEKLUTH, H.; BERTRAM. V. (1998), *Ship Design for Efficiency and Economy*, Butterworth + Heinemann, Oxford

TSARSITALIDIS, V.; ROSSOPOULOS, S. (2018), *ISO 19030 - The Good, the Bad and the Ugly*, 3rd HullPIC Conf., Redworth

Human Factor, the Double-Side Effect

Matteo Barsotti, IB, Genoa/Italy, m.barsotti@ib-marine.com

Abstract

There is now the trend of the autonomous ship, but it has to be clarified that is not a "we don't need a human in the ship's handling" but it's just a "we do not need him located on the vessel". Why is so important and sometime tricky the human factor? The IoT and the machine learning are of course replacing the humans in most of the activity, but the decision will have to be always coming from a human. So, it is always important to keep in mind that we can digitalize everything and bring onshore al the sensor data, create all the alerting and the analytics but then the human, his expertise is the key. Usually there is the idea that human factor is the human error that is correct but, in any case, this is not the only meaning, the human factor is also the human understanding and interpretation of an information that a system can give. Nowadays we have plenty of system that promises wonderful saving and claims to be fully automatic. Sometimes it is true but there is something behind, the expertise from whom give you the software and then the expertise of the customer in understanding and then using the information received. Here will be the focus on three main topics that have to be accompanied by the human factor to be fully used: Alerting, ISO19030 and Machine Learning.

1. Introduction

One of the bullet points of IMO's Strategic Plan (2018-2023) is to "integrate new and advancing technologies in the regulatory framework". This involves balancing the benefits derived from new and advancing technologies against safety and security concerns, the impact on the environment and on international trade facilitation, the potential costs to the industry, and finally their impact on personnel, both on board and ashore. In 2017, following a proposal by several Member States, IMO's Maritime Safety Committee (MSC) agreed to include the issue of marine autonomous surface ships on its agenda. This was in the form of a scoping exercise to determine how the safe, secure, and environmentally sound operation of Maritime Autonomous Surface Ships (MASS) may be introduced in IMO instruments.

For MASS vessels, the IMO has established four degrees of autonomy:

- Degree one: Ship with automated processes and decision support: Seafarers are on board to operate and control shipboard systems and functions. Some operations may be automated and at times be unsupervised but with seafarers on board ready to take control.
- Degree two: Remotely controlled ship with seafarers on board: The ship is controlled and operated from another location. Seafarers are available on board to take control and to operate the shipboard systems and functions.
- Degree three: Remotely controlled ship without seafarers on board: The ship is controlled and operated from another location. There are no seafarers on board.
- Degree four: Fully autonomous ship: The operating system of the ship can make decisions and determine actions by itself.

The scoping exercise was seen as a starting point that would touch on an extensive range of issues, including the human element, safety, security, liability and compensation for damage, interactions with ports, pilotage, responses to incidents and protection of the marine environment. The regulatory scoping exercise (RSE) was finalized at the 103rd Session of the MSC in May 2021. The outcome highlights several high-priority issues, cutting across several instruments, that would need to be addressed at a policy level to determine future work.

It has been defined the new concepts of

- <u>global degree of automation of a ship</u> that is the lowest degree of automation of main system covering essential services, Fig.1.
- <u>degrees of control</u> that represents the degree of availability of human operating the ship aboard (crew) or remotely outside the ship from a remote-control centre (operators), Fig.2.

Degree of automation		Manned	Definition	Information Acquisition	Information Analysis	Authority to make decisions	Action initiated by
A0	Human operated	Yes	Automated or manual operations are under human control. Human makes all decisions and controls all functions.	System Human	Human	Human	Human
A1	Human directed	Yes/No	Decision support: system suggests actions. Human makes decisions and actions.	System	System Human	Human	Human
A2	Human delegated	Yes/No	System invokes functions. Human must confirm decisions. Human can reject decisions.	System	System	Human	System
A3	Human supervised	Yes/No	System invokes functions without waiting for human reaction. System is not expecting confirmation. Human is always informed of the decisions and actions.	System	System	System	System
A4	Full automation	Yes/No	System invokes functions without informing the human, except in case of emergency. System is not expecting confirmation. Human is informed only in case of emergency	System	System	System	System

Fig.1: Degree of automation

Degree of control			Human presence	Location of control station
Direct control	DC0	No direct control	No crew available to monitor and control the system, nor to take control in case of warning or alert.	
	DC1	Available direct control	Crew available aboard, ready to take control in case of warning or alert. But they may be not at the control station	Aboard
	DC2	Discontinuous direct control	Monitoring and control may be discontinuous during a short period Crew always available at the control station, ready to take control	Aboard
	DC3	Full direct control	System is actively monitored and controlled at any time	Aboard
Remote control	RC0	No remote control	No operator available to monitor and control remotely the system, nor to take control in case of warning or alert.	
	RC1	Available remote control	Operators available in the RCC, ready to take control in case of warning or alert But they may be not at the remote control station	RCC
	RC2	Discontinuous remote control	Remote monitoring and control may be discontinuous during a short period Operators always available at the remote control station, ready to take control	RCC
	RC3	Full remote control	System is actively monitored and controlled remotely at any time	RCC

Fig.2: Degree of control

As a result, the guidelines introduce the concept of the Remote-Control Centre that is exactly the place where the ship management is moved along with the knowledge, that previously was on board; this is exactly where the crew is now needed, so it can be considered as just a relocation.

Of course, this is not easy and it takes time, but we have to consider that all the system that are available today in terms of automatic data collection and performance monitoring have behind the idea of Decision Support System.

Decision Support System (DSS) is an information system that supports business or organizational decision-making activities. DSSs serve the management, operations, and planning levels of an

organization (usually mid and higher management) and help people make decisions about problems that may be rapidly changing and not easily specified in advance.

The Human Factor is clear then where it fits in this environment and then the positivity that can bring. There is then also negative aspect related to the Human Factor that can be either voluntary or not voluntary. If a crew member wants to hide something to an Owner, an Operator or a Charterer and the ship has no other means of reporting than the noon report (manual) then for him is very simple.

Nowadays with more restriction in Emission, security, and all other aspect there is no possibility to not get as much information from a vessel that override the human intervention. This is where is the dilemma, from one side we have the good Human Factor because it means experience and valuable help but on the other side there is the bad Human Factor that hide something; it is in the human nature but the system available today can help in this dilemma so as said in Middle Ages and coming from Aristoteles " in medio stat Virtus", the solution will be take the Human knowledge but also use Human-independent means to get the information. Nevertheless, not all is on the crew's shoulder but there is other two parties with their Human Factor in the data handling. The first is the provider of a solution, as there should be the expertise to explain and make the customer really use the solution and not just sell the solution to make money and then forgot about us. The second is obviously the support on shore, someone in office with the expertise and capabilities to read the data and support the crew. Selling a performance monitoring system could be easy if we promise wonderful savings, fully automatic system and no crew intervention; but it is not exactly like that, it is important to understand the goal of the customer and then to be clear with him about the capability of a system but also about the action from the ships or the office onshore.

2. Alerting

When it comes to alerting, we receive always a very good feedback from the customer because the Human Factor in reporting could be a tricky element. There is more and more the need of the Shipowner/Ship operator to know immediately if something happens and this is because when you trust only on noon report you have only to trust in one report per day and hoping that is not so wrong (because it is wrong!). This could be due to the human error in the evaluation but also on meeting a charter party, covering some bad weather that cannot be avoided etc. What is sometimes not considered or told from some vendors is the fact that there is always the need to interpret a data coming from a sensor or at least someone to receive the alert and manage it. Furthermore, on a single signal we could have a problem and not find until some time, no matter how many alerts you put on it because it is there when human factor do its part. Let's take an example: if a from a flowmeter we take only the actual flow and use this to evaluate the daily consumption of course we will obtain a value that is different from the consumption measured by a very well-done manual sounding. If the flow has a minimum bias, it means that at every measurement it will add some consumption and then at the end the total consumption will be more than the real one. In a case like this we must combine to the following actions:

➢ Do the maintenance of the flowmeters as per maker recommendations.
➢ Integrate the flow of the flowmeter with additional data to evaluate the correctness of the signal received (example the Shaft Power and calculate the SFOC)
➢ Integrate with the tank sounding signals.

It is only a very simple example, but it is just to underline that depending on the data we get we can build alert together with the customer plus involving the crew in order to cover all the cases and issues that may arise. The crew or the operator on shore are a valuable help in understanding what can be monitored otherwise the risk is to have on shore a thousand of signal but then missing an important one.

Not every customer is structured to have a dedicated person or department in analyzing the data and then the alerts can be useless in fact it is important to set alerts that the customer can use. Creating an

alert to highlight when the vessel has 2 out of 3 Diesel generators at sea with MCR below 40% is extremely good but then, which is the point if all (onshore and on-board) will disregard it?

The job is not easy, as in most cases, it is a change of mentality, "we used to do like this", "we always do like that", "we receive too many emails", "you are spying on us" but at the end it worth if it is managed in the proper way because the incident and failure prevention along with emission saving will re-pay all the efforts. Alerting is a very helpful tool but should be set up in the proper way according to the customer need and Humans' participation.

3. ISO 19030

When it is presented a module that cover the ISO 19030 it is then strictly important to have clearly in mind the capabilities, the requirement, and the outcome of this ISO standard. The aim of this International Standard is to prescribe practical methods for measuring changes in ship specific hull and propeller performance and to define a set of relevant performance indicators for hull and propeller maintenance, repair, retrofit activities. Hull and propeller performance refers to the relationship between the condition of a ship's underwater hull and propeller and the power required to move the ship through water at a given speed. Hull and propeller performance is related to variations in power because ship hull resistance and propeller efficiency are not directly measurable quantities. Changes in underwater hull resistance are due to alterations in the condition of the hull. Changes in the propeller efficiency are due to both alterations in the condition of the propeller and to modifications to the flow of water to the propeller (the hull wake) as consequence of alterations to the hull condition. In order to measure changes in the speed-power relationship for a vessel in service, it is necessary to compare two periods (a reference period and an evaluation period) where the environmental conditions and the operational profile are adequately comparable (filter the observed data) and/or apply corrections (normalize the observed data). Hull and propeller maintenance, repair and retrofit activities influence the energy efficiency of a ship in service. An indication of these effects can be obtained by measurement of changes in the delivered power required to move the ship through water at a given speed between two periods for which the environmental conditions and operational profiles have been made adequately comparable through filtering and/or normalization of the observed data.

The above definition gives ship's speed through the water and delivered power as the two primary parameters when measuring changes in hull and propeller performance -> Primary Parameters. In order to apply the filtering and normalization procedures necessary to make the reference period and evaluation period adequately comparable, measurements of both the environmental conditions and the ship's operational profile are required -> Secondary Parameters. For both parameters, the parameters are set up as shown in Fig.3.

It then follows, in the standard, the chapter related to the sensor installation maintenance and calibration because otherwise the standard cannot be applied, and it is one strong point to be stressed here; the human factor it is essential in the evaluation and the management of the various system.

Not only on the accuracy of the measurement the standards give indications but also on the data acquisition frequency, Fig.4, and here is one of the most critical point of the standard. If the data collection system has not this requirement, then the system is not ISO 19030 compliant.

After the data acquisition there is the data filtering and validation:

- ➢ One outlier in a 10-minutes dataset determine the invalidity of the whole dataset
- ➢ Correction for environmental factors
- ➔ The data filtering and validation provides the Corrected Dataset

Excluding the dataset that contains one dataset it is another criticality and it means that the system will require a bigger amount of data to be collected in order to build a valid Corrected Dataset.

Parameter	Acceptable measurement device / source[a]	Unit
Relative wind speed and direction measured at the height of the anemometer	Ship anemometer - minimum sensor accuracy of ±1m/s, ±5°	[m/s], [°]
Speed over ground	(D) GPS	[knots]
Ship heading	Gyro compass, or compass - DGPS	[°]
Shaft revolutions	Pick-up, optical sensor, ship revs counter w/ minimum sensor accuracy of ±0,5 %, 1σ	[rev/min]
Static draught fore and aft	Information from loading or stability computer or equivalent sources for static draught. NOTE Preference for observed draft – when available.	[m]
Water depth	Ship echo sounder w/ minimum sensor accuracy of - +/- 0,5 m on the 20m range scale, respectively +/- 5m on the 200m range scale; or - +/-2,5% of the indicated depth, whichever is greater.	[m]
Rudder angle	Rudder angle indicator - minimum sensor accuracy of ±1°	[°]
Seawater temperature	Thermometer	[°C]
Ambient air temperature	Thermometer	[°C]
Air pressure	Barometer	[Pa]

[a] Minimum sensor accuracy refers to the by the sensor manufacturer's specified accuracy

Fig.3: Minimum sensor requirements

Then it is possible to calculate the Performance Values that is the percentage of speed loss compared to a reference speed power relation.

From the Performance Values it is possible to evaluate the Performance Indicator PI, Fig.5, as the differences between the average percentage speed loss of Reference period and Evaluation period.

The next step is to create the Reference Period and here is another hot point because it is possible to consider a period as reference if they are all met simultaneously the following:

➢ water temperature is >2°C and if there is no other indication that the vessel is trading in ice;
➢ the wind speed is between 0 – 7.9 m/s (BF 0 and BF 4);
➢ water depth is greater than the larger of the values obtained from two formulae dependent on ship breadth, ship speed and mean draft
➢ delivered power has to be within the range of power values covered by the available speed-power reference curves,
➢ displacement has to be within ±5% of the displacement values for the available speed-power reference curves,
➢ absolute rudder angle value is smaller than 5°

	Parameter	Minimum Data acquisition rate
Primary Parameters	Vessel speed through water	Once every 15 seconds (0,07Hz)
	Delivered Power ᵃ	Same as for vessel speed and same time stamp as vessel speed
Secondary Parameters	Shaft revolutions	Once every 15 seconds (0,07Hz)
	Relative wind speed/direction	Once every 15 seconds (0,07Hz)
	Speed over ground and ship heading	Once every 15 seconds (0,07Hz)
	Rudder angle	Once every 15 seconds (0,07Hz)
	Water depth	Once every 15 seconds (0,07Hz)
	Static draught fore and aft	Whenever loading condition changes
	Water temperature	Once every 15 seconds (0,07Hz)

a The sensor measurements needed to estimate delivered power by either Annex B or Annex C shall be logged at the minimum acquisition rate for the primary parameters and with the same time stamp

Fig.4: Minimum data acquisition rates

Performance indicator (PI)	Definition
Dry-docking performance: Determining the effectiveness of the dry-docking (repair and/or retrofit activities)	Change in hull and propeller performance following present out-docking (Evaluation period) as compared with the average from previous out-dockings (Reference periods).
In-service performance: Determine the effectiveness of the underwater hull and propeller solution (including any maintenance activities that have occurred over the course of the full dry-docking interval)	Average change in hull and propeller performance from a period following out-docking (Reference period) to the end of dry-docking interval (Evaluation period).
Maintenance trigger: Trigger underwater hull and propeller maintenance, including propeller and/or hull inspection	Change in hull and propeller performance from the start of the dry-docking interval (Reference period) to a moving average at a given point in time (Evaluation period)
Maintenance effect: Determine the effectiveness of a specific maintenance event, including any propeller and/or hull cleaning	Change in hull and propeller performance from before (Reference period) to after a maintenance event (Evaluation period).

Fig.5: Basic hull and performance indicators

Reference Period and Evaluation periods:

- <u>Dry-docking performance:</u>
  One year Period
  Reference Period: immediately before dry-docking
  Evaluation Period: immediately after dry-docking

- <u>In-service performance</u>
  Minimum One year Period
  Reference Period: immediately after Dry-dock
  Evaluation Period: from the end of Reference Period until the end of the same dry-docking period
- <u>Maintenance Trigger</u>
  Minimum three months Period
  Reference Period: immediately after Dry-dock
  Evaluation Period: from the end of Reference Period of the same length in the same dry-docking period
- <u>Maintenance Effect</u>
  Minimum three months Period
  Reference Period: immediately before maintenance event
  Evaluation Period: immediately after maintenance event

As a result, the general feeling is that is not easy and even if in the Part 3 of the standard are provided "Alternative Methods" not every data collection is feasible to the standard, so it is better to take care when it is presented an ISO 19030 compliant system. Or better, maybe a system can be compliant but not the ship or the company if not all the required data are mapped. The Human factor here is less visible but is in the expertise of explaining on how to deal with the requirements and on how to use the four PIs. These PIs can give a ship manager and especially a shipowner the possibility to do a lot of analysis and have information, not only "clean the ship is dirty" that a well-experienced Master can give without an ISO standard but long-term analysis on Dry-docking interval, the best time to clean and also to create a sort of ranking of the Hull/Propeller cleaning providers, etc.

Again, all of this is possible if there is the human on both sides that understand and interpret the data and analysis created.

4. Machine Learning

Machine Learning is another topic that is in almost all presentation about performance monitoring and data collection but most of the time is presented as Black box but not as the definition of the algorithm but as a sort of miracle with no possibility of questions, like "do you believe in machine learning?" as it is a new religion. Of course, as an algorithm that learns from the data can be considered as a sort of mystery but again here some explanations are needed for everybody's comprehension.

Machine learning is a branch of artificial intelligence (AI) and computer science which focuses on the use of data and algorithms to imitate the way that humans learn, gradually improving its accuracy. Machine learning is an important component of the growing field of data science. Through the use of statistical methods, algorithms are trained to make classifications or predictions, uncovering key insights within data mining projects. These insights subsequently drive decision making within applications and businesses, ideally impacting key growth metrics. As big data continues to expand and grow, the market demand for data scientists will increase, requiring them to assist in the identification of the most relevant business questions and subsequently the data to answer them.

Machine learning algorithm can is divided into three main parts:

1. <u>Decision Process</u>: In general, machine learning algorithms are used to make a prediction or classification. Based on some input data, which can be labelled or unlabeled, your algorithm will produce an estimate about a pattern in the data.
2. <u>Error Function</u>: An error function serves to evaluate the prediction of the model. If there are known examples, an error function can make a comparison to assess the accuracy of the model.
3. <u>Model Optimization Process</u>: If the model can fit better to the data points in the training set,

then weights are adjusted to reduce the discrepancy between the known example and the model estimate. The algorithm will repeat this evaluate and optimize process, updating weights autonomously until a threshold of accuracy has been met.

There are three types of machine learning:

1. Supervised machine learning
   Supervised machine learning is defined by its use of labeled datasets to train algorithms that to classify data or predict outcomes accurately. As input data is fed into the model, it adjusts its weights until the model has been fitted appropriately. This occurs as part of the cross-validation process to ensure that the model avoids overfitting or underfitting. Some methods used in supervised learning include neural networks, naïve bayes, linear regression, logistic regression, random forest, support vector machine (SVM), and more.

2. Unsupervised machine learning
   Unsupervised machine learning uses machine learning algorithms to analyze and cluster unlabeled datasets. These algorithms discover hidden patterns or data groupings without the need for human intervention. Its ability to discover similarities and differences in information make it the ideal solution for exploratory data analysis, cross-selling strategies, customer segmentation, image and pattern recognition. Other algorithms used in unsupervised learning include neural networks, k-means clustering, probabilistic clustering methods, and more.

3. Semi-supervised learning
   Semi-supervised learning offers a happy medium between supervised and unsupervised learning. During training, it uses a smaller labeled data set to guide classification and feature extraction from a larger, unlabeled data set. Semi-supervised learning can solve the problem of having not enough labeled data (or not being able to afford to label enough data) to train a supervised learning algorithm.

The most available machine learning algorithm in the shipping are the supervised machine learning algorithm with a labeled data set to predict a measure, usually Power or Slip. What is usually hidden and where is the Human Factor, is the selection of the dataset because different dataset as input will provide a different output that will be more accurate or less accurate. It is a matter of measured data, how they are measured, and which are selected; it helps again experience from the vendors in giving the best advice on the standard measures but also from the customer because a measured data cannot be available or maybe is better to use another measure that is more significant for a specific vessel. In other words, if not well prepared the machine learning algorithm can give very bad information, it is a very good example of "Garbage In - Garbage Out", Human factor then in the selection of the inputs is essential.

5. Conclusions

Human factor has a double side effect, good and bad. Bad is when the Human want to hide something from someone, or it can be related to the error in the evaluation of a measure that is intrinsic of a human. Human factor is also bad when there is lack of expertise and then someone want to make benefit of it. The expertise is the good of the Human Factor but it has to come along with honesty and willing to teach. Whenever there is a change, it is always a battle to change the mentality and to focus on what really worth in the jungle of the providers. From a provider's point of view, the biggest value is to have a dedicated customer with experience because this enables both to improve using both experience in developing and updating the system to a better and competitive result. Together it is possible to reduce the bad side effect of the Human factor enabling the crew and then the ship owner/ship operator to really use what they are paying for otherwise it will be only a good marketing tool to show to third parties.

References

https://www.ibm.com/cloud/learn/machine-learning

https://www.imo.org/en/MediaCentre/HotTopics/Pages/Autonomous-shipping

BUREAU VERITAS (2019), *Guidelines for Autonomous Shipping*

ISO 19030 Standard: *Ships and marine technology — Measurement of changes in hull and propeller performance part 1, 2 and 3,* Int. Standard Org., Geneva

SONCINI, G. (2020), *MASS Autonomous Ships: Current Status, Developments and Pitfalls!*, HIPER Conf., Cortona

Accurate Vessel Performance Quantification using Noon Reports Data Collection Systems

Javier Zamora, Navalytica, New York/USA, javier@navalytica.com

Abstract

Noon reports data is often deemed unsuitable to perform any accurate performance analysis. This paper identifies reporting of the daily averages of vessel speed, propeller rpm, and shaft power demand as an intrinsic source of error of noon reports data collection systems. To prove that hypothesis, first a mathematical model is derived such that it accurately characterizes the shaft and effective power demand of a vessel, which is then validated with Series 60 and KVLCC2 data. This model is used to derive a methodology to evaluate the performance of a vessel, which is tested over a synthetic dataset, ensuring reproducibility and validation against a known benchmark. Then the proposed performance evaluation procedure is applied to a noon report dataset. The results identify vessel speed variability as an intrinsic source of error of noon reports, and show that by omitting these noon reports, it is possible to conduct an accurate performance evaluation of a vessel.

Symbols

A_e/A_o	Expanded blade area ratio
D	Propeller diameter
J	Advance coefficient
J_{oq}	Zero-torque advance ratio
J_{ot}	Zero-thrust advance ratio
K_Q	Torque coefficient
K_{Qo}	Zero-speed torque coefficient
k_q	Curvature parameter of the torque closed-form equation
K_T	Thrust coefficient
K_{To}	Zero-speed thrust coefficient
k_t	Curvature parameter of the thrust closed-form equation
n	Propeller rotation rate
P/D	Pitch to diameter ratio.
P_D	Delivered power
P_E	Effective power
P_S	Shaft Power
Q	Torque
Rn	Reynolds number
R_T	Total resistance of the hull when towed
R^2	Coefficient of determination
T	Propeller thrust
t	Thrust deduction fraction
V	Ship speed
V_A	Propeller advance speed
w	Taylor wake fraction
Z	Number of propeller blades
η_o	Propeller efficiency in open water
η_R	Relative rotative efficiency
η_S	Shafting efficiency
ρ	Mass density of fluid

1. Introduction

In January 2014, the International Maritime Organization (IMO) introduced amendments to MARPOL Annex VI "Regulations for the prevention of air pollution from ships", *IMO (2009)*, to quantify the ratio of the environmental costs to the transport capacity-mile achieved by ship through the mandatory Energy Efficiency Design Index (EEDI) for new ships, and Ship Energy Efficiency Management Plan (SEEMP) for all ships.

In parallel, the shipping industry nowadays operates in an economic sphere in which the markets of the goods transported, as well as the particularities of the shipping markets, determine operating profiles, costs and prices, *Lindstad et al. (2013)*. In addition, strategic investments oriented to increase fuel efficiency face the intricacies of the interactions between ship owner, charterer, and ship manager, *Agnolucci et al. (2014)*.

The increase of voyage costs as a percentage of revenue, either due to the rise of fuel costs or the reduction of freight rates due to the overcapacity of ships, makes fuel efficiency to become a key element in the ability of a ship owner to remain competitive. Thus, operational decisions by ship owners and managers trend towards fuel reduction.

To realize savings, assess investment risks and remain competitive in tough financial and regulatory times, changes in performance must be quantified for their conversion to a monetary impact. As described by *Armstrong (2013)*, quantification is a significant aspect of the development of optimization initiatives.

The arrival of data acquisition systems and improvement of sensor accuracy provides large amounts of operational vessel sailing data to stakeholders, already incentivized due to fuel costs and international regulation, to find ways to reduce operational costs by increasing vessel efficiency.

However, a significant share of the world fleet still relies on Noon Reports data acquisition systems. Noon reports are a vessel data collection system in which the captain submits a daily report detailing the fuel consumption and other relevant parameters that reflect the ship operational profile over the previous 24 hours. The uncertainty related to the manual entry round-off error in these reports is accepted as an impassable barrier to perform any meaningful performance analysis. However, it will be shown that a source of error in the noon reports data happens due to the loss of information sustained by submitting simple averages as aggregated measures of vessel speed and propeller revolutions.

2. State of the art of vessel performance modeling

According to ISO 19030, *ISO (2016)*, vessel performance refers to the relationship between the condition of hull and propeller, and the power required to move the ship at a given speed. A straightforward approach to characterize this relationship is to somehow control all the influential variables: draft, trim, weather, etc. which could be done in the following ways:

1. <u>Sea trial tests</u>. Sea trials at specific range of speeds and loading conditions produce accurate results, which are easy to analyze and interpret. Both *ITTC (2012)* and ISO 15016, *ISO (2015)*, provide sea trial guidelines. Even though the latter provides additional corrections for resistance due to wind, waves, depth, and water density and temperature, they are fully compatible with each other, *Strasser et al. (2015)*. Sea trials for ship performance evaluation are advocated by Bazari (2007) and by hull and propeller performance monitoring companies. However, sea trials are disruptive, costly and time-consuming activities, *Munk (2006)*.

2. <u>Normalization</u>. Normalization implies correcting each influential variable: wind, waves, draft and water depth to a baseline by employing a model that quantifies the expected shaft power for all operational conditions. The main problem of this approach is that the model used for the corrections may lead to uncertainties that arise from incorrect model functional form or model parameters due to either omitted variables or unknown effects.

3. <u>Data filtering</u>. Filtering implies decimating the dataset, eliminating the data afar from reference conditions. The filtering approach is easy to implement and interpret, *Flikkema (2013)*, as no assumptions are made regarding the inner consistency of the data. However meaningful data might be lost, and longer evaluation periods are required to collect adequate volumes to infer statistically significant results.

Current approaches to ship performance modelling can be broadly categorized into theoretical, statistical and hybrid methods:

1. <u>Theoretical Models</u>. Theoretical models are based on model tests that determine calm water resistance, on top of which the added resistance due to wind, waves, current, ice, and fouling is considered. The calm water resistance is the sum of frictional, residual and air resistance. A standard model-ship correlation line, ITTC'57, accounts for scale effects. The exact total resistance calculation method is outlined in the 1978 ITTC Performance Prediction Method. *Hansen (2010)* includes theoretical models for added resistance in wind, waves, steering and shallow water. *Eljart (2006)* includes the effect of sea state, wind, course-keeping and shallow water. *Hansen (2010)* corrects for wind/weather to calculate the power demand at a reference speed and draft to quantify the fouling effect. Also, there are some semi-empirical models, acceptable from an initial design perspective, such as those by *Holtrop and Mennen (1982), Guldhammer and Harvald (1965), Hollenbach (1998)* and *Gertler (1954)*.

   However, the underlying formulae in all theoretical models have assumptions and associated uncertainties. *Logan (2011)* indicates that many of the theoretical models that measure the ship's resistance remain un-validated in the scenario in which they are applied. Also, the hull and propeller fouling create difficulties for validating models, as each added resistance cannot be attributed to its source. The weather conditions limit opportunities for validation since calm conditions are needed. Further, full validation requires a large dataset that represents a wide range of ship operating conditions which may take many years to accumulate. There are as well inconsistencies surrounding which specific added resistance factors should be included. And there is no described method that accounts for interaction effects between each component of added resistance.

2. <u>Statistical and Machine Learning Models</u>. *Pedersen and Larsen (2009)* describe methods of predicting ship propulsion power, and they compare the prediction accuracy of artificial neural networks (ANN) and regression models. They concluded that ANNs successfully predict propulsion power, yet they also find validation errors insensitive to different combinations of input variables. *Petersen et al. (2011a)* compare gaussian processes (GP) to ANNs predicting fuel consumption and speed from a set of measured features. *Petersen et al. (2012)* implement a time-delay neural network to predict the response of speed, trim, draught, and heading to a change in a control variable (pitch, rudder angle, current, headwind and crosswind).

   Brandsaeter and Vanem (2018) applied regression models to predict ship's speed using a set of 18 vessel parameters collected from high-frequency sensors over 3 months. The goal of outperforming the Admiralty coefficient formula ($C_{ADM} = \Delta^{\frac{2}{3}} V^3 / P_S$) was not achieved for the complete range of operational speeds. *Perera and Mo (2016,2018)* proposed a three-steps procedure for operational data processing: sensor faults detection, data classification and data compression using Principal Components Analysis and Gaussian Mixture models, but no quantitative metrics were published. *Ahlgren and Thern (2018)* relied on an unsupervised machine learning algorithm to predict ship fuel consumption. Their best performing model achieved accuracy similar to previous researchers but with lower number of used features. *Soner et al. (2018)* developed ship propulsion models based on shrinkage models such as Ridge and Lasso over high-frequency data. They utilized the same dataset as *Petersen et al. (2012)* and reported similar accuracy.

   Wang et al. (2018) also uses a Lasso regression to model the FOC of containerships from a dataset that included 97 vessels, significantly improving the accuracy of predictions. *Gkerekos et al. (2019)* developed a three-step process: data pre-processing, the training of a family of regression models and selection of the best performing over the test set.

   Farag and Olçer (2020) combined high frequency data with weather data with an ANN and a multi-regression model to predict a VLCC tanker's break power and specific fuel oil consumption,

achieving high accuracy (99.6%) predicting the dataset used to train the model. *Gkerekos and Lazakis (2020)* combined a deep-neural network prediction model with a weather routing algorithm. Anomalies in the ship dataset were filtered by applying a ±3σ cut-off value in each parameter. *Coraddu et al. (2017)* used random forests as feature selection strategy. *Coraddu et al. (2019a)* blend auto-logged and AIS data from a research vessel to train a Support Vector Machines and k-nearest neighbors to classify the vessel's hull and propeller condition as "clean" or "fouled". *Coraddu et al. (2019b)* used a large dataset obtained from on-board sensors of two Handymax chemical/product tankers to develop the ships' digital twin with Neural Networks with the goal to estimate the speed loss due to marine fouling, outperforming the ISO 19030 standard approach. *Aldous (2015)* and *Themelis et al. (2018)* compare data from noon reports (NR) to continuous monitoring (CM) data, concluding that there is a significant reduction of uncertainty by using CM. Statistics and machine learning models make it difficult to detect the significance of input variables and to understand the inner consistency between parameters. Also, these approaches require the dataset to be an unbiased sample, and this seldom happens, because operational constraints produce preferred speeds, drafts, and trims in vessel operational sailing datasets.

3. Hybrid Models. *Telfer (1926)* assumes a linear relationship between the torque coefficient and the slip, and proposes the Generalized Power Diagram (GPD) which relates power, ship speed, propeller revolutions and slip, for a particular wake fraction in one diagram. The generalized power diagram can be derived either from speed trials, *Telfer (1926), Townsin et al. (1975),* or propeller open-water characteristics from model tests, *Telfer (1926), Garg (1972)*. Fig.1 shows an example of a GPD for a cargo liner for shaft power, slip, ship speed and propeller revolutions for a wake fraction of 0.22. *Journée et al. (1987)* developed a hybrid model of a ship's fuel consumption. Measured signals were used to adjust the coefficients of the hydrodynamic model over various draft, trim and speed combinations in calm sea, to predict vessel speed, power, and fuel consumption. Predictions were found to be poor in bad weather conditions assumed due to inaccurate weather measurements.

Munk (2006) describes a commercial model that predicts hull fouling using weekly recordings of performance data taken with constant navigation, calm weather, and controlled draft. The added resistance due to fouling was obtained by comparing the observed values and the model output. The model is based on first principles and approximation formulae with empirical constants, although accuracy of results was not disclosed.

Leifsson et al. (2008) developed a hybrid model that integrates hydrodynamic constraints with a feed forward neural network to predict the fuel consumption and speed of a container vessel. They compare and report the advantage of using a hybrid model over a theoretical-only model for fuel consumption predictions during validation in extreme environmental conditions, although it is noted that their theoretical model does not include the effect of added resistance in waves. Also, the theoretical model seems to be superior over the range of operating values, which suggests that its performance could have been improved in the more extreme environmental conditions if wave data and a theoretical wave model were included. Also, the data is collected over a narrow vessel speed variance, which may have limited the network training and have affected the comparisons between methods.

3. The open-water propeller

The open-water propeller refers to a propeller working in uniform inflow, independent of the influence of the ship to which it may be fitted. Open-water tests allow to take measurements of thrust (T) and torque (Q) taken for a range of speeds of advance (V_A) and propeller revolutions (n) of a propeller running in undisturbed water. The recorded thrust and torque are then nondimensionalized applying the relationships shown in Eqs. (1) and (2).

$$K_T = \frac{T}{\rho \cdot n^2 \cdot D^4} \tag{1}$$

$$K_Q = \frac{Q}{\rho \cdot n^2 \cdot D^5} \tag{2}$$

D is the diameter of the propeller and ρ is the mass density of the water. The open-water performance of the propeller can be computed using Eq.(3).

$$\eta_o = \frac{J \cdot K_T}{2 \cdot \pi \cdot K_Q} \tag{3}$$

J is the advance ratio:

$$J = \frac{V_A}{nD} \tag{4}$$

Now, let us define K_{To} as the zero-speed thrust coefficient or the thrust coefficient K_T when the value of the propeller advance ration J is zero ($K_{To} = K_T(J = 0)$), and K_{Qo} as the zero-speed torque coefficient or the torque coefficient K_Q when the value of the propeller advance ratio J is zero ($K_{Qo} = K_Q(J = 0)$). We can further define the coefficient J_{ot} as a zero-thrust propeller advance ratio or the propeller advance ratio J such that the thrust developed by the propeller is zero ($J_{ot} = J(K_T = 0)$), and J_{oq} as the zero-torque propeller advance ratio or the propeller advance ratio J such that the torque delivered to the propeller is zero ($J_{oq} = J(K_Q = 0)$). Since K_Q is a smooth continuous curve connecting the points $(J_{oq}, 0)$ and $(0, K_{Qo})$, let us express K_Q as

$$K_Q = K_{Qo} \cdot \left(1 - \frac{f(J)}{f(J_{oq})}\right) \tag{5}$$

The Taylor Series expansion of f(J) around a point "a" such that it would have been neglected the terms of order J^2 and higher, would give a straight line connecting the points $(J_{oq}, 0)$ and $(0, K_{Qo})$,

$$K_Q = K_{Qo} \cdot \left(1 - \frac{f(a) + \frac{f'(a)}{1!}(J - a) + \frac{f''(a)}{2!}(J - a)^2 + \cdots}{f(a) + \frac{f'(a)}{1!}(J_{oq} - a) + \frac{f''(a)}{2!}(J_{oq} - a)^2 + \cdots}\right) \approx K_{Qo} \cdot \left(1 - \frac{J}{J_{oq}}\right) \tag{6}$$

from where it is apparent that $a = 0$ and $f(0) = 0$. At the same time, the Eq.(5) can be rewritten as:

$$K_Q = K_{Qo} - \frac{K_{Qo}}{f(J_{oq})} f(J) \tag{7}$$

such that the first derivative of K_Q respect to J is

$$\frac{dK_Q}{dJ} = -\frac{K_{Qo}}{f(J_{oq})} \frac{d}{dJ} f(J) \tag{8}$$

and since

$$-\frac{K_{Qo}}{f(J_{oq})} = \frac{K_Q - K_{Qo}}{f(J)} \tag{9}$$

then

$$\frac{dK_Q}{dJ} = \frac{K_Q - K_{Qo}}{f(J)} \cdot \frac{d}{dJ} f(J) \tag{10}$$

From where it seems to be possible expressing the first derivative of K_Q as a function of K_Q:

$$\frac{dK_Q}{dJ} = f(K_Q) \tag{11}$$

such that $f(K_Q)$ could be approximated by a Maclaurin series expansion,

$$\frac{dK_Q}{dJ} = f(K_Q) = f(K_Q = 0) + \frac{f'(K_Q = 0)}{1!} \cdot K_Q + \frac{f''(K_Q = 0)}{2!} \cdot K_Q^2 \tag{12}$$
$$+ \cdots$$

Then, the simplest approximation of $\frac{dK_Q}{dJ} = f(K_Q)$ could be of $\frac{dK_Q}{dJ}$ approximately equal to a constant value c_1,

$$\frac{dK_Q}{dJ} \approx c_1 \tag{13}$$

Solving for K_Q by integrating the Eq.(13) would lead to expressing K_Q as the straight line connecting the points $(J_{oq}, 0)$ and $(0, K_{Qo})$ mentioned before. It follows that the simplest non-trivial approximation for $\frac{dK_Q}{dJ}$ could be that of linear dependency with K_Q:

$$\frac{dK_Q}{dJ} \approx c_1 + c_2 \cdot K_Q \tag{14}$$

Solving for K_Q by integrating Eq.(14) yields:

$$K_Q = c_3 \cdot e^{c_2 \cdot J} - \frac{c_1}{c_2} \tag{15}$$

c_1, c_2 and c_3 are constants and combining Eq.(15) with Eq.(5) leads to:

$$K_{Qo} \cdot \left(1 - \frac{f(J)}{f(J_{oq})}\right) = c_3 \cdot e^{c_2 \cdot J} - \frac{c_1}{c_2} \tag{16}$$

To satisfy Eq.(16), the following holds: (1) $K_{Qo} = c_3 - \frac{c_1}{c_2}$; (2) $J_{oq} = \frac{1}{c_2} \cdot \ln\left(\frac{c_1}{c_2 \cdot c_3}\right)$; and (3) $k_q = c_2$, thus f(J),

$$f(J) = e^{k_q \cdot J} - 1 \tag{17}$$

which yields the following expression for K_Q:

$$K_Q = K_{Qo} \cdot \left(1 - \frac{e^{k_q \cdot J} - 1}{e^{k_q \cdot J_{oq}} - 1}\right) \tag{18}$$

Similarly, the thrust coefficient (K_T) can be represented by the following expression:

$$K_T = K_{To} \cdot \left(1 - \frac{e^{k_t \cdot J} - 1}{e^{k_t \cdot J_{ot}} - 1}\right) \tag{19}$$

And in view of Eqs.(18) and (19), the efficiency of the open-water propeller (η_o) can be expressed as

$$\eta_o = \frac{J}{2\pi} \cdot \frac{K_{To}}{K_{Qo}} \cdot \frac{\left(e^{k_q \cdot J_{oq}} - 1\right)}{\left(e^{k_t \cdot J_{ot}} - 1\right)} \cdot \frac{\left(e^{k_t \cdot J_{ot}} - e^{k_t \cdot J}\right)}{\left(e^{k_q \cdot J_{oq}} - e^{k_q \cdot J}\right)} \tag{20}$$

4. Wageningen B-Series Propellers

The Wageningen B series is a general purpose, fixed pitch, non-ducted propeller series extensively used for analysis and design. The series was presented by *Troost (1937,1939,1951)* in the late 1940s. Reviewing early results, inconsistencies due to the scale effects from different model tests were observed, and complete re-appraisal of the series was conducted by van *Lammeren et al. (1969)*. Table I shows the extent of the series in terms of a blade number versus blade area ratio.

Table I: Wageningen B series – blade number versus blade area ratio

Z	Blade area ratio A_E/A_O											
2	0.3		0.38									
3		0.35			0.5			0.65		0.80		
4			0.40			0.55			0.70		0.85	1.00
5				0.45			0.60		0.75		0.90	1.05
6					0.5		0.65		0.80		0.95	
7						0.55		0.70		0.85		

Oosterveld and Oossanen (1975) reported a multiparametric regression analysis of the original open-water test data of 120 propeller models, in which the open-water characteristics of the series are represented at a Reynolds number $2 \cdot 10^6$ by the Eqs.(21) and (22).

$$K_T = \sum_{n=1}^{39} C_n \cdot (J)^{s_n} \cdot \left(\frac{P}{D}\right)^{t_n} \cdot \left(\frac{A_e}{A_o}\right)^{u_n} \cdot (Z)^{v_n} \tag{21}$$

$$K_Q = \sum_{n=1}^{47} C_n \cdot (J)^{s_n} \cdot \left(\frac{P}{D}\right)^{t_n} \cdot \left(\frac{A_e}{A_o}\right)^{u_n} \cdot (Z)^{v_n} \tag{22}$$

Table II shows the open-water characteristics (J, K_T, K_Q) of the propeller B5-75, $P/D = 1.0$ generated with the B-Series polynomials for $Rn = 2 \cdot 10^6$. Regressing equations (18)-(20) to the open-water propeller data J, K_T and K_Q set of values listed in Table II leads to the fitting parameters K_{To}, J_{ot}, k_t, K_{Qo}, J_{oq}, and k_q used to calculate the estimated values $\widehat{K_T}$ and $\widehat{K_Q}$ shown in Table III, achieving the goodness-of-fit characterized by the determination coefficients $R^2(K_T)$, $R^2(K_Q)$ and $R^2(\eta_o)$ shown in

Table III. Fig.1 shows the J, K_T and K_Q values generated using the polynomials and the Eqs.(18)-(20) fitting curves.

Table II: Open-water characteristics (J, K_T, K_Q) of the propeller B5-75, $P/D = 1.0$

J	K_T	K_Q	$\widehat{K_T}$	$\widehat{K_Q}$
0	0.468994	0.068961	0.473452	0.069412
0.1	0.441187	0.065404	0.440648	0.065361
0.2	0.408566	0.06126	0.405672	0.060977
0.3	0.371608	0.056558	0.368381	0.056234
0.4	0.330794	0.051328	0.328622	0.051102
0.5	0.286604	0.045598	0.28623	0.045548
0.6	0.239516	0.039399	0.241032	0.039539
0.7	0.190011	0.03276	0.192842	0.033037
0.8	0.138567	0.025709	0.141462	0.026001
0.9	0.085666	0.018277	0.086681	0.018387
1.0	0.031785	0.010493	0.028273	0.010149
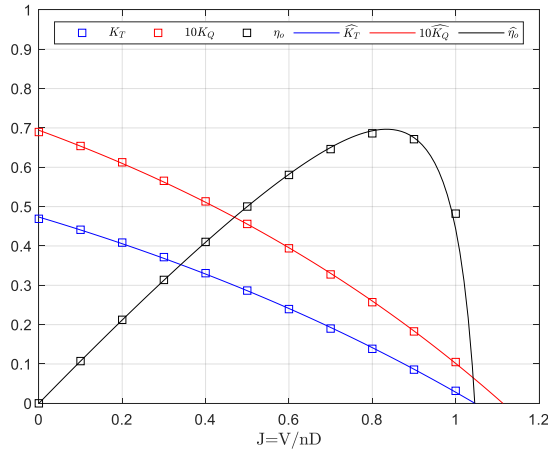
Table III

K_{To}	0.4735
J_{ot}	1.0462
k_t	0.6410
K_{Qo}	0.0694
J_{oq}	1.1133
k_q	0.7886
$R^2(K_T)$	0.999651
$R^2(K_Q)$	0.999804
$R^2(\eta_o)$	0.997127

Fig.1: B5-75, P/D=1.0, K_T, K_Q, and η_o values and fitting expressions $\widehat{K_T}$, $10\widehat{K_Q}$, $\widehat{\eta_o}$

This process was repeated for each one of the propellers with number of blades and blade aspect ratio listed in Table I, for pitch ratios in the range $(0.5, 0.6, ..., 1.4)$. Fig.2 shows the histograms of the resulting coefficients of determination obtained by fitting the Eqs.(18) - (20) to the K_T, K_Q and η_o curves obtained during the simulation.
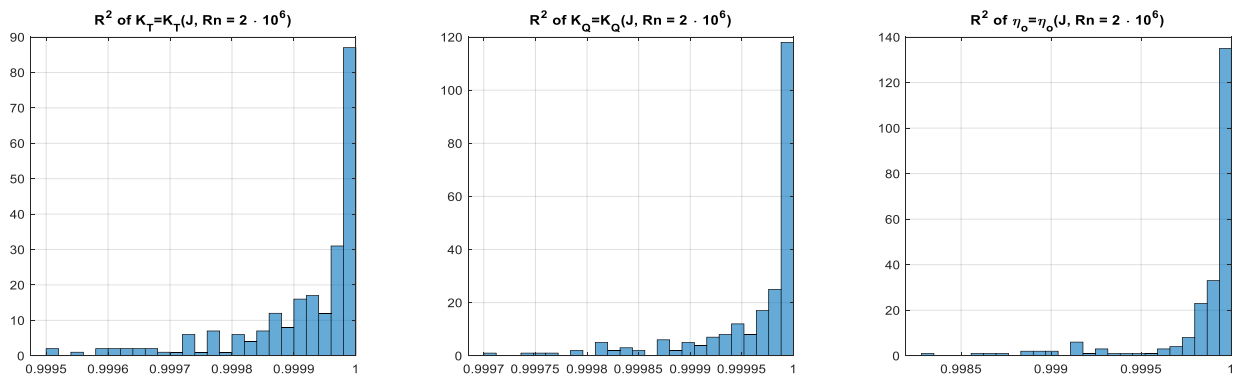
Fig.2: Histograms of R^2 obtained fitting Eqs.(18)-(20) to the Wageningen B-Series simulated propellers at $Rn = 2 \cdot 10^6$

5. Full-scale vessel

The effect of moving the propeller from an open-water scenario to a behind the hull scenario is typically quantified through the inclusion of the wake fraction (w), the thrust deduction coefficient (t), and the rotative relative efficiency (η_R).

The wake fraction coefficient (w) accounts for the loss of speed of the water due to the presence of the hull at the propeller position. The wake is the combination of the boundary layer associated with skin friction, the flow velocities occasioned by the streamlined form of the ship and the orbital velocities of the waves created by the ship. If the ship speed is V and the average velocity of the water relative to the hull at the propeller position is V_A, the wake speed, $V - V_A$, leads to the definition of the non-dimensional wake fraction coefficient as $w = 1 - V_A/V$.

The action of the propeller causes the water in front of it to be sucked towards the propeller. This results in extra resistance on the hull. The thrust force (T) on the propeller must overcome both the ship's towing resistance (R_T) and the extra resistance on the hull due to the sucking action of the propeller. The difference between the thrust force (T) and the towing resistance (R_T), $T - R_T$, corresponds to a loss of thrust. Thus, a non-dimensional thrust deduction coefficient (t) can be defined as $t = 1 - R_T/T$.

Since water closes in around the stern, the flow through the propeller disc will not be the same everywhere and will not, in general, be parallel to the shaft line. These effects can be combined and expressed as a relative rotative efficiency (η_R) as $\eta_R = \eta_B/\eta_o$, where η_B is the behind-the-hull propeller efficiency and η_o is the open water propeller efficiency. Both η_B and η_o express a ratio between the thrust power (P_T) and the delivered power (P_D). The thrust power (P_T) is the power developed by the thrust (T) of the propeller at the speed of advance (V_A) ($P_T = T \cdot V_A$), and the delivered power (P_D) is the power absorbed by the propeller.

The power measured in the shaft is the shaft power (P_S) delivered to the shafting system by the propelling machinery ($P_S = P_D/\eta_S$), where the shafting efficiency (η_s) is a measure of the power lost in shaft bearings and a stern tube. The effective power demand (P_E) needed to tow a ship at a constant speed V ($P_E = R_T \cdot V$). Thus, shaft power (P_S) and effective power (P_E) can be expressed as shown in equations (45) and (46) respectively.

$$P_S = \frac{1}{\eta_S \cdot \eta_R} \cdot 2 \cdot \pi \cdot \rho \cdot n^3 \cdot D^5 \cdot K_Q \tag{23}$$

$$P_E = (1 - t) \cdot \rho \cdot n^2 \cdot D^4 \cdot V \cdot K_T \tag{24}$$

And in view of Eqs.(18) and (19) providing mathematical expressions for K_Q and K_T, it follows:

$$P_S = \frac{1}{\eta_s \cdot \eta_R} \cdot 2 \cdot \pi \cdot \rho \cdot n^3 \cdot D^5 \cdot K_{Qo} \cdot \left(\frac{e^{k_q \cdot J_{oq}} - e^{k_q \cdot \frac{(1-w) \cdot V}{n \cdot D}}}{e^{k_q \cdot J_{oq}} - 1} \right) \tag{25}$$

$$P_E = (1 - t) \cdot \rho \cdot D^4 \cdot V \cdot n^2 \cdot K_{To} \cdot \left(\frac{e^{k_t \cdot J_{ot}} - e^{k_t \cdot \frac{(1-w) \cdot V}{n \cdot D}}}{e^{k_t \cdot J_{ot}} - 1} \right) \tag{26}$$

Telfer's Generalized Power Diagram (GPD) can be seen now as a polynomial approximation of the surface represented in Fig.3. Telfer predicts a GPD for each value of wake coefficient. Eq.(25) indicates that there is a shaft power surface for each pair (w, η_R). A few examples illustrate the applicability of Eqs.(25) and (26). Figs.5-9 show the open-water characteristics of a few propellers used to test several Series 60 Models, *Todd (1964)*. Fig.10 shows the open-water characteristics of the propeller KP458, http://www.simman2008.dk/PDF/MOERI%20propeller%20for%20KVLCC's.zip, used to test the KRISO Very Large Crude-oil Carrier 2 (KVLCC2), *Seo et al. (2020)*.

Regressing Eqs.(18)-(20) to the open-water propeller data J, K_T and K_Q selected set of values listed in Tables IV-IX leads to the fitting parameters K_{To}, J_{ot}, k_t, K_{Qo}, J_{oq}, and k_q achieving the goodness-of-fit characterized by the determination coefficients $R^2(K_T)$, $R^2(K_Q)$, $R^2(P_S)$ and $R^2(P_E)$ shown in Table X.
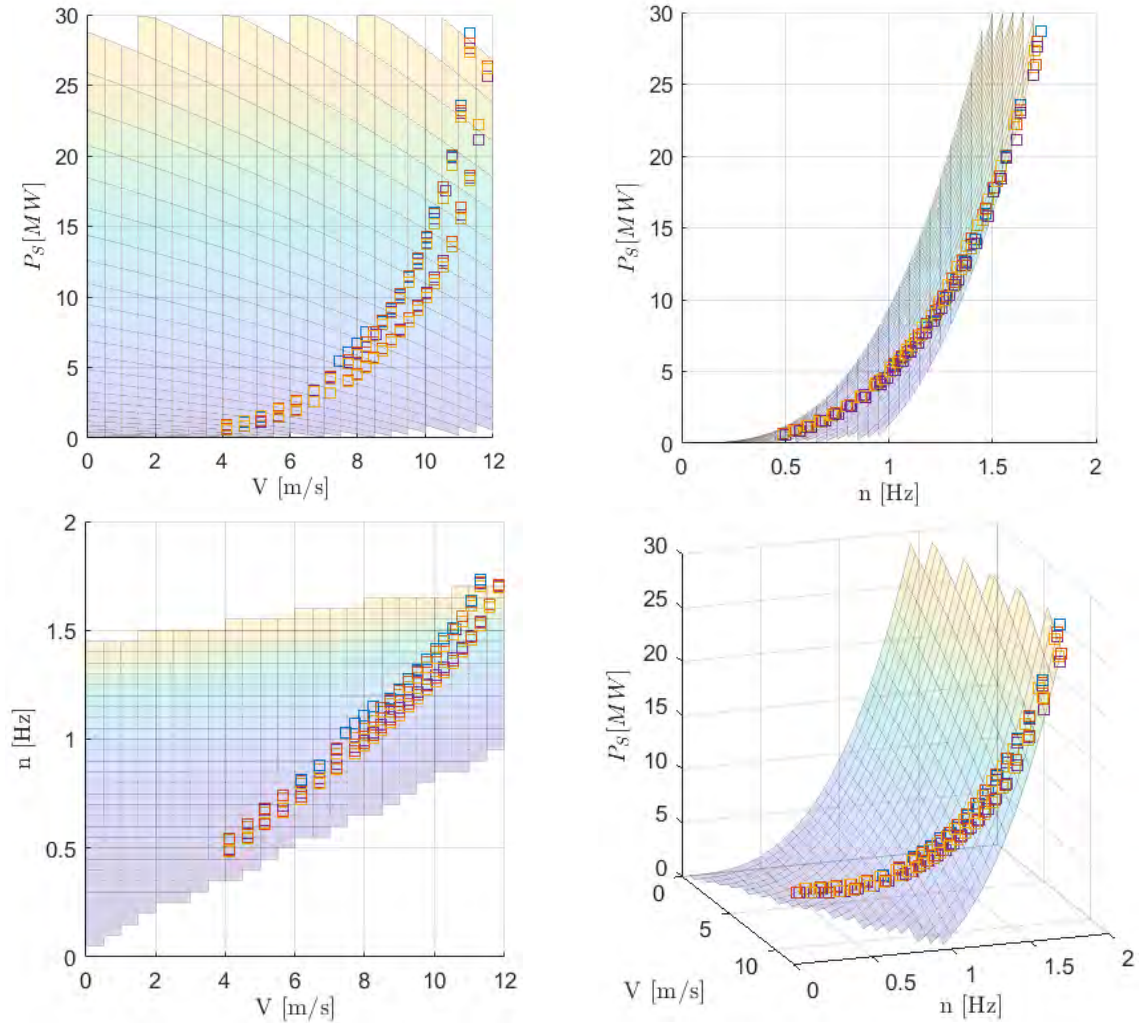
Fig.3: P_S surface from Eq (25) assumed w=0.319 and η_R=1.018; and Series 60 Models 4221, 4280, 4281, 4282 published data

6. Estimation of the vessel performance evolution over time

Vessel performance evaluation tries to quantify the speed reduction or increase of the power demand that results from the in-service degradation of the vessel. In a general sense, it can be assumed that the wake fraction coefficient depends on the vessel sailing parameters. It also makes sense that the progressive increase of frictional resistance due to the biofouling growth in the hull must have some effect in the set of all the possible values of the wake fraction coefficient. Should this effect happen uniformly over the whole set of possible values of w, then the time evolution of the average of the wake fraction coefficient ($\overline{w}$) must capture the increase of hull frictional resistance over time.

In other words, it is expected that the average of all the possible wake fraction values of a smooth hull to be smaller than the average of all the wake fraction values of an otherwise same hull but with significant higher level of roughness. Similar reasoning can be applied to the relative rotative efficiency, where the time evolution of the average of the relative rotative efficiency ($\overline{\eta_R}$) could be seen as a manifestation of the variability over time of the propeller efficiency range.

Zamora (2021) describes the following method to estimate the evolution of the performance of a vessel over time: given a time series of operational vessel sailing data, a series of values $(\overline{\eta_R}, \overline{w})_i$ can be obtained by iteratively applying regression analysis of the Eq.(27) over a moving window of data along the time series.

189
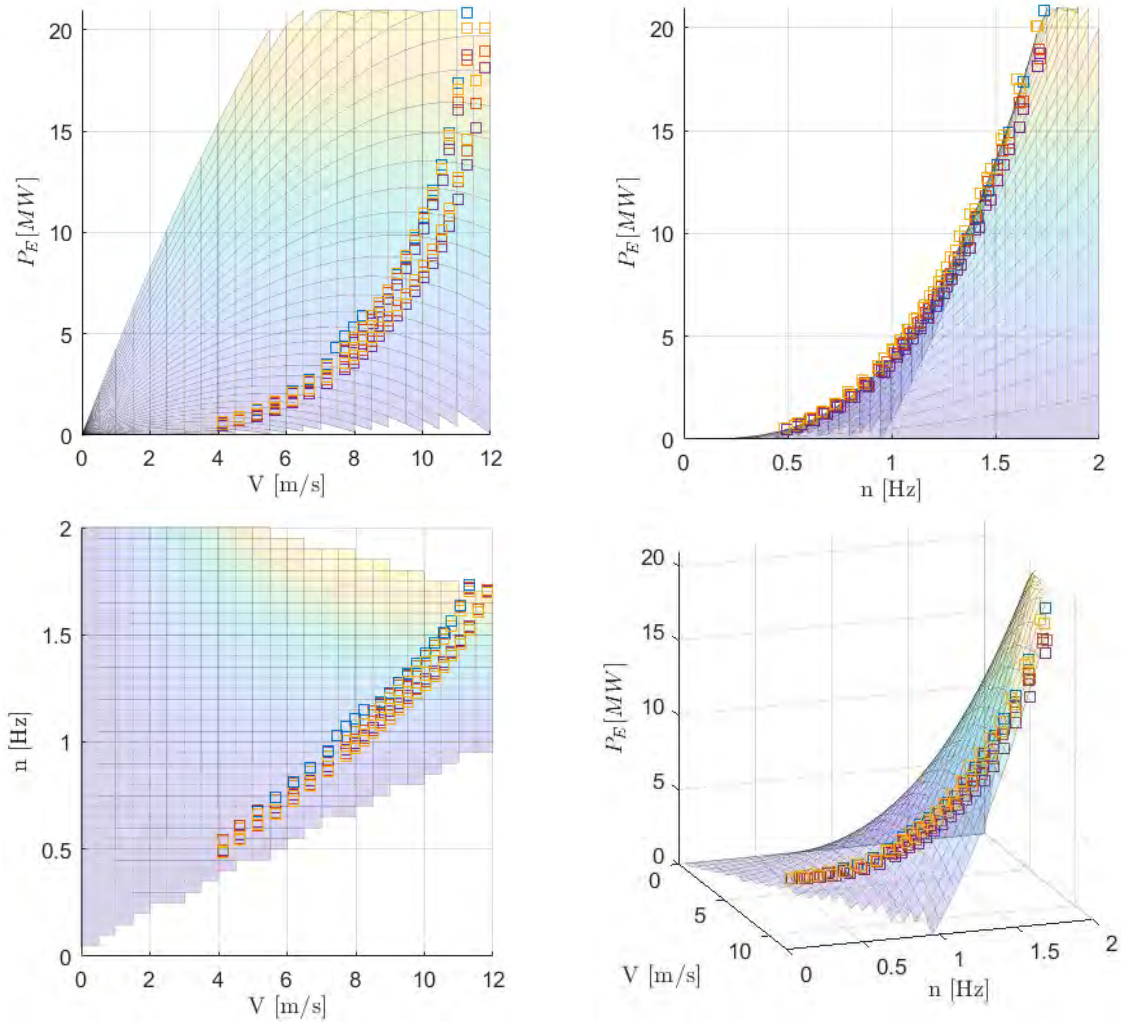
Fig.4: P_E surface from Eq.(26) assumed t=0.1977; and Series 60 Models 4221, 4280, 4281, 4282 published data

The evolution of the values $(\overline{\eta_R}, \overline{w})_i$ captures the average time degradation of the set of values $(\eta_R, w)_i$.

$$\widehat{P_S} = \frac{1}{\eta_s \cdot \overline{\eta_R}} \cdot 2 \cdot \pi \cdot \rho \cdot n^3 \cdot D^5 \cdot K_{Qo} \cdot \left(\frac{e^{k_q \cdot J_{oq}} - e^{k_q \cdot \frac{(1-\overline{w}) \cdot V}{n \cdot D}}}{e^{k_q \cdot J_{oq}} - 1} \right) \qquad (27)$$

Then, given pre-defined nominal conditions (n_o, V_o), the calculation of the vessel power demand at (n_o, V_o) for each pair $(\overline{\eta_R}, \overline{w})_i$ would yield the evolution over time of the vessel power demand as if the vessel had continuously sailed at the nominal conditions (n_o, V_o), thus reflecting the evolution over time of the performance of the vessel.

As a simple but illustrative example of the application of this patented method, consider a synthetic dataset of 8740 data points (each point corresponding to one hour along a year). A variable "h_t" can be defined as an incremental counter between 1 and 8740. For this example, it will be assumed that the vessel speed, expressed in knots, changes daily following the equation

$$V_{synth} = 15 + 7 \cdot (-1)^{\left\lfloor \frac{3}{400} \cdot h_t \right\rfloor} \qquad (28)$$

The draft, in percent displacement, changes weekly following the equation,

$$Draft_{synth} = 60 + 40 \cdot \left(WN - 2 \left\lfloor \frac{WN}{2} \right\rfloor \right) \qquad (29)$$

Where "WN" is calculated as

$$WN = 1 + \left\lfloor \frac{DN}{14} \right\rfloor \qquad (30)$$

190
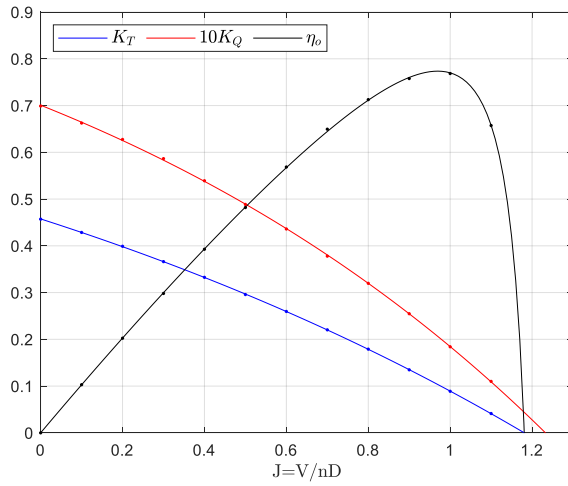
Fig.5: Propeller DTMB 3376 open-water characteristics, *Moss (1963)*

Fig.6: Propeller DTMB 3378 open-water characteristics, *Moss (1963)*

Fig.7: Propeller DTMB 3380 open-water characteristics, Moss (1963)

Table IV		
J	K_T	K_Q
0	0.4570	0.06990
0.1	0.4286	0.06626
0.2	0.3990	0.06275
0.3	0.3662	0.05865
0.4	0.3326	0.05392
0.5	0.2958	0.04885
0.6	0.2596	0.04360
0.7	0.2203	0.03779
0.8	0.1790	0.03198
0.9	0.1348	0.02548
1.0	0.0889	0.01841
1.1	0.0413	0.01100

Table V		
J	K_T	K_Q
0	0.48595	0.07214
0.1	0.4537	0.06819
0.2	0.4191	0.06387
0.3	0.3845	0.05936
0.4	0.3455	0.05447
0.5	0.303	0.04923
0.6	0.26176	0.04357
0.7	0.21887	0.03758
0.8	0.1731	0.03128
0.9	0.1273	0.02452
1.0	0.0779	0.01706
1.1	0.02599	0.00905

Table VI		
J	K_T	K_Q
0	0.4762	0.07568
0.1	0.4481	0.07127
0.2	0.416	0.06631
0.3	0.3807	0.06105
0.4	0.3425	0.05591
0.5	0.3043	0.05052
0.6	0.2636	0.04488
0.7	0.2241	0.03902
0.8	0.1821	0.0329
0.9	0.13806	0.02621
1.0	0.09206	0.01941
1.1	0.04419	0.01231
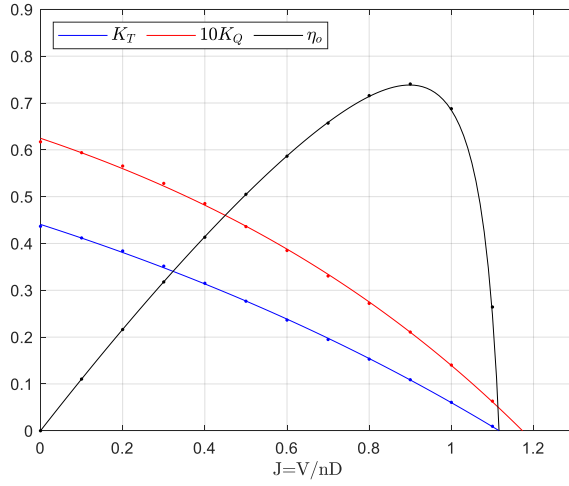
Fig.8: Propeller DTMB 3379 open-water
characteristics, *Moss (1963)*

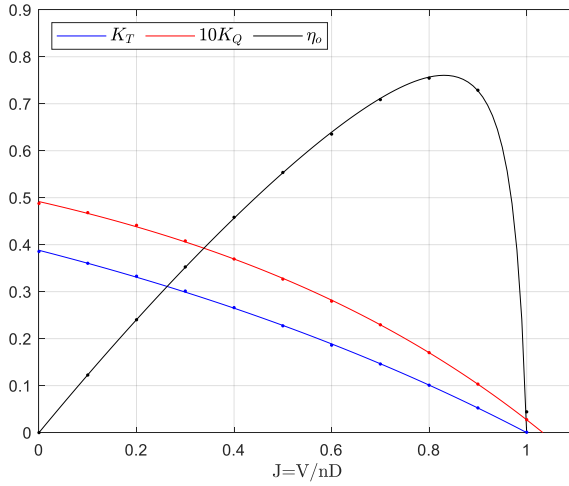| J	K_T	K_Q
0	0.4366	0.06171
0.1	0.4118	0.05939
0.2	0.384	0.05654
0.3	0.3516	0.05283
0.4	0.315	0.04852
0.5	0.2767	0.0436
0.6	0.2364	0.0385
0.7	0.1949	0.03305
0.8	0.1529	0.0272
0.9	0.10898	0.02108
1.0	0.06067	0.01404
1.1	0.00956	0.00633

Table VII

Fig.9: Propeller DTMB 3377 open-water
characteristics, *Moss (1963)*

J	K_T	K_Q
0	0.3856	0.04877
0.1	0.3604	0.04682
0.2	0.3329	0.04412
0.3	0.3013	0.0408
0.4	0.266	0.03695
0.5	0.2273	0.03267
0.6	0.1861	0.02797
0.7	0.146	0.02295
0.8	0.10086	0.01702
0.9	0.05253	0.01032
1.0	0.00077	0.00276

Table VIII
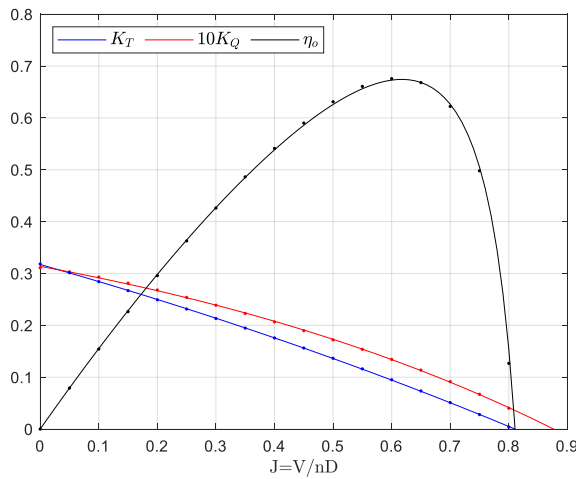
Fig.10: Propeller KP458 open-water characteristics

J	K_T	K_Q
0	0.3183	0.0311
0.10	0.2843	0.02932
0.20	0.2493	0.02682
0.30	0.2132	0.02388
0.40	0.1757	0.02067
0.50	0.1365	0.01721
0.60	0.0951	0.01344
0.70	0.0511	0.00915
0.75	0.028	0.00671
0.80	0.004	0.00402

Table IX

Table X

Model	Prop.	K_{Qo}	J_{oq}	k_q	K_{To}	J_{ot}	k_t	$R^2(K_Q)$	$R^2(K_T)$	$R^2(P_S)$	$R^2(P_E)$
4210	3378	0.072	1.2082	0.6835	0.4872	1.1486	0.4307	0.99999	0.99995	0.99992	0.99935
4213	3379	0.062	1.1732	0.9210	0.4407	1.1165	0.5654	0.99954	0.99975	0.99983	0.99996
4214	3377	0.049	1.0331	1.2231	0.3880	1.0000	0.7115	0.99982	0.99984	0.99997	0.99993
4215	3378	0.072	1.2082	0.6835	0.4872	1.1486	0.4307	0.99999	0.99995	0.99990	0.99974
4218	3380	0.076	1.2654	0.4292	0.4791	1.1879	0.4017	0.99996	0.99989	0.99991	0.99987
4221	3376	0.070	1.2327	0.7298	0.4575	1.1810	0.5122	0.99992	0.99999	0.99994	0.99912
4256	3380	0.076	1.2654	0.4292	0.4791	1.1879	0.4017	0.99997	0.99989	0.99989	0.99989
4260	3377	0.049	1.0331	1.2231	0.3880	1.0000	0.7115	0.99982	0.99984	0.99999	0.99999
4272	3378	0.072	1.2082	0.6835	0.4872	1.1486	0.4307	0.99999	0.99995	0.99987	0.99967
4280	3376	0.070	1.2327	0.7298	0.4575	1.1810	0.5122	0.99992	0.99999	0.99967	0.99889
4281	3376	0.070	1.2327	0.7298	0.4575	1.1810	0.5122	0.99992	0.99999	0.99962	0.99871
4282	3376	0.070	1.2327	0.7298	0.4575	1.1810	0.5122	0.99992	0.99999	0.99970	0.99921
KVLCC2	KP458	0.031	0.8765	1.1326	0.3174	0.8107	0.4702	0.99979	0.99997	0.99803	0.99034

The values of propeller revolutions, wake fraction, relative rotative efficiency, and shaft power demand are obtained by matching the synthetic speed and draft values obtained before to the Series 60 Model 4280 data.

Then, to simulate the progressive increase of power demand due to biofouling, the synthetic shaft power demand is multiplied by a coefficient that starts at a value of 1 and increases linearly over time. An event such as a hull cleaning, propeller polishing or the application of a new coating during dry dock, is simulated by dropping the biofouling coefficient back to a value of 1, before increasing over time once more. For example, if the vessel begins operation on January 1 having a biofouling coefficient with a value of 1 and rises to a value of 1.02 by June 30, the vessel can be cleaned at the half year mark on July 1 such that the biofouling coefficient drops back down to 1. Fig.11 shows the time evolution of the biofouling coefficient.
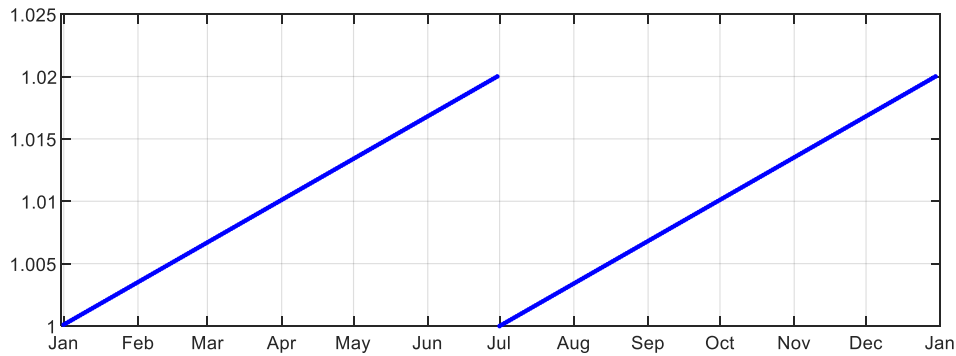

Fig.11: Biofouling coefficient

Fig.12 shows the resulting vessel synthetic speed (V_{synth}), synthetic draft ($Draft_{synth}$), synthetic rate of propeller rotation (n_{synth}), and synthetic shaft power demand ($P_{S,synth}$) with the biofouling coefficient already applied.
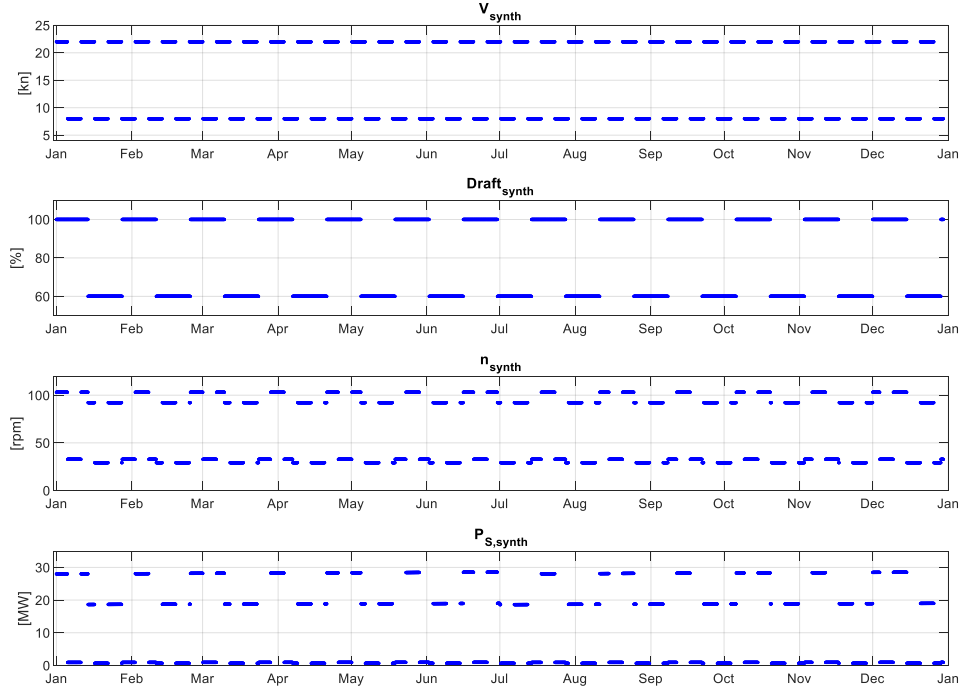
Fig.12: Synthetic dataset

We can now specify the vessel nominal conditions as $V_o = 20$ knots $= 10.3$ m/s and $n_o = 90$ rpm $= 1.5$ Hz. Also, in this case, the size of the moving window is defined as 30 days. The first step is to take data within the first 30 days. An example of a first 30-day window, between January 1 and January 30, extracted from the synthetic dataset is provided in Fig.13. Using regression analysis, we can fit the Eq.(27) to the data selection over the 30-day window and obtain the fitting parameters $\overline{\eta_R}$ and $\overline{w}$. Then, the fitting parameters can be used to calculate the shaft power demand at the selected nominal sailing conditions. For example, if $\overline{\eta_R} = 1.149$ and $\overline{w} = 0.405$, then, using Eq.(27):

$$P_{S,i} = \frac{1}{\eta_S \cdot \overline{\eta_{R,i}}} \cdot 2 \cdot \pi \cdot \rho \cdot n_o^3 \cdot D^5 \cdot K_{Qo} \cdot \left(1 - \frac{e^{k_q \frac{(1-\overline{w_i})V_o}{n_o D}} - 1}{e^{k_q J_{oq}} - 1} \right) =$$

$$= \frac{1}{1.0 \cdot 1.149} \cdot 2 \cdot \pi \cdot 1025 \cdot 1.5^3 \cdot 7.315^5 \cdot 0.070 \cdot \left(1 - \frac{e^{0.730 \cdot \frac{(1-0.405) \cdot 10.288}{1.5 \cdot 7.315}} - 1}{e^{0.730 \cdot 1.233} - 1} \right) = 18.2 \text{ MW}$$

The 30-day moving window can then be advanced by 1 day, repeating the process in the data range January 2 – January 31, and so on. The process finalizes when the 30-day moving window arrives at the end of the dataset. We can interpret the series of values $P_{S,i}$ as the shaft power demand that would have been obtained if the vessel had continuously sailed at the fixed conditions of $V_o = 20$ knots and $n_o = 90$ rpm.
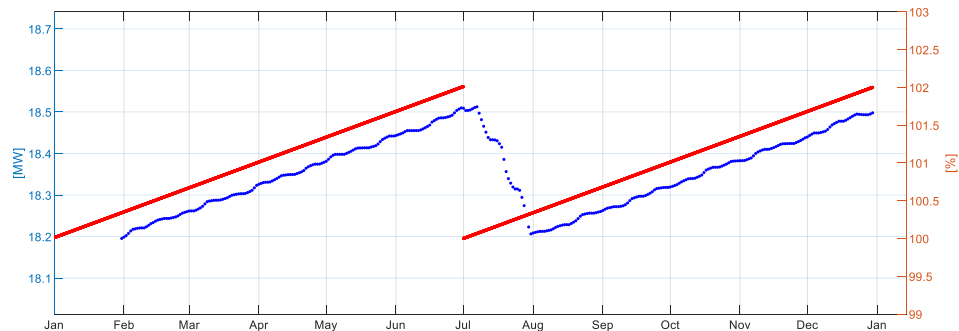

Fig.13: Time evolution of vessel performance

194

Fig.13 shows the series of values $P_{S,i}$ obtained in the example, as well as the biofouling coefficient previously defined. The graph shows that the series of values $P_{S,i}$ reflect changes in the in-service degradation of the hull, successfully identifying the hull cleaning event that occurred on July 1, the maximum increase of shaft power demand, and the hull degradation rate.

7. Intrinsic error of Noon Reports data collection systems

Let us consider a KVLCC2 vessel sailing at 16.5 kn for 12 h, and at 12.5 kn for another 12 h. The captain would submit a Noon Report summarizing the performance metrics of the 24 h reporting period as follows:

- Average vessel speed: 14.5 kn
- Average propeller rpm: 67.76 rpm
- Average shaft power demand: 17.324 MW
- Main Engine fuel consumption: 74.8 mt

For simplicity, it is assumed that $\eta_S = 1$ and SFOC = 180 g/kWh. If the same vessel had sailed with same draft, trim, and weather conditions at 14.5 kn during 24 h, the fuel consumption would have been 69.1 mt, and the reported 74.8 mt would have been interpreted as 8.2% higher than expected.

If the sailing speed pattern during the reporting period happened due to justified operational constraints, it cannot be said that the vessel underperformed with an 8.2% fuel consumption increase above the expected baseline. Moreover, it cannot be said that the Noon Report was wrong. However, it is apparent that this noon report doesn't reflect the baseline performance of the vessel, and it should be omitted when evaluating the performance of the vessel.

This simple example illustrates that reporting simple average values of vessel speed, propeller rpm, and shaft power demand produces unreliable noon report data whenever the vessel experiences high speed variability during the reporting period.

A more rigorous proof can be derived from Eq.(25). Let us consider a series of values $P_{S,i}$, V_i, and n_i, $1 \leq i \leq 24$, one data-point per hour during the 24-h reporting period, during which it is assumed that the draft, trim, and weather sailing conditions did not change. Each data-point will verify the internal consistency captured by Eq.(25):

$$P_{S,i} = \frac{1}{\eta_s \cdot \eta_R} \cdot 2 \cdot \pi \cdot \rho \cdot n_i^3 \cdot D^5 \cdot K_{Qo} \cdot \left(\frac{e^{k_q \cdot J_{oq}} - e^{k_q \cdot \frac{(1-w) \cdot V_i}{n_i \cdot D}}}{e^{k_q \cdot J_{oq}} - 1} \right) \qquad (31)$$

Reporting average values as summarizing metrics of power, speed and rpm is sustained on the assumption that

$$\overline{P_S} \overset{?}{=} \frac{1}{\eta_s \cdot \eta_R} \cdot 2 \cdot \pi \cdot \rho \cdot \bar{n}^3 \cdot D^5 \cdot K_{Qo} \cdot \left(\frac{e^{k_q \cdot J_{oq}} - e^{k_q \cdot \frac{(1-w) \cdot \overline{V}}{\bar{n} \cdot D}}}{e^{k_q \cdot J_{oq}} - 1} \right) \qquad (32)$$

Which can happen if, and only if,

$$V_1 = \cdots = V_i = \cdots = V_{24} = \overline{V}$$
$$n_1 = \cdots = n_i = \cdots = n_{24} = \bar{n}$$
$$P_{S_1} = \cdots = P_{S_i} = \cdots = P_{S_{24}} = \overline{P_S}$$

i.e., i.i.f. speed, rpm, and sailing conditions are kept constant during the reporting period.

8. Vessel performance with Noon Reports data

In section 6, a synthetic dataset of hourly values was created to illustrate the applicability of a performance evaluation method. This dataset was used to create a secondary synthetic dataset by calculating the average speed, rpm and shaft power demand at every 24 h period. Applying the vessel

performance evaluation procedure described in section 6 over this secondary synthetic noon reports dataset would yield Fig.15. Fig.16 shows that the noon reports covering periods with high vessel speed variability introduce a significant level of error, masking the actual baseline performance of the vessel.
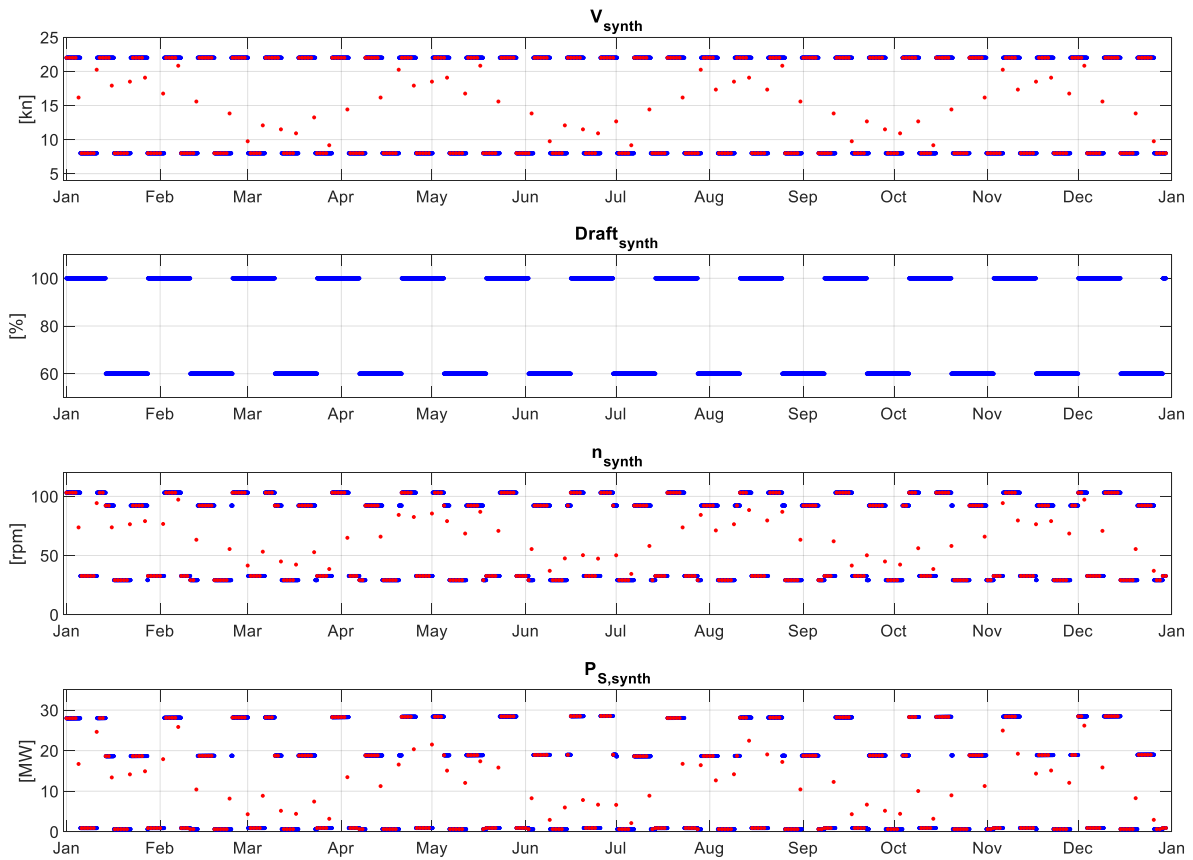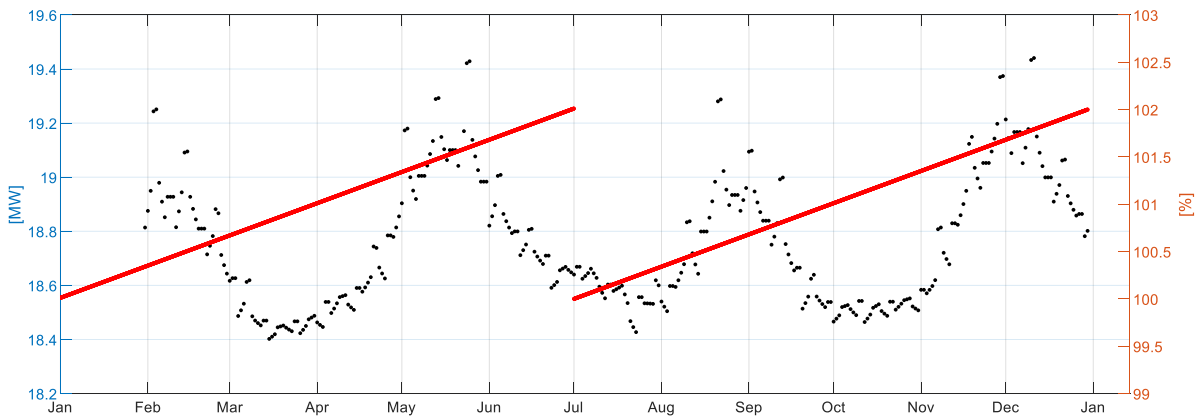

Fig.15: Noon Reports synthetic dataset

Fig.16: Time evolution of vessel performance with Noon Reports synthetic dataset

Fig.17 shows the synthetic noon reports dataset, in which the noon reports covering periods where the vessel experienced high speed variability have been omitted. Applying the vessel performance evaluation procedure described in section 6 over the dataset yields the Fig.18, which coincides with the expected vessel performance evolution over time.
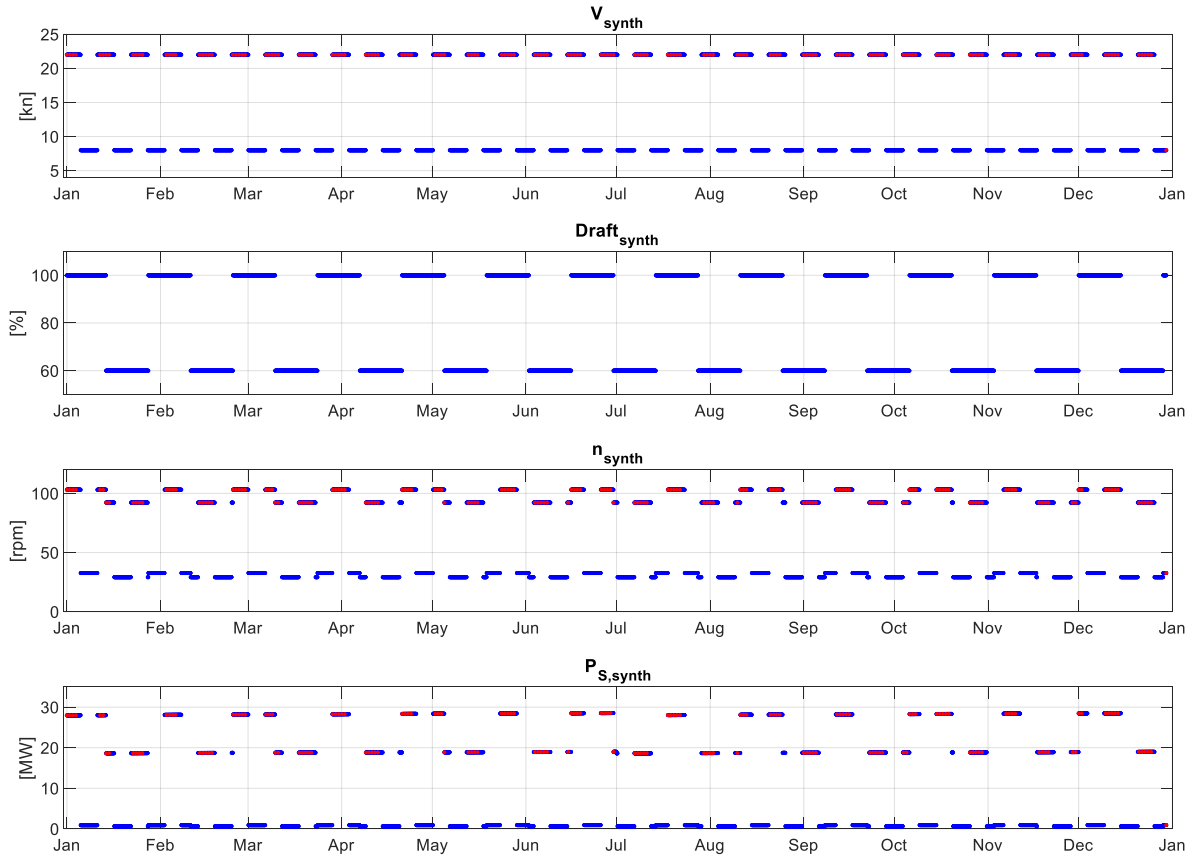
Fig.17: Synthetic dataset of filtered Noon Reports
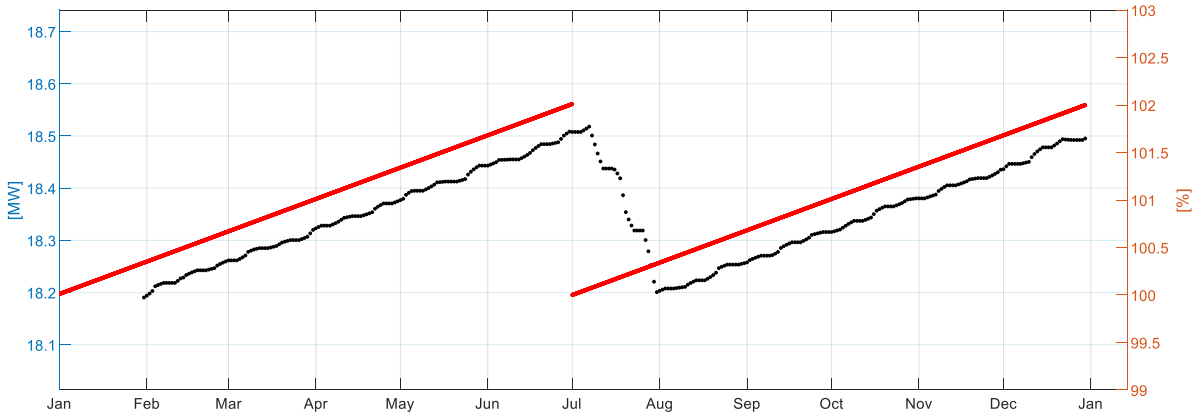
Fig.18: Time evolution of vessel performance with Noon Reports selected data

9. Conclusion

Closed-form mathematical expressions were derived that allow expressing the shaft and effective power as a function of the open-water characteristics of a propeller, the vessel speed, propeller revolutions, propeller diameter, fluid density, wake fraction coefficient, thrust deduction fraction, shaft efficiency and relative rotative efficiency.

The Series 60 and KVLCC2 model data was used to test the feasibility of these equations. The coefficients of determination obtained indicate that this mathematical model can be used to characterize the power demand of a full-scale vessel. Furthermore, a method was introduced to estimate the evolution of vessel performance over time such that it does not require knowledge of the maintenance history of the vessel.

197

A synthetic dataset was created using the Series 60 Model 4280 as a baseline reference. The baseline power demand was affected by a sawtooth waveform, thus replicating the effects of progressive performance degradation due to fouling as well as a hull cleaning event. Then, from this data, a secondary dataset was created, mimicking the noon reports that the captain would have submitted. Then the proposed performance evaluation procedure was used to identify vessel speed variability as an intrinsic source of error of noon reports, and show that by omitting these noon reports, it is possible to conduct an accurate performance evaluation of a vessel with noon reports as data collection system.

References

AGNOLUCCI, P.; SMITH, T.W.P.; REHMATULLA, N. (2014), *Energy efficiency and time charter rates: Energy efficiency savings recovered by ship owners in the Panamax market*, Transportation Research Part A: Policy and Practice 66, pp.173-184

AHLGREN, F.; THERN, M. (2018), *Auto machine learning for predicting ship fuel consumption*, 31st Int. Conf. Efficiency, Cost, Optimization, Simulation and Environmental Impact of Energy Systems

ALDOUS, L. (2015), *Ship Operational Efficiency: Performance Models and Uncertainty Analysis*, University College London, London

ARMSTRONG, V.N. (2013), *Vessel optimisation for low carbon shipping*, Ocean Engineering

BAZARI, Z. (2007), *Ship energy performance monitoring and benchmarking,* J. Marine Eng. and Technology A9

BRANDSÆTER, A.; VANEM, E. (2018), *Ship speed prediction based on full scale sensor measurements of shaft thrust and environmental conditions*, Ocean Eng. 162

CORADDU, A.; ONETO, L.; BALDI, F.; AGUITA, D. (2017), *Vessel fuel consumption forecast and trim optimisation: A data analytics perspective,* Ocean Eng. 130, pp.351-370

CORADDU, A.; LIM, S.; ONETO, L.; PAZOUKI, K.; NORMAN, R.; MURPHY, A.J. (2019a), *A novelty detection approach to diagnosing hull and propeller fouling,* Ocean Eng. 176, pp.65-73

CORADDU, A.; ONETO, L.; BALDI, F.; CIPOLLINI, F.; ATLAR, M.; SAVIO, S. (2019b), *Data-driven ship digital twin for estimating the speed loss caused by the marine fouling,* Ocean Eng. 186

ELJARDT, G. (2006), *Development of a fuel oil consumption monitoring system*, TU Hamburg-Harburg

FARAG, Y.B.; OLÇER, A.I. (2020), *The development of a ship performance model in varying operating conditions based on ANN and regression techniques,* Ocean Eng. 198

FLIKKEMA, M. (2013), *Approaches to Measuring Hull and Propeller Performance, Hull and Propeller Performance Measurement Standard*, MARIN, Oslo

GARG, B.R. (1972), *The service performance of ships with special reference to tankers,* MSc Thesis, University of Newcastle upon Tyne

GERTLER, M. (1954), *A reanalysis of the original test data for the Taylor standard series*, DTMB report 806, Washington

GKEREKOS, C.; LAZAKIS, I. (2020), *A novel, data-driven heuristic framework for vessel weather routing*, Ocean Eng. 197

GKEREKOS, C.; LAZAKIS, I.; THEOTOKATOS, G. (2019), *Machine Learning models for predicting ship main engine Fuel Oil Consumption: A comparative study,* Ocean Eng. 188

GULDHAMMER, H.E.; HARVALD, S.A. (1965), *Ship Resistance Effects of Form and Principal Dimensions,* Akademisk Forlag, Copenhagen (revised 1974)

HANSEN, A. (2010), *Monitoring of hull condition of ships*, MSc Thesis, NTNU, Trondheim

HELMA, S. (2020), *Surprising Behaviour of the Wageningen B-Screw Series Polynomials*, J. Marine Science and Engineering

HOLLENBACH, K.U. (1998), *Estimating resistance and propulsion for single screw and twin-screw ships,* Ship Technology Research 45/2

HOLTROP, J.; MENNEN, G.G.J. (1982), *An Approximate Power Prediction Method*, Int. Shipb. Progress 29, pp.166-170

IMO (2009), *Prevention of Air Pollution From Ships - Update of the 2000 IMO GHG Study*, Int. Maritime Org., London

ISO (2015), *ISO 15016:2015 Guidelines for the assessment of speed and power performance by analysis of speed trial data*, Int. Standard. Org., Geneva

ISO (2016), *ISO 19030:2016 Measurement of changes in hull and propeller performance*, Int. Standard. Org., Geneva

ITTC (2012), *Speed and Power Trials Part 1 Preparation and Conduct. ITTC - Recommended Procedures and Guidelines. 7.5-04-01-01.1,* Int. Towing Tank Conf.

JOURNEE, J.M.J. ; RIJKE, R.J.; VERLEG, G.J.H. (1987), *Marine Performance Surveillance with a Personal Computer*, Report 753-P, TU Delft

LEIFSSON, L.P. ; SÆVARSDOTTIR, H.; SIGURDSSON, S.; VESTEINSSON, A. (2008), *Grey-box modeling of an ocean vessel for operational optimization,* Simulation Modelling Practice and Theory 16(8), pp.923-932

LINDSTAD, H.; ASBJØRNSLETT, B.E.; JULLUMSTRØ, E. (2013), *Assessment of profit, cost and emissions by varying speed as a function of sea conditions and freight market*, Transportation Research Part D: Transport and Environment 19:5

LOGAN, K.P. (2011), *Using a Ships Propeller for Hull Condition Monitoring*, ASNE Intelligent Ships Symp. IX, Philadelphia

MOSS, J.L. (1963), *Hull Form Development and Resistance and Propulsion Tests Results of a Series of ship hulls having extreme "V" Sections*, University of Michigan

MUNK, T. (2006), *Fuel Conservation Through Managing Hull Resistance*, Motorship Propulsion Conf., Copenhagen

OOSTERVELD, M.W.C.; VAN OSSANNEN, P. (1975), *Further computer-analysed data of the Wageningen B-screw series,* ISP 22

PEDERSEN, J.P.; LARSEN, J. (2009), *Prediction of Full-Scale Propulsion Power using Artificial Neural Networks*, 8th COMPIT Conf., Budapest, pp.537-550

PERERA, L.; MO, B. (2016), *Machine Intelligence for Energy Efficient Ships: A Big Data Solution*, Maritime Engineering and Technology III, Vol. 1, Taylor & Francis Group, London, pp.143-150

PERERA, L.; MO, B. (2018), *Ship performance and navigation data compression and communication under autoencoder system architecture*, J. Ocean Eng. Sci. 3, pp.133-143

PETERSEN, J.P.; JACOBSEN, D.J.; WINTHER, O. (2011a), *Gaussian Mixture Models for Analysing Operational Ship Data*, Technical Report, DTU, Lyngby

PETERSEN, J.P.; WINTHER, O.; JACOBSEN, D.J. (2012), *A Machine-Learning Approach to Predict Main Energy Consumption*, Ship Technology Research, 59/1, pp.64-72

PETERSEN, J.P.; JACOBSEN, D.J.; WINTHER, O. (2012), *Statistical modelling for ship propulsion efficiency*, J. Mar. Sci. Technol. 17, pp.30-39

SEO, J.H.; LEE, C.M.; JIN, W.Y.; CHOI, J.E., LEE, I.W. (2020), *Power increase and propulsive characteristics in regular head waves of KVLCC2 using model tests*, Ocean Eng. 216

SONER, O.; AKYUZ, E.; CELIK, M. (2018), *Statistical modelling of ship operational performance monitoring problem*, J. Mar. Sci. Technol. 24/2, pp.543-552

STRASSER, G.; TAKAGI, K.; WERNER, S.; HOLLENBACH, U.; TANAKA, T.; YAMAMOTO, K.; HIROTA, K. (2015), *A Verification of the ITTC/ISO Speed/Power Trials Analysis*, J. Marine Science Technology 20, pp.2-13

TELFER, E.V. (1926), *The practical analysis of merchant ships trials and service performance*, Trans. NECIES Vol 43

THEMELIS, N.; SPANDONIDIS, C.C.; CHRISTOPOULOS, G.; GIORDAMLIS, C. (2018), *A comparative study on ship performance assessment based on noon report and continuous monitoring datasets*, 12th Conf. Hellenic Institute of Marine Technology, pp.55-64

TODD, F.H. (1964), *Series 60. Methodical Experiments with Models of Single-Screw Merchant Ships*, Report 1712, Dept of the Navy

TOWNSIN, R.L.; MOSS, B.; WYNNE, J.B.; WHYTE, I.M. (1975), *Monitoring the speed performance of ships*, Trans. NECIES Vol. 91, pp.159

TROOST, L. (1938), *Open water test series with modern propeller forms*, Trans. NECIES 54

TROOST, L. (1939), *Open water test series with modern propeller forms. Part 2 – three bladed propellers*, Trans NECIES

TROOST, L. (1951), *Open water test series with modern propeller forms. Part 3 – two bladed and five bladed propellers – extension of the three and four bladed B-series*, Trans. NECIES 67

VAN LAMMEREN, W.P.A.; VAN MANEN, J.D.; OOSTERVELD, M.W.C. (1969), *The Wageningen B-screw series*, Trans. SNAME

WANG, S.; JI, B.; ZHAO, J.; LIU, W.; XU, T. (2018), *Predicting ship fuel consumption based on LASSO regression*, Transport. Res. D 65, pp.817-824

ZAMORA, J. (2021), *Obtaining and Utilizing Power Demand data of Self-Propelled Vehicles*, U.S. Patent Application No. 17/225,019, U.S. Patent and Trademark Office

A Case Study of Speed Optimization

Pavlos Karagiannidis, GreenSteam, Athens/Greece, pavlos.karagiannidis@greensteam.com
Jonas S. Frederiksen, GreenSteam, Lyngby/Denmark, jsf@greensteam.com
Matthew Streeter, GreenSteam, Lyngby/Denmark, matthew.streeter@greensteam.com
Chresten Søndergaard, GreenSteam, Lyngby/Denmark, cs@greensteam.com
John Harrington, GreenSteam, Eastleigh/UK, jh@greensteam.com
Daniel Jacobsen, GreenSteam, Lyngby/Denmark, dj@greensteam.com
Jóan Petur Petersen, GreenSteam, Lyngby/Denmark, jpp@greensteam.com
Ivana Melillo, d'Amico International Shipping, Rome/Italy, melillo.i@damicoship.com

Abstract

This joint article between D'Amico and GreenSteam will investigate speed optimization (SO) for the vessel Cielo di Cagliari. The SO problem consists of a given route, which is broken into stretches by the SO algorithm, and for each stretch, the algorithm finds the best speed to reduce the total fuel consumption – in this example we achieved a saving of 3.7% fuel. We will compare the propulsion model's influence on the results by comparing a classical naval architecture approach and a data-driven machine learning approach. We will also compare the models' ability to predict the actual fuel consumption for voyages, and the impact of fouling and weather are also studied.

1. Introduction

Speed Optimization solves the problem of sailing from point A to point B in the most fuel cost-efficient way given the departure and arrival times, and possible other constraints. The primary way it can save fuel is to avoid bad weather, adverse currents, and other factors such as taking ECA zones into account. The problems include modeling the vessel's fuel consumption, weather forecasts, and the speed optimization algorithm. Weather forecasts include total sea currents, waves, and wind. The fuel consumption models can be independently developed, *Coraddu et al. (2019), Petersen et al. (2011), Karagiannidis and Themelis (2021)*, for various applications, out of which SO is one of the most popular. Speed optimization algorithms are discussed further in the literature review section.

The importance of SO application has gained momentum following the global efforts to reduce Green House Gasses (GHG) emissions and the strict targets set by IMO (MEPC 74, 75 and 76), the Sea Cargo Charter, and other initiatives as mentioned by IMO's (2018) initial strategy on reduction of GHG emissions from ships, operational measures appeared as one of the prominent short-term measures to achieve them. They require minimum capital expenditures (in comparison to other measures) and can be implemented on every type of vessel without major modifications or time delays. However, in order to successfully implement these measures (i.e. Speed Optimization) and reduce emissions, it is crucial to develop accurate and sophisticated models and algorithms.

Nevertheless, the race to reduce emissions is going to have many side effects on the competitiveness and the commercial benchmark of the ships worldwide. Ship managers or owners that demonstrate lower CO2 emissions will get higher ratings from IMO, as per the CII scheme. Inevitably, there will be incentives for the charterers to transfer cargo with more efficient and less emitting ships to demonstrate eco-friendly operations and increased sustainability of their business. In this context, speed optimization of every voyage could be considered as a competitive advantage or even as an industry standard.

2. Literature Overview

Speed Optimization is approached as a mathematical problem of optimization. Studies model the ship speed profile problem using an objective function that estimates the total fuel cost of the voyage with the constraints of the problem being the ETA and any intermediate deadlines that need to be met. The solution is found by minimizing the objective function while respecting the constraints. Variations

between different studies/approaches appear in the mathematical modeling i.e. the definition of the objective function and/or the constraints but also in the method selected for solving the optimization problem i.e. finding the local or global minima.

However, the mathematical modelling of the optimization problem and its proper solution do not guarantee an effective SO application. The main source of uncertainty in SO applications has its roots in the assumed speed-consumption relation. The framework of SO is generic but to apply it successfully to each vessel it is essential to have a highly accurate ship-specific speed-consumption model that is incorporated in the objective function. Such a model needs to take into account all the parameters that influence the vessel's propulsion efficiency i.e. wind, waves, currents, temperature, hull and propeller condition, trim, draft etc. Only then, the minimization of the objective function will produce a realistically optimized speed profile that will allow the subject vessel to arrive on time and save fuel, hence reducing costs and emissions.

Some examples of SO studies are listed here. *Kim et al. (2016)* suggests a speed optimizer for multiple ports based on a nonlinear mixed-integer program that can find optimal speed considering multiple time windows for each port. This work doesn't consider the optimal speed between ports concerning the weather. *Psaraftis (2019)* compares speed optimization and slow steaming, highlighting some problems with the latter. *Yang et al. (2020)* describes a speed optimization approach using a Genetic Algorithm. Their propulsion model uses STW instead of SOG to estimate the vessel's resistance and considers involuntary speed loss due to added resistance in wind and waves.

3. GreenSteam Approach

3.1 Modeling

GreenSteam's ML model consists of a Bayesian model with prior knowledge about the physical system. In a Bayesian model, the posterior distribution for the model parameters and predictions are found using Bayes theorem. This way, the model can learn from operational data collected from the vessel and update its view. The statistical priors are defined using probability distributions, which can tell the model what reasonable values to begin with.

The ML model can handle fouling as added fouling resistance, this in a Bayesian way, so for example, we can indicate to the model using the priors what we expect the fouling levels to be before the model sees any data.

3.2 Speed Optimization Algorithm

We define a route between points A and B by dividing it into legs, which are given as a number of waypoints. The route is broken into smaller stretches by the SO algorithm. Each stretch has a fixed distance for which the SO finds the optimal advice speed based on the optimal solution for the route respecting the ETA and other constraints on power and speed. The SO problem is solved using a Dynamic Programming approach, where the problem of reaching a point on the route using the least fuel can be broken into similar subproblems, resolving them recursively.

4. Case Study

Developing advanced algorithms for optimization and complex machine learning models is of limited value in the real world, unless validated with actual experiments. In the following case-study a D'Amico managed tanker, whose principal particulars are presented in Table I, is chosen to optimize her speed profile using GreenSteam's advanced Speed Optimization service. Details of the live trial voyage are also given in Table II.

Table I: Ship Principal Particulars

Ship Type	Oil products tanker
Year of Built	2018
Summer Deadweight	74999 tons
Length Over all	228 m
Max Breadth	36 m
Draft (laden)	11.6 m

The scope of the case-study is to validate through a real-life trial the effectiveness of the algorithm and the ship propulsion model behind it. This was achieved by a close collaboration among three parties: owner (D'Amico), charterer, and provider (GreenSteam). For the subject voyage, the vessel is given specific speed advice daily from GS. The algorithm runs on updated weather forecast data every few hours and so the crew is requested to adjust the ship speed. The charter is providing the requested ETA to the next port of call.

Table II: Live Trial Voyage Details

Start of Voyage leg	Balboa, Panama Canal
Date of Departure	12 June 2021
End of Voyage leg	Gwangyang, South Korea
Date of Arrival	09 July 2021
Total Distance	8,353 nm
Loading Condition	Laden

5. Results

The above-mentioned effectiveness of GreenSteam's solution can be quantified by the vessel's timely arrival at the port and the total cost of fuel consumption and emissions emitted. However, before reviewing the live trial results we need to establish some confidence on the ship propulsion model which is the key element to the success of this process.

5.1 Model accuracy

In this study, the GreenSteam Machine Learning model (GS ML model) is tested and compared to a reference model that resembles the state-of-the-art academic ship propulsion model from DTU (DTU Ship Simulation Workbench). The main difference between these models lies in the hybrid nature of the GS ML model that incorporates data-driven Bayesian components and its ability to take fouling into account. The DTU Ship Simulation Workbench model doesn't account for the fouling and pure empirical naval architecture models are inaccurate in heavy sea states by nature because of their empirical towing tank inheritance, so the model has a clear disadvantage, and will most likely tend to underpredict the power. Not taking fouling into account reflects a quite common practice in the industry today when looking at speed optimization.

Both models can predict the required shaft power or fuel consumption of the vessel by having as input a set of operational parameters and ship geometry characteristics. Hence, the error of the models' predictions on the measured shaft power of the vessel is estimated. The evaluation period extends over all the available data of the vessel, and it covers a period of about 3 years (07/2018 to 07/2021). The error is given as a Normalized Root Mean Square Error (NRMSE) value, and it is computed for four different aggregation intervals.

Table III: Ship Propulsion models' error comparison

Aggregation	GS ML Model	Reference model
10 minutes	12.75 %	22.56%
1 hour	12.26%	22.37%
6 hours	10.87%	21.89%
24 hours	9.02%	21.32%

Fig.1 shows the 10-minute values of measured and predicted Shaft Power as a function of the Speed Through Water. From Table III the error of the GS ML model is 12.75% while that of the reference model is 22.56%. The same gap between these two models is maintained in the rest aggregation intervals. The reference model is under-predicting the required shaft power in most cases since it is not compensating properly for the hull fouling, in contrast with the GS ML model that explicitly models fouling as well.
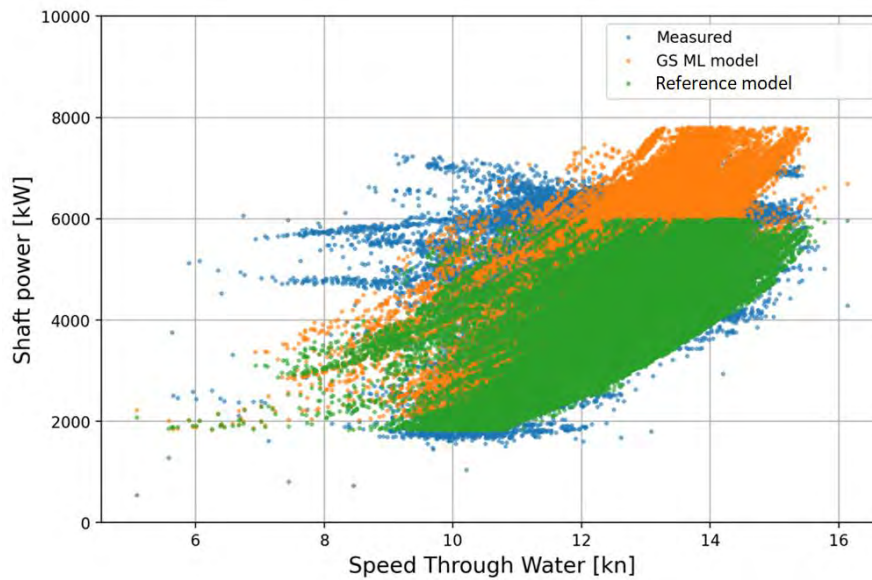
Fig.1: Measured STW vs Shaft Power values and the respective models' predictions

5.2 Live Speed Optimization

The next step of the process is to optimize the subject voyage of the vessel (ref. Table 2) with Green-Steam's optimization algorithm. The algorithm is executed to optimize the exact same voyage under the following two scenarios:

1. The GS ML model is used as the ship propulsion model and
2. The reference model is used as the ship propulsion model.

The optimization process is sensitive to the shaft power and fuel consumption prediction, and therefore different models may produce significantly different speed advice. The advised Speed Over Ground (SOG) profiles for the two scenarios and the voyage route are shown in Figs.2 and 3, respectively.
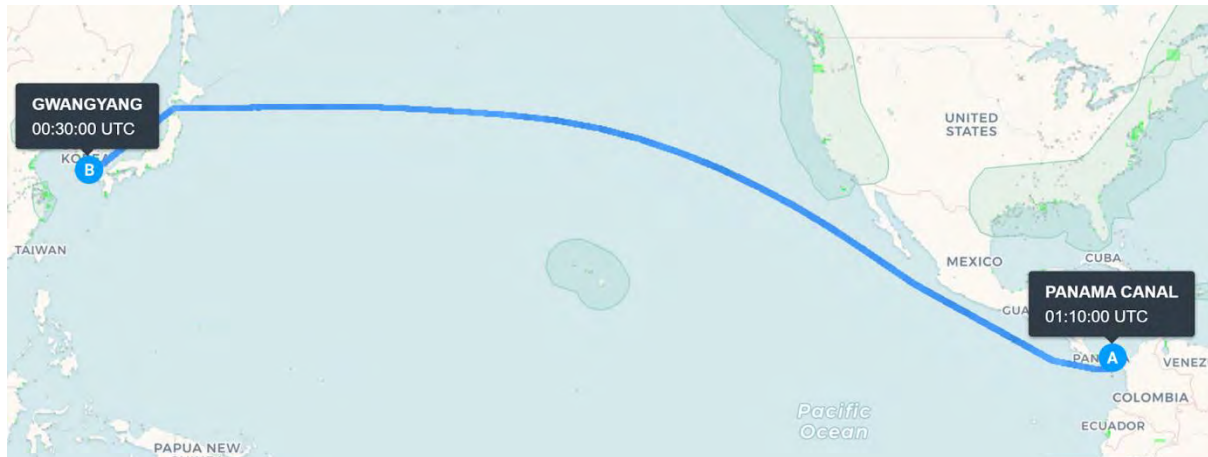
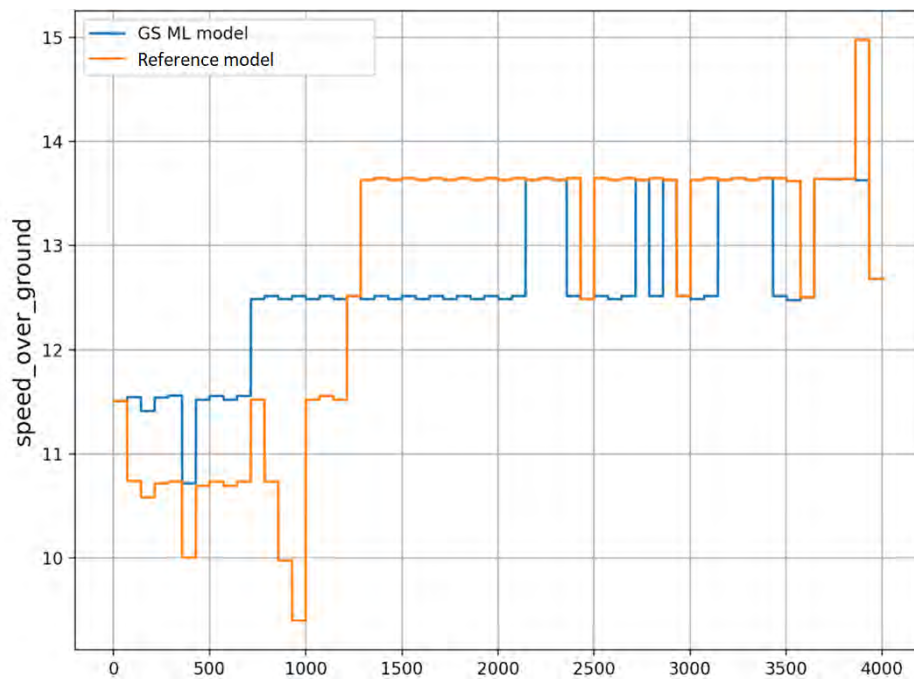

Fig.2: Ship's route for the Speed Optimization voyage

Fig.3: The advised SOG from the SO using the GS ML model and the reference model

Table IV: Summary of optimal costs for both scenarios.

GS ML Model total fuel cost	221,761$
Reference Model total fuel cost	176,479$
Difference	45,282$ or 20.4%

Simply by adopting a different ship propulsion model in the Speed Optimization process the encountered weather conditions would also change. The encountered wind speed and significant wave height for both scenarios are plotted in Figs.4 and 5. The average relative wind speed and wave height, though, are almost the same for the voyage in total, estimated to be average relative wind speed of 10.7 kn and

average wave height of 1.7 m. However, the fuel consumption prediction from the two models, presented in Fig.6, differs by almost 20% and so does the total voyage cost, presented in Table IV.
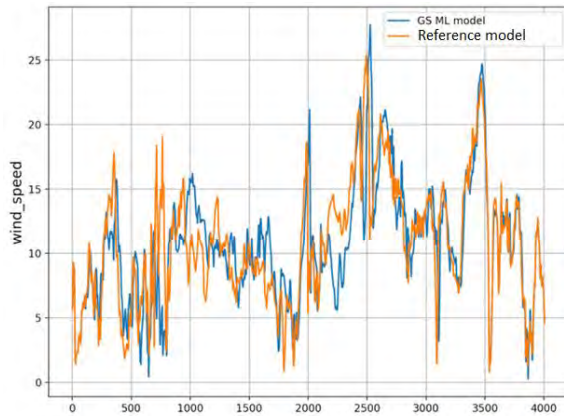
Fig.4: Encountered Relative Wind Speed (kn) by the vessel in each scenario
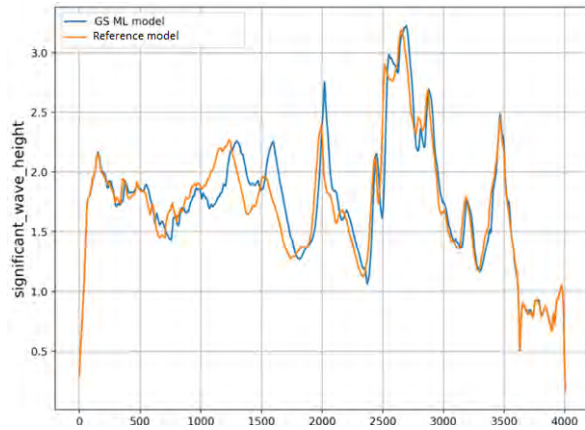

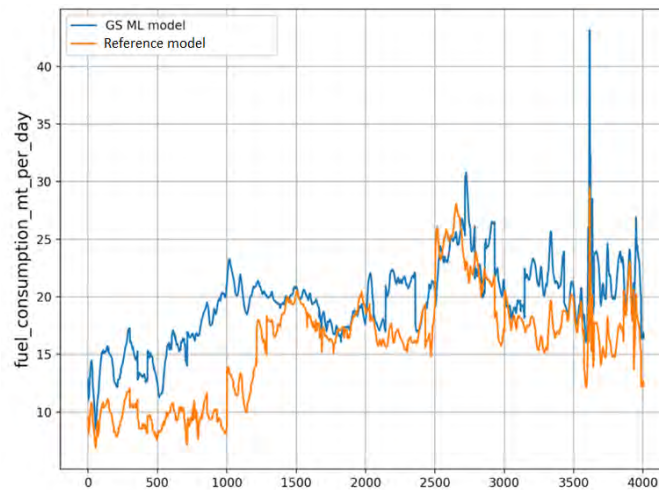Fig.5: Encountered Significant Wave Height (m) by the vessel in each scenario

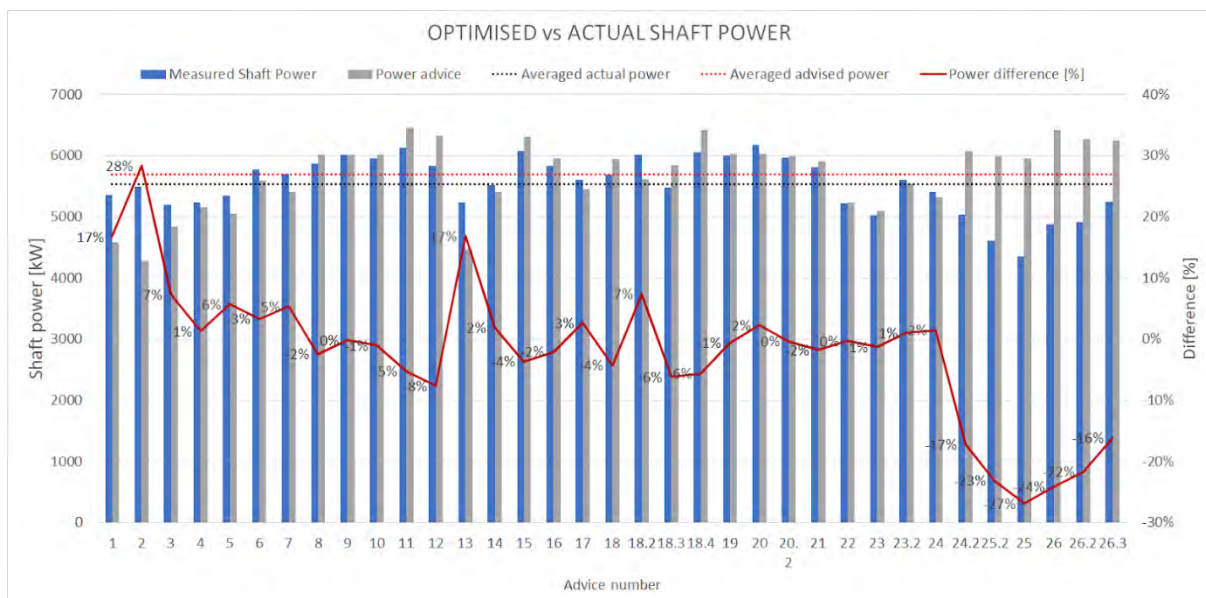Fig.6: Model's Fuel Consumption Prediction in each scenario

Fig.7: The optimized power value (power advice) against the actual (measured shaft power), for each fraction of the voyage, and the percentage difference between them.

206

The above direct comparison of the SO advice and the models' prediction is legitimate since all the constraints of the problem are identical, however the comparison of the actual live trial with the SO predictions is not totally plausible. One reason is that the crew receives instructions in terms of power required to achieve the "optimal" SOG for a particular fraction of the voyage and so, some error might be introduced in the process of implementation. This is demonstrated in Fig.7, where the advised and the measured Shaft Power are plotted as well as the percentage difference among these two. The average power difference is just 2% but it is important to note the much higher deviation from "advice" at the very start and close to the end of the sea passage due to local restrictions related with port traffic.

Another unforeseeable reason for deviation among the optimized voyage total cost and the actual cost is that of the weather forecast. Even with a ship propulsion model that achieves 100% accuracy, the slight difference of the forecasted against the actual weather conditions faced by the vessel will introduce some error in the final result.

Table V compares actual voyage data and the GS Optimisation predictions. The middle column, "Actual Voyage Predictions" refers to the model prediction under the actual speeds and weather conditions that the vessel experienced which differ from the optimal voyage predictions for the above stated reasons. The error from the actual voyage consumption is 6.3% which is well within the expected error range.

Table V: Comparison of actual, predicted and optimal voyage cost and consumption

	GS Optimal Values	Actual Voyage Predictions	Actual Voyage Values
Total Cost:	221,761$	249,260$	273,813$
Total Consumption:	548 tons	605 tons	643 tons

The most meaningful comparison though would be among the actual voyage and the simulated voyage at constant average speed, hence without the GS SO advice. The constant speed scenario, which is selected as reference for the actual savings, provides a pessimistic estimation of the savings because the vessel only at the best-case scenario would sail at constant speed and not in an arbitrary, sub-optimal speed profile. The estimated actual savings are presented in Table VI.

Table VI: Actual voyage data against constant speed consumption prediction

	Constant Speed	Actual Voyage	Difference
Average Voyage Speed	12.84 knots	12.84 knots	
Total Fuel Consumption	666.4 tons	643 tons	24.7 tons or 3.7%

Table VII: Estimation of emissions reduction and CII rating

	Attained CII (g.CO2/DWT.nm)	Reduction in CII - Compared to 2019
IMO DCS 2019	3.9470	
IMO DCS 2020	3.9004	1.2%
Voyage (Actual)	3.5590	10.9%
Voyage (Constant speed)	3.6821	7.2%
Attained CII Rating	A	

The fuel consumption savings of the optimized voyage are also translated into emissions reduction for the particular voyage and into CII benchmark. An estimated reduction of 3.7% is found in the mass of CO_2 and a CII rating A is achieved. The voyage is compared with the total average rating for the vessel from 2019 and 2020 respectively in the Table VII.

6. Conclusion

Using a precise model that can adapt to operational data from the vessel and handle fouling can considerably improve the SO applications' overall performance and metrics. Not accounting for the fouling will lead the SO application to assume that the vessel can make the voyage with less fuel than needed. The underpredicted required propulsion power will result in the ship constantly lagging behind, compromising the ETA and resulting in suboptimal speeds.

References

CORADDU, A.; ONETO, L.; BALDI, F.; CIPOLLINI, F.; ATLAR, M.; SAVIO, S. (2019), *Data-driven ship digital twin for estimating the speed loss caused by the marine fouling,* Ocean Eng. 186, 106063

IMO (2018), *Initial IMO Strategy on Reduction of GHG Emissions from Ships*, Resolution MEPC.304(72), Int. Mar. Org., London

KIM, J.; KIM, H.; JUN H. B.; KIM, C. (2016), *Optimizing Ship Speed to Minimize Total Fuel Consumption with Multiple Time Windows*, Mathematical Problems in Eng.

KARAGIANNIDIS, P.; THEMELIS, N. (2021), *Data-driven modelling of ship propulsion and the effect of data pre-processing on the prediction of ship fuel consumption and speed loss*, Ocean Eng. 222, 108616

PETERSEN, J.P.; JAKOBSEN, D.J.; WINTHER, O. (2011), *A Machine-Learning Approach to Predict Main Energy Consumption under Realistic Operational Conditions*, 10th COMPIT Conf. Berlin, pp.305-316

PSARAFTIS, H.N. (2019), *Speed Optimization vs Speed Reduction: The Choice between Speed Limits and a Bunker Levy*, Sustainability 11(8)
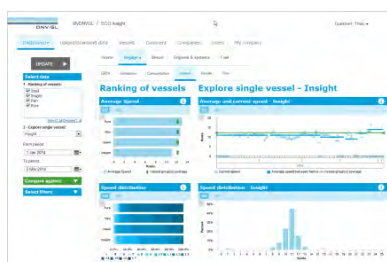
YANG, L.; CHEN, G.; ZHAO, J.; RYTTER, N. G. M. (2020), *Ship Speed Optimization Considering Ocean Currents to Enhance Environmental Sustainability in Maritime Shipping*, Sustainability 12(9)

Index by Authors

'

7th Hull Performance & Insight Conference (HullPIC)

Tullamore/Ireland, 9-11.5.2022

Topics:	ISO 19030 and beyond / EEXI and CII / sensor technology / human factors in reporting & understanding performance / information fusion / big data / uncertainty analysis / hydrodynamic models / business models / coating technology / Energy Saving Devices and how to prove they work
Organiser:	Volker Bertram (VB conferences) Stein Kjolberg (Jotun)

Advisory Committee:

Francesco Bellusci	Scorpio Group	Liz Haslbeck	NSWC-CD	Beom-Jin Park	KRISO
Johnny Eliasson	Chevron Shipping	Jeppe S. Juhl	BIMCO	Daniel Schmode	Wärtsilä
Wojciech Gorski	Enamor	Carsten Manniche	Ultranav	Giampiero Soncini	IB
Erik Hagestuen	Kyma	Ivana Melillo	D'Amico	Geoff Swain	FIT
Gilyong Han	Intertanko	Geir Axel Oftedahl	Jotun	Diego M. Yebra	Hempel

Venue:	The conference will be administered in Hamburg/Germany and held in Tullamore/Ireland
Format:	Papers to the above topics are invited and will be selected by a selection committee. The proceedings will be made freely available to the general public.

Deadlines:	anytime	Optional "early warning" of interest to submit paper / participate
	23.12.2021	First round of abstract selection (1/3 of available slots)
	24.02.2022	Second round of abstract selection (remaining slots)
	07.04.2022	Final papers due
Admin. Fees:	700 €	– early registration (by 01.04.2021)
	800 €	– late registration
		Fees are subject to German VAT

Sponsors:	Jotun, Tutech Innovation, COACH Solutions, Hasytec, Hoppe Marine, HullWiper, Idealship, Miros Mocean, Wärtsilä (further sponsors to be announced)
Information:	volker@vb-conferences.com or volker.bertram@dnv.com